

JOURNAL OF

CHROMATOGRAPHY A

INCLUDING ELECTROPHORESIS AND OTHER SEPARATION METHODS

EDITORS

U.A.Th. Brinkman (Amsterdam)

R.W. Giese (Boston, MA)

J.K. Haken (Kensington, N.S.W.)

L.R. Snyder (Orinda, CA)

S. Terabe (Hyogo)

EDITORS, SYMPOSIUM VOLUMES,

E. Heftmann (Orinda, CA), Z. Deyl (Prague)

EDITORIAL BOARD

D.W. Armstrong (Rolla, MO)

W.A. Aue (Halifax)

P. Boček (Brno)

A.A. Boulton (Saskatoon)

P.W. Carr (Minneapolis, MN)

N.H.C. Cooke (San Ramon, CA)

V.A. Davankov (Moscow)

G.J. de Jong (Weesp)

Z. Deyl (Prague)

S. Dilli (Kensington, N.S.W.)

Z. El Rassi (Stillwater, OK)

H. Engelhardt (Saarbrücken)

F. Erni (Basle)

M.B. Evans (Hatfield)

J.L. Glajch (N. Billerica, MA)

G.A. Guiochon (Knoxville, TN)

P.R. Haddad (Hobart, Tasmania)

I.M. Hais (Hradec Králové)

W.S. Hancock (Palo Alto, CA)

S. Hjertén (Uppsala)

S. Honda (Higashi-Osaka)

Cs. Horváth (New Haven, CT)

J.F.K. Huber (Vienna)

K.-P. Hupe (Waldbronn)

J. Janák (Brno)

P. Jandera (Pardubice)

B.L. Karger (Boston, MA)

J.J. Kirkland (Newport, DE)

E. sz. Kováts (Lausanne)

K. Macek (Prague)

A.J.P. Martin (Cambridge)

L.W. McLaughlin (Chestnut Hill, MA)

E.D. Morgan (Keele)

J.D. Pearson (Kalamazoo, MI)

H. Poppe (Amsterdam)

F.E. Regnier (West Lafayette, IN)

P.G. Righetti (Milan)

P. Schoenmakers (Amsterdam)

R. Schwarzenbach (Dübendorf)

R.E. Shoup (West Lafayette, IN)

R.P. Singhal (Wichita, KS)

A.M. Sioffi (Marseille)

D.J. Strydom (Boston, MA)

N. Tanaka (Kyoto)

K.K. Unger (Mainz)

R. Verpoorte (Leiden)

Gy. Vigh (College Station, TX)

J.T. Watson (East Lansing, MI)

B.D. Westerlund (Uppsala)

EDITORS, BIBLIOGRAPHY SECTION

Z. Deyl (Prague), J. Janák (Brno), V. Schwarz (Prague)

ELSEVIER

JOURNAL OF CHROMATOGRAPHY A

INCLUDING ELECTROPHORESIS AND OTHER SEPARATION METHODS

Scope. The *Journal of Chromatography A* publishes papers on all aspects of **chromatography, electrophoresis** and related methods. Contributions consist mainly of research papers dealing with chromatographic theory, instrumental developments and their applications. In the *Symposium volumes*, which are under separate editorship, proceedings of symposia on chromatography, electrophoresis and related methods are published. *Journal of Chromatography B: Biomedical Applications*—This journal, which is under separate editorship, deals with the following aspects: developments in and applications of chromatographic and electrophoretic techniques related to clinical diagnosis or alterations during medical treatment; screening and profiling of body fluids or tissues related to the analysis of active substances and to metabolic disorders; drug level monitoring and pharmacokinetic studies; clinical toxicology; forensic medicine; veterinary medicine; occupational medicine; results from basic medical research with direct consequences in clinical practice.

Submission of Papers. The preferred medium of submission is on disk with accompanying manuscript (see *Electronic manuscripts* in the Instructions to Authors, which can be obtained from the publisher, Elsevier Science B.V., P.O. Box 330, 1000 AH Amsterdam, Netherlands). Manuscripts (in English; *four* copies are required) should be submitted to: Editorial Office of *Journal of Chromatography A*, P.O. Box 681, 1000 AR Amsterdam, Netherlands, Telefax (+31-20) 5862 304, or to: The Editor of *Journal of Chromatography B: Biomedical Applications*, P.O. Box 681, 1000 AR Amsterdam, Netherlands. Review articles are invited or proposed in writing to the Editors who welcome suggestions for subjects. An outline of the proposed review should first be forwarded to the Editors for preliminary discussion prior to preparation. Submission of an article is understood to imply that the article is original and unpublished and is not being considered for publication elsewhere. For copyright regulations, see below.

Publication information. *Journal of Chromatography A* (ISSN 0021-9673): for 1995 Vols. 683–714 are scheduled for publication. *Journal of Chromatography B: Biomedical Applications* (ISSN 0378-4347): for 1995 Vols. 663–674 are scheduled for publication. Subscription prices for *Journal of Chromatography A*, *Journal of Chromatography B: Biomedical Applications* or a combined subscription are available upon request from the publisher. Subscriptions are accepted on a prepaid basis only and are entered on a calendar year basis. Issues are sent by surface mail except to the following countries where air delivery via SAL is ensured: Argentina, Australia, Brazil, Canada, China, Hong Kong, India, Israel, Japan, Malaysia, Mexico, New Zealand, Pakistan, Singapore, South Africa, South Korea, Taiwan, Thailand, USA. For all other countries airmail rates are available upon request. Claims for missing issues must be made within six months of our publication (mailing) date. Please address all your requests regarding orders and subscription queries to: Elsevier Science B.V., Journal Department, P.O. Box 211, 1000 AE Amsterdam, Netherlands. Tel.: (+31-20) 5803 642; Fax: (+31-20) 5803 598. Customers in the USA and Canada wishing information on this and other Elsevier journals, please contact Journal Information Center, Elsevier Science Inc., 655 Avenue of the Americas, New York, NY 10010, USA, Tel. (+1-212) 633 3750, Telefax (+1-212) 633 3764.

Abstracts/Contents Lists published in Analytical Abstracts, Biochemical Abstracts, Biological Abstracts, Chemical Abstracts, Chemical Titles, Chromatography Abstracts, Current Awareness in Biological Sciences (CABS), Current Contents/Life Sciences, Current Contents/Physical, Chemical & Earth Sciences, Deep-Sea Research/Part B: Oceanographic Literature Review, Excerpta Medica, Index Medicus, Mass Spectrometry Bulletin, PASCAL-CNRS, Referativnyi Zhurnal, Research Alert and Science Citation Index.

US Mailing Notice. *Journal of Chromatography A* (ISSN 0021-9673) is published weekly (total 52 issues) by Elsevier Science B.V., (Sara Burgerhartstraat 25, P.O. Box 211, 1000 AE Amsterdam, Netherlands). Annual subscription price in the USA US\$ 5389.00 (US\$ price valid in North, Central and South America only) including air speed delivery. Second class postage paid at Jamaica, NY 11431. **USA POSTMASTERS:** Send address changes to *Journal of Chromatography A*, Publications Expediting, Inc., 200 Meacham Avenue, Elmont, NY 11003. Airfreight and mailing in the USA by Publications Expediting.

See inside back cover for Publication Schedule, Information for Authors and information on Advertisements.

© 1994 ELSEVIER SCIENCE B.V. All rights reserved.

0021-9673/94/\$07.00

No part of this publication may be reproduced, stored in a retrieval system or transmitted in any form or by any means, electronic, mechanical, photocopying, recording or otherwise, without the prior written permission of the publisher, Elsevier Science B.V., Copyright and Permissions Department, P.O. Box 521, 1000 AM Amsterdam, Netherlands.

Upon acceptance of an article by the journal, the author(s) will be asked to transfer copyright of the article to the publisher. The transfer will ensure the widest possible dissemination of information.

Special regulations for readers in the USA – This journal has been registered with the Copyright Clearance Center, Inc. Consent is given for copying of articles for personal or internal use, or for the personal use of specific clients. This consent is given on the condition that the copier pays through the Center the per-copy fee stated in the code on the first page of each article for copying beyond that permitted by Sections 107 or 108 of the US Copyright Law. The appropriate fee should be forwarded with a copy of the first page of the article to the Copyright Clearance Center, Inc., 222 Rosewood Drive, Danvers, MA 01923, USA. If no code appears in an article, the author has not given broad consent to copy and permission to copy must be obtained directly from the author. The fee indicated on the first page of an article in this issue will apply retroactively to all articles published in the journal, regardless of the year of publication. This consent does not extend to other kinds of copying, such as for general distribution, resale, advertising and promotion purposes, or for creating new collective works. Special written permission must be obtained from the publisher for such copying.

No responsibility is assumed by the Publisher for any injury and/or damage to persons or property as a matter of products liability, negligence or otherwise, or from any use or operation of any methods, products, instructions or ideas contained in the materials herein. Because of rapid advances in the medical sciences, the Publisher recommends that independent verification of diagnoses and drug dosages should be made.

Although all advertising material is expected to conform to ethical (medical) standards, inclusion in this publication does not constitute a guarantee or endorsement of the quality or value of such product or of the claims made of it by its manufacturer.

Ⓢ The paper used in this publication meets the requirements of ANSI/NISO Z39.48-1992 (Permanence of Paper).

Printed in the Netherlands

CONTENTS

(Abstracts/Contents Lists published in Analytical Abstracts, Biochemical Abstracts, Biological Abstracts, Chemical Abstracts, Chemical Titles, Chromatography Abstracts, Current Awareness in Biological Sciences (CABS), Current Contents/Life Sciences, Current Contents/Physical, Chemical & Earth Sciences, Deep-Sea Research/Part B: Oceanographic Literature Review, Excerpta Medica, Index Medicus, Mass Spectrometry Bulletin, PASCAL-CNRS, Referativnyi Zhurnal, Research Alert and Science Citation Index)

REGULAR PAPERS

Column Liquid Chromatography

- New hybrid displacement technique for preparative liquid chromatography
by J. Newburger and B. DeLange (Princeton, NJ, USA) and G. Guiochon (Knoxville and Oak Ridge, TN, USA)
(Received 14 June 1994) 1
- N-Alkylcarbamoyl derivatives of amino acids as chiral stationary phases for high-performance liquid chromatography. I. An example of enhancing enantioselectivity by deleting the non-enantioselective π - π interaction site on the chiral stationary phase
by J.-Y. Lin (Tainan, Taiwan) and M.-H. Yang (Taipei, Taiwan) (Received 14 June 1994) 13
- Chiral ion-pair chromatographic separation of two dihydropyridines with camphorsulfonic acids on porous graphitic carbon
by M. Josefsson, B. Carlsson and B. Norlander (Linköping, Sweden) (Received 13 June 1994) 23
- Separation of the *R*(-)- and *S*(+)-enantiomers of the ethyl ester of tiagabine·HCl using a Chiralcel-OG column
by A.M. Rustum (North Chicago, IL, USA) (Received 16 May 1994) 29
- Temperature-induced displacement of proteins from dye-affinity columns using an immobilized polymeric displacer
by I.Yu. Galaev, C. Warrol and B. Mattiasson (Lund, Sweden) (Received 2 June 1994) 37
- Interaction of Cibacron Blue with polymers: implications for polymer-shielded dye-affinity chromatography of phosphofructokinase from baker's yeast
by I.Yu. Galaev, N. Garg and B. Mattiasson (Lund, Sweden) (Received 9 June 1994) 45
- Presence of a preferred anion-exchange binding site on cytochrome *b*₅: structural and thermodynamic considerations
by D.S. Gill, D.J. Roush and R.C. Willson (Houston, TX, USA) (Received 10 June 1994) 55
- Separation of arachidonic acid metabolites by on-line extraction and reversed-phase high-performance liquid chromatography optimized by computer simulation
by H. Fritsch (Chatillon-sur-Chalaronne, France), I. Molnar (Berlin, Germany) and M. Wurl (Hannover, Germany)
(Received 9 June 1994) 65
- Chromatographic behaviour of phenylurea pesticides in high-performance liquid chromatography with nitrile- and amino-bonded stationary phases
by J. Fischer and P. Jandera (Pardubice, Czech Republic) (Received 21 June 1994) 77
- Evaluation of liquid chromatography-ion spray mass spectrometry for the determination of substituted benzoic acids and their glycine conjugates
by F. Kasuya, K. Igarashi and M. Fukui (Kobe, Japan) (Received 31 May 1994) 93
- Analysis of neutral nitrogen compounds in diesel oil by direct injection high-performance liquid chromatography-mass spectrometry-ultraviolet spectrometry methods
by J. Mao (Kingston, RI and Wareham, MA, USA), C.R. Pacheco (Kingston, RI, USA and Rio de Janeiro, Brazil) and D.D. Traficante and W. Rosen (Kingston, RI, USA) (Received 21 June 1994) 103
- Identification of potentially mutagenic contaminants in the aquatic environment by liquid chromatographic-thermospray mass spectrometric characterization of in vitro DNA adducts
by D.W. Kuehl, J. Serrano and S. Naumann (Duluth, MN, USA) (Received 20 June 1994) 113
- Gas Chromatography*
- Automated headspace analysis of fumigants 1,3-dichloropropene and methyl isothiocyanate on charcoal sampling tubes
by J. Gan, S.R. Yates, W.F. Spencer and M.V. Yates (Riverside, CA, USA) (Received 17 June 1994) 121
- Evaluation of Tenax TA for the determination of chlorobenzene and chloronitrobenzenes in air using capillary gas chromatography and thermal desorption
by S.F. Patil (Poona, India) and S.T. Lonkar (Rasayani, India) (Received 9 June 1994) 133

ห้องสมุดกรมวิทยาศาสตร์บริการ

(Continued overleaf)

13 S.ศ. 2537
J. 233/

Contents (continued)

Electrophoresis

Simple approach to eliminating disturbances in isoelectric focusing caused by the presence of salts by J.-L. Liao and R. Zhang (Uppsala, Sweden) (Received 22 June 1994)	143
Model of electrophoretic focusing in a natural pH gradient moving in a tapered capillary by K. Šlais (Brno, Czech Republic) (Received 14 June 1994)	149

SHORT COMMUNICATIONS

Column Liquid Chromatography

Diastereomeric and enantiomeric separation of monoesters prepared from <i>meso</i> -cyclopentane-1,2-diols and racemic carboxylic acids on a silica phase and on amylose and cellulose chiral stationary phases by A. Kunath and F. Theil (Berlin-Adlershof, Germany) and J. Wagner (Berlin, Germany) (Received 15 July 1994)	162
In vivo O-dealkylation of resorufin and coumarin ethers by the green alga <i>Chlorella fusca</i> analysed by a rapid and sensitive high-performance liquid chromatographic assay by F. Thies and L.H. Grimme (Bremen, Germany) (Received 27 May 1994)	168

JOURNAL OF CHROMATOGRAPHY A

VOL. 684 (1994)

JOURNAL OF CHROMATOGRAPHY A

INCLUDING ELECTROPHORESIS AND OTHER SEPARATION METHODS

EDITORS

U.A.Th. BRINKMAN (Amsterdam), R.W. GIESE (Boston, MA), J.K. HAKEN (Kensington, N.S.W.),
L.R. SNYDER (Orinda, CA)

EDITORS, SYMPOSIUM VOLUMES

E. HEFTMANN (Orinda, CA), Z. DEYL (Prague)

EDITORIAL BOARD

D.W. Armstrong (Rolla, MO), W.A. Aue (Halifax), P. Boček (Brno), A.A. Boulton (Saskatoon), P.W. Carr (Minneapolis, MN), N.H.C. Cooke (San Ramon, CA), V.A. Davankov (Moscow), G.J. de Jong (Weesp), Z. Deyl (Prague), S. Dilli (Kensington, N.S.W.), Z. El Rassi (Stillwater, OK), H. Engelhardt (Saarbrücken), F. Erni (Basle), M.B. Evans (Hatfield), J.L. Glajch (N. Billerica, MA), G.A. Guiochon (Knoxville, TN), P.R. Haddad (Hobart, Tasmania), I.M. Hais (Hradec Králové), W.S. Hancock (Palo Alto, CA), S. Hjertén (Uppsala), S. Honda (Higashi-Osaka), Cs. Horváth (New Haven, CT), J.F.K. Huber (Vienna), K.-P. Hupe (Waldbronn), J. Janák (Brno), P. Jandera (Pardubice), B.L. Karger (Boston, MA), J.J. Kirkland (Newport, DE), E. sz. Kováts (Lausanne), K. Macek (Prague), A.J.P. Martin (Cambridge), L.W. McLaughlin (Chestnut Hill, MA), E.D. Morgan (Keele), J.D. Pearson (Kalamazoo, MI), H. Poppe (Amsterdam), F.E. Regnier (West Lafayette, IN), P.G. Righetti (Milan), P. Schoenmakers (Amsterdam), R. Schwarzenbach (Dübendorf), R.E. Shoup (West Lafayette, IN), R.P. Singhal (Wichita, KS), A.M. Siouffi (Marseille), D.J. Strydom (Boston, MA), N. Tanaka (Kyoto), S. Terabe (Hyogo), K.K. Unger (Mainz), R. Verpoorte (Leiden), Gy. Vigh (College Station, TX), J.T. Watson (East Lansing, MI), B.D. Westerlund (Uppsala)

EDITORS, BIBLIOGRAPHY SECTION

Z. Deyl (Prague), J. Janák (Brno), V. Schwarz (Prague)



ELSEVIER

Amsterdam – Lausanne – New York – Oxford – Shannon – Tokyo

J. Chromatogr. A, Vol. 684 (1994)

© 1994 ELSEVIER SCIENCE B.V. All rights reserved.

0021-9673/94/\$07.00

No part of this publication may be reproduced, stored in a retrieval system or transmitted in any form or by any means, electronic, mechanical, photocopying, recording or otherwise, without the prior written permission of the publisher, Elsevier Science B.V., Copyright and Permissions Department, P.O. Box 521, 1000 AM Amsterdam, Netherlands.

Upon acceptance of an article by the journal, the author(s) will be asked to transfer copyright of the article to the publisher. The transfer will ensure the widest possible dissemination of information.

Special regulations for readers in the USA – This journal has been registered with the Copyright Clearance Center, Inc. Consent is given for copying of articles for personal or internal use, or for the personal use of specific clients. This consent is given on the condition that the copier pays through the Center the per-copy fee stated in the code on the first page of each article for copying beyond that permitted by Sections 107 or 108 of the US Copyright Law. The appropriate fee should be forwarded with a copy of the first page of the article to the Copyright Clearance Center, Inc., 222 Rosewood Drive, Danvers, MA 01923, USA. If no code appears in an article, the author has not given broad consent to copy and permission to copy must be obtained directly from the author. The fee indicated on the first page of an article in this issue will apply retroactively to all articles published in the journal, regardless of the year of publication. This consent does not extend to other kinds of copying, such as for general distribution, resale, advertising and promotion purposes, or for creating new collective works. Special written permission must be obtained from the publisher for such copying.

No responsibility is assumed by the Publisher for any injury and/or damage to persons or property as a matter of products liability, negligence or otherwise, or from any use or operation of any methods, products, instructions or ideas contained in the materials herein. Because of rapid advances in the medical sciences, the Publisher recommends that independent verification of diagnoses and drug dosages should be made.

Although all advertising material is expected to conform to ethical (medical) standards, inclusion in this publication does not constitute a guarantee or endorsement of the quality or value of such product or of the claims made of it by its manufacturer.

Ⓢ The paper used in this publication meets the requirements of ANSI/NISO Z39.48-1992 (Permanence of Paper).

Printed in the Netherlands

New hybrid displacement technique for preparative liquid chromatography[☆]

J. Newburger^a, B. DeLange^a, G. Guiochon^{b,c,*}

^aBristol-Myers Squibb Pharmaceutical Research Institute, P.O. Box 4000, Princeton, NJ 08543-4000, USA

^bDepartment of Chemistry, University of Tennessee, 575 Buehler Hall, Knoxville, TN 37996-1600, USA

^cDivision of Analytical Chemistry, Oak Ridge National Laboratory, Oak Ridge, TN 37831-6120, USA

First received 15 May 1993; revised manuscript received 14 June 1994

Abstract

A new hybrid displacement technique (patent pending) for separating mixtures which incorporates the positive aspects of displacement chromatography and sample self-displacement, has been developed. Immediately after injection of the separation mixture, a relatively large, but finite amount of an inert material is injected onto the column to act as a “displacing compound”. The purpose of this displacing compound is to drive the separation by providing additional adsorption site competition, *thus enhancing the displacement effect*. It functions to help maintain the concentrations of the actual separation components so that tailing and/or fronting, yield limiting factors in sample self-displacement, are mitigated. The displacing compound is distinct from a true displacer because it is introduced in a limited quantity at the outset of the separation, not as a continuous additive.

Feasibility has been demonstrated and operational parameters investigated. Using a displacing compound sharpens zone boundaries between mixture components. The practical significance of this effect includes increased loading capability and the ability to achieve high yields when the major component elutes first. The impact of adding a displacing compound is greater when *the separation factors (α) between the mixture components are smaller*.

1. Introduction

The practice of preparative HPLC is undergoing dramatic changes as understanding of column overload phenomena grows. One new method, sample self-displacement [1–3], takes advantage of a displacement effect which occurs when a column is heavily loaded. When component

bands overlap in the chromatographic column, their behavior is not independent. It differs markedly from their behavior when they elute individually. For example, in the case of a binary mixture, the second component displaces the first, literally pushing the first component ahead of itself through the column. A sharp delineation between component zones results even though visual resolution is often negligible [4,5]. Modeling studies have shown very good correlation with experimental work [6–8]. Similar separations can be achieved with multi-component mixtures [9]. The practical outcome of this

* Corresponding author. Address for correspondence: Department of Chemistry, University of Tennessee, 575 Buehler Hall, Knoxville, TN 37996-1600, USA.

[☆] Patent pending, US Serial No. 868 075; filed 13 April 1992.

displacement effect is a large increase in the production rate of pure material.

Although the underlying mechanisms are similar, sample self-displacement differs significantly from conventional displacement chromatography in that an external displacing agent is not added to promote displacement. Consequently, a lengthy column re-equilibration between successive cycles is unnecessary, and separation optimization is much less involved. Unfortunately, because there is no constant forward push from a constant concentration displacer, the separation between successive bands remains incomplete. In a binary mixture, for example, as the material elutes and the concentration of the second component decreases, the competitive interaction between the two components is weakened and the first component band tails into the second. Depending on such factors as sample load, mixture ratios, relative retention, or requisite purity, the effect of this tailing on the recovery yield of both components can be negligible or substantial.

By considering and comparing the features of sample self-displacement and displacement chromatography, one solution to the yield loss problem becomes evident. In the former mode, contamination by tailing results from dilution of the mixture material as it elutes down the column. In the latter, the constant addition of an external displacing agent suppresses dilution and, consequently, tailing. In the present work, a new hybrid technique is described which incorporates some positive features of both chromatographic modes. A limited amount of an external compound is introduced onto the column at the start of a run, subsequent to the injection of the feed sample. This "displacing compound" provides competition for adsorption with the last-eluted component of the feed. In this way, it enhances the degree of competition between all component pairs of the feed, increasing the concentration of each of the component bands, and significantly reducing their tailing. Unlike working in the sample self-displacement mode, an external agent is added. However, the hybrid technique differs from displacement chromatography because the addition of the displac-

ing compound is not continuous. Instead, a single, adjustable pulse is injected. Furthermore, the composition of the mobile phase in which the column is initially equilibrated remains constant, so column regeneration is not necessary.

2. Experimental

2.1. Apparatus

Preparative experiments were carried out on a Varex (Burtonsville, MD, USA) VersaPREP preparative liquid chromatograph, equipped with a Kipp and Zonen (Delft, Netherlands) Model BD40 strip-chart recorder.

Component ratios in the regions between bands where these components interfere were determined on an analytical HPLC system consisting of a Perkin-Elmer (Norwalk, CT, USA) Series 4 liquid chromatograph, an Applied Biosystems (Foster City, CA, USA) Model 783A variable-wavelength absorbance detector, a Perkin-Elmer ISS-100 autosampler and a VG (Cheshire, UK) Multichrom data acquisition system.

2.2. Reagents

Solvents were HPLC grade, purchased from J.T. Baker (Phillipsburg, NJ, USA). Diethyl phthalate, dimethyl phthalate, dipropyl phthalate, α -tetralone, β -tetralone and benzosuberone rated 99% + purity were purchased from Aldrich (Milwaukee, WI, USA). The benzyl butyl phthalate, also from Aldrich, was 98% pure.

2.3. Preparative chromatographic conditions

The preparative column consisted of three identical 250 × 21.4 mm Dynamax 8- μ m silica columns (Rainin Instruments, Woburn, MA, USA) connected in series with a minimum length of 0.040-in. (1 in. = 2.54 cm) tubing. Prior to use, the column was washed with the following series of solvents: 1.5 l of tetrahydrofuran (THF)–hexane (30:70), 1.0 l of THF–hexane–ethyl acetate (10:75:15) and 1 l of ethyl acetate–

hexane (15:85). The column was finally washed with 4.0 l of ethyl acetate–hexane (4:96). This procedure was found to be necessary to remove any trace of silica-deactivating solvents (e.g., water) present in the shipping solvent. Failure to wash the columns as indicated resulted in a substantial reduction of the displacement effect.

For all experiments reported, the mobile phase was ethyl acetate–hexane (4:96). The flow-rate was 50 ml/min. Peaks were monitored at a wavelength of 310 nm for experiments separating the benzosuberone/ α -tetralone mixture and 290 nm for the dipropyl phthalate/benzyl butyl phthalate mixture.

2.4. Procedures

Compounds were weighed out according to the desired ratio and loadings, added to volumetric flasks, and dissolved in concentrations of 4–8 g/10 ml of 12–14% ethyl acetate in hexane. (Some extra ethyl acetate was added to improve solubility if necessary). Sample mixtures were injected onto the column by filling a 10-ml Rheodyne (Cotati, CA, USA) high-pressure valve injection loop.

The following routine was followed when making injections: (1) the flow-rate was reduced from 50 to 10.5 ml/min; (2) the 10-ml loop was loaded with the separation mixture (12 ml were flushed through to ensure thorough filling) and the injection valve ports opened to the column; (3) after 75 s, the flow was stopped; (4) the 10-ml loop was filled with displacing compound and the valve ports opened to the column; (5) the flow-rate was increased from 0 to 50 ml/min over 20 s; at the same time, the strip-chart recorder was started.

For each experiment, fraction collection began as soon as a slope change was noted in the detector signal. Fraction volumes were monitored indirectly by counting chart paper units. The fraction volumes were approximately 10 ml.

The fractions were analyzed to determine the concentration ratio of the two components, using a Waters Nova-Pak 4 μ m silica column, 150 \times 3.9 mm. In all studies, a mobile phase of ethyl acetate–hexane (4:96) was used at a flow-rate of

0.9 ml/min monitored at a wavelength of 285 nm. A standard of each component was made up fresh and injected as a single-point calibration standard for every fraction set analysis. Standard curves were run showing that absorbance was linear for the concentration ranges encountered for all compounds used in the experiments.

2.5. Calculations

Recovery yields were determined from each chromatogram by counting the number of chart paper units under the curve for each fraction. This procedure was reproducible within several percents. Because the extinction coefficients of benzosuberone and α -tetralone differ significantly, the “true” chromatographic (i.e., concentration) profile had to be derived first. The elution profiles shown in this paper for these compounds are the concentration profiles, and not the original detector response (i.e., absorbance) profiles. The elution profiles of the dipropyl phthalate and benzyl butyl phthalate mixture are the original chromatograms, not the concentration profiles. To determine the true concentration profiles of benzosuberone and α -tetralone, individual injections of 2, 2.5 and 3 g were made for these two compounds. In both cases, the peak areas increased linearly with increasing sample size, with the average area ratio of benzosuberone to α -tetralone equal to 2.16. Using this factor, the relative composition of each fraction, and the area measured under the curve for each fraction, normalized profiles were derived. From these profiles, the recovery yields were calculated as in previous studies [2,3].

3. Results and discussion

To investigate the potential of displacing compounds for yield enhancement, binary mixtures were selected for study because their behavior in the sample self-displacement mode is well-characterized [1,2]. In choosing a substance to act as a displacing compound, the following factors were considered:

(1) The relative retention of the displacing compound to the feed components should be large enough that these components did not trail significantly into it, but small enough that interaction with them on the column would occur.

(2) The displacing compound should be completely eluted in a reasonable time using the mobile phase selected for the separation.

(3) The increase in separation yield should be sufficient to offset the increase in cycle time in terms of overall production rate.

With these criteria in mind, k' was determined for a number of compounds using a 750×21.4 mm silica column and a mobile phase of ethyl acetate-hexane (4:96). Of these compounds, benzosuberone ($k' = 2.4$) and α -tetralone ($k' = 3.2$) were chosen to make the separation mixtures ($\alpha = 1.33$). Diethyl phthalate ($k' = 5.4$) was chosen to be the displacing compound.

The injection technique was developed to minimize premature elution of the mixture components prior to the addition of the displacing compound. After filling the loop with the separation mixture and triggering the injection valve, flow was continued for a period of 75 s at 10.5 ml/min to completely empty the loop. Flow was then stopped to allow time to fill the injection loop with the displacing compound. Flow was resumed at the elution flow-rate of 50 ml/min immediately after triggering the injection valve.

A possible alternative procedure, injecting the separation mixture and the displacing compound in one solution, simultaneously, was investigated. This method caused severe tailing of the benzosuberone and fronting of the diethyl phthalate with recovery considerably less than for the sample self-displacement yield.

3.1. Effect of the addition of a displacing compound on separations of benzosuberone and α -tetralone (50:50 mixtures)

Fig. 1a shows the chromatogram for a mixture injection of 2.5 g of benzosuberone and 2.5 g of α -tetralone under sample self-displacement conditions. Fig. 1b shows a separation of the same mixture when diethyl phthalate is injected as a displacing compound. Diethyl phthalate does not

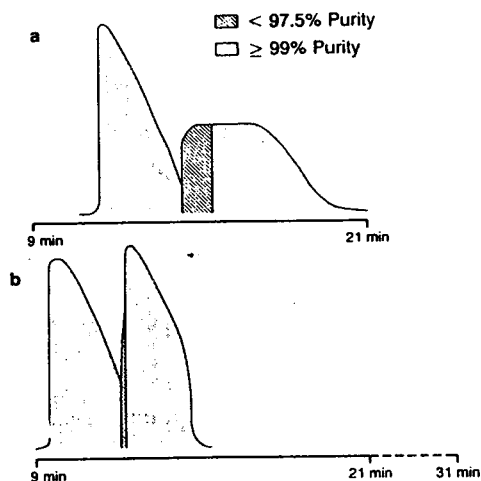


Fig. 1. Comparison of a self-displacement separation and a separation with a displacing compound added. Column: 750×21.4 mm I.D., packed with $8\text{-}\mu\text{m}$ silica particles. Mobile phase: ethyl acetate-*n*-hexane (4:96, v/v). Flow-rate: 50 ml/min. Sample: (a) 2.5 g benzosuberone (elutes first) and 2.5 g α -tetralone; (b) 2.5 g benzosuberone and 2.5 g α -tetralone with 7 g diethyl phthalate added.

absorb light at the 310 nm wavelength used for the experiment so its presence is not detected (as determined with refractive index detection, it elutes during the period from 14.5 to 31 min). When Fig. 1a is compared to Fig. 1b, peak compression is noted when a displacing compound is added. Furthermore, there is an important decrease in the amount of impure material found at the component interface. This decrease results from a reduction in tailing of the benzosuberone which occurs when using a displacing compound.

Fig. 2 is a graph which helps visualize the effect of adding a displacing compound on the mixed band interface between the two component bands. The extent of the tailing by the benzosuberone into the α -tetralone band can be expressed by plotting the percentage of benzosuberone present in α -tetralone fractions after the benzosuberone fractions cease to be 99% pure. Each point on the graph represents a collected fraction which has been analyzed to determine the mixture ratio. Points are plotted until the α -tetralone fractions attain a purity of $\geq 99.5\%$. The y-intercept is equal to 99% pure

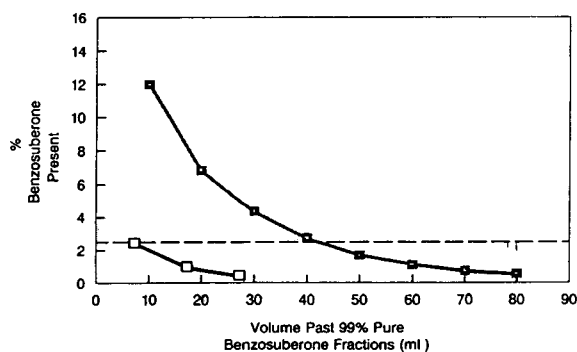


Fig. 2. Effect of the addition of a displacing compound on α -tetralone purity for a 5-g sample of benzosuberone and α -tetralone (50:50). Plot of benzosuberone concentration in collected fractions vs. the volume of solvent eluting past the last 99% pure benzosuberone fraction. Conditions as in Fig. 1. Diethyl phthalate: \blacksquare = 0 g; \square = 7 g.

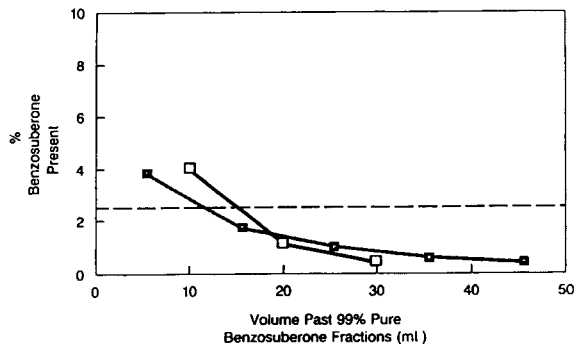


Fig. 4. Effect of the addition of a displacing compound on α -tetralone purity for a 4-g mixture of benzosuberone and α -tetralone (50:50). Plot of benzosuberone concentration in collected fractions vs. the volume of solvent eluting past the last 99% pure benzosuberone fraction. Conditions as in Fig. 1. Diethyl phthalate: \blacksquare = 0 g; \square = 7 g.

benzosuberone. When the hybrid technique is used, the boundary between peaks is sharper and the benzosuberone tailing is greatly reduced.

In sample self-displacement, as loading increases, tailing increases as well. This effect is shown in Fig. 3, a traditional loading study plot for sample self-displacement. As can be seen in Fig. 4, for the 4-g mixture of benzosuberone and α -tetralone (50:50), no significant reduction in tailing is obtained by adding a displacing com-

pound. Therefore, the sample self-displacement technique, which is less complicated and has shorter run times, is a more appropriate technique to use for this injection amount. However, as can be seen in Fig. 5, for 6 g of the 50:50 mixture, the addition of a displacing compound does cause a substantial decrease in tailing. The addition of 8 g of diethyl phthalate gives a better tailing profile than 7 g and is significantly better than adding no displacing compound at all.

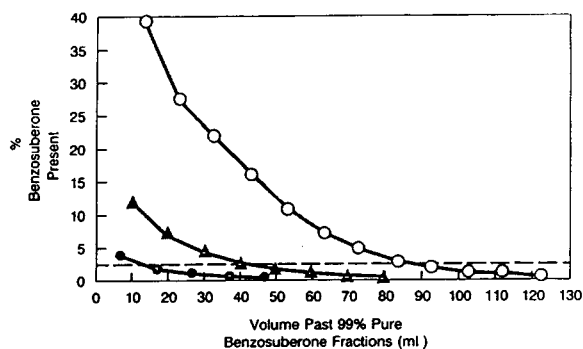


Fig. 3. Effect of loading on α -tetralone purity for a sample self-displacement separation. Plot of benzosuberone concentration in collected fractions vs. the volume of solvent eluting past the last 99% pure benzosuberone fraction. Conditions as in Fig. 1. Sample: 4- (\bullet), 5- (\blacktriangle) and 6-g (\circ) mixtures of benzosuberone and α -tetralone (50:50).

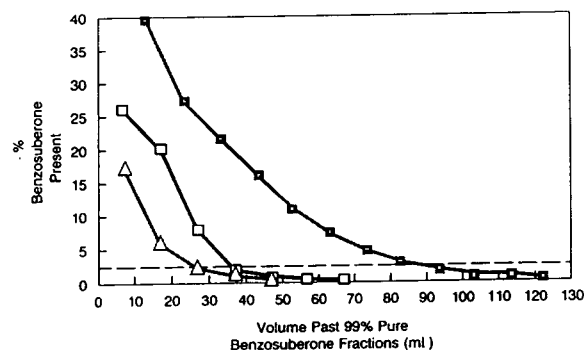


Fig. 5. Effect of the addition of a displacing compound on α -tetralone purity for a 6-g sample of benzosuberone and α -tetralone (50:50). Plot of benzosuberone concentration in the collected fractions vs. the volume of solvent eluting past the last 99% pure benzosuberone fraction. Conditions as in Fig. 1. Diethyl phthalate: \blacksquare = 0 g; \square = 7 g; \triangle = 8 g.

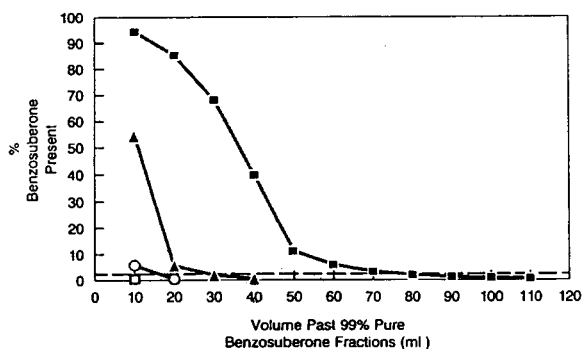


Fig. 6. Effect of the addition of a displacing compound on α -tetralone purity for a 5-g sample of benzosuberone and α -tetralone (75:25). Plot of benzosuberone concentration in collected fractions vs. the volume of solvent eluting past the last 99% pure benzosuberone fraction. Conditions as in Fig. 1. Diethyl phthalate: \blacksquare = 0 g; \blacktriangle = 5 g; \circ = 6 g; \square = 7 g.

3.2. Comparison of separations of benzosuberone and α -tetralone with and without a displacing compound added for different mixture ratios

In sample self-displacement, tailing increases with increasing ratio of the preceding to the subsequent component. In a binary mixture, for example, as the ratio of the first eluting component to the second eluting component in-

creases from 50:50 (Fig. 2) to 75:25 (Fig. 6) to 90:10 (Fig. 7) and no diethyl phthalate is added, tailing becomes greater. Furthermore, the sharp boundary between the first and second components becomes less defined at higher mixture ratios, with the second component beginning to front, i.e., trail forward, into the first band. This fronting results in contamination of the later eluting benzosuberone fractions as seen in the more gradual change in slope for the initial points plotted in Figs. 6 and 7.

When Figs. 2, 6 and 7 are compared, it can be seen that the effect of adding a displacing compound on both tailing and fronting is substantially more significant at the higher concentration ratios. Thus the derived benefit of using the new hybrid technique is even greater at higher mixture ratios.

The impact of the displacing compound on the band shape of the separation components becomes greater as the mixture ratio of preceding component(s) to subsequent component(s) increases. Comparing the 50:50 mixture (Fig. 1) and the 90:10 mixture (Fig. 8), a dramatic difference is seen when a displacing compound is used.

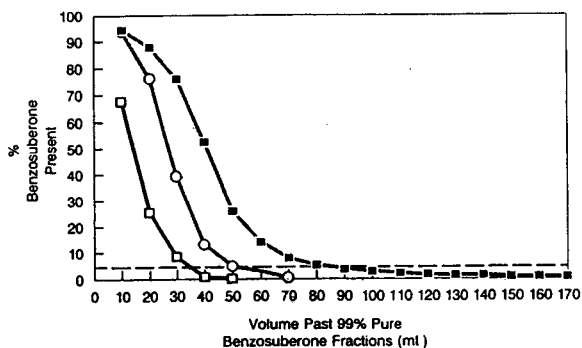


Fig. 7. Effect of the addition of a displacing compound on α -tetralone purity for a 5-g sample of benzosuberone and α -tetralone (90:10). Plot of benzosuberone concentration in the collected fractions vs. the volume of solvent eluting past the last 99% pure benzosuberone fraction. Conditions as in Fig. 1. Diethyl phthalate: \blacksquare = 0 g; \circ = 6 g; \square = 7 g.

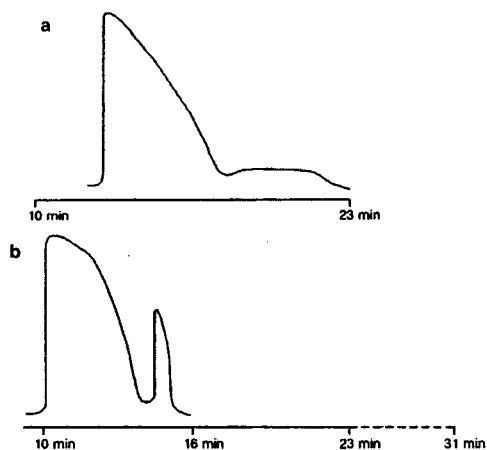


Fig. 8. Comparison of a self-displacement separation and a separation with a displacing compound added. Sample: (a) 4.5 g benzosuberone and 0.5 g α -tetralone; (b) 4.5 g benzosuberone and 0.5 g α -tetralone with 7 g diethyl phthalate added. Conditions as in Fig. 1.

3.3. Factors contributing to yield and production when displacing compounds are used

While the purification of the first component of the feed is made easier and its recovery yield is improved for a given sample size, the situation is somewhat different for the second component as it can become polluted by the displacing compound. This auxiliary to the separation must be chosen for its compatibility with the product. The yield of the second component depends on its acceptable degree of purity.

The value of the desired purity for an individual component of the feed depends on the type of separation being performed. For example, if the mixture to be separated is an end product, i.e., a material that will undergo no further chemical processes or purifications before use, a higher percentage of purity, with little or no contamination from the displacing compound, would be preferable. If, however, the recovered material is an intermediate, which will undergo further chemical processes or purifications, removal of the displacing compound may not be critical at this stage, and a lower purity would be acceptable. The determination of the acceptable or desired purity for a particular separation component can be made by the chromatographer. Further, in any separation, the percentage purity deemed acceptable may be a function of the recovery yield required.

From Figs. 5-7, it can be seen that increasing the amount of displacing compound injected leads to a narrower mixed zone at the interface between the two component bands by reduction in the first band's tailing and, when a factor, reduction in the second band's fronting as well. However, tailing and fronting are not the only factors which affect production rate and recovery yield of pure material. The potential formation of a second mixed zone, between the second component and the displacer must be taken into account.

From the plot in Fig. 7 and the chromatograms in Fig. 9 for the 90:10 mixture, we see that the displacement effect is strongest when 7 g of diethyl phthalate are added. With the 7-g addition, however, there is a greater overlap between

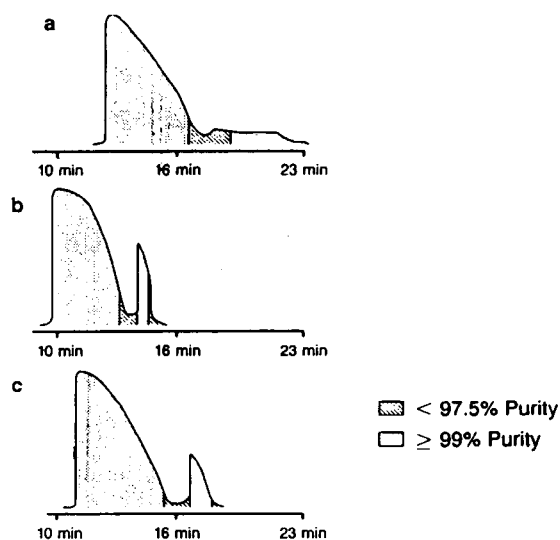


Fig. 9. Effect of the amount of displacing compound added on a 5-g sample of benzosuberone and α -tetralone (90:10). Sample: (a) No diethyl phthalate added; (b) 7 g diethyl phthalate added; (c) 6 g diethyl phthalate added. Conditions as in Fig. 1.

the diethyl phthalate and the α -tetralone than for the 6-g addition, resulting in a larger loss of material due to its contamination with the displacing compound. In both cases, using the new hybrid technique produces significantly higher yields than the sample self-displacement separation. Overall, the addition of 6 g of displacing compound gives the highest yield (Table 1). The choice of how much displacing compound to

Table 1
Influence of the amount of displacing compound on the recovery yield

Amount of diethyl phthalate (g)	Amount of α -tetralone recovered with $\leq 1\%$ of each impurity (%) ^a
0	68.7
6	95.7
7	81.7

^a Benzosuberone and diethyl phthalate (the latter detected at 285 nm).

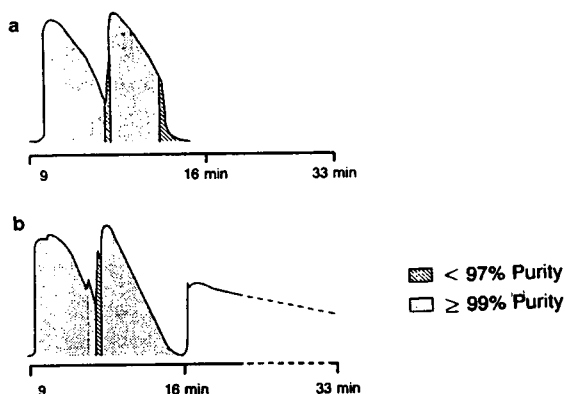


Fig. 10. Importance of the relative retention between the separation mixture and the displacing compound. Sample: (a) 2.5 g benzosuberone and 2.5 g α -tetralone with 7 g diethyl phthalate added; (b) 2.5 g benzosuberone and 2.5 g α -tetralone with 7 g β -tetralone added. Conditions as in Fig. 1.

inject is a compromise between minimizing the size of the mixed zone between the two components and minimizing the mixed zone between the last eluted component and the displacing compound. For maximum recovery of α -tetralone, 7 g of the displacing compound would be optimum when displacing compound contamination is not an issue, while 6 g would be optimum for an end product.

Yield enhancement is just one advantage gained by using the new hybrid technique. Al-

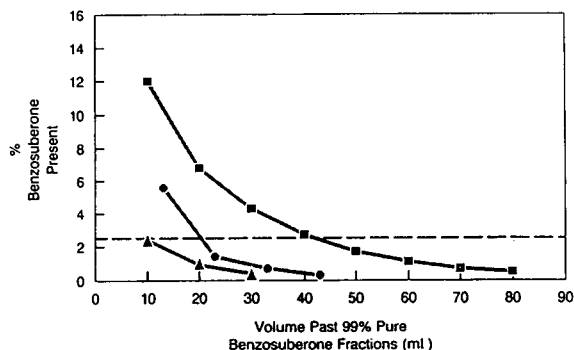


Fig. 11. Comparison of the choice of displacing compound on α -tetralone purity for a 5-g sample of benzosuberone and α -tetralone (50:50). Plot of benzosuberone concentrations in the collected fractions vs. the volume of solvent eluting past the last 99% pure benzosuberone fraction. Conditions as in Fig. 1. \blacksquare = No displacing compound; \blacktriangle = diethyl phthalate; \bullet = β -tetralone.

though the run time increases from 23 to 31 min in Figs. 1 and 8 to 10 because the displacing compound must also elute during a cycle, overall production rates can increase. Zone boundaries are sharper and less ambiguous when the displacing compound is added. Fewer fractions must be checked by analytical HPLC to determine cut points for 99% pure material. Therefore, the total time needed to both collect and process fractions for one injection is less. The production rate can also increase when the displacing compound is added because larger feed samples can be used.

As a separation methodology, the hybrid displacement technique is particularly well suited to high-volume production runs. Both injection and fractionation process are easily amenable to an automated approach and the columns do not require washing between runs, a marked advantage compared to classical displacement chromatography. Follow-up fraction checking is minimal and the displacing compound is easily recovered by solvent stripping. Correspondingly, mobile phase can be recovered and recycled since the process is isocratic. Furthermore, material production is good. For the separation pictured in Fig. 10 (with $\alpha = 1.3$), an hourly throughput of almost 10 g, with 95% recovery, is achieved using a column of only 2.5 cm in diameter. The process was found to be as robust as conventional overloaded elution.

3.4. Importance of the relative retention between the displacing compound and the separation mixture

Different compounds can act as displacing compounds for the same mixture to be separated. The deciding factor will be the relative retention between the last eluting component of the separation mixture and the displacing compound. The relative retentions between α -tetralone and diethyl phthalate and between α -tetralone and β -tetralone are 1.7 and 1.9, respectively. As can be seen in the chromatograms in Fig. 10 and the plot in Fig. 11, when β -tetralone is the displacing compound, the intensity of the displacement effect is reduced. There is more benzosuberone tailing into the α -tetralone band,

Table 2
Comparison between two displacing compounds

Displacing compound (7 g)	α Value	Amount of α -tetralone recovered with $\leq 1\%$ of each impurity ^a
Diethyl phthalate	1.7	89.7
β -Tetralone	1.9	95.0

^a Benzosuberone, diethyl phthalate or β -tetralone.

and the peaks are less compressed. Nevertheless, the α -tetralone recovery yield is slightly higher with β -tetralone, as shown in Table 2, because the displacing compound does not contaminate the α -tetralone.

When the relative retention between the last-eluting mixture component and the displacing compound is too great, there is an adverse effect on the separation. The α value for α -tetralone and dimethyl phthalate is 2.9. As can be seen in Fig. 12, using dimethyl phthalate as the displacing compound causes more tailing than when the sample self-displacement technique is used.

3.5. Effect of using a displacing compound for difficult separations

In sample self-displacement, less material per injection can be separated when the α values

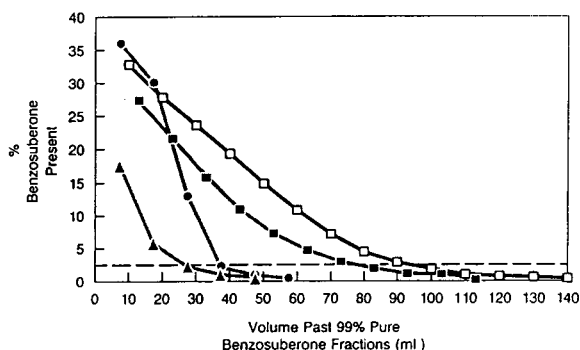


Fig. 12. Comparison of the choice of displacing compound on α -tetralone purity for a 6-g mixture of benzosuberone and α -tetralone (50:50). Plot of benzosuberone concentrations in the collected fractions vs. the volume of solvent eluting past the last 99% pure benzosuberone fraction. Conditions as in Fig. 1. \blacksquare = No displacing compound; \blacktriangle = diethyl phthalate; \bullet = β -tetralone; \blacklozenge = dimethyl phthalate.

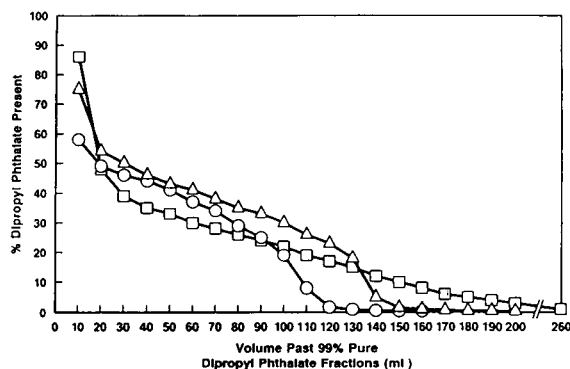


Fig. 13. Effect of the addition of a displacing compound on benzyl butyl phthalate purity for a 2-g mixture of dipropyl phthalate and benzyl butyl phthalate (50:50). Plot of dipropyl phthalate concentration in the collected fractions vs. the volume of solvent eluting past the last 99% pure dipropyl phthalate fraction. Conditions as in Fig. 1. β -Tetralone: \square = 0 g; \triangle = 4 g; \circ = 5 g.

between the separation components are small. For benzosuberone and α -tetralone, the α value is 1.33; for dipropyl phthalate and benzyl butyl phthalate, it is only 1.15. Due to considerable tailing (see Fig. 13), the amount of material collected as mixed fractions during this latter separation is much greater than for the previous separations. Pure material is recovered in a lower yield even though less is injected (2 g in Fig. 13 vs. 5 or 6 g in Figs. 2 and 5, respectively). When β -tetralone is added as a displacing compound, the recovery of benzyl butyl phthalate increases significantly as seen in Figs. 13 and 14. The effect of the β -tetralone on the tailing of the dipropyl phthalate band into the benzyl butyl phthalate fractions is substantial as can be seen in Fig. 13. Many more fractions have $>99.5\%$ purity when the displacing compound is added. The advantage to using the new hybrid technique instead of sample self-displacement is even greater when α is small.

4. Conclusions

Sample self-displacement offers significant advantages over traditional preparative elution chromatography with touching band separations. However, there is a potential for yield loss with

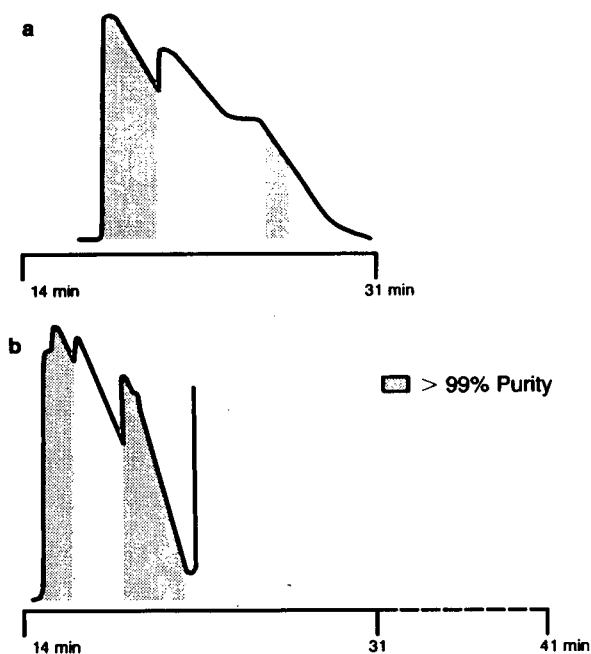


Fig. 14. Comparison of a self-displacement separation and a separation with a displacing compound added when α is small. Sample: (a) 1 g dipropyl phthalate (elutes first) and 1 g benzyl butyl phthalate; (b) 1 g dipropyl phthalate and 1 g benzyl butyl phthalate with 5 g β -tetralone added. Conditions as in Fig. 1.

this technique, depending on sample loading, mixture ratio and the difficulty of the separation. Yield loss, which results from the tailing and fronting of the component bands to form mixed zones at their interface, appears to be less a factor in displacement chromatography. However, the optimization and mechanics of working with displacers is often cumbersome. Chemists avoid it particularly for the rapid separation of batches of limited size where the cost of method development would be too large a component of the total separation cost.

The new hybrid displacement technique described, addition of a displacing compound in a discreet quantity at the outset of a separation subsequent to injection of the mixture, addresses and overcomes the limitations of both techniques. When zone boundaries between separation components are sharp, the sample self-

displacement technique is the easiest preparative method to use. However, when zone boundaries between components are diffuse, especially for the elimination of the impurities which are less retained than the main component, the addition of a displacing compound can result in a substantial reduction in tailing and fronting. The practical outcome of fewer mixed fractions is a higher loading and a greater recovery yield. Like overloaded elution and displacement chromatography, this new hybrid technique is a mode of operating chromatographic separations. As such, it is applicable independently of the retention mechanism used for the separation. Its suitability for large-scale separations depends on economical rather than technical considerations.

In order to realize the optimum benefit from a displacing compound, one must determine which displacing compound to use and how much to inject. The displacing compound which produces the sharpest boundaries between mixture components is not necessarily the best candidate. Similarly, the amount of displacing compound which provides the strongest displacement effect may not be the most appropriate injection quantity. Instead, the choice of a displacing compound and the quantity to use are related to its potential encroachment upon the feed components. The reduction in the number of mixed fractions at the separation component interfaces may be of mere academic interest if an unacceptable amount of useful material is lost through contamination with the displacing compound. The use of the purified materials and the criteria for purity are the controlling factors.

Given these considerations, the practice of this hybrid technique is relatively easy to implement. For the experiments described in this paper, the choice of the displacing compound was made based on analytical retention times. The optimized load, amount of displacing compound, and retention difference between displacing compound and components of the sample were determined with three or four exploratory injections. In all cases, the recovery yields were improved when the hybrid technique was employed. It is a viable approach, without some of the inconvenience of true displacement chroma-

tography, when yield losses from sample self-displacement separations are unacceptable.

References

- [1] J. Newburger, L. Liebes, H. Colin and G. Guiochon, *Sep. Sci. Technol.*, 22 (1987) 1933.
- [2] J. Newburger and G. Guiochon, *J. Chromatogr.*, 484 (1989) 153.
- [3] J. Newburger and G. Guiochon, *J. Chromatogr.*, 523 (1990) 63.
- [4] G. Guiochon and S. Ghodbane, *J. Phys. Chem.*, 92 (1988) 3682.
- [5] S. Golshan-Shirazi and G. Guiochon, *J. Phys. Chem.*, 93 (1989) 4143.
- [6] S. Golshan-Shirazi and G. Guiochon, *Anal. Chem.*, 60 (1988) 2364.
- [7] S. Golshan-Shirazi and G. Guiochon, *Anal. Chem.*, 61 (1989) 1368.
- [8] A.M. Katti, M. Czok and G. Guiochon, *J. Chromatogr.*, 556 (1991) 205.
- [9] J. Newburger, S. Taylor and G. Guiochon, presented at the *7th International Symposium on Preparative Liquid Chromatography, Ghent, April 1990*.

N-Alkylcarbamoyl derivatives of amino acids as chiral stationary phases for high-performance liquid chromatography I. An example of enhancing enantioselectivity by deleting the non-enantioselective π – π interaction site on the chiral stationary phase

Jer-Yann Lin^{a,*}, Mei-Hui Yang^b

^aDepartment of Mathematics and Science Education, National Tainan Teachers College, Tainan, Taiwan

^bDepartment of Chemistry, National Taiwan University, Taipei, Taiwan

First received 14 April 1994; revised manuscript received 14 June 1994

Abstract

The role of the π – π interaction provided by the benzyl group of N-benzylcarbamoyl-derived chiral stationary phases (CSPs) was studied. Based on deleting the non-enantioselective π – π interaction site on an N-benzylcarbamoyl-(*S*)-phenylglycine-derived CSP, a series of seven CSPs were prepared by bonding N-alkylcarbamoyl derivatives of (*S*)-phenylglycine or (*S*)-phenylalanine either ionically or covalently on 3-aminopropyltriethoxysilane-modified silica gel. The chromatographic behaviour on the CSPs with regard to the resolution of dinitrobenzamide or dinitrobenzanilide derivatives of enantiomeric amino acids, amino alcohols, amines and carboxylic acid was studied. The best chromatographic results were found on ionic-type CSPs containing N-*n*-stearylcarbamoyl-(*S*)-phenylglycine or N-cyclohexylcarbamoyl-(*S*)-phenylglycine. It was also found that the chiral recognition abilities of all of the four ionic-type N-alkylcarbamoyl-(*S*)-phenylglycine CSPs were better than that of the ionic-type CSP containing N-benzylcarbamoyl-(*S*)-phenylglycine for the discrimination of the same enantiomeric analytes. The results clearly confirm that enhancement of enantioselectivity is achieved by deleting the non-enantioselective π – π interaction site on the N-benzylcarbamoyl-(*S*)-phenylglycine-derived CSP.

1. Introduction

The study of the chiral recognition mechanism is important in that it not only affords insight into which chiral stationary phase (CSP) should be used for the effective resolution of a given analyte but also aids in the design of CSPs with enhanced enantioselectivity. Among the hun-

dreds of chiral stationary phases, the chiral recognition mechanisms on π donor–acceptor phases have been studied intensively and reviewed [1]. It was proposed that the separation of enantiomers on these CSPs is dependent on the formation of diastereomeric complexes with different free energies between the CSP and the enantiomeric analyte. The formation of these complexes requires enantioselective interactions (chiral interactions), which are formed by an

* Corresponding author.

appropriate combination of suitably located functionalities on the CSP with complementary sites on the analyte. The enantioselective interactions are essential in recognizing the enantiomers, while non-enantioselective interactions are the interactions in excess of those required for chiral recognition. Däppen *et al.* [2] demonstrated that the retention of an analyte on a CSP can be described as the sum of non-chiral and chiral interactions. The enantioselective interactions are important in distinguishing the enantiomeric analyte and can affect the elution order of enantiomers.

However, the non-enantioselective interactions may also influence the magnitude of enantioselectivity of the chiral resolution by increasing retention. For example, the residual silanol groups on the underlying silica support often influence the enantioselectivity of the chiral resolution by the non-chiral interaction [3–6]. The chromatographic results on a tandem array of chiral and achiral columns also showed that a decrease in the magnitude of the enantioselectivity was observed owing to adsorption stemming from sites on the achiral packing [7]. Thus, the concept suggested by Pirkle and Welch [8] that the design of a CSP with enhanced enantioselectivity may be achieved by deleting the non-productive interaction sites on the original CSPs is reasonable.

Owing to the conformational rigidity and polar nature of the urea functionality, many CSPs contain a urea linkage as their connection arm to silica gel [9–14]. In a previous study, the chiral recognition behaviour for the resolution of dinitrobenzamide or dinitroanilide derivatives of enantiomeric amino acids, amino alcohols, amines and carboxylic acid on N-arylcarbamoyl-derived CSPs containing either one or two chiral centres was studied [9]. Various magnitudes of enantioselectivities were observed, and in some instances CSPs containing two chiral centres provided better resolution than a commercially available CSP [Supelcosil LC-(R)-urea]. The chiral resolution on the N-benzylcarbamoyl-(*S*)-phenylglycine CSP (CSPA; Fig. 1) was found to be the best among the series of N-arylcarbamoyl-derived CSPs containing one chiral centre. It

showed that the phenylglycine moiety of CSPA provides the enantioselective π - π interaction that is important in chiral resolution and dominates the elution order of enantiomeric analytes. However, the role of the π - π interaction provided by the N-benzylcarbamoyl moiety has not been reported.

This study was focused on the influence of the π - π interaction provided by the benzyl group of CSPA (Fig. 1). A series of seven CSPs containing N-alkylcarbamoyl derivatives of (*S*)-phenylglycine and (*S*)-phenylalanine were prepared. The chromatographic results of this study show that the benzyl group of CSPA provides a non-enantioselective π - π interaction and that the CSPs designed by deleting the non-enantioselective π - π interaction site have a more effective recognition ability than the original CSPA.

2. Experimental

2.1. Chemicals

The silica gel (Nucleosil; pore size 100 Å, particle size 10 μ m, surface area 350 m²/g), was obtained from Macherey-Nagel. 3-Aminopropyltriethoxysilane (APS) was purchased from Chisso. The analytes used in the chromatographic experiments were of synthetic reagent grade (Merck). The N-alkylcarbamoyl derivatives of amino acids were obtained by the method described previously [9].

2.2. Preparation of APS-modified silica gel

The procedure for the preparation of APS-modified silica gel was the same as reported previously [9]. The results of elemental analysis are given in Table 1.

2.3. Preparation of ionic-type CSPs

To a solution of 0.01 mol of an N-alkylcarbamoyl derivative of an L-amino acid in 100 ml of tetrahydrofuran (THF), 2.5 g of APS-modified silica gel were added. The mixture was

$$\left[\text{O}-\text{Si}(\text{CH}_2\text{CH}_2\text{CH}_2-\text{Z}-\overset{\text{(S)}}{\underset{\text{R}^2}{\text{C}}}\text{NH}\overset{\text{O}}{\parallel}\text{CNH}-\text{R}^1) \right]_n$$

CSP	-R ¹	-R ²	-Z-
CSPA	-CH ₂ ⊙	⊙	-NH ₃ ⁺ -OOC-
CSPB	⊙	-CH(CH ₃) ₂	-NH ₃ ⁺ -OOC-
CSP1	-CH ₂ ⊙	-CH(CH ₃) ₂	-NH ₃ ⁺ -OOC-
CSP2	⊙	-CH ₂ ⊙	-NH ₃ ⁺ -OOC-
CSP3	⊙	⊙	-NH ₃ ⁺ -OOC-
CSP4	-CH ₂ CH ₂ CH ₃	⊙	-NH ₃ ⁺ -OOC-
CSP5	-CH(CH ₃) ₂	⊙	-NH ₃ ⁺ -OOC-
CSP6	-CH ₂ (CH ₂) ₁₆ CH ₃	⊙	-NH ₃ ⁺ -OOC-
CSP7	-CH ₂ CH ₂ CH ₃	⊙	-NHCO-
CSP8	-CH(CH ₃) ₂	⊙	-NHCO-

Fig. 1. Structures of chiral stationary phases.

subjected to ultrasonic vibration for 10 min followed by stirring for 4 h. The product was filtered, washed with THF and dried under vacuum overnight.

2.4. Preparation of covalent-type CSPs

A solution of 0.01 mol of an N-alkylcarbamoyl derivative of an L-amino acid in 100 ml of

Table 1
Characteristics of the 3-aminopropylsilica and the CSPs

Sample	Elemental analysis (%)			Loading capacity ^a	
	C	H	N	mmol/g	groups/nm ²
3-Aminopropylsilica	3.71	1.06	1.27	0.91	1.59
CSPA ^b	11.29	1.82	2.35	0.39	0.67
CSPB ^b	11.12	1.80	2.58	0.47	0.81
CSP1	11.67	1.92	2.41	0.41	0.71
CSP2	12.25	1.62	2.33	0.38	0.65
CSP3	11.63	1.57	2.31	0.37	0.64
CSP4	10.68	1.77	2.36	0.39	0.67
CSP5	10.65	1.37	2.34	0.38	0.65
CSP6	19.26	1.99	2.28	0.36	0.62
CSP7	10.60	1.52	2.38	0.40	0.69
CSP8	10.64	1.27	2.34	0.38	0.65

^a Based on the percentage of nitrogen.

^b The results have been published in a previous paper [9].

dimethylformamide was cooled in an ice-bath. Next, 0.01 mol of N-hydroxysuccinimide and 0.01 mol of dicyclohexylcarbodiimide (DCC) were added to the above solution at 0°C and the mixture was stirred at room temperature for 24 h. After removal of the suspended solid dicyclohexylurea, 2.5 g of APS-modified silica gel were added and stirred for 48 h. After filtration, the product was suspended in 100 ml of toluene and end-capped by reaction with trimethylchlorosilane at 40°C for 4 h. The final product was filtered and washed with methanol, water and acetone and then dried under vacuum overnight.

The results of elemental analyses of all the CSPs prepared are given in Table 1.

2.5. Chromatographic studies

The chromatographic studies were carried out with a liquid chromatographic system consisting of an Alphatech solvent-delivery system and an Applied Biosystems Model 757 variable-wavelength UV detector. The recorder used was a Model 21 SIC Chromatocorder. Stainless-steel columns (300 mm × 4 mm I.D.) were packed by the balanced-density slurry method using an Econo-packing pump (Inpac International) at 400 kg/cm². Mixtures of *n*-hexane and 2-propanol (90:10–99:1, v/v) were used as the mobile phase, which was filtered through a 0.45- μ m membrane filter and degassed by ultrasonic vibration prior to use. The flow-rate was 1.0 ml/min. The detector was operated at 254 nm. Experiments were carried out at 25°C. Analytes were dissolved in methanol and suitable amounts of the solutions were injected. Chromatographic peaks were assigned by injecting the corresponding derivative of enantiomeric enriched analyte.

3. Results and discussion

Fig. 1. shows the structures of the ten chiral stationary phases (CSPs) studied. The preparation and enantioselectivities of CSPA and CSPB have been reported previously [9]. Seven N-

alkylcarbamoyl-derived CSPs and CSP1 were successfully prepared by bonding chiral entities either ionically or covalently to APS-modified silica gel, as shown in Fig. 2. In order to compare the enantioselectivities of the N-alkylcarbamoyl-derived CSPs with that of CSPA, the preparation and the packing of all these CSPs were carried out under identical conditions. The support of CSPA was 10- μ m silica gel, so the same silica gel was used as the support of the other CSPs in this study, even though the small particle size of silica gel often increases the efficiency of chiral resolution. According to the results of elemental analyses (Table 1), the surface coverages of chiral ligands on these CSPs were found to range from 0.36 to 0.47 mmol/g (0.62–0.81 groups/nm²).

The chiral recognition abilities of the amide derivatives of amino acids, amino alcohols, amines and carboxylic acid on these CSPs were examined, and the results are summarized in Tables 2 and 3. Typical chromatograms are shown in Figs. 3 and 4. According to the separation factors (α), nearly all of the seven N-alkylcarbamoyl-derived CSPs, except CSP2, provide sufficient resolution for the analytes chosen in this study. In general, the ionic-type CSPs were found to be more effective than the corresponding covalent-type CSPs for the separation of the enantiomeric analytes. The better results observed on the ionic-type CSP may be ascribed to the stronger chiral interaction provided by the ionic bond of the ionic-type CSP.

3.1. Non-enantioselective nature of the π - π interaction provided by the *N*-benzylcarbamoyl moiety of CSPs

Although CSPA, CSPB and CSP1 contain a urea linkage, CSPA is derived from (*S*)-phenylglycine, whereas CSPB and CSP1 are derived from (*S*)-valine (Fig. 1). Further, CSPA and CSP1 contain an N-benzylcarbamoyl moiety, whereas CSPB contains an N-phenylcarbamoyl moiety. Hence two phenyl groups are present in CSPA and only one in CSPB and CSP1. Different chiral resolutions were observed on these CSPs (Table 2). CSPB provides chiral recogni-

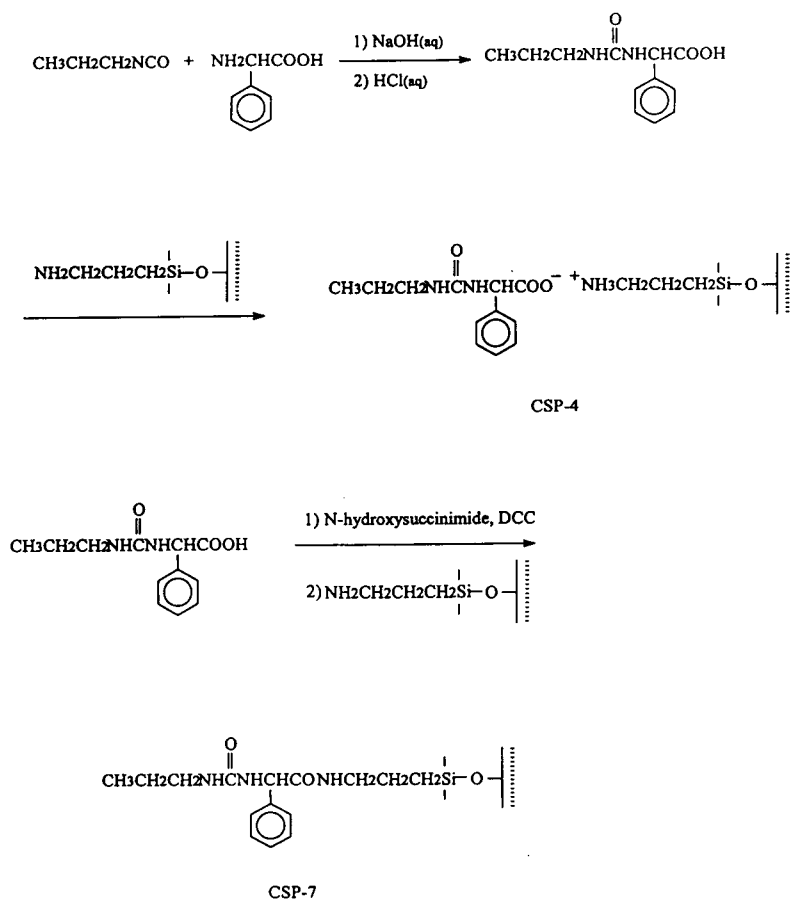


Fig. 2. Examples of the preparation of N-alkylcarbamoyl-derived chiral stationary phases.

tion ability for the separation of the DNB derivatives of amino acids, amino alcohols and diamine enantiomers. CSPA, having a better resolution ability than CSPB, could resolve all of the DNB derivatives of the chosen enantiomers. As expected, no significant chiral resolution was observed on CSP1. It is worth noting that opposite elution orders were observed on CSPA and CSPB. The *R*-enantiomer was first eluted on CSPB, whereas the *S*-enantiomer was eluted first on CSPA. The opposite elution order suggests that the π - π interactions provided by the phenylcarbamoyl and phenylglycine dominate two different chiral recognition models. The results observed on CSP1 infer that the *N*-benzylcarbamoyl moiety provides only a non-enantioselective π - π interaction.

3.2. Chromatographic behaviour of the *N*-alkylcarbamoyl-derived CSPs

Two amino acids, (*S*)-phenylglycine and (*S*)-phenylalanine, were used as chiral entities of the *N*-alkylcarbamoyl-derived CSPs in this study. As shown in Fig. 1, the structures of CSP2 and CSP3 are identical except that CSP3 contains (*S*)-phenylglycine and CSP2 contains (*S*)-phenylalanine. In a previous study [9], the benzyl group of phenylalanine was characterized as a non-enantioselective π - π interaction site and the phenyl group of phenylglycine as an enantioselective π - π interaction site. Comparing the chromatographic results on CSP2 with those on CSP3 for the separation of a series of twelve enantiomeric analytes under identical

Table 2
Resolution of derivatized enantiomers on CSPA, CAPB and CSP1

Analyte	CSPA			CSPB			CSP1		
	k'_1	α	M	k'_1	α	M	k'_1	α	M
<i>Amino acids</i> ^a									
Valine	3.23(S)	1.67	A	1.92(R)	1.18	A	2.49	1	A
Alanine	6.91(S)	1.18	A	3.50(R)	1.26	A	4.78	1	A
Leucine	3.60(S)	1.58	A	1.81(R)	1.26	A	2.92	1	A
Methionine	5.87(S)	1.30	A	6.54(R)	1.31	A	8.61	1	A
Phenylalanine	7.03(S)	1.39	A	3.07(R)	1.18	A	3.71	1	A
<i>Amino alcohols</i> ^b									
2-Aminobutanol	7.85(S)	1.41	A	4.30(R)	1.17	A	5.03	1	A
2-Aminopropanol	11.74(S)	1.24	A	7.26(R)	1.11	A	8.17	1	A
Norephedrine	9.63	1.02	A	5.12	1.12	A	6.04	1	A
<i>Amines</i> ^b									
Phenylethylamine	8.60(R)	1.09	A	4.35	1	C	5.52	1	C
1-Methylbutylamine	4.46	1.18	A	2.68	1	C	3.48	1	C
1,2-Diaminopropane	42.41	1.09	A	12.96	1.19	A	13.11	1	A
<i>Carboxylic acid</i> ^c									
Ibuprofen	6.82(S)	1.16	A	13.02	1	B	14.23	1	B

k'_1 is the capacity factor of the first-eluted enantiomer; k'_1 (R/S) indicates the absolute configuration of the first-eluted enantiomer. The separation factor (α) is the ratio of the capacity factors of the enantiomers. Mobile phase (M): A-*n*-hexane–2-propanol (90:10); B-*n*-hexane–2-propanol (97:3); C-*n*-hexane–2-propanol (99:1). Chromatographic results for CSPA and CSPB are from Ref. [9].

^a As N-dinitrobenzamide-O-methyl ester derivatives.

^b As N-dinitrobenzamide derivatives.

^c As dinitroanilide derivative.

chromatographic conditions, it was found that there was no significant resolution on CSP2 for any chosen analytes, whereas good resolution was observed on CSP3. This illustrates that the enantioselective π - π interaction provided by phenylglycine is necessary for enantiomer separation in the N-alkylcarbamoyl-derived CSPs.

Four different N-alkylcarbamoyl moieties, N-*n*-propyl-, N-isopropyl-, N-*n*-stearyl-, and N-cyclohexylcarbamoyl, were used as the terminus of the brush of CSPs. In order to investigate the influence of the N-alkylcarbamoyl moiety of CSPs on the chiral recognition, chromatographic results for the resolution of twelve enantiomeric analytes on these CSPs (CSP3–8) were compared (Table 3). In most instances, the enantioselectivities of these CSPs decrease with the order of the N-alkyl terminal groups N-*n*-stearyl,

N-cyclohexyl > N-isopropyl > N-*n*-propyl, according to the separation factors of the chosen enantiomeric analytes. It is also worth noting that the retention of a given analyte on the ionic-type CSP6 is shorter than those on any other ionic-type CSPs (CSP3–5) according to the capacity factors of the more retained enantiomers. The shorter retention and higher separation factors on CSP6 can be illustrated by the non-polar character of the *n*-stearyl group in a normal-phase separation.

3.3. Influence of the non-enantioselective π - π interaction

As shown in Fig. 1, both CSPA and CSP3-6 contain phenylglycine as a chiral entity. However, CSPA bears an additional benzyl group

Table 3
Resolution of derivatized enantiomers on CSP2–8

Analyte	CSP2		CSP3		CSP4		CSP5		CSP6		CSP7		CSP8	
	k'_1	α	k'_1	α	k'_1	α	k'_1	α	k'_1	α	k'_1	α	k'_1	α
<i>Amino acids</i> ^a														
Valine	2.79	1	2.14(S)	1.72	2.08(S)	1.69	2.02(S)	1.71	1.58(S)	1.77	2.88(S)	1.16	3.34(S)	1.29
Alanine	4.42	1	4.30(S)	1.18	4.31(S)	1.19	4.27(S)	1.19	3.67(S)	1.20	5.35(S)	1.06	5.19(S)	1.14
Leucine	2.58	1	2.37(S)	1.90	2.20(S)	1.76	2.19(S)	1.76	1.66(S)	1.93	3.02(S)	1.21	3.41(S)	1.31
Methionine	5.47	1	5.20(S)	1.57	5.39(S)	1.47	5.28(S)	1.47	4.29(S)	1.53	4.98(S)	1.13	7.40(S)	1.22
Phenylalanine	3.58	1	3.97(S)	1.70	3.91(S)	1.56	3.90(S)	1.57	3.15(S)	1.68	5.10(S)	1.15	7.14(S)	1.25
<i>Amino alcohols</i> ^b														
2-Aminobutanol	5.89	1	6.62(S)	1.43	5.81(S)	1.42	7.20(S)	1.42	5.73(S)	1.55	6.46(S)	1.10	6.22(S)	1.19
2-Aminopropanol	8.82	1	8.68(S)	1.26	9.58(S)	1.25	10.64(S)	1.25	8.38(S)	1.33	8.80(S)	1.06	9.00(S)	1.14
Norephedrine	8.01	1	9.05	1.04	8.59	1.03	8.73	1.05	7.85	1.06	7.99	1	7.32	1
<i>Amines</i> ^b														
Phenylethylamine	6.43	1	7.10	1.24	5.62(R)	1.18	5.35(R)	1.18	4.56(R)	1.25	5.89(R)	1.01	6.69	1
1-Methylbutylamine	3.71	1	3.90	1.28	3.24	1.24	3.07	1.24	2.27	1.28	3.19	1.04	3.70	1
1,2-Diaminopropane	28.22	1	26.92	1.11	24.50	1.10	24.34	1.10	23.77	1.22	21.48	1	21.53	1
<i>Carboxylic acid</i> ^c														
Ibuprofen	5.98	1	5.45(S)	1.17	5.56(S)	1.17	5.55(S)	1.17	4.34(S)	1.18	4.57	1	4.95	1

k'_1 is the capacity factor of the first-eluted enantiomer; k'_1 (R/S) indicates the absolute configuration of the first-eluted enantiomer. The separation factor (α) is the ratio of the capacity factors of enantiomers. Mobile phase: 2-propanol–*n*-hexane (10:90).

^a As N-dinitrobenzamide-O-methyl ester derivatives.

^b As N-dinitrobenzamide derivatives.

^c As dinitroamide derivative.

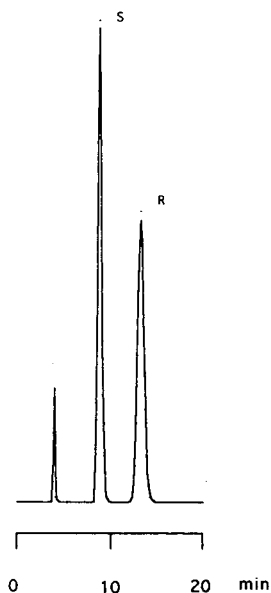


Fig. 3. Chromatogram for the resolution of N-dinitrobenzoyl-D,L-leucine-O-methyl ester on CSP6. Mobile phase, *n*-hexane–2-propanol (90:10); flow-rate, 1 ml/min.

which was characterized as a non-enantioselective π – π interaction. Comparing the chiral resolution results on CSPA with those on CSP3–6,

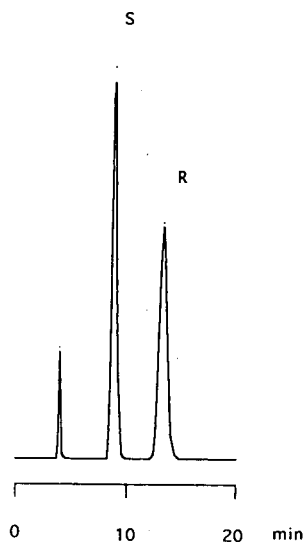


Fig. 4. Chromatogram for the resolution of N-dinitrobenzoyl-D,L-valine-O-methyl ester on CSP3. Mobile phase, *n*-hexane–2-propanol (90:10); flow-rate, 1 ml/min.

the capacity factor of a given analyte on CSPA is larger than any of those on CSP3–6 under the same chromatographic conditions. For example, the capacity factor of (*R*)-phenylalanine is 9.77 on CSPA, whereas that on CSP6 is only 5.29. Further, the separation factor of a given racemic analyte on CSPA was smaller than any of those on CSP3–6 under the same chromatographic conditions. For example, the separation factor of D,L-leucine on CSP6 is 1.93 whereas it is only 1.58 on CSPA.

Because the silica supports are the same and the surface coverages are similar for CSPA and CSP3–6, the differences in the chromatographic results between CSPA and CSP3–6 may be ascribed to the additional non-enantioselective π – π interaction provided by the benzyl group of CSPA. The longer retentions and smaller separation factors on CSPA can be illustrated by the non-enantioselective π – π interaction. In other words, the enantioselectivity is enhanced by deleting this non-enantioselective π – π interaction site on CSPA.

4. Conclusions

Based on deleting the non-enantioselective π – π interaction site on the N-benzylcarbamoyl-(*S*)-phenylglycine, a series of seven chiral stationary phases containing N-alkylcarbamoyl-(*S*)-phenylglycine were prepared. It is found that (*S*)-phenylglycine is better than (*S*)-phenylalanine for acting as a chiral entity of the series of N-alkylcarbamoyl-driven CSPs. The best chromatographic results on the series of seven CSPs were found on the ionic-type N-*n*-stearylcarbamoyl-(*S*)-phenylglycine- and N-cyclohexylcarbamoyl-(*S*)-phenylglycine-derived CSPs. The chiral recognition abilities on all of the ionic-type CSPs derived from N-alkylcarbamoyl-(*S*)-phenylglycine are better than that on the ionic-type N-benzylcarbamoyl-(*S*)-phenylglycine CSP for the discrimination of the same enantiomers. The results clearly show that the enantioselectivity is enhanced by deleting the non-enantioselective π – π interaction site on the N-benzylcarbamoyl-(*S*)-phenylglycine CSP.

Acknowledgement

Financial support from the National Science Council (Taiwan) is gratefully acknowledged.

References

- [1] W.H. Pirkle and T.C. Pochapsky, *Chem. Rev.*, 89 (1989) 347.
- [2] R. Däppen, V.R. Meyer and H. Arm, *J. Chromatogr.*, 464 (1989) 39.
- [3] W.H. Pirkle and R.S. Readnour, *Chromatographia*, 31 (1991) 129.
- [4] H. Engelhardt, H. Low, W. Eberhardt and N. Nauss, *Chromatographia*, 27 (1989) 535.
- [5] Y. Dobashi and S. Hara, *J. Org. Chem.*, 52 (1987) 2490.
- [6] R. Brugger and H. Arm, *J. Chromatogr.*, 592 (1992) 309.
- [7] W.H. Pirkle and J.L. Schreiner, *J. Org. Chem.*, 46 (1981) 4988.
- [8] W.H. Pirkle and C.J. Welch, *J. Chromatogr.*, 589 (1992) 45.
- [9] M.H. Yang and J.Y. Lin, *J. Chromatogr.*, 631 (1993) 165.
- [10] N. Oi, H. Kitahara and R. Kira, *J. Chromatogr.*, 535 (1990) 213.
- [11] N. Oi, H. Kitahara and R. Kira, *J. Chromatogr.*, 515 (1990) 441.
- [12] N. Oi and H. Kitahara, *J. Chromatogr.*, 285 (1984) 198.
- [13] N. Oi and H. Kitahara, *Bunseki Kagaku*, 33 (1984) 386.
- [14] W.H. Pirkle and M.H. Hyun, *J. Chromatogr.*, 322 (1985) 295.



ELSEVIER

Journal of Chromatography A, 684 (1994) 23–27

JOURNAL OF
CHROMATOGRAPHY A

Chiral ion-pair chromatographic separation of two dihydropyridines with camphorsulfonic acids on porous graphitic carbon

Martin Josefsson*, Björn Carlsson, Björn Norlander

Department of Clinical Pharmacology, Faculty of Health Sciences, Linköping University, S-581 85 Linköping, Sweden

First received 14 March 1994; revised manuscript received 13 June 1994

Abstract

The direct enantiomeric separation of the two racemic dihydropyridines amlodipine (AML) and UK52.829 (UK) with (1*S*)-(+)10-camphorsulfonic acid [(+)-CSA] as a chiral counter-ion, on porous graphitic carbon Hypercarb-S, is described. The enantiomers of AML and UK were separated in a mobile phase system consisting of 5 mM (+)-CSA in dichloromethane–methanol (25:75, v/v). When the enantiomeric separation of AML and UK was studied in a mobile phase system consisting of 5 mM (1*S*)-(+)3-bromo-10-camphorsulfonic acid [Br-(+)-CSA] in dichloromethane–methanol (25:75, v/v) the capacity factor, k' , was markedly increased while the separation factor, α , was slightly decreased compared to the mobile phase with (+)-CSA as chiral counter-ion. No enantiomeric separation of AML or UK was seen in a chromatographic system with acetonitrile substituted for methanol as mobile phase solvent, neither with (+)-CSA nor Br-(+)-CSA as chiral counter-ion.

1. Introduction

Recently a number of methods for chromatographic resolution of drug enantiomers have been developed. One of the main reasons is the increasing interest in finding robust systems for evaluation of differences and similarities in pharmacodynamics and pharmacokinetics of the enantiomers [1].

In high-performance liquid chromatography (HPLC) there are several possibilities for enantiomeric separation on conventional non-chiral columns. Enantiomers can be separated indirectly as diastereomeric derivatives generated by derivatization with a homochiral reagent, or

directly by using a chiral additive in the mobile phase (e.g., cyclodextrin, crown ether, metal complex) that promotes enantiomeric separation [2]. Furthermore, a chiral counter-ion dissolved in the mobile phase can be used to separate enantiomers of acids and amines [3]. The enantiomers of some β -amino alcohols, for instance, have been separated with (+)-10-camphorsulfonate as chiral counter-ion in a normal-phase chromatographic system on a LiChrosorb-DIOL column [4].

Porous graphitic carbon (PGC) is a non-polar chromatographic adsorbent that allows special stereoselectivity. It has been considered a "pure" reversed-phase adsorbent with an extremely uniform surface [5,6]. The PGC Hypercarb-S has successfully been used in resolu-

* Corresponding author.

tion of enantiomeric amines as diastereomeric ion pairs with N-carbobenzyloxyglycyl-L-proline (L-ZPG) or (–)-2,3:4,6-di-O-isopropylidene-2-keto-L-gulonic acid [(–)-DIKGA] as chiral counter-ion [7,8]. The enantiomers of acids like 10-camphorsulfonic acid (CSA) and N-carbobenzyloxyglycylproline (ZPG), have been separated with quinine as chiral counter-ion [8].

In a previous paper we showed a fast chromatographic separation of the (–)-menthyl chloroformate derivatives of some drug enantiomers (e.g., dihydropyridines, β -amino alcohols) [9]. In this paper we have further investigated chiral separations on PGC, of the dihydropyridines amlodipine (AML), UK52.829 (UK) and felodipine (FEL) with (1*S*)-(+)-10-camphorsulfonic acid [(+)-CSA] or (1*S*)-(+)-3-bromo-10-camphorsulfonic acid [Br-(+)-CSA] as counter-ion.

2. Experimental

2.1. Chemicals

Acetonitrile (far UV), dichloromethane and methanol, all HPLC grade, were purchased from LabScan Analytical Sciences (Dublin, Ireland).

Racemic AML and UK, and *R*-(+)-amlodipine were obtained from Pfizer (New York,

USA) and racemic FEL from Astra Hässle (Mölndal, Sweden). (+)-CSA was purchased from Merck (Darmstadt, Germany) and Br-(+)-CSA from Fluka (Buchs, Switzerland). The structures of the chiral substances are shown in Fig. 1.

2.2. Instrumentation

The HPLC system consisted of a Varian 2510 pump (Walnut Creek, CA, USA) a Waters 486 UV detector (Milford, MA, USA), a Spectra-Physics 4270 integrator (San Jose, CA, USA), a Jones Chromatography column heater (Hengoed, Mid Glamorgan, UK) a Rheodyne 7125 injector with a 20- μ l loop and a Rheodyne 0.5- μ m column inlet filter (Cotati, CA, USA).

Chromatography was carried out on a PGC Hypercarb-S column, 100 \times 4.6 mm I.D. (Shandon, Runcorn, England), with well degassed HPLC-grade solvents. The PGC column was thermostated to 30°C and the mobile phase was recirculated for at least 12 h before use. In studies with only minor variations in temperature or counter-ion concentration the mobile phase was recirculated for at least 2 h before use. Mobile phase flow-rate was 1.5 ml/min. Samples containing 2 μ g of the free drug were manually injected into a 20- μ l loop. The ion pairs were all detected at 250 nm and the elution order of the enantiomers of amlodipine was determined with

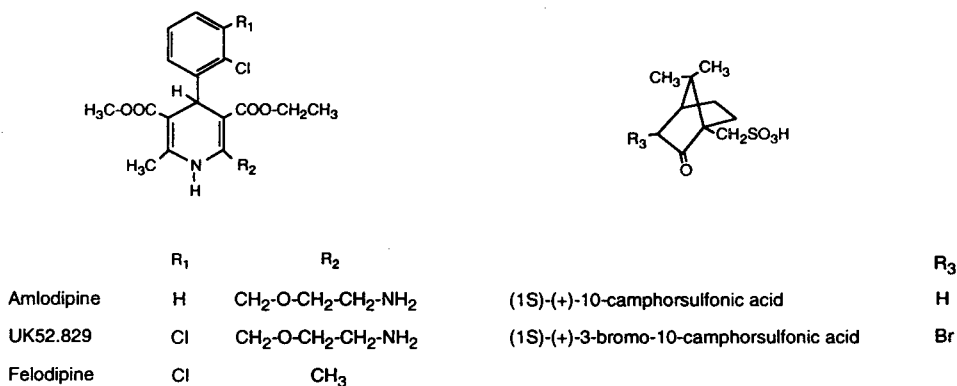


Fig. 1. Molecular structures.

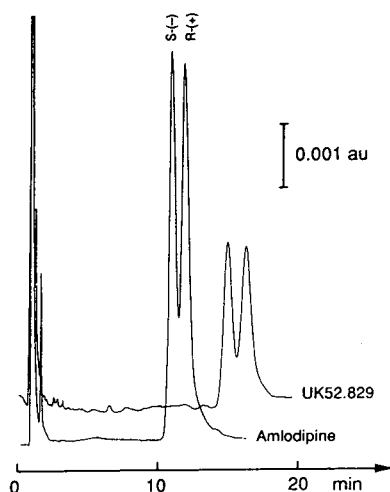


Fig. 2. Separation of racemic amlodipine and UK52.829 on Hypercarb-S. Column temperature: 30°C. Mobile phase: 5 mM (1S)-(+)-10-camphorsulfonic acid in dichloromethane-methanol (25:75, v/v). Flow-rate: 1.5 ml/min.

help of the enantiomerically pure *R*-(+)-amlodipine.

2.3. Solutions

Stock solutions of racemic AML, UK and FEL (1 mg/ml) were prepared with 10 mg of the free

base in 10 ml methanol. Working solutions (0.1 $\mu\text{g}/\mu\text{l}$) for all the dihydropyridines were prepared in methanol and acetonitrile.

3. Results and discussion

Enantiomeric separation of the two dihydropyridines AML and UK was achieved in a mobile phase system consisted of 5 mM (+)-CSA in dichloromethane-methanol (25:75, v/v) (Fig. 2). The capacity factor, k' , and the separation factor, α , of the chiral ion-pairs are presented in Table 1.

The dihydropyridine structure does not act as either a proton acceptor or a proton donor, and dihydropyridines that do not contain other groups with such properties are neutral over the whole pH range [10]. However, the primary amino group on the side chain of AML and UK gives these dihydropyridines basic properties. To verify that the primary amino group was responsible for the electrostatic interaction with the sulfonic acid in (+)-CSA, felodipine (FEL) that lacks this substituent (Fig. 1), was studied in the same chromatographic system.

The optimum (+)-CSA concentration for enantiomeric separation, with acceptable k' values, of AML and UK was determined to be

Table 1
Capacity and separation factors of the enantiomers of three dihydropyridines on Hypercarb-S

Solute	Solvent X: methanol						Solvent X: acetonitrile					
	Y: (+)-CSA		Y: Br-(+)-CSA		No Y		Y: (+)-CSA		Y: Br-(+)-CSA		No Y	
	k'_1	α	k'_1	α	k'_1	α	k'_1	α	k'_1	α	k'_1	α
Amlodipine	22.1	1.08	39.1	1.05	^a	—	77.6	1	18.5	1	^a	—
UK52.829	30.9	1.08	53.1	1.05	^a	—	129	1	30.3	1	^a	—
Felodipine	58.6	1	55.6	1	60.0	1	71.6	1	59.4	1	55.3	1

Column temperature: 30°C. Mobile phase: 5 mM counter-ion Y in dichloromethane-solvent X (25:75, v/v). Flow-rate: 1.5 ml/min.

^a No peaks visible within 90 min.

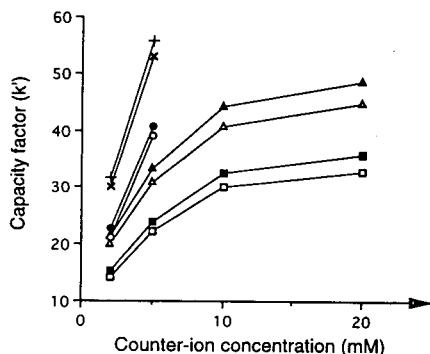


Fig. 3. Capacity factors of the enantiomers of amlodipine (AML) and UK52.829 (UK) at different counter-ion concentrations in a mobile phase system based on dichloromethane–methanol (25:75, v/v). Column: Hypercarb-S. Column temperature: 30°C. Counter-ion: (1*S*)-(+)-10-camphorsulfonic acid [(+)-CSA] or (1*S*)-(+)-3-bromo-10-camphorsulfonic acid [Br-(+)-CSA]. Flow-rate: 1.5 ml/min. □ = AML/(+)-CSA (1); ■ = AML/(+)-CSA (2); △ = UK/(+)-CSA (1); ▲ = UK/(+)-CSA (2); ○ = AML/Br-(+)-CSA (1); ● = AML/Br-(+)-CSA (2); × = UK/Br-(+)-CSA (1); + = UK/Br-(+)-CSA (2).

about 5 mM (Fig. 3). At (+)-CSA concentrations above 10 mM no further increase in the separation factor, α (k'_2/k'_1) was achieved (Fig. 3). The halogenated counter-ion Br-(+)-CSA was compared with (+)-CSA in the same chromatographic system. A marked increase in k' for AML and UK but no rise in α compared to (+)-CSA, was seen (Fig. 3). When the dihydropyridines were studied in a chromatographic system without counter-ion (i.e., dichloromethane–methanol, 25:75) no peaks of AML or UK were visible, but FEL was eluted within 50 min. Migration of the enantiomers of AML and UK was restored when 1 mM (+)-CSA was added to the mobile phase.

When the aprotic solvent acetonitrile was substituted for the protic methanol forming a mobile phase system of 5 mM (+)-CSA in dichloromethane–acetonitrile (25:75, v/v), no enantiomeric separation of AML and UK was visible. The dihydropyridines, however, both were markedly more retained in this slightly less polar chromatographic system (Table 1). Furthermore, when the halogenated camphorsulfonic acid was studied as counter-ion in the chromatographic system based on acetonitrile no

enantiomeric separation was visible while AML and UK surprisingly were much less retained both compared to (+)-CSA in this chromatographic system as well as Br-(+)-CSA in the mobile phase system based on methanol (Table 1).

In chiral ion-pair chromatography the electrostatic interaction alone between the two moieties may not be sufficient for enantiomeric separation [3]. A two-point attractive interaction between the selector (counter-ion) and the enantiomers might be necessary to give different solvations in the mobile phase or different interactions with the stationary phase, which can resolve the diastereomeric ion pairs. The second attachment could be another electrostatic interaction or a hydrogen bond. Beside the ion pairing of AML and UK with (+)-CSA or Br-(+)-CSA as counter-ion there is a possible hydrogen bonding. The keto group in the CSAs might form a bond with the hydrogen atom attached to the nitrogen in the dihydropyridine structure. X-Ray studies on the (–)-(1*S*)-camphoric acid derivatives of AML shows that this is quite possible [11].

Our results indicate that the primary amino group of AML and UK is responsible for a strong interaction with the PGC surface. In the mobile phase system without counter-ion, described above, no peaks of AML or UK were observed while FEL was eluted within 50 min. Charge transfer between unshared electron pairs of the primary amine in AML and UK and the delocalized band of electrons on PGC, might be the explanation [9,12]. Bassler et al. [12] showed that the k' values of some substituted aromates increased linearly, on PGC, with increasing electron donor ability. The migration observed when (+)-CSA successively was added to the mobile phase indicates increasing grade of ion pairing. Further on, we show that the choice of organic solvents play an important role for the retention and selectivity of the diastereomeric ion pairs of AML and UK. Surprisingly no separation was visible in a solvent system based on acetonitrile neither with (+)-CSA nor Br-(+)-CSA as chiral counter-ion. The ability to form stable intermolecular bonds with the coun-

ter-ion ought to be stronger in acetonitrile than in the protic methanol that is able to compete in hydrogen bonding. In a previous paper [9] we showed that an organic solvent with a high content of oxygen lone pairs (e.g., acetic acid or formic acid) in the mobile phase markedly decreased the retention of the (–)-menthyl chloroformate derivatives of AML and UK compared to solvents like acetonitrile or alcohols, on the PGC Hypercarb-S. However, in that chromatographic system the enantioselectivity was higher with acetonitrile in the mobile phase than with alcohol.

The enantiomers of dihydropyridines are generally hard to separate. Vandenbosch et al. [13] showed in their evaluation of six stationary phases, for direct separation of enantiomers, that the dihydropyridines in most systems gave α -values around 1.1. The best results were obtained on protein columns (e.g., Chiral α -glycoprotein, Ovomuroid) with α values, for some of the dihydropyridines, above 1.1.

4. Conclusions

Our results show that the dihydropyridines AML, FEL and UK are highly retained on the PGC. With addition of a chiral counter-ion enantioselective migration of AML and UK is achieved. However, since ion pairs of the solutes, counter-ions and mobile phase solvents seem to competitively interact with the PGC

surface the retention mechanisms and selectivity are hard to predict. The strong retention of planar non-polar solutes on PGC are a drawback since chromatography requires high contents of organic solvents, but the stereoselectivity of the material makes it still an interesting complement as a chromatographic tool in chiral separations.

References

- [1] A.R. Fassihi, *Int. J. Pharm.*, 92 (1993) 1.
- [2] S. Allenmark, *Chromatographic Enantioseparation, Methods and Applications*, Ellis Horwood, Chichester, 2nd ed. 1991, pp. 60, 160.
- [3] C. Pettersson, in A.M. Krstulovic (Editor), *Chiral Separations by HPLC*, Ellis Horwood, Chichester, 1991, p. 124.
- [4] C. Pettersson and G. Schill, *J. Chromatogr.*, 204 (1981) 179.
- [5] J.H. Knox and B. Kaur, *J. Chromatogr.*, 352 (1986) 3.
- [6] B. Kaur, *The Use of Porous Graphitic Carbon in HPLC*, Shandon Scientific, Runcorn, 1991.
- [7] A. Karlsson and C. Pettersson, *Chirality*, 4 (1992) 323.
- [8] C. Pettersson and C. Gioeli, *Chirality*, 5 (1993) 241.
- [9] M. Josefsson, B. Carlsson and B. Norlander, *Chromatographia*, 37 (1993) 129.
- [10] M. Ahnoff and B.-A. Persson, *J. Chromatogr.*, 531 (1990) 181.
- [11] S. Goldmann, J. Stoltefuss and L. Born, *J. Med. Chem.*, 35 (1992) 3341.
- [12] B.J. Bassler, R. Kaliszan and R.A. Hartwick, *J. Chromatogr.*, 461 (1989) 139.
- [13] C. Vandenbosch, D. Massart and W. Lindner, *J. Pharm. Biomed. Anal.*, 10 (1992) 895.

Separation of the *R*(–)- and *S*(+)-enantiomers of the ethyl ester of tiagabine · HCl using a Chiralcel-OG column

Abu M. Rustum

Department 41G (R13), Bioanalytical Research, Abbott Laboratories, 1401 Sheridan Road, North Chicago, IL 60064, USA

First received 15 February 1994; revised manuscript received 16 May 1994

Abstract

The *R*(–)- and *S*(+)-enantiomers of ethyl-*N*-[4,4-di(3-methyl-thien-2-yl)-but-3-enyl]-nipecotate-hydrochloride are separated by a normal-phase chiral HPLC on a commercially available chiral stationary phase. Samples of *R*(–)- and *S*(+)-enantiomers were first dissolved in a few drops of 2-methyl-2-propanol, diluted with the mobile phase, and then injected directly into the HPLC system. The HPLC system was equipped with a Daicel, Chiralcel-OG column. The mobile phase consisted of hexane–2-methyl-2-propanol–1-octanol, (990:8:2, v/v/v) to which approximately 0.5 ml of diethylamine was added. The method is able to separate the *R*(–)- and *S*(+)-enantiomers with a resolution factor of 1.2 and a selectivity factor of 1.16. The limit of quantification of the *S*(+)-enantiomer is 0.2% in the *R*(–)-enantiomer. The analytical procedure was validated by conducting standard addition and recovery of the *S*(+)-enantiomer in the *R*(–)-enantiomer. The precision of the method was determined by multiple analysis of each of the two samples of *R*(–)-enantiomer containing approximately 1% of the *S*(+)-enantiomer.

1. Introduction

The differences in biological activity between the enantiomers of pharmaceutical agents have been reported in the literature [1]. In recent years, interest in the stereochemical aspects of drug action has been intensified [2–4] because of the more stringent regulations for the marketing of optically active drugs by the United States Food and Drug Administration (U.S.F.D.A.) and other regulatory agencies of the world.

High-performance liquid chromatography (HPLC) and gas chromatography (GC) have been used to separate and quantitate the enantiomers of pharmacologically active compounds [5–12]. To understand the separation mechanism of the enantiomers on a chiral

stationary phase, numerous theoretical studies have been conducted by the early pioneers of this field [13–16]. Gal [17] conducted studies on derivatization of optically active compounds with pure optically active reagents, forming diastereoisomers. The diastereoisomers were separated using various chromatographic conditions. Wainer [18,19] has classified all the commercially available chiral stationary phases according to their mode of separation mechanism of the optically active compounds having different functional groups. To ensure the optical purity of a chiral drug, and to determine the pharmacokinetic profiles and pharmacodynamic effects of individual enantiomers of a chirally active drug, a simple reproducible and sensitive analytical method is required.

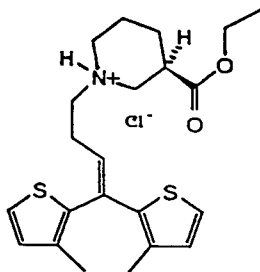


Fig. 1. Chemical structure of the ethylester of Tiagabine·HCl.

In this report, a commercially available chiral stationary phase (Chiralcel-OG) was used to separate and quantitate the *R*(-)- and *S*(+)-enantiomers of ethyl-*N*-[4,4-di(3-methyl-thien-2-yl)-but-3-enyl] nipecotate-hydrochloride (ethyl ester of Tiagabine·HCl) without derivatization. The chemical structure of the ethyl ester of Tiagabine·HCl is shown in Fig. 1. This compound is a pro-drug and is the penultimate intermediate in the synthesis of Tiagabine·HCl, which is under development as an anti-convulsive agent. The *R*(-)-enantiomer of the drug has been found to be pharmacologically more active than the *S*(+)-enantiomer. Several commercially available columns were investigated using normal-phase and reversed-phase modes to obtain the maximum resolution and sensitivity of the two enantiomers.

2. Experimental

2.1. Equipment

A HPLC solvent-delivery system (SP 8800) equipped with an injector/autosampler (SP 8780), an integrator (SP 4270), and a variable-wavelength UV-visible detector (SP 8450) was used in the experiment (Spectra-Physics, San Jose, CA, USA). A 25 cm × 4.6 mm I.D., Chiralcel-OG column was used in the method finally developed (Daicel, USA). The other chiral stationary phase columns investigated in this experiment were 25 cm × 4.6 mm I.D., 5 μm, *D*-phenylglycine (Regis, Morton Grove, IL, USA), 25 cm × 4.6 mm I.D., 5 μm, β-cyclo-

dextrin column, cyclobond-1 (Rainin Instruments, Woburn, MA, USA), 25 cm × 4.6 mm I.D., 5 μm, phenylalanine (Jones Chromatography, Mid Glamorgan, UK), 25 cm × 4.6 mm I.D., 10 μm, Chiralcel-OJ (Daicel, USA), and 15 cm × 7.5 mm, 10 μm, bovine serum albumin column (manufactured by Machery-Nagel, bought from Alltech Assoc., Deerfield, IL, USA).

2.2. Materials

A HPLC-grade hexane and 1-octanol were purchased from Fisher Scientific (Fairlawn, NJ, USA). Diethylamine (reagent grade) and 2-methyl-2-propanol were purchased from Aldrich (Milwaukee, WI, USA). The racemic mixture, *R*(-)- and *S*(+)-enantiomers of the ethyl ester of Tiagabine·HCl, was from Abbott Laboratories (North Chicago, IL, USA).

2.3. Preparation of the sample

Approximately 10 mg of the samples were weighed and transferred into a 10-ml volumetric flask. Aliquots of 5–10 drops of 2-methyl-2-propanol were added into the sample flask to dissolve the sample. The sample was then diluted with the mobile phase. The standard solutions of *R*(-)- and *S*(+)-enantiomers and the racemic (±) mixture were similarly prepared. The mobile phase was injected as a blank.

2.4. Preparation of the mobile phase

To 990 ml of hexane, 8.0 ml of 2-methyl-2-propanol, 2.0 ml of 1-octanol, and 0.50 ml of diethylamine were added and mixed. The mobile phase mixture was degassed for approximately 5 min and used for analysis.

2.5. Chromatographic conditions

The typical chromatographic conditions used in this experiment are as follows: the flow-rate of the mobile phase was 0.8 ml/min; the samples were monitored with a UV detector at 280 nm

and 0.10 to 0.20 AUFS; 10 μ l of the sample were injected into the HPLC system.

2.6. Calculation

Quantification of the *S*(+)-enantiomer present in the *R*(-)-enantiomer was done using the following equation:

$$\% \text{ of } S(+)\text{-enantiomer} = 100 \cdot$$

$$\frac{\text{Peak area of the } S(+)\text{-enantiomer}}{\text{Sum of the peak areas of the } S(+)\text{- and } R(-)\text{-enantiomers}}$$

2.7. Limit of quantification (LOQ)

Samples of *R*(-)-enantiomer of tiagabine-ethyl ester were analyzed to determine the lowest level of *S*(+)-enantiomer which can be quantitated with good reproducibility (% R.S.D. less than 10). The limit of quantification (LOQ) of the method for *S*(+)-enantiomer present in the *R*(-)-enantiomer was about 0.2% at a signal-to-noise ratio of about 3.

3. Results and discussion

The blank (mobile phase) was injected and no peak eluted with the same retention times as those of the *S*(+)- and *R*(-)-enantiomers. Fig. 2 is a typical chromatogram of the racemic (\pm) mixture of the chiral compound which shows that the peaks of *S*(+)- and *R*(-)-enantiomers are adequately resolved from each other. Figs. 3 and 4 are typical chromatograms of the racemic (\pm) and *R*(-)-enantiomers of the ethyl ester of Tiagabine \cdot HCl when 1-octanol was not present in the mobile phase.

The capacity factors (k') of the *S*(+)- and *R*(-)-enantiomers were approximately 2.80 and 3.25 under the chromatographic conditions used in this experiment. The resolution between the two enantiomers was approximately 1.2 with a selectivity factor (α) of 1.16.

The amount of the *S*(+)-enantiomer present in the *R*(-)-enantiomer was quantified by peak area percent. The response of the UV detector

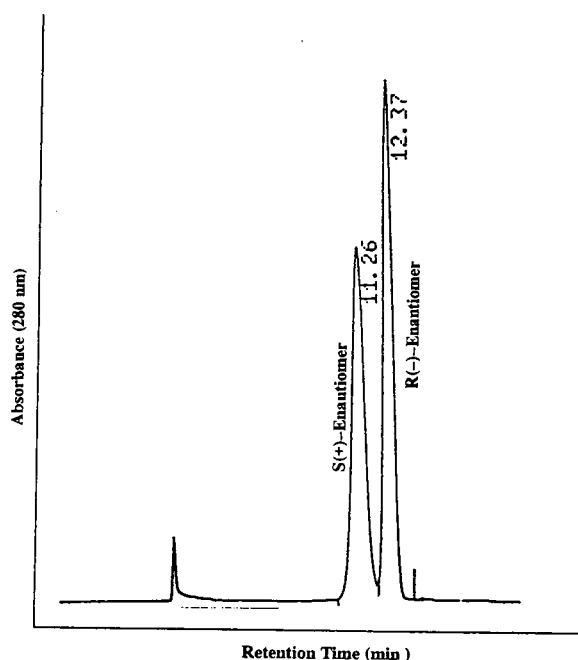


Fig. 2. Typical chromatogram of a racemic (\pm) mixture of the ethyl ester of Tiagabine \cdot HCl using the mobile phase (with 1-octanol) described in this report.

was linear from 0.10 to 1.0 mg/ml for 10- μ l injections. Typical regression line equation of the analyte has a correlation coefficient of >0.999 with a negligible y-intercept, and essentially passes through the origin. Authentic reference materials of the pure *S*(+)- and *R*(-)-enantiomers were available for the determination of relative retention volumes, *i.e.* elution order. Under the chromatographic conditions of these experiments, the *S*(+)-enantiomer elutes before the *R*(-)-enantiomer. Elution of the *S*(+)-enantiomer prior to the *R*(-)-enantiomer makes this method ideal for trace analysis of the *S*(+)-enantiomer present in the *R*(-)-enantiomer.

Experiments were conducted to obtain a mobile phase which will give optimum separation and sensitivity on the Chiralcel-OG column. The stationary phase of the Chiralcel-OG column is the methylphenyl carbamate derivative of cellulose, agglomerated on silica. Therefore, the type and amount of solvents which can be used in the mobile phase on Chiralcel-OG column are lim-

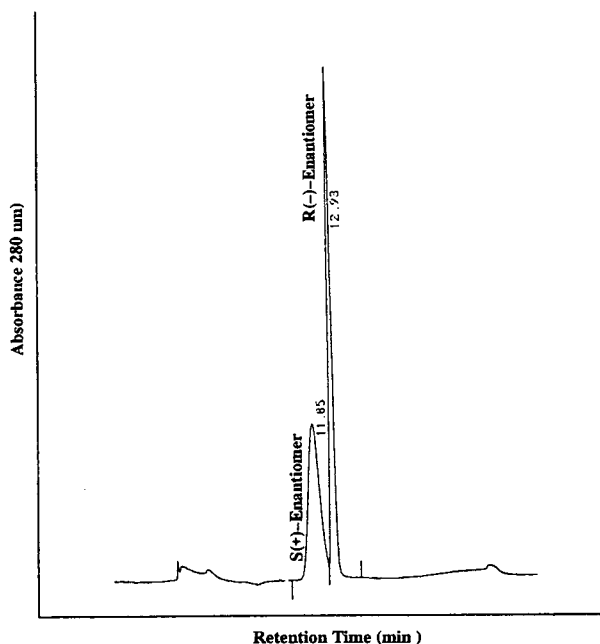


Fig. 3. Typical chromatogram of a racemic (\pm) mixture of the ethyl ester of Tiagabine·HCl using the same mobile phase as of Fig. 2, except 1-octanol was not added in the mobile phase.

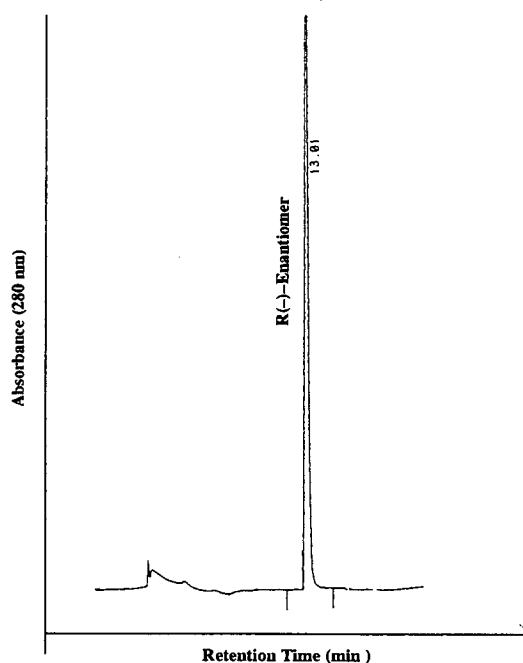


Fig. 4. Typical chromatogram of the $R(-)$ -enantiomer of the ethyl ester of Tiagabine·HCl. Mobile phase is same as that of Fig. 2, except 1-octanol was not added in the mobile phase.

ited. Typically, isopropanol is used in the range of 5 to 10%, mixed with hexane or heptane as the mobile phase. Other solvents which can be used in the mobile phase in small quantities are *tert.*-butanol, ethanol and other long chain alcohols. If solvents other than the above are used in the mobile phase, the column may lose selectivity, and the back pressure may also increase (due to the swelling of the stationary phase) and may destroy the column. Trace amounts of diethylamine (less than 0.5%) can be used in the mobile phase when the analyte molecule contains an amine functionality.

The selectivity and resolution of the two enantiomers varies with the choice of alcohol. For example, if 2-propanol is used in the mobile phase instead of 2-methyl-2-propanol, the resolution between the two enantiomers of the ethyl ester of Tiagabine·HCl is totally lost. The presence of a second alcohol in the mobile phase in trace amounts can also enhance the resolution between the two enantiomers. The resolution

between the $R(-)$ and $S(+)$ -enantiomers of the ethyl ester of Tiagabine·HCl is approximately 1.1 without 1-octanol in the mobile phase. The resolution between the two enantiomers increases to 1.5, when 0.2% of 1-octanol is added in the mobile phase. For the ethyl ester of Tiagabine·HCl, in addition to resolution enhancement, addition of 0.2% 1-octanol in the mobile phase has also broadened the peak width of the unusual sharp peak of the $R(-)$ -enantiomer which elutes after the $S(+)$ -enantiomer (Figs. 3 and 4).

The unusual chromatographic behavior of the $R(-)$ -enantiomer (later eluting peak) is difficult to explain satisfactorily with the established phenomena of chromatography. Typically, in isocratic chromatography, the later eluting peak is wider than the early eluting peak when the core structures (active sites) of both the molecules are similar, except for the number of carbon atoms. The broadening of the $R(-)$ -enantiomer peak, which elutes later, cannot be

satisfactorily explained with the known theories and phenomena of chromatography, such as eddy diffusion, mass transfer of the analyte from mobile phase to stationary phase and vice versa, viscosity of the mobile phase and other various interactions (hydrophobic, ionic, charge dispersion, etc.) between the analyte and the stationary phase. Addition of 1-octanol in the mobile phase improved the resolution and also broadened the peaks of the two enantiomers. However, the relative peak-broadening for the *R*(–)-enantiomer was found to be greater than the *S*(+)-enantiomer. This observation suggests that the interaction of the two enantiomers with the active sites of the chiral stationary phase or with the active sites of the silica backbone of the stationary phase increases in the presence of 1-octanol in the mobile phase, hence resulting in a broader peak. However, because of different spatial configurations of the two enantiomers, the chiral interaction of the *R*(–)-enantiomer with the chiral stationary phase (when 1-octanol is added in the mobile phase) appears to be greater than the *S*(+)-enantiomer, hence resulting in a higher percentage of peak-broadening than the *S*(+)-enantiomer.

Inspection of Figs. 3 and 4 reveals that the peak shape and width of the pure *R*(–)-enantiomer in the standard solution is the same as the peak shape and width of *R*(–)-enantiomer in the standard solution of the racemic (\pm) mixture. It is not possible to explain satisfactorily by the known theories and phenomena of chromatography the sharper peak shape of the *R*(–)-enantiomer (later eluting is sharper) than the *S*(+)-enantiomer; however, a possible explanation could be that the secondary interactions of the *S*(+)-enantiomer directly with the chiral stationary phase or with the silica backbone of the stationary phase are stronger than the interactions of the *R*(–)-enantiomer with the stationary phase. In chiral chromatography, the retention of the enantiomers is primarily dictated by the chiral interaction between the chiral sites of the analyte and stationary phase. Therefore, due to different spatial configurations of the two enantiomers, one enantiomer can have stronger secondary interactions with the stationary phase

(or its backbone) but weak chiral interaction with the chiral stationary phase, resulting into a broader peak but a shorter retention time than the other enantiomer. In general, the mass transfer of the analyte from stationary phase to mobile phase is poor when the analyte experiences strong secondary interactions with the active sites of the stationary phase or with the active sites of the backbone of the stationary phase. It is difficult to prove the above hypothesis regarding the band widths of the two enantiomers with the data available at this time. However, the explanation given above seems logical and may quite possibly be true.

The presence of diethylamine in the mobile phase plays an important role in the chromatographic efficiency and the separation. If diethylamine is not present in the mobile phase, the two enantiomers elute as overlapping wide peaks with a resolution factor of less than one. The extra broadening of the peaks of the two enantiomers in the absence of diethylamine in the mobile phase can be explained in terms of strong interaction of the nitrogen atom of the nipecotic acid moiety of the analyte with the silanols of the silica backbone of the stationary phase, or with the carbamate or hydroxyl functionality of the chiral stationary phase. Therefore, the sharper peaks of the analyte in presence of diethylamine is due to the suppression of the secondary interactions between the basic sites of the analyte and the stationary phase. Two other amines such as *N,N*-dimethyloctylamine and triethylamine were also tested. Both of these amines were found to be less effective than diethylamine in terms of decreasing the overlapping of the two peaks, and increasing the resolution.

The stationary phase of the Chiralcel-OG column is very susceptible to trace amounts of mobile phase modifiers; the effects on the retention and selectivity behavior of the original stationary phase by different mobile phase modifier may be either temporary or permanent. Therefore, columns should be used for dedicated analyses. When a new column is obtained, it should be conditioned with at least 1 l of mobile phase at a flow-rate of 0.5 ml/min to 0.8 ml/min to achieve a reproducible separation.

The separation of two enantiomers on a chiral stationary phase can only take place if one enantiomer, on a time average basis, has stronger interaction than the other enantiomer. The elution order of the *S*(+)- and *R*(-)-enantiomers of the analyte is dictated by the absolute configuration of the chiral stationary phase. The elution of the undesired enantiomer prior to the desired enantiomer is always preferred. Otherwise, a large resolution factor and good chromatographic efficiency would be required between the two enantiomers for accurate quantitation of the undesired enantiomer.

Columns packed with phenylglycine, phenylalanine (Pirkle type) and β -cyclodextrin were also investigated (both under normal- and reversed-phase conditions) for enantiomeric separation of the ethyl ester of Tiagabine · HCl. Solvents, such as hexane, isopropanol, ethanol and 0.1% trifluoroacetic acid were used at various combination, to obtain retention times from 10 to 60 min. For reversed-phase conditions, various ratios of 0.01 M phosphate buffer at different pH (2.2 to 7.5) with different percentages of organic modifiers such as methanol, acetonitrile and isopropanol were used to obtain retention time ranged from 10 to 50 min. There was no indication of enantiomeric separation from any of the above experiments.

A bovine serum albumin (BSA) column was also investigated using mobile phases having different percentages of isopropanol (1 to 10%) in a 0.01 M aqueous phosphate buffer. The pH of the mobile phase was varied from 3 to 7 and the retention time of the analyte ranged from 12 to 35 min. Again, no indication of enantiomeric separation was obtained from any experiments conducted by using the BSA column.

A Chiralcel-OJ column was also investigated for enantiomeric separation of the ethyl ester of Tiagabine. Solvents such as hexane, isopropanol, ethanol, trace amounts of diethylamine and trifluoroacetic acid (0.1%, v/v) were used at different solvent strengths. The retention time of the analyte varied from 10 to 30 min. This column (Chiralcel-OJ), showed some indication of enantiomeric separation when a mobile phase of hexane–isopropanol–ethanol–trifluoroacetic

acid at a ratio of 93:5:2:0.1 (v/v) was used. However, the resolution and selectivity of the analyte did not improve to any significant magnitude when the ratios of the solvents were varied from 100% hexane to hexane–isopropanol (90:10), and hexane–ethanol (90:10).

The column-to-column reproducibility of the separation between the two enantiomers of the analyte was tested by using three Chiralcel-OG columns of different lots. The separation was found to be reproducible on columns having different lot numbers, but conditioning of the new column with the mobile phase was required to achieve reproducibility. Typically, 1 l of the mobile phase at a flow-rate of approximately 0.5 ml/min was needed to condition a new column.

Standard addition and recovery experiments were conducted by two analysts to determine the accuracy of the method for the quantification of trace amounts of *S*(+)-enantiomer present in the *R*(-)-enantiomer. The range of addition levels used in this study was approximately 0.5% to 2.0%. The recovery of the *S*(+)-enantiomer averaged 100.5% with 2.1% R.S.D. The data for the standard addition and recovery experiments are summarized in Table 1.

The precision and short-term ruggedness of the method were also determined by two analysts using one lot of Tiagabine ethyl ester

Table 1
Standard addition and recovery data for *S*(+)-enantiomer

Baseline signal (%) ^a	Addition level (%)	Percent theory	Percent found	Percent recovery
(A)	(B)	(A + B)	(C)	$\left(\frac{C}{A+B} \cdot 100\right)$
1.00	0.55	1.55	1.56	100.6
1.00	1.00	2.00	1.99	99.5
1.00	2.00	3.00	3.00	100.0
1.05	0.55	1.60	1.67	104.4
1.05	1.00	2.05	2.07	101.0
1.05	2.00	3.05	2.97	97.4
Mean				100.5
S.D.				±2.1
R.S.D. (%)				±2.1

^a Baseline signal is the percent of *S*(+)-enantiomer already present in the sample used in this experiment.

which contained trace amount of *S*(+)-enantiomer. Two samples of *R*(-)-enantiomer of Tiagabine ethyl ester were prepared by each of the two analysts. The samples were analyzed using two different instruments, columns, and on two different days. The precision (R.S.D.) of the method is 6.4%. The results of this experiment are presented in Table 2. Fig. 5 is a typical sample chromatogram of the ethyl ester of Tiagabine·HCl containing approximately 0.3% of the *S*(+)-enantiomer.

The Chiralcel-OG column used in this method to separate the two enantiomers was found to be very stable under mobile phase conditions used in the final method. The efficiency, selectivity, resolution, and other chromatographic properties of the Chiralcel-OG column did not show any significant change after approximately 500 sample injections with the following maintenance procedure applied. On several occasions (three times), the resolution and efficiency of the column deteriorated after 20 to 30 injections of the sample. The column was easily regenerated to its original activity simply by washing it with approximately 200 ml of hexane–isopropanol–ethanol (70:20:10, v/v/v) at a flow-rate of 0.2 ml/min. After the washing, the column was re-conditioned with approximately 200 ml of the mobile phase. The occasional deterioration of

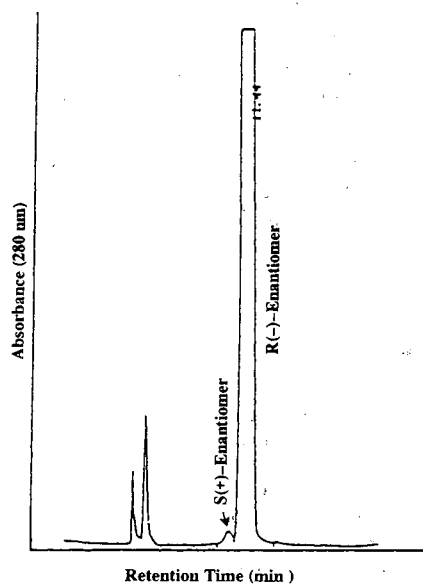


Fig. 5. Typical chromatogram of a sample of the ethyl ester of Tiagabine·HCl containing trace amount of the *S*(+)-enantiomer. Mobile phase is same as that of Fig. 2.

the column performance was probably due to the presence of some unknown impurities in the samples. This method is also used to analyze the in-process samples. The in-process samples at R&D stage of any project usually contain impurities of unknown characteristics and varies widely from lot to lot. Some of these unknown impurities may not elute from the column with the mobile phase used, and therefore could be the potential cause of deterioration of the efficiency, selectivity and resolution.

Table 2
Precision data for analysis of *S*(+)-enantiomer present in the *R*(-)-enantiomer

Analyst identification	Peak area (%) of <i>S</i> (+)-enantiomer
1	0.481
1	0.463
1	0.474
1	0.459
1	0.489
1	0.472
2	0.429
2	0.414
2	0.402
Mean	0.454
S.D.	±0.029
R.S.D. (%)	±6.4

4. Conclusions

An analytical method was required to determine the presence of *S*(+)-enantiomer in the ethyl ester of Tiagabine·HCl in order to assure the chiral purity of the final product. If the content of the *S*(+)-enantiomer at this stage of synthesis is higher than the desired level, then it can be reduced, to some extent, by recrystallization. Once this synthetic step is completed and the final product is obtained, the *S*(+)-enantiomer cannot be further reduced to any significant

amount by recrystallization. Therefore, it was important to control the final enantiomeric purity at this stage of synthesis. The normal-phase HPLC method described in this paper to separate the two enantiomers of the analyte is simple, reproducible, and relatively sensitive. The separation of the two enantiomers was reproducible on three different columns obtained from three different lots.

References

- [1] A.R. Cushny, *Biological Relations of Optically Isomeric Substances*, Williams & Wilkins, Baltimore, MD, 1926.
- [2] E.J. Ariens, *Med. Res. Rev.*, 6 (1986) 451.
- [3] J.W. Hubbard, D. Ganes, H.K. Lim and K.K. Midha, *Clin. Biochem.*, 19 (1986) 107.
- [4] D.W. Drayer, *Clin. Pharmacol. Ther.*, 40 (1986) 125.
- [5] E. Gil-Av, A. Tishbee and P.E. Hare, *J. Am. Chem. Soc.*, 102 (1980) 5115.
- [6] A. Sioufi, G. Kaiser, F. Leroux and J.P. Dubois, *J. Chromatogr.*, 450 (1988) 221.
- [7] N. Nimura, Y. Kasahara and T. Kinoshita, *J. Chromatogr.*, 213 (1981) 327.
- [8] B. Blessington and N. Crabb, *J. Chromatogr.*, 454 (1988) 450.
- [9] H. Furukawa, *Chem. Pharm. Bull.*, 23 (1975) 1625.
- [10] M. Gazdag, G. Szepesi and K. Milhalyfi, *J. Chromatogr.*, 450 (1988) 145.
- [11] T. Arai, H. Koike, K. Hirata and H. Oizumi, *J. Chromatogr.*, 448 (1988) 439.
- [12] L.R. Gelber and J.L. Neumeyer, *J. Chromatogr.*, 257 (1983) 317.
- [13] J.D. Morrison (Editor), *Asymmetric Synthesis*, Vol. 1, Academic Press, New York, 1983.
- [14] D.W. Armstrong, *Anal. Chem.*, 59 (1987) 84A.
- [15] M. Zief and L.J. Crane (Editors), *Chromatographic Chiral Separations*, Marcel Dekker, New York, 1988.
- [16] D.W. Armstrong, X. Xang, S.M. Han and R.A. Menges, *Anal. Chem.*, 59 (1987) 2594.
- [17] J. Gal, *LC·GC*, 5 (1987) 106.
- [18] I.W. Wainer, *A Practical Guide to the Selection and Use of HPLC Chiral Stationary Phases*, 1988.
- [19] I.W. Wainer, *Trends Anal. Chem.*, 6 (1987) 125.



ELSEVIER

Journal of Chromatography A, 684 (1994) 37–43

JOURNAL OF
CHROMATOGRAPHY A

Temperature-induced displacement of proteins from dye-affinity columns using an immobilized polymeric displacer

Igor Yu. Galaev, Cecilia Warrol, Bo Mattiasson*

Department of Biotechnology, Chemical Centre, Lund University, P.O. Box 124, S-221 00 Lund, Sweden

First received 25 January 1994; revised manuscript received 2 June 1994

Abstract

Poly(N-vinylcaprolactam) (PVCL), a polymer with a cloud point of 38°C, was used for the polymer shielding of Blue Sepharose. The globule-coil transition of the polymer was exploited in a dye-affinity column for the displacement of bound lactate dehydrogenase (LDH); elution was carried out without any change in the buffer composition by changing the temperature of the column. LDH from porcine muscle was bound to the PVCL-shielded column at 40°C. At this temperature LDH could not be eluted from the column with 0.1 M KCl. The decrease in temperature to *ca.* 23°C (room temperature) resulted in LDH elution with 0.1 M KCl. Crude porcine muscle extract was applied on the PVCL-shielded column at 40°C and the foreign proteins were washed out with 0.1 M KCl at 40°C. The flow was then interrupted, the column was cooled to room temperature and virtually homogeneous LDH was eluted with the same buffer. The purification factor was 17 and the recovery of LDH was 90%. This appears to be the first reported successful enzyme purification in which a temperature shift was used as the only eluting factor without changing the buffer composition.

1. Introduction

Reversible phase transitions in polymer solutions and critical phenomena in polymer gels have recently attracted attention because of their scientific and technological potential. These transitions may be initiated by small changes of temperature, pH, ionic strength, light, electric field or solvent composition [1]. Temperature change seems to be one of the most attractive triggers of such transitions. By using temperature-responsive polymers solutions can be manipulated without the addition of any substances, hence eliminating their removal at a

later stage. In addition, the response of the system may be exploited many times simply by heating and cooling it repeatedly. The use of temperature-responsive polymers and non-ionic surfactants in biotechnology [2], as separation agents [3,4], for the preparation of biocatalysts [5], and for the design of intelligent materials [6] has been reviewed in detail during the last year.

Temperature-responsive polymers have serious potential in the development of chromatographic systems, as a small temperature shift can modify the binding and elution of target substances. One such attempt was made by Gewehr et al. [7]. Gel permeation chromatography was carried out using porous glass modified with a temperature-responsive polymer, poly(N-iso-

* Corresponding author.

propylacrylamide). The elution of dextrans of various molecular masses was strongly affected by the temperature due to a change in the effective pore size of the matrix. This can be attributed largely to the transition of polymer molecules from coils to globules on the surface of the pores of the glass beads.

Previously we have developed a concept of polymer-shielded dye-affinity chromatography [8,9]. Poly(N-vinyl pyrrolidone) (PVP) treatment of a Blue Sepharose column resulted in the binding of the polymer due to multi-point interaction with the dye ligands. The bound polymer molecules significantly decreased both the adsorption of foreign proteins and non-specific binding of the target enzymes without seriously impairing enzyme interactions with the dye ligands via specific nucleotide binding sites. The realization of only specific interactions improved recoveries and elution efficiency. In other words, the bound polymer served as a lid, opening the ligand for strong specific interactions but preventing more weak non-specific interactions [8,9].

The use of a temperature-responsive polymer, poly(N-vinylcaprolactam) (PVCL), for shielding in dye-affinity chromatography was believed not only to decrease the non-specific interactions, but also to manage the specific interactions in response to temperature. This work was carried out with the idea of developing a system in which the globule-coil transition of the polymer caused by a temperature shift could be used for the displacement of bound proteins without changing the buffer composition, and hence as the only eluting factor.

2. Experimental

Lactate dehydrogenase type XXX-S from porcine muscle, β -NADH Grade III, and Cibacron Blue 3GA were purchased from Sigma (St. Louis, MO, USA). Cibacron Blue 3GA was used as such, its concentrations were determined using extinction $13\,600\text{ l mol}^{-1}\text{ cm}^{-1}$ [10]. Oxamic acid was purchased from BDH (Poole, UK) and a molar absorptivity of N-vinylcap-

rolactam from Polysciences (Warrington, PA, USA). Blue Sepharose was synthesized by coupling Cibacron Blue 3GA to Sepharose CL-4B according to Ref. [11]. The Cibacron Blue content, determined according to Ref. [12], was $4.2\ \mu\text{mol g}^{-1}$ dry gel. PVCL was synthesized by radical bulk polymerization according to Ref. [13] and had a molecular mass of about 40 000 (determined from intrinsic viscosity using the equation $[\eta] = 3.5 \cdot 10^{-4} M_w^{0.57}$ [14]) and a cloud point of 38°C in 20 mM Tris-HCl buffer (pH 7.3) in the presence of 0.1 M KCl.

Ground pork was purchased in a local shop and homogenized in ice-cold 20 mM Tris-HCl buffer (pH 7.3) containing 0.1 M KCl (10 ml of buffer per gram of muscle tissue). The homogenate was filtered through a synthetic fibre pad to remove larger particulate matter, centrifuged for 15 min to remove cell debris and the supernatant was filtered through Munktell filter-paper (Grycksbo, Sweden) to remove traces of fat. The porcine muscle extract was kept frozen without any loss of LDH activity and was applied directly after thawing and filtering on the Blue Sepharose column.

All chromatographic experiments with Blue Sepharose were carried out using a thermostated $1.3 \times 0.9\text{ cm}$ I.D. column at a flow-rate of 0.17 ml min^{-1} . All solutions introduced on to the column were in 20 mM Tris-HCl buffer (pH 7.3). The elution of LDH was performed with 0.1 or 1.5 M KCl. Elution by a temperature shift was carried out as follows: the sample was applied at 40°C and eluted with 0.1 M KCl at the same temperature (in the case of pure LDH, to show that the enzyme was not eluted at these conditions, or in the case of the porcine muscle extract, to wash out foreign proteins). Then the pump was stopped, the column was cooled to 25°C and elution was continued at this temperature with the same buffer. The porcine muscle extract was applied to the column until breakthrough of LDH was observed. The column was washed with 0.1 M KCl in buffer until no further protein (monitored by the absorbance at 280 nm) was detected in the eluate. Fractions of 10 min (with commercial LDH) or 5 min (with crude extract) were collected.

The PVCL shielding of columns was performed with an excess of 1% polymer solution (about 50 column volumes) followed by washing with 1.5 M KCl (pH 3.4) and re-equilibration of the column with an appropriate buffer.

The complex formation of PVCL with Cibacron Blue in solution was studied by differential spectroscopy using a Shimadzu UV-260 double-beam spectrophotometer as described in Ref. [15].

LDH activity was measured in the fractions according to a reported procedure [16]. The inhibition of the LDH reaction in NADH to NAD⁺ direction by Cibacron Blue was performed at 25 and 40°C in 20 mM Tris-HCl (pH 7.3) in the presence and absence of 0.1 M KCl.

Sodium dodecyl sulfate polyacrylamide gel electrophoresis (SDS-PAGE) with 12% gel was performed according to Ref. [17] using soybean trypsin inhibitor (M_r 21 500), carbonic anhydrase (M_r 31 000), ovalbumin (M_r 45 000), bovine serum albumin (M_r 66 200), and phosphorylase B (M_r 97 400) as standards.

3. Results and discussion

Fig. 1 presents elution profiles (with 0.1 M KCl followed by 1.5 M KCl) of pure LDH from untreated and PVCL-shielded columns at room temperature (ca. 23°C) and at 40°C. The elution profiles at room temperature and at 40°C from the untreated column were similar, suggesting that this temperature shift had not substantial effect on the behaviour of the untreated column. This behaviour was in complete agreement with the effect of temperature on the specific binding of Cibacron Blue to LDH, which was estimated using the competitive inhibition constants.

Cibacron Blue binding constants to LDH determined by different methods are virtually identical [18]. Moreover, the inhibition constant reflects specific binding of the Cibacron Blue ligand with an active site of LDH without a contribution of non-specific binding. Addition of 0.1 M KCl increased the inhibition constants (and hence decreased the efficiency of Cibacron Blue binding) from 0.1 to 0.65 μ M at 23°C and

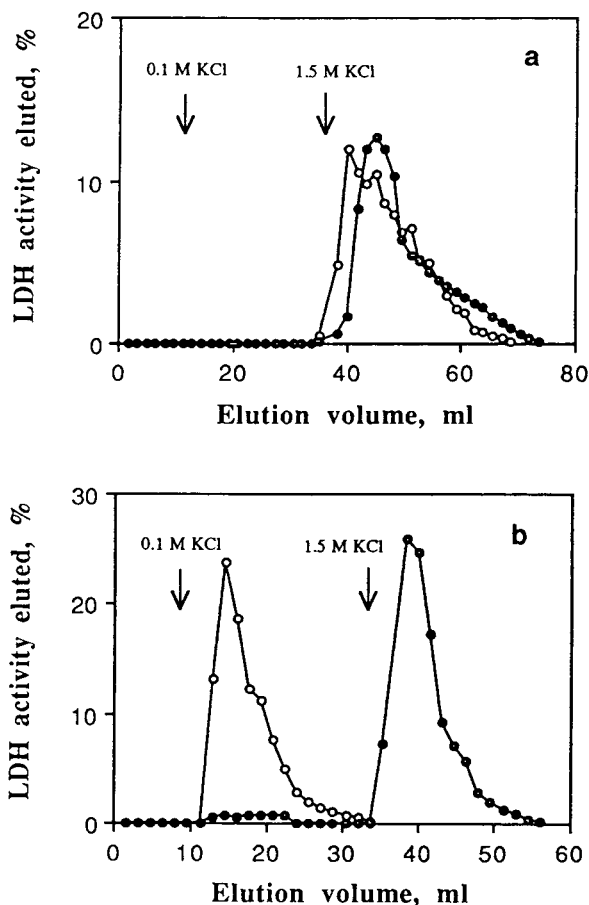


Fig. 1. Elution profile of LDH at (○) room temperature and (●) 40°C from (a) unmodified and (b) PVCL-shielded Blue Sepharose with 0.1 M KCl, followed by elution with 1.5 M KCl. Arrows indicate when elution with 0.1 M KCl and elution with 1.5 M KCl were begun. Experimental conditions: column, 1.3 × 0.9 cm I.D.; flow-rate, 0.17 ml min⁻¹; fractions collected every 10 min. The total amount of LDH eluted from the column was taken as 100% in all instances for the sake of comparison.

from 0.14 to 0.76 μ M at 40°C. This small decrease in binding efficiency caused by 0.1 M KCl was not sufficient to elute LDH from untreated columns at either room temperature or 40°C.

The elution behaviour using the PVCL-shielded column was different from that using the unshielded column. PVCL shielding resulted in sharper elution profiles at 40°C, an observation in line with PVP shielding of Blue Sepha-

rose [8,9]. Most important was the temperature-induced change in the elution profiles. Whereas LDH was not eluted at all with 0.1 M KCl at 40°C, the enzyme was easily eluted with the same eluent from the PVCL-shielded column at room temperature. Hence the column behaviour was completely different at 23°C, a temperature below the cloud point of PVCL, and at 40°C, a temperature above the cloud point.

Fig. 2 presents the elution profiles of LDH from the PVCL-shielded column with 0.1 M KCl at different temperatures. The temperature was lowered to room temperature in the course of elution by interrupting the flow, cooling the column and continuing the elution again at room temperature. LDH is readily eluted with 0.1 M KCl at room temperature. Raising the temperature hindered elution, and virtually no enzyme was eluted at 40 and 45°C, the temperatures above the cloud point of PVCL. Cooling the column to room temperature resulted in elution of LDH with the same buffer. The buffer containing 0.1 M KCl is a much milder eluent, resulting in broader LDH elution profiles from polymer-shielded columns than those obtained by elution with 1.5 M KCl [9].

It is conceivable that PVCL binds to the matrix via multi-point interaction with Cibacron Blue ligands. In solution one polymer molecule of PVCL efficiently bound 7–8 molecules of Cibacron Blue with a binding constant of 1.8 μM . Owing to the multi-valent interaction of PVCL with Cibacron Blue ligands, the effective avidity of the polymer to the matrix is much higher than its affinity to the ligand.

Unfortunately, there is no convenient and sensitive method for the determination of PVCL. Hence it is difficult to determine amount of PVCL bound to the column. The binding of polymer to the column resulted in a decrease in the enzyme binding capacity of the column. This effect has been demonstrated and discussed in detail [8]. The dye-affinity column was treated with an excess of PVCL solution. Hence the polydispersity of the polymer bound to the column will be determined not only by the polydispersity of the applied PVCL but also by the relative avidity of polymer molecules with different molecular masses to the matrix.

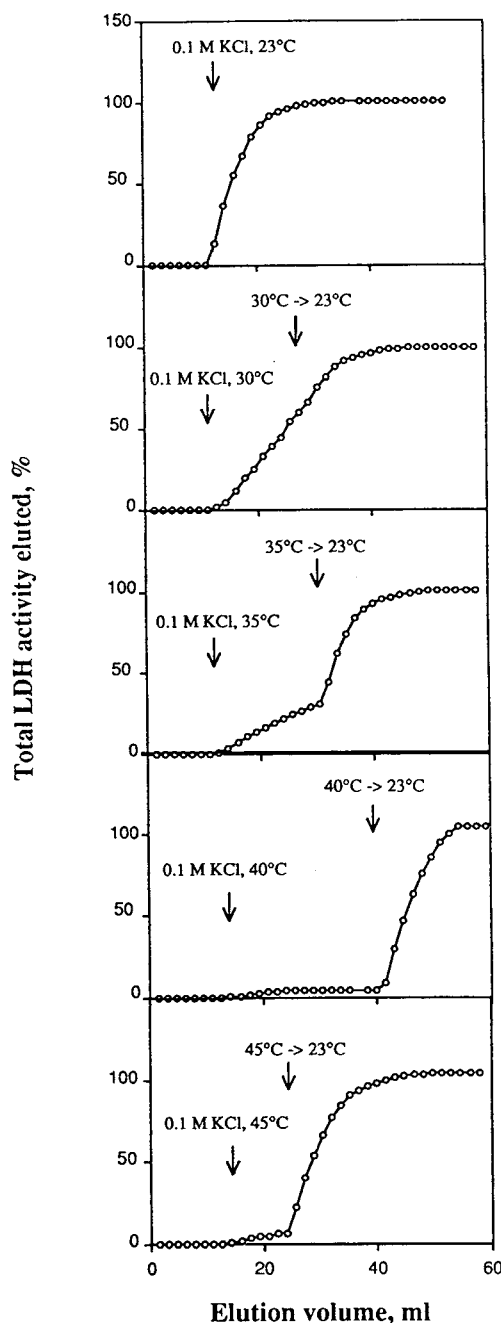


Fig. 2. Elution profile of LDH from PVCL-shielded Blue Sepharose with 0.1 M KCl at different temperatures. Arrows indicate when elution was interrupted, the column was cooled to room temperature and elution was continued at this temperature. Experimental conditions: column, 1.3 × 0.9 cm I.D.; flow-rate, 0.17 ml min⁻¹; fractions collected every 10 min. The total amount of LDH eluted from the column was taken as 100% in all instances for the sake of comparison.

The binding of Cibacron Blue to PVCL was independent of temperature at temperatures below the cloud point of PVCL where the polymer molecules were in the form of loose coils. When bound to the Cibacron Blue molecules coupled to the matrix, polymer molecules could efficiently compete with LDH for dye-ligands. The small decrease in LDH binding efficiency caused by the addition of 0.1 M KCl was sufficient to elute the enzyme from PVCL-shielded column at room temperature. The strong multi-point attachment of the PVCL to the matrix protects against complete removal of the polymer from the column. The PVCL-shielded column was used repeatedly for about ten runs without losing its temperature-responsive property. Above the transition temperature, PVCL molecules form compact globules striving for aggregation and formation of a separate phase. The polymer shielding decreased, so Cibacron Blue ligands were more available for both specific and non-specific interactions with LDH. Elution with 0.1 M KCl in that event was inefficient, and a more robust eluent was required. Above the transition temperature the PVCL-shielded column behaved similarly to the untreated column, although some effect of the polymer resulted in a sharper elution profile. Cooling of the PVCL-shielded column with bound LDH resulted in the transition of immobilized polymer molecules from globules to flexible coils. Owing to their relative flexibility, these coils could interact with more ligands than could compact polymer globules. This interaction of PVCL molecules is efficient enough to displace the LDH molecules bound to the Cibacron Blue ligands. Hence cooling the column resulted in displacement of bound LDH by immobilized polymer and hence in complete elution of enzyme without any changes in buffer composition.

The effect of temperature on the elution of different proteins is well documented in protein chromatography [7,19–26]. The increase in the affinity of monoclonal antibodies to oligosaccharides with decrease in temperature was used to optimize the resolution [24]. sAMP synthetase elutes in a sharper elution peak from a Cibacron Blue column at 20 than 4°C under otherwise

identical conditions [25]. Binding of 6-phosphogluconate dehydrogenase from the thermophilic organism *Bacillus stearothermophilus* to Cibacron Blue and Procion Red HE 3B columns increases with increasing temperature from 5 to 50°C [26]. Nevertheless, the temperature was never a critical variable in binding or elution in dye-affinity chromatography [26].

The effect of temperature in hydrophobic chromatography is also not so drastic. In hydrophobic chromatography to alter the binding efficiency significantly by changing only the temperature requires the use of exotic conditions. We were able to find only one report of elution by means of a temperature shift [23]. A mixture of ovalbumin, catalase and chymotrypsinogen A was separated by hydrophobic chromatography on phenylbutylamine at sub-zero temperatures. At –15°C, ovalbumin and catalase were eluted with 30% ethylene glycol in a void volume, while chymotrypsinogen A remained bound to the column. An increase in temperature to 4°C resulted in the elution of chymotrypsinogen A with the same eluent. While low temperatures are healthy for enzyme purification, although the work at –15°C might be complicated, the use of 30% ethylene glycol is harmful to the activity of many enzymes. Certainly, the use of such procedures is restricted to analytical applications.

The drastic difference in the elution of LDH from the PVCL-shielded column at room temperature and 40°C can hardly be attributed to a simple decrease in efficiency of hydrophobic interaction. No LDH was eluted from the untreated Blue Sepharose column either at room temperature or at 40°C with 20% ethylene glycol (the use of higher ethylene glycol concentrations was prohibited by the progressive inactivation of LDH). Subsequent elution with 1.5 M KCl resulted in LDH recoveries of 71% and 48%, respectively. Hence the coil–globule transition of PVCL polymer bound to the Blue Sepharose induced by raising the temperature is the most reasonable explanation for the different column behaviours at room temperature and 40°C.

This property of a PVCL-shielded column was used for the development of a dye-affinity system where temperature was the only means of elution without changing the buffer composition.

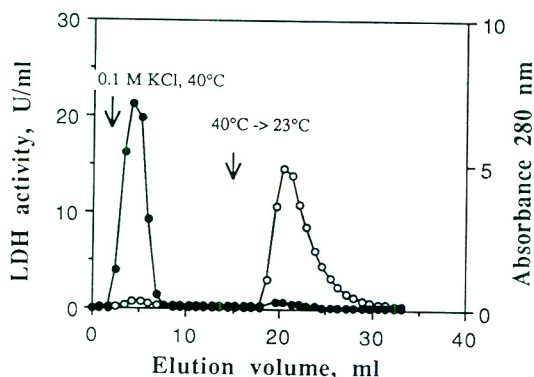


Fig. 3. Elution profile of (○) LDH activity and (●) protein with 0.1 M KCl from PVCL-shielded Blue Sepharose. The crude extract was applied on a column at 40°C. Arrows indicate when elution with 0.1 M KCl at 40°C was begun and when the column was cooled to room temperature and elution was continued at this temperature. Experimental conditions; column, 1.3 × 0.9 cm I.D.; flow-rate, 0.17 ml min⁻¹; fractions collected every 5 min.

Crude porcine muscle extract was applied to a column at 40°C until breakthrough, the foreign proteins were washed out with 0.1 M KCl at 40°C, the flow was interrupted, the column was cooled to room temperature and finally LDH was eluted with the same buffer (Fig. 3). The chromatographic procedure resulted in virtually homogeneous LDH (Fig. 4) with a purification factor of 17 and recovery of 90% of the enzyme.

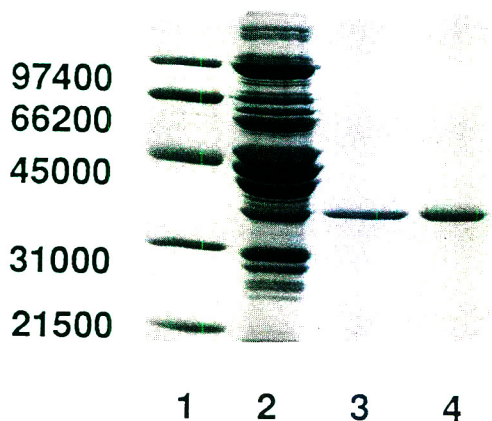


Fig. 4. SDS-PAGE patterns for LDH. Lanes: 1 = marker proteins; 2 = crude extract; 3 = LDH eluted after a temperature decrease from 40°C to room temperature (PVCL-shielded Blue Sepharose, 0.1 M KCl); 4 = commercial sample.

To the best of our knowledge, this is the first reported successful enzyme purification where the temperature shift is used as the only eluting factor without changing the buffer composition. PVCL, a polymer with a globule-coil transition temperature of 38°C, was used in this work. The properties of the polymer forced us to operate at a fairly high temperature (40°C) from the biotechnological point of view. Modern polymer chemistry can provide polymers with different transition temperatures, low enough to meet the requirements of biomolecule stability [2]. The use of a temperature shift as the only eluting factor in polymer-shielded dye-affinity chromatography is quite attractive. Relatively small temperature changes can be designed in a fast and convenient mode, replacing tedious procedures of column re-equilibration after elution buffer and purification of target enzyme from high salt concentrations used for elution in traditional dye-affinity chromatography.

Acknowledgements

The support of the Swedish Royal Academy of Sciences (KVA), the National Swedish Board for Technical and Industrial Development (NUTEK), the Swedish Agency for Cooperation with Developing Countries (SAREC) and the Swedish Research Council for Engineering Sciences (TFR) is gratefully acknowledged. The authors thank Nandita Garg for the synthesis of Blue Sepharose and Dr. Scott Bloomer for linguistic advice.

References

- [1] E. Kokufuta and T. Tanaka, *Macromolecules*, 24 (1991) 1605; and references cited therein.
- [2] I.Yu. Galaev and B. Mattiasson, *Enzyme Microb. Technol.*, 15 (1993) 354.
- [3] K.L. Wang, J.H. Burban and E.L. Cussler, *Adv. Polym. Sci.*, 104 (1993) 68.
- [4] W.L. Hinze and E. Pramauro, *CRC Crit. Rev. Anal. Chem.*, 24 (1993) 133.
- [5] E. Kokufuta, *Adv. Polym. Sci.*, 104 (1993) 159.
- [6] T. Okano, *Adv. Polym. Sci.*, 104 (1993) 180.

- [7] M. Gewehr, K. Nakamura, N. Ise and H. Kitano, *Macromol. Chem.*, 193 (1993) 249.
- [8] I.Yu. Galaev and B. Mattiasson, *J. Chromatogr.*, 648 (1993) 367.
- [9] I.Yu. Galaev and B. Mattiasson, *J. Chromatogr.*, 662 (1994) 27.
- [10] S.T. Tompson and E. Stellwagen, *Proc. Natl. Acad. Sci. U.S.A.*, 73 (1976) 361.
- [11] W. Heyns and P. De Moor, *Biochim. Biophys. Acta*, 358 (1974) 1.
- [12] G.K. Chambers, *Anal. Biochem.*, 83 (1977) 551.
- [13] O.F. Solomon, M. Corciovel and C. Boghina, *J. Appl. Polym. Sci.*, 12 (1968) 1843.
- [14] Yu.E. Kirsh, I.Yu. Galaev, T.M. Karaputadze, A.M. Margolin and V.K. Svedas, *Biotekhnologiya (Engl. Trans.)*, No. 2 (1987) 184.
- [15] J. Hubble, A.G. Mayes and R. Eisenthal, *Anal. Chim. Acta*, 279 (1993) 167.
- [16] *Worthington Enzymes and Related Biochemicals*, Worthington Biochemical, Freehold, NJ, 1982, p. 109.
- [17] U.K. Laemmli, *Nature*, 227 (1970) 680.
- [18] Y.C. Liu, R. Ledger and E. Stellwagen, *J. Biol. Chem.*, 259 (1984) 3796.
- [19] H.P. Jennissen, *J. Chromatogr.*, 159 (1978) 71.
- [20] S. Hjerten, in *Proceedings of the International Workshop on Technology for Protein Separation and Improvement of Blood Plasma Fractionation; DHEW Publ. (NIH) (U.S.)*, NIH-78-21422, National Institutes of Health, Reston, VA, 1978, p. 410.
- [21] J. Visser and M. Strating, *Biochim. Biophys. Acta*, 384 (1975) 69.
- [22] T.G.I. Ling and B. Mattiasson, *J. Chromatogr.*, 254 (1983) 83.
- [23] C. Le Peuch and C. Balny, *FEBS Lett.*, 87 (1978) 232.
- [24] S. Ohlson and D. Zopf, in T.T. Ngo (Editor), *Molecular Interactions in Bioseparations*, Plenum Press, New York, 1993, p. 15; and references cited therein.
- [25] G. Markham and G. Reed, *Arch. Biochem. Biophys.*, 184 (1977) 24.
- [26] *Dye-Ligand Chromatography. Application, Method, Theory of Matrex Gel Media*. Amicon, Lexington, MA, 1980, p. C24.



ELSEVIER

Journal of Chromatography A, 684 (1994) 45–54

JOURNAL OF
CHROMATOGRAPHY A

Interaction of Cibacron Blue with polymers: implications for polymer-shielded dye-affinity chromatography of phosphofructokinase from baker's yeast

Igor Yu. Galaev, Nandita Garg, Bo Mattiasson*

Department of Biotechnology, Chemical Centre, Lund University, P.O. Box 124, Lund S-221 00, Sweden

First received 16 February 1994; revised manuscript received 9 June 1994

Abstract

Interactions between Cibacron Blue F3GA and water-soluble non-ionic polymers were investigated by monitoring the spectral shift that accompanies the binding phenomena. Polyvinylpyrrolidone (PVP) and poly(vinyl alcohol) were the only polymers among those tested found to interact effectively with the dye. The difference spectra for the PVP–dye complex was typical of “electrostatic interaction spectra” at low ionic strength and typical of “hydrophobic interaction spectra” in the presence of 1.5 M KCl. The binding constant and the number of binding sites per polymer molecule were calculated using the simplest model of independent binding sites. One dye molecule was bound by a PVP segment with a molecular mass of 1000–1300. Regardless of the size of the polymer molecules, the binding constants were in the micromolar range. Poly(vinyl alcohol) bound less efficiently to Cibacron Blue than PVP. One dye molecule was bound by a polymer segment with a molecular mass of about 10 000. The data on PVP complexing with Cibacron Blue were used to develop the concept of polymer-shielded dye-affinity chromatography. This concept was successfully applied to the chromatography of phosphofructokinase (EC 2.7.1.11) from baker's yeast. Specific elution of the bound enzyme from PVP-shielded column resulted in an efficient process with 27-fold purification.

1. Introduction

Affinity chromatography has traditionally been used in the last stages of purification processes owing to the high costs of matrices and ligands and instability of ligands towards degradative enzymes present in very crude extracts [1]. Recent efforts have been directed to the application of this high-resolution technique to the earlier stages of a purification scheme so as to

reduce working volumes and processing times, thereby reducing the overall costs. One approach has been to replace the more expensive protein ligands with cheaper triazine dyes, which serve as group-specific ligands [2]. Purification of nucleotide-dependent enzymes such as dehydrogenases and kinases, and also non-nucleotide-dependent proteins such as bovine serum albumin (BSA) on dye-linked supports is well documented [3–11]. The commonly used triazine dyes provide possibilities for a range of different interactions between the protein and the dye. As

* Corresponding author.

a well defined biological affinity site is not always present, a number of non-specific binding interactions may occur. These interactions may lead to the irreversible binding of the protein, thereby obstructing the selectivity of the process [2].

The selectivity of affinity chromatographic procedures is governed in general by the ratio

$$\frac{\text{efficiency of specific interaction of the target protein with the ligand}}{\text{efficiency of non-specific interaction of foreign proteins with the ligand}}$$

The use of more specific ligands increases selectivity owing to the increase of the numerator. Another way to improve the selectivity is to reduce the denominator, in other words, to reduce the non-specific interactions and to allow only specific interactions. This approach is also promising because it can improve the recovery of the target molecule. In fact, target molecules interact with the ligand-containing matrix via specific binding sites and non-specifically due to various comparatively weak hydrophobic and electrostatic interactions. Reduction of these non-specific interactions would probably improve the recovery, especially during specific elution of the target molecule. One possible way to reduce non-specific interactions is to block such sites on the ligand with an inert agent. This agent must bind to the ligand tightly enough to prevent the

non-specific interactions but not strongly enough to disturb the specific interaction. The multi-point attachment of such an agent to numerous ligands allows it to stick constantly to the column and protects its displacement by the target protein, hence the agent must be of polymeric nature. This agent must not interact with the proteins in the sample. All these requirements of the blocking agent restrict its choice to water-soluble non-ionic polymers.

Previously we proposed the concept of polymer-shielded dye-affinity chromatography [12, 13]. Poly-N-vinylpyrrolidone (PVP) treatment of the column results in the binding of the polymer due to multi-point interaction with the dye ligands. The bound polymer molecules significantly decrease both adsorption of foreign proteins and non-specific binding of the target enzymes, while not seriously impairing enzyme interactions with the dye ligands via specific nucleotide binding sites. The realization of only specific interactions results in improved recoveries and elution efficiency.

The dye-affinity chromatography of phosphofructokinase (PFK) from baker's yeast (*Saccharomyces cerevisiae*) usually results in relatively low degrees of purification (3–13-fold) (see Table 1 and references therein). In the dye-affinity chromatography of other nucleotide-dependent enzymes, the degree of purification usually varies between 20- and 80-fold [11]. The

Table 1
Purification of yeast PFK by dye-affinity techniques using Cibacron Blue ligand

Matrix	Mode	Eluent	Yield (%)	Purification (-fold)	Ref.
Sephadex G-100	Batch adsorption	Ammonium sulfate	59	3.5	[37]
Sephadex G-200	Column chromatography	1.5 M ammonium sulfate	84	13.0	[36]
Sephadex G-200	Column chromatography	1.5 M ammonium sulfate	85	5.5	[36]
Sephadex G-200	Column chromatography	1.5 M ammonium sulfate	75	6.0	[36]
Sepharose CL6B	Column chromatography	1 M potassium chloride	91	— ^a	[38]
Sepharose CL6B	Column chromatography	10 mM ATP	69	— ^a	[38]
		1 mM ATP	26	— ^a	[38]
PEG-CB-Dextran	Affinity partitioning	0.34 M K ₂ HPO ₄ – 0.37 M KH ₂ PO ₄	75	9.0	[21]
Matrex Blue	Column chromatography	2 mM ATP	81	5.4	[39]
Sepharose CL4B	Column chromatography	50 mM ATP	56	27.0	This work

^a With pure enzyme preparation.

intention of this work was to study the complexation of non-ionic water-soluble polymers with Cibacron Blue and to apply the concept of polymer shielding to the dye-affinity chromatography of PFK.

2. Theory

The simplest model of independent binding of n Cibacron Blue molecules to the polymer molecule was used, and it was treated according to a slightly modified procedure [14]. The observed absorbance, A , can be described mathematically by

$$A = E_{\text{CB}}[\text{CB}] + E_{\text{X}}[\text{X}] \quad (1)$$

where E_{CB} and E_{X} are molar absorptivities and $[\text{CB}]$ and $[\text{X}]$ are concentrations of uncomplexed and complexed Cibacron Blue, respectively. The path length was taken as 1 cm.

In the absence of polymer, the absorbance A' can be written as

$$A' = E_{\text{CB}}[\text{CB}]_0 \quad (2)$$

where the subscript zero indicates total concentration. Also,

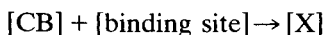
$$[\text{CB}] + [\text{X}] = [\text{CB}]_0 \quad (3)$$

The change in absorbance, ΔA , due to the complexation of Cibacron Blue with the polymer may be written as

$$\Delta A = A - A' = (E_{\text{X}} - E_{\text{CB}})[\text{X}] \quad (4)$$

E_{CB} was determined by direct measurement of Cibacron Blue absorbance, and E_{X} was determined by measurement of Cibacron Blue absorbance in the presence of the excess of polymer.

The complex formation may be described as



where $[\text{binding site}]$ is the concentration of free binding sites on the polymer molecule. The equilibrium constant taken as the dissociation constant will be

$$K = [\text{CB}][\text{binding site}]/[\text{X}] \quad (5)$$

The simplest assumption of independent binding of n Cibacron Blue molecules with one polymer molecule corresponds to

$$[\text{binding site}]_0 = n[\text{polymer}]_0 \quad (6)$$

From material balance,

$$[\text{binding site}] + [\text{X}] = [\text{binding site}]_0 \quad (7)$$

Substituting Eqs. 3, 6 and 7 in Eq. 5, we obtain

$$K = ([\text{CB}]_0 - [\text{X}])(n[\text{polymer}]_0 - [\text{X}])/[\text{X}] \quad (8)$$

Solving Eq. 8 for $[\text{X}]$ gives the physically significant root

$$[\text{X}] = 0.5\{([\text{CB}]_0 + K + n[\text{polymer}]_0) - ([\text{CB}]_0 + K + n[\text{polymer}]_0)^2 - 4[\text{CB}]_0n[\text{polymer}]_0\}^{1/2} \quad (9)$$

The experimental data obtained for $[\text{X}]$ from Eq. 4 over a range of polymer concentrations were fitted to Eq. 9 allowing best-fit values of the parameters K and n . These best fit values were obtained by minimizing the sum of square deviations weighted with the squares of the values, allowing the K and n terms to float freely. A good fit of experimental values was obtained using only two variable, independent parameters. The use of any other combination of parameters significantly different from the best-fit values resulted in a curve clearly different from that obtained experimentally. This was clearly seen by the significant increase in the sum of square deviations.

3. Experimental

PVP with average molecular masses of 10 000 (PVP-10) and 40 000 (PVP-40), ATP, AMP, β -NADH, fructose-6-phosphate and bicinechonic acid solution were purchased from Sigma (St. Louis, MO, USA). Polyethylene glycol (PEG) with molecular mass 20 000, poly(vinyl alcohol) (PVA) with molecular mass 13 000, methylcellulose 15, hydroxymethylcellulose 20 and dextran F70 were purchased from Serva (Heidelberg, Germany). When PVA was dissolved some insoluble material was removed by centrifugation,

and the actual polymer content was determined on a dry mass basis. PEG 8000 was purchased from Union Carbide, Sepharose CL 4B from Pharmacia (Uppsala, Sweden) and fresh baker's yeast from a local supermarket. Cibacron Blue 3GA was purchased from Sigma and used as received. The heterogeneous character of commercially available dye preparations is well known [15]; nevertheless it is common to use Cibacron Blue in spectral studies without additional purification [14,16–18].

The spectral titration was performed at room temperature according to Ref. [14]. Sample and reference cuvettes each containing a solution of ca. $80 \mu\text{M}$ Cibacron Blue in 50 mM Tris (pH 8.0) were placed in a Shimadzu UV-260 double-beam spectrophotometer. Small volumes ($1\text{--}10 \mu\text{l}$) of 5% PVP solution were added to the sample cuvette and equal volumes of buffer were added to the reference cuvette. The contents of the cuvettes were mixed and spectra in the range $400\text{--}800 \text{ nm}$ were registered (Figs. 1 and 2).

Blue Sepharose was synthesized by coupling Cibacron Blue 3GA to Sepharose CL 4B accord-

ing to Ref. [19]. The Cibacron Blue content was determined according to Ref. [20] as $41.8 \mu\text{mol/g}$ dried gel, after drying the gel for 48 h at 80°C .

Yeast homogenate was prepared according to Ref. [21]. Fresh baker's yeast was homogenized with twice its mass of dry-ice in 100-g portions in a household blender. The resulting powder was layered on a tray and, after evaporation of the dry-ice, the liquified material was mixed with 0.05 M sodium phosphate buffer (pH 7.0) containing 5 mM 2-mercaptoethanol, 0.2 mM EDTA and 0.5 mM phenylmethanesulfonyl fluoride (PMSF). It was centrifuged at $16\,000 \text{ g}$ for 15 min and the supernatant was subjected to fractional precipitation with PEG 8000. The precipitate between 4 and 8% (w/w) was collected and dissolved in the extraction buffer. This preparation was either used immediately or frozen at -20°C . The frozen material was thawed and centrifuged at 3000 g and the supernatant was applied to the column.

Chromatographic procedures were performed at 4°C . The column dimensions were $8.0 \text{ cm} \times 2.0 \text{ cm}$ I.D. and the flow-rate was 0.1 ml/min .

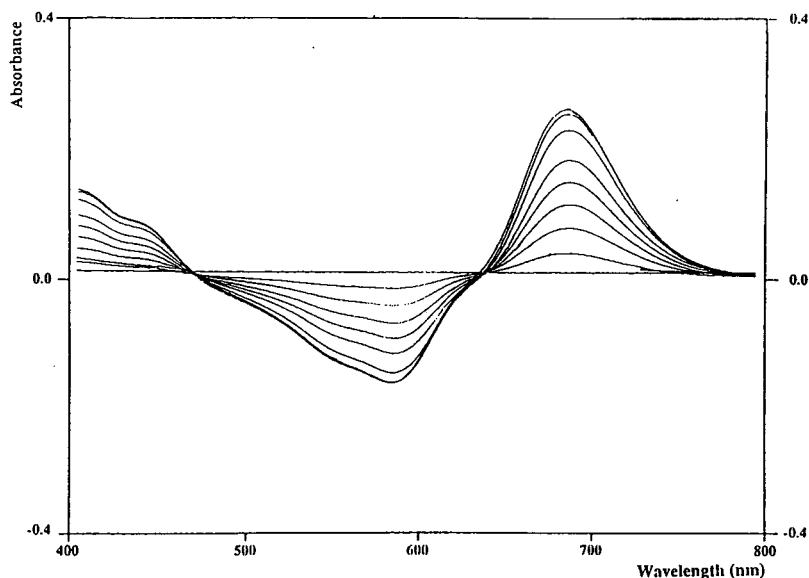


Fig. 1. Difference spectra obtained when Cibacron Blue was titrated with increasing concentrations of PVP-40. Both the sample and reference cuvettes contained 2 ml of $81 \mu\text{M}$ Cibacron Blue in 50 mM Tris (pH 8.0). Identical volumes of polymer [1.25 mM PVP-40 in 50 mM Tris (pH 8.0)] and buffer were added to the reference and sample cuvettes. The final concentration of PVP-40 in the sample cuvette was 0.6, 1.2, 1.9, 2.5, 3.1, 4.4, 5.6 and $6.8 \mu\text{M}$.

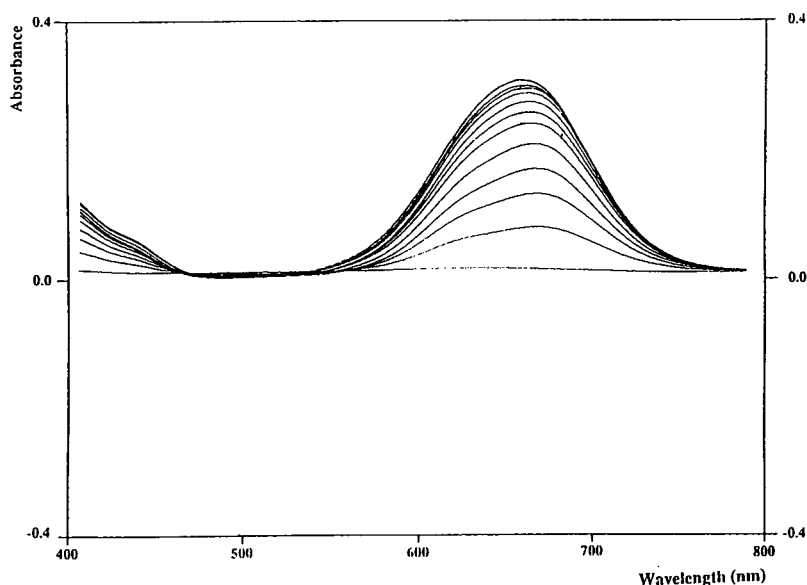


Fig. 2. Difference spectra obtained when Cibacron Blue was titrated with increasing concentrations of PVP-40 in the presence of salt. Both the sample and reference cuvettes contained 2 ml of $81 \mu\text{M}$ Cibacron Blue in 50 mM Tris (pH 8.0) containing 1.5 M KCl. Identical volumes of polymer [1.25 mM PVP-40 in 50 mM Tris (pH 8.0)] and buffer were added to the sample and reference cuvette. The final concentration of PVP-40 in the sample cuvette was 0.6, 1.2, 1.9, 2.5, 3.1, 3.7, 5.0, 6.2, 7.4 and $9.3 \mu\text{M}$.

PVP shielding of the column was done by percolating a 1% PVP solution and washing the column with 1.5 M KCl (pH 3.4). The column was re-equilibrated with 0.05 M sodium phosphate buffer (pH 7.0) containing 5 mM 2-mercaptoethanol, 0.2 mM EDTA and 0.5 mM PMSF before protein application; all solutions were subsequently introduced in the same buffer. Fractions were collected every 10 or 50 min. After application of the requisite amount of yeast extract, the column was washed extensively with buffer until the absorbance of the effluent at 280 nm was below 0.2. Specific elution was performed with ATP (0.05 M).

PFK activity was measured according to Ref. [22] using a Shimadzu UV-120-02 spectrophotometer. Protein concentration was determined by the BCA assay using the method given by the manufacturer of the reagent (Sigma procedure No. TPRO-562). The incubation time at 37°C was 60 min, and after cooling at room temperature for 10 minutes the absorbance of the samples was measured at 562 nm .

4. Results and discussion

Spectra of Cibacron Blue in the visible range are sensitive to the environment of the dye chromophore. The difference spectra according to Subramanian [16] can be classified as “electrostatic interaction spectra” (positive peak in the 690-nm region and negative double minima in the $630\text{-}585\text{-nm}$ region) and “hydrophobic interaction spectra” (positive peak at 655 nm , a shoulder at 610 nm and a small negative contribution below 550 nm). Using a difference spectroscopic technique we studied the interaction of Cibacron Blue with various non-ionic, water-soluble polymers. No appreciable interaction of the dye with dextran, polyacrylamide, hydroxyethylcellulose or PEG was observed. A very weak interaction of hydrophobic type was detected with methylcellulose (data not shown). Only PVP and PVA interacted with the dye. PVA interactions were weaker than interactions with PVP.

PVP interaction with Cibacron Blue resulted

in difference spectra with a peak at 680–690 nm, a minimum at 580–590 nm with a shoulder around 550 nm and an isosbestic point at 630–640 nm, indicating complex formation (Fig. 1). This type of difference spectra is typical of dye interaction with proteins, and can be classified as “electrostatic interaction spectra” according to Subramanian [16]. The difference spectra were significantly changed in the presence of 1.5 M KCl and characterized by a positive peak at 650–660 nm and a small negative contribution below 550 nm (Fig. 2). This spectrum type is similar to “hydrophobic interaction spectra” [16]. PVP is well known to complex both with negatively charged and hydrophobic substances [23]. The contribution of electrostatic interaction in the difference spectra was more pronounced at low ionic strength. The increase in ionic strength suppressed the electrostatic component and made the contribution of the hydrophobic interaction more pronounced.

The binding constant for PVP complexing with Cibacron Blue in solution was calculated as 2.1 μM (Fig. 3). A molecule of the polymer with a molecular mass of 40 000 contained 30 sites, capable of binding Cibacron Blue ligands. For PVP-10 with a molecular mass of 10 000 the calculated value of the binding constant was 6.1 μM and the number of binding sites per polymer molecule was 8. Note should be taken that the calculated dependence of complex concentration on polymer concentration was very sensitive to the number of binding sites per polymer molecule. Even minimal changes in the number of binding sites resulted in significant changes of the binding curve (Fig. 3, dashed curves).

The dye ligand was bound by a polymer segment having a molecular mass of 1000–1300 irrespective of the size of the polymer molecule. This supported the assumption of independent binding sites and is in agreement with the direct measurement of I_3 and 1-anilinonaphthalene-8-sulfonate complexation with vinylpyrrolidone oligomers of different molecular masses. The complexation takes place only when the oligomer molecular mass is higher than 1500 [24].

Although the type of the difference spectra was changed with increase in ionic strength, the

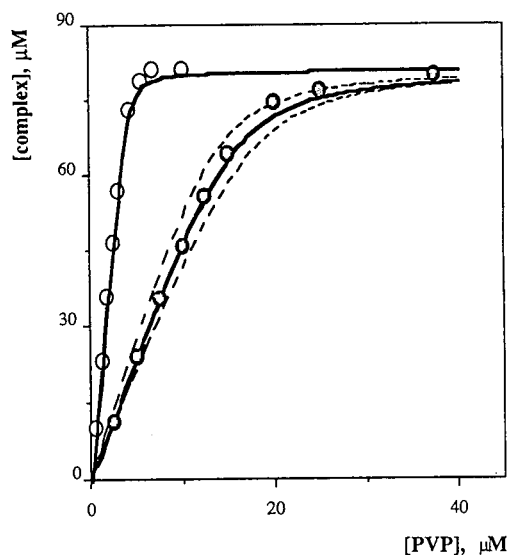


Fig. 3. PVP-40 (○) and PVP-10 (●) complexation with Cibacron Blue [81 μM Cibacron Blue, 50 mM Tris (pH 8.0)]. The open circle values were taken from Fig. 1 except the last point. The spectrum for this point and the one before it coincide. The values for E_{CB} and E_{x} at 680 nm are 6500 and 9600 $\text{l mol}^{-1} \text{cm}^{-1}$, respectively. The solid curves were calculated using the binding constants 2.1 and 6.1 μM and 30 and 8 binding sites for PVP-40 and PVP-10, respectively. The dashed curves were calculated using binding constant 6.1 μM and numbers of binding sites 7 (lower curve) and 9 (upper curve) for PVP-10.

binding constant of PVP-40 with Cibacron Blue was relatively insensitive to the high ionic strength. In the presence of 1.5 M KCl, which is frequently used as a non-specific eluent in affinity chromatography, the binding constant was 5.7 μM , the number of binding sites being practically the same, 32. A small regular shift of the wavelength at the maximum indicated a more complicated process of Cibacron Blue binding to the polymer under these conditions.

The interaction of PVA with Cibacron Blue was of the same type as for PVP: a positive maximum at 670–680 nm, an isosbestic point at 600–610 nm and a minimum at 570–580 nm with a shoulder around 540 nm. In contrast to PVP, the interaction with PVA was significantly weaker. The calculated value of the binding constant was 16.7 μM and the number of binding sites per polymer molecule was only 1.4. A

polymer segment with a molecular mass of about 10 000 complexed one Cibacron Blue molecule, ten times less than in the case of PVP. PVA with a molecular mass of 13 000 interacted with the dye nearly stoichiometrically. This polymer could not provide multi-point attachment when interacting with a Cibacron Blue-containing matrix, and for this reason it could not be used for polymer shielding in dye-affinity chromatography.

The interaction of Cibacron Blue with PVA reduces the access to the ligand in dye–PVA conjugates. That explains the previously reported result [25] that lactate dehydrogenase (LDH) from bovine heart was inhibited ten times less efficiently by Cibacron Blue–PVA conjugate than by Cibacron Blue–dextran conjugate, in which no interaction was detected between the dye and the polymer. The absence of a Cibacron Blue interaction with dextran and hence good access to the dye–ligand in such conjugates explains clearly the observation that the same values of the inhibition constants of lactate dehydrogenase by free and dextran-coupled triazine dyes are obtained [26]. The coupling of Cibacron Blue to Sepharose, which is carbohydrate in nature (as is dextran), does not alter the binding constant of LDH to the dye. The interaction of BSA with free and PEG-coupled Cibacron Blue is characterized by virtually the same half-saturation dye concentrations, whereas for PVA–Cibacron Blue it is about ten times higher [27]. The absence of a Cibacron Blue interaction with PEG is the reason for the extensive use of such conjugates in affinity partitioning [28]. Restricted access of the dye–ligand in the Cibacron Blue–PVA conjugates might be the reason for unsuccessful affinity precipitation of LDH using these conjugates [25,29].

Among the polymers studied, only PVP could bind efficiently and via multi-point attachment to the Cibacron Blue ligands of the Blue Sepharose and serve as an inert blocking agent of non-specific protein–dye interactions. The binding constant of one PVP segment with the dye ligand was in the micromolar range. The binding constants of Cibacron Blue to the nucleotide-binding sites of enzymes are in the same range or even

lower [26,29–34]. Thus enzymes can successfully compete with PVP segments for the ligand. The non-specific interaction of the dye ligands with the proteins is much weaker and characterized by higher binding constants. For instance, binding of Cibacron Blue to bovine serum albumin, which is considered to take place due to non-specific hydrophobic interactions, is characterized by a binding constant estimated to be 35–85 μM [27]. The data on Cibacron Blue binding to cytochrome *b₅* reductase can be rationalized assuming non-specific interaction with a binding constant of 85 μM together with specific binding (binding constant 1 μM) [35]. Hence the PVP segments, when bound to the dye–ligand, would protect it from relatively weak non-specific interactions with proteins. In other words, PVP molecules bound to the Blue Sepharose could serve as a lid, making the ligand available for strong specific interactions and protecting it from relatively weaker non-specific interactions. In dye affinity chromatography, retention of the target protein is governed by the sum of specific and non-specific interactions. When an affinity eluent is introduced, the specific interactions are minimized. If the non-specific interactions in the presence of affinity eluent are insufficient to retain the protein, it starts to move down the column. If the non-specific interactions are sufficiently strong, the protein remains bound and, as a result, the recovery is low [2]. Another consequence of the non-specific interactions is that even though they may be insufficient to retain the protein in the absence of the specific interactions, they may interact weakly with the protein as it moves down the column. These weak interactions will give rise to peak tailing and reduce the efficiency of the elution step. In the case of polymer treatment, it is assumed that the polymer prevents these non-specific interactions between the matrix and the target protein. As a result, only specific interactions occur. One consequence of this is an improved yield and elution efficiency. This forms the concept of polymer-shielded dye-affinity chromatography [12,13]. Table 2 summarizes the effects of polymer shielding. In all instances a decrease in capacity is seen with improved yields. There is a marginal

Table 2
Influence of PVP treatment in dye-affinity chromatography

System	Elution mode	Yield	Purification (-fold)	Efficiency	Capacity
Blue Sepharose–LDH	Non-specific	+	Marginal	+	–
	Specific	+	Marginal	+	–
Scarlet Sepharose–LDH	Non-specific	Marginal	+	+	–
	Specific	+	Marginal	Marginal	–
Scarlet Sepharose–sADH	Non-specific	Marginal	+	Marginal	–
	Specific	+	Marginal	+	–
Blue Sepharose–PFK	Specific	+	Marginal	+	–

The results are taken from Ref. [13] and this work; + indicates an increase; – indicates a decrease; marginal indicates marginal effects.

effect on the degree of purification fold, but the overall efficiency in terms of the elution volume is generally increased.

Like many other kinases, PFK has been shown to interact effectively with Cibacron Blue [36]. Binding is believed to occur at the ATP binding sites of the enzyme. A number of procedures that take advantage of this fact have been published for the purification of PFK on Cibacron Blue linked supports (Table 1). The degrees of purification achieved are significantly lower than those obtained in dye-affinity chromatography of other nucleotide-dependent enzymes, where they usually vary between 20- and 80-fold [11]. The low degrees of purification suggest strong non-specific interactions in the case of dye-affinity chromatography of PFK and makes this system suitable for evaluating the potential of polymer-shielded dye-affinity chromatography.

Specific elution of PFK (with its nucleotide substrate ATP) from an untreated and a PVP-shielded column is presented in Fig. 4 and Table 3. PVP shielding resulted in improved efficiency of the column. PFK concentration in the peak fractions was 5–6 times higher from the PVP-shielded column, and peak tailing, characteristic of the untreated column, was absent with the PVP-shielded column. PVP shielding also resulted in an improved PFK recovery, without significantly affecting the degree of purification (Table 3).

The purification factor obtained, 27, was sig-

nificantly higher than that reported previously in Cibacron Blue-based chromatography of PFK [21,36–39], but the recovery of PFK by specific elution was lower. The high recovery reported

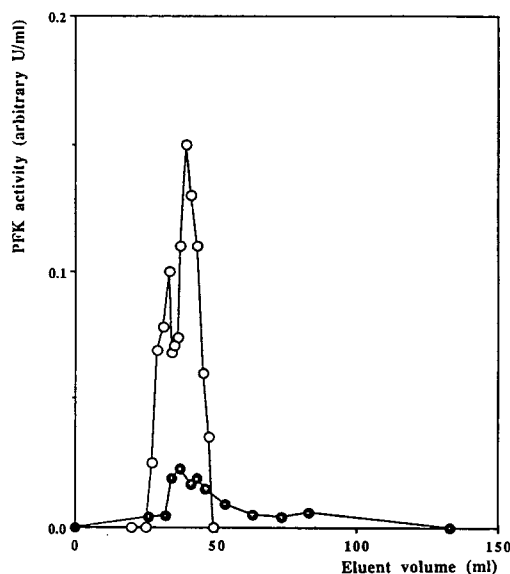


Fig. 4. Specific elution profile of PFK with 0.05 M ATP from untreated (●) and PVP-treated (○) Blue Sepharose column. Chromatographic procedures were performed at 4°C. Experimental conditions: 8.0 cm × 2.0 cm I.D. column; all solutions were introduced in 0.05 M sodium phosphate buffer (pH 7.0) containing 5 mM 2-mercaptoethanol, 0.2 mM EDTA and 0.5 mM PMSF; PVP treatment was done by percolating a 1% PVP solution through the column and then washing with 1.5 M KCl (pH 3.4); the column was re-equilibrated with 0.05 M sodium phosphate buffer (pH 7.0) containing 5 mM 2-mercaptoethanol, 0.2 mM EDTA and 0.5 mM PMSF; the flow-rate was 0.1 ml/min.

Table 3
Elution of PFK from Blue Sepharose

Column	Enzyme activity applied (U)	Enzyme activity bound (U)	Enzyme activity recovered			Specific activity of enzyme (U mg ⁻¹)		Purification (-fold)
			U	Volume (ml)	Yield (%)	Before affinity chromatography	After affinity chromatography	
Untreated	4.80	4.70	0.53	133	11.3	0.63	15.0	24.0
PVP-treated	4.30	2.30	1.30	47	56.0	0.60	16.0	27.0

Chromatographic procedures were performed at 4°C. The column dimensions were 8.0 cm × 2.0 cm I.D. and the flow-rate was 0.1 ml/min. The column was equilibrated before protein application with 0.05 M sodium phosphate buffer (pH 7.0) containing 5 mM 2-mercaptoethanol, 0.2 mM EDTA and 0.5 mM PMSF and all solutions were subsequently introduced in the same buffer. Fractions were collected every 10 or 50 min. After application of the requisite amount of yeast extract, the column was washed extensively with buffer until the absorbance 280 nm of the effluent was below 0.2. The specific elution was performed with ATP (0.05 M).

may be a result of the use of purified PFK, whereas crude yeast extract was used in these experiments.

The improvement of column efficiency and PFK recovery can be attributed to the PVP blockage of Cibacron Blue ligands capable of non-specific binding of PFK. The specific binding of PFK to the column was not seriously impaired. Some decrease in PFK binding by the PVP-shielded column was probably due to the decrease in non-specific PFK binding, which was much more significant with the untreated column.

Previously we have shown that PVP shielding results in improved efficiency of specific elution for systems such as porcine muscle lactate dehydrogenase–Blue Sepharose and secondary alcohol dehydrogenase from *Thermoanaerobium brockii*–Scarlet Sepharose. The present data provide a further example of the benefits of PVP shielding. These data, along with the results on the PVP binding to a Cibacron Blue, form a consistent concept of polymer-shielded dye affinity chromatography.

Acknowledgements

The support of the Swedish Royal Academy of Sciences (KVA), the National Swedish Board for Technical and Industrial Development (NUTEK), the Swedish Agency for Research

Cooperation with Developing Countries (SAREC) and the Swedish Research Council for Engineering Sciences (TFR) is gratefully acknowledged. The authors thank Mats Nilsson for help with the calculations and Dr. Scott Bloomer for linguistic advice.

References

- [1] E. Stellwagen, *Methods Enzymol.*, 182 (1990) 343.
- [2] R.K. Scopes, *Anal. Biochem.*, 165 (1987) 235.
- [3] F. Qadri, *Trends Biotechnol.*, 3 (1985) 7.
- [4] C.V. Stead, *Bioseparation*, 2 (1991) 129.
- [5] M.A. Vijayalakshmi, *Trends Biotechnol.*, 7 (1989) 71.
- [6] T. Makriyannis and Y.D. Clonis, *Process Biochem.*, 28 (1993) 179.
- [7] Y.D. Clonis, T. Atkinson, C.J. Bruton and C.R. Lowe (Editors), *Reactive Dyes in Protein and Enzyme Technology*, Macmillan, Basingstoke, 1987.
- [8] Y.D. Clonis, in M.T.W. Hearn (Editor), *HPLC of Proteins and Polynucleotides*, VCH, New York, 1991, Ch. 13, p. 453.
- [9] Y.D. Clonis, *CRC Crit. Rev. Biotechnol.*, 7 (1988) 263.
- [10] M. Allary, J. Saint-Blancard, E. Boschetti and P. Girot, *Bioseparation*, 2 (1991) 167.
- [11] R.K. Scopes, *J. Chromatogr.*, 376 (1986) 131.
- [12] I.Yu. Galaev and B. Mattiasson, *J. Chromatogr.*, 648 (1993) 367.
- [13] I.Yu. Galaev and B. Mattiasson, *J. Chromatogr. A*, 662 (1994) 27.
- [14] A.G. Mayes, R. Eissenthal and J. Hubble, *Biotechnol. Bioeng.*, 40 (1992) 1263.
- [15] S.J. Burton, S.B. McLoughlin, C.V. Stead and C. Lowe, *J. Chromatogr.*, 435 (1988) 127.

- [16] S. Subramanian, *Arch. Biochem. Biophys.*, 216 (1982) 116.
- [17] S. Subramanian and B. Kaufman, *J. Biol. Chem.*, 255 (1980) 10587.
- [18] P.S. Appukuttan and B.K. Bachhawat, *Biochim. Biophys. Acta*, 580 (1979) 15.
- [19] W. Heyns and P. De Moor, *Biochim. Biophys. Acta*, 358 (1974) 1.
- [20] G.K. Chambers, *Anal. Biochem.*, 83 (1977) 551.
- [21] G. Kopperschläger and G. Johansson, *Anal. Biochem.*, 124 (1982) 117.
- [22] E. Hofmann and G. Kopperschläger, *Methods Enzymol.*, 90 (1982) 49.
- [23] Yu.E. Kirsh, *Prog. Polym. Sci.*, 11 (1985) 283.
- [24] Yu.E. Kirsh, T.A. Soos and T.M. Karaputadze, *Eur. Polym. J.*, 19 (1983) 639.
- [25] J.E. Morris and R.R. Fisher, *Biotechnol. Bioeng.*, 36 (1990) 737.
- [26] A.R. Ashton and G.M. Polya, *Biochem. J.*, 175 (1978) 501.
- [27] G. Johansson and M. Joelsson, *J. Chromatogr.*, 537 (1991) 219.
- [28] G. Johansson, in H. Walter, D.E. Brooks and D. Fisher (Editors), *Partitioning in Aqueous Two-Phase Systems: Theory, Methods, Uses and Applications to Biotechnology*, Academic Press, New York, 1985, p. 161.
- [29] R.R. Fisher, B. Machiels, K.C. Kyriacou and J.E. Morris, in M.A. Vijayalakshmi and O. Bertrand (Editors), *Protein-Dye Interactions: Developments and Applications*, Elsevier, London, 1989, p. 190.
- [30] B.B. Chambers and R.B. Dunlap, *J. Biol. Chem.*, 254 (1979) 6515.
- [31] B.H. Weber, K. Willeford, J.G. Moe and D. Piszkie-wicz, *Biochem. Biophys. Res. Commun.*, 86 (1979) 252.
- [32] P. Bull, H. McDonald and P. Valenzuela, *Biochim. Biophys. Acta*, 653 (1981) 368.
- [33] Y.C. Liu, R. Ledger and E. Stellwagen, *J. Biol. Chem.*, 259 (1984) 3796.
- [34] Y.C. Liu and E. Stellwagen, *J. Biol. Chem.*, 262 (1987) 583.
- [35] D. Pompon, B. Guiard and F. Lederer, *Eur. J. Biochem.*, 110 (1980) 565.
- [36] H.-J. Böhme, G. Kopperschläger, J. Schulz and E. Hoffmann, *J. Chromatogr.*, 69 (1972) 209.
- [37] W. Diezel, H.-J. Böhme, K. Nissler, R. Frever, W. Heilmann, G. Kopperschläger and E. Hofmann, *Eur. J. Biochem.*, 38 (1973) 479.
- [38] R.S. Beissner and F.R. Rudolph, *J. Chromatogr.*, 161 (1978) 127.
- [39] P. Welch and R.K. Scopes, *Anal. Biochem.*, 112 (1981) 154.



ELSEVIER

Journal of Chromatography A, 684 (1994) 55-63

JOURNAL OF
CHROMATOGRAPHY A

Presence of a preferred anion-exchange binding site on cytochrome b_5 : structural and thermodynamic considerations

Davinder S. Gill¹, David J. Roush², Richard C. Willson*

Department of Chemical Engineering, University of Houston, 4800 Calhoun Avenue, Houston, TX 77204-4792, USA

First received 7 September 1993; revised manuscript received 10 June 1994

Abstract

A preferred chromatographic contact region for adsorption of recombinant soluble tryptic fragment of rat cytochrome b_5 on the hydrophilic anion-exchanger Mono Q has been identified using conservative carboxylate-to-amide mutations of charged residues. Equilibrium adsorption isotherms were measured under conditions of full reversibility by high ionic strength, as confirmed by explicit mass balances performed for each experiment. Although cytochrome b_5 displays several clusters of negative charge, mutations in one cluster consistently reduce binding affinity and the stoichiometric displacement parameter Z by much greater factors than do mutations in other areas of the molecule. Adsorption heterogeneity derived by fitting isotherms to the Hill equation is reduced by factors which reduce the overall affinity of adsorption. Van 't Hoff analyses gave uniformly positive enthalpies of adsorption, and mutational changes in adsorption enthalpy were relatively independent of the site of mutation. These results suggest that enthalpy does not play a dominant role in either affinity or selectivity of anion-exchange adsorption in this system.

1. Introduction

Ion-exchange chromatography is widely used for the high-resolution purification of proteins [1,2]. For optimal design of processes and adsorbents for protein ion exchange, it is desirable to have a clear understanding of the structural and thermodynamic factors governing its performance. Ion-exchange adsorption is conventionally regarded as requiring that the net charge

of the protein be opposite that of the exchanger. However, both neutral proteins and proteins with net charge of the same sign as the exchanger have been shown to adsorb in certain cases [3-6]. This is because the three-dimensional geometry of the protein sterically precludes all the charged residues contacting the ion-exchange surface simultaneously [7]. If the distribution of charged amino acids on the protein surface is sufficiently asymmetric, then electrostatic screening can make a cluster of charges on the protein surface a preferred chromatographic contact region which dominates adsorption behavior.

The phenomenon of "patch-controlled" adsorption was first predicted by Boardman and Partridge [8]. The first experimental demonstra-

* Corresponding author.

¹ Present address: Department of Surgery, Massachusetts General Hospital and Harvard Medical School, Boston, MA 02114, USA.

² Present address: Bioprocess R & D, Merck and Co., Inc., P.O. Box 2000, Rahway, NJ 07065, USA.

tion was provided by Brautigam et al. [9] using cation-exchange separation of chemically modified variants of cytochrome *c*. More recent work has clearly documented the adsorption of proteins with net charge equal to zero, or of the same sign as that of the ion exchanger [3–5]. Direct evidence of the dominant role of specific amino acid clusters in adsorption has been provided by chromatographic studies of charge mutant forms of single proteins [10–13]. The importance of local charge clusters has been further investigated by computational analysis [14,15]. We have also recently applied computational electrostatics modeling to understanding cytochrome *b*₅ adsorption [16].

We have characterized the anion-exchange adsorption of recombinant soluble rat cytochrome *b*₅ in order to test the contributions of specific amino acid residues to the thermodynamic driving forces for adsorption. We employed batch adsorption isotherm measurements under equilibrium conditions to avoid potential complications associated with flow systems. The equilibrium adsorption data support interpretation of the results in terms of thermodynamic driving forces. We have chosen conservative (carboxylate to amide) site-directed mutant forms to systematically examine the surface of cytochrome *b*₅ for preferred chromatographic contact region(s). Isotherm data were analyzed in several ways. Values for the equilibrium affinity parameter (*K*) were derived from Hill analysis [17] and were interpreted in terms of the stoichiometric displacement model of Kopaciewicz et al. [5] to obtain the apparent number of binding sites on the protein surface (*Z*). Hill analysis was also used to estimate the degree of heterogeneity of adsorption. Apparent enthalpies of adsorption were calculated using Van 't Hoff analysis.

2. Materials and methods

Recombinant soluble wild type rat cytochrome *b*₅ and its surface charge mutants were prepared in *Escherichia coli*. Synthetic genes for most of these proteins were the generous gift of Dr.

Stephen Sligar (see Ref. [18]). The E96Q mutation was introduced into the wild type gene by replacing an *Nru*I-*Eco*RI fragment of the gene with synthetic oligonucleotides as described elsewhere [19]. Proteins were purified by ion-exchange and size-exclusion chromatography, and characterized using sodium dodecyl sulfate–polyacrylamide gel electrophoresis (SDS-PAGE), spectrophotometry, and HPLC as described previously [18,20,21].

The monodisperse polymeric quaternary amine-based strong anion exchanger Mono Q (Pharmacia) was used as the adsorbent. It was equilibrated according to the manufacturer's protocol [22] and then recovered from fast protein liquid chromatography (FPLC) columns. The fresh, equilibrated Mono Q was used for initial adsorption experiments and then regenerated by washing with 50 volumes of high ionic strength buffer (10 mM Tris, pH 8.0 + 0.1 mM EDTA + 1.0 M NaCl) followed by washing (10 steps of 50 volumes each) with 10 mM Tris, pH 8.0 + 0.1 mM EDTA. The effectiveness of regeneration was confirmed by observation of the absorbance of the wash solution at 280 nm. Adsorption behavior was not observably affected by several cycles of regeneration after adsorption at low loading; the results reported here were obtained using adsorbent which had been regenerated in this manner.

Equilibrium batch adsorption experiments were performed in triplicate, as previously described [20]. Briefly, protein samples were equilibrated with the adsorbent in microcentrifuge tubes rotated at 3 rpm for 1 h. This period had been found in control experiments to be more than sufficient to ensure equilibration as judged by isotherm invariance. The tubes were completely filled with liquid to avoid protein denaturation at the gas–liquid interface. Samples were prepared in 10 mM Tris buffer adjusted to pH 8.0 in an environmental room at the experimental temperature and supplemented with NaCl to the desired concentration. Measurements were carried out at pH 8.0 to minimize the variability of ionization of weakly acidic and basic groups (histidine 19 and the termini) and to ensure that the surface charge was dominated by the highly

ionizable acidic groups of aspartic and glutamic acids in addition to heme propionates, and basic groups of lysine and arginine. At pH 8.0, far from their pK_a values, mutations made in these residues lead directly to a unit change in the net charge of the protein. Tris buffer was chosen because neither of its buffer species were expected to interact with the positively charged adsorbent. The amount of protein adsorbed was always less than 400 nmol protein per 10^8 adsorbent particles, less than 20% of the demonstrated capacity of Mono Q for cytochrome b_5 .

The amount of protein remaining in the supernatant after equilibration was calculated from the absorbance at 412 nm using the known molar absorbance in the strong cytochrome b_5 Soret band at this wavelength ($130 \text{ mM}^{-1} \text{ cm}^{-1}$; the oxidized form of the protein was used throughout). The amount of protein adsorbed was separately determined by elution of adsorbed protein with 10 mM Tris, pH 8.0 + 0.5 M NaCl over 1 h. Salt at this concentration was found to achieve quantitative elution within 30 min, and also did not alter the molar absorbance of the protein. An explicit mass balance on the free and adsorbed protein was calculated for each sample to control for the potentially confounding effects of denaturation, proteolysis, incomplete elution, etc. Mass balances for all experiments reported here closed to within 5%. Some of the cytochrome b_5 mutants were found to be less tightly adsorbed to Mono Q than was the wild type protein under similar conditions. These mutants were studied over a range of salt concentrations (75 to 150 mM NaCl) extending to somewhat lower values than used for the wild type protein (100–175 mM).

Values for the equilibrium affinity parameter (K) were derived from Hill analysis [17]. Each K value reported here was derived from an isotherm defined by at least six points. The standard deviations reported were calculated from the results of triplicate experiments. Values of the stoichiometric displacement parameter Z were obtained through linear least squares fits of $\log K$ versus \log (reciprocal ionic strength) for four salt concentrations. Van 't Hoff enthalpies of adsorption were calculated from fits of $\log K$

versus reciprocal absolute temperature for at least five temperatures in the range of 4 to 37°C.

The mutations studied in this work were chosen based on the high-resolution X-ray structure determined for cytochrome b_5 [23]. The mutations used were conservative, with typically a single negatively charged aspartic or glutamic acid residue at the surface mutated to the corresponding neutral amide (asparagine or glutamine). An important consideration was that mutant forms of cytochrome b_5 be used that were not structurally different from the wild type protein. Characterization of rat cytochrome b_5 and its mutants by two-dimensional NMR indicates that none of the mutations studied induces any significant change in the tertiary structure of the protein [24], with the exception of the double mutant E47,48Q. Mutating residue 47 to glutamine abolishes a salt link to Arg51, which may perturb the local structure of the protein [25]. It should also be noted that mutants E82Q and E96Q have not been subjected to characterization by NMR. As discussed below, the acidic residue at each of these positions is thought to be involved in one or more salt bridges whose disruption may alter the local tertiary structure.

Selection of mutants was based on examination of the structure of cytochrome b_5 using the molecular graphics utilities in QUANTA (version 3.2) and CHARMM 20.3 (Polygen) on a Silicon Graphics 4D/20 workstation. Although no complete structural determination for rat cytochrome b_5 is yet available, nearly complete high-resolution coordinates for the crystal structure of the 93% homologous bovine protein are available through the Brookhaven Protein Data Bank [23]. We have recently reported [26] a homology model for rat cytochrome b_5 based on the bovine cytochrome b_5 structure. The missing termini were added to the core in configurations derived from the coordinates of homologous proteins identified by an exhaustive search of the Brookhaven Protein Data Bank. The six amino acid differences between the bovine and rat proteins occur at the surface, and are largely conservative. These mutations were built into the bovine protein, and the resulting structure explicitly solvated (a 10 Å annulus consisting of

942 TIPS3P waters) and minimized over 500 steps of the adopted-basis Newton–Raphson algorithm. The homology-based model structure provided a basis for selection of mutants for this study as well as interpretation of the results, as described below.

The solvent-accessible surface of cytochrome b_5 displays several clusters of negative charges. The assignment of residues to clusters depends on the cutoff radius used. Based on a $C\alpha$ to $C\alpha$ distance of ca. 5.0 Å, the clusters of two or more charges on wild type cytochrome b_5 are: (1) Glu14 and Glu15; (2) Glu41, Glu42 and Glu47; (3) Glu47, Glu48 and Glu52; (4) Glu60, Glu63 and Asp64; and (5) Asp70 and Glu73 (see Fig. 1). The protoporphyrin propionates may contribute to adsorbent interactions involving residues Glu47, Asp70 and others nearby. Additional

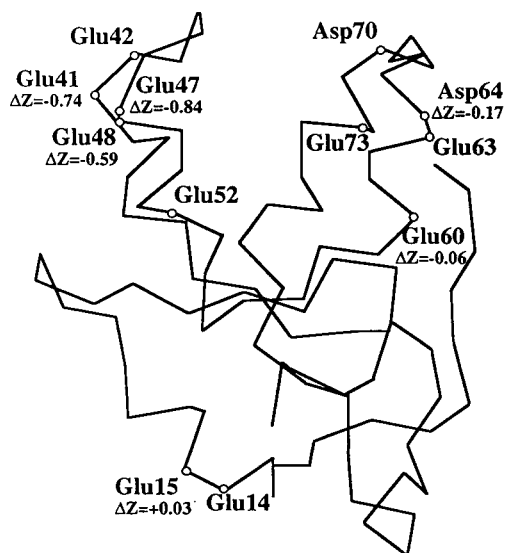


Fig. 1. $C\alpha$ trace of the three-dimensional structure of rat cytochrome b_5 (see Ref. [26]) depicting the distribution of negative charge on the protein surface. Only surface charges in clusters of two or more are shown. The molecule is oriented with the N-terminus on the right and the heme-binding pocket shown as the open area at the top of the diagram. Circles represent positions of negatively charged amino acids where substitutions were studied. Wild type residues are labeled using the three-letter code for amino acids. ΔZ is the difference in the value of the stoichiometric displacement parameter Z relative to that for the wild type protein.

charge is contributed by carboxylic acid residues which are not clustered with any patch and/or which are salt linked with positive residues, as discussed below. Although it was difficult to predict a priori whether a given part of the protein surface would prove to be a preferred chromatographic contact region, the major clusters were targeted by the mutations initially used. We avoided mutations in residues salt-bridged with neighboring, positively charged amino acids (i.e., Glu47–Arg51, Glu63–Arg72) as these would be only partially available to interact coulombically with the ion-exchange surface. Except for E47,48Q, all mutations studied were single carboxylate-to-amide substitutions (Table 1).

3. Results and discussion

Values of the Hill affinity constant (K) at 25°C in the presence of 100 mM NaCl, the apparent number of contacts estimated from the salt-dependence of adsorption using the stoichiometric displacement model (Z), and Van 't Hoff enthalpies of adsorption (ΔH_{ads}) are shown in Table 1. The values given for K , Z and ΔH_{ads} for the wild type protein have been reported previously [20].

The largest clusters of negative charge on rat cytochrome b_5 are two groupings of three negative charges, one on each side of the heme-binding pocket (Fig. 1). Residues 41, 47 and 48 comprise a cluster located at one end of the heme plane while residues 60, 63 and 64 lie on the other side (Fig. 1). If any cluster functions as a chromatographic contact region in anion-exchange adsorption, mutations that neutralize one or more of the negative charges in the cluster would be expected to reduce the observed Z number and adsorption affinity. From Table 1, it can be seen that compared to the wild type protein ($Z = 2.92$), the single-charge mutants E41Q and E48Q show reductions of Z by 0.74 and 0.59, respectively, and also produce the largest reductions in adsorption affinity at 100 mM NaCl. Each of these mutations affects residues lying in the major cluster composed of

Table 1

Values of the Hill binding constant K , stoichiometric displacement parameter Z , and Van 't Hoff enthalpy of adsorption ΔH_{ads} for adsorption of wild type cytochrome b_5 and its mutants on Mono Q in 0.010 M Tris buffer at pH 8.0

Protein	K	Z	ΔZ	ΔH_{ads} (kcal/mol)	$\Delta\Delta H_{\text{ads}}$ (kcal/mol)
Wild type	0.081 ± 0.002	2.92 ± 0.32	0.00 (0.0)	2.87 ± 0.26	0.00
E41Q ^a	0.032 ± 0.005	2.18 ± 0.27	-0.74 (-1.0)	2.51 ± 0.47	-0.36
E48Q	0.020 ± 0.000	2.33 ± 0.34	-0.59 (-1.0)	2.44 ± 0.52	-0.43
E47,48Q	0.016 ± 0.001	2.08 ± 0.42	-0.84 (-2.0)	2.51 ± 0.60	-0.36
E15Q	0.100 ± 0.002	2.95 ± 0.25	0.03 (-1.0)	2.32 ± 0.37	-0.55
E60Q	0.046 ± 0.001	2.86 ± 0.05	-0.06 (-1.0)	2.49 ± 0.25	-0.38
D64N	0.051 ± 0.000	2.75 ± 0.33	-0.17 (-1.0)	2.40 ± 0.28	-0.47

Reported values of Hill binding constants ($K \pm \text{S.D.}$) were measured at 25°C in buffer containing 0.100 M NaCl. Values of Z were obtained by linear regression of $\log K$ versus $\log (1/[\text{NaCl}])$; values obtained at 25°C are shown. ΔH_{ads} values were calculated from a Van 't Hoff linear regression of $\log K$ versus $1/T$ for at least five temperatures in the range 4–37°C. Z and ΔH_{ads} values for wild type cytochrome b_5 are from Ref. [20]. ΔZ denotes the difference of the Z value for the mutant from Z obtained for the wild type protein. Numbers in parentheses beside the ΔZ values indicate the expected change in net charge for the given mutation, as compared to the wild type protein (see Ref. [16]). $\Delta\Delta H_{\text{ads}}$ are the differences from the wild type ΔH_{ads} . The reported standard deviations were calculated from the results of triplicate experiments.

^a In naming the variants the single-letter amino acid code for the wild type carboxylate residue is followed by the position of the amino acid, followed by the single-letter amino acid code for the new amide residue. For example, E41Q indicates that glutamic acid (E) in position 41 was mutated to glutamine (Q). D = Aspartic acid; N = asparagine.

residues 41, 47 and 48. In contrast, neutralization of Glu15 at the N-terminus of the protein produces no statistically significant change in the value of Z , and appears to slightly *increase* the affinity of adsorption at 100 mM NaCl. Neutralization of Asp64 or Glu60 in the secondary charge cluster produces an intermediate change in the values of Z and K . These results strongly imply that the major charge cluster plays a dominant role in adsorption of the protein.

The observed values of Z reflect fractional contributions from multiple charged residues, rather than a direct correspondence between Z and the number of charged residues in a particular cluster. No single mutation in the major contact region produces a change in Z of more than -0.74. The double mutant E47,48Q shows a reduction in Z value of -0.84, well below the $\Delta Z = -2.0$ expected from unit contributions by dominant contact residues. The further reduction in Z produced by incorporating the E47Q mutation into the E48Q protein ($\Delta\Delta Z = -0.25$) is larger than the change produced by the first mutation in other charge clusters. This behavior presumably reflects the continued importance of

this cluster in adsorption even after deletion of one charge by mutation. The small ΔZ produced by the second mutation also illustrates the lack of a one-to-one correspondence between Z and the number of residues interacting with the adsorbent surface.

The differences in Z number between proteins bearing mutations in the apparent major contact region (E41Q and E48Q) and proteins bearing mutations outside this region (E15Q, E60Q, D64N) are larger than the sum of the standard deviations of the individual values (Table 1). The complex nature of the measurement procedure, however, introduces more scatter than one would prefer. Further limitations arise from the fact that the largest ΔZ expected for single substitutions is only -1.0. Double or triple substitutions would increase the expected difference, but would risk perturbing the tertiary fold of the protein. These measurements do show reduced scatter compared to the first (and only other) study to report Z numbers measured using equilibrium adsorption experiments [27]. The principal conclusions drawn from the ΔZ values are supported by the disproportionate

responsiveness of binding affinity (K) to mutations in this region. In addition, the present results are in good agreement with (significantly lower scatter) Z values for this system derived from our independent HPLC studies of a partially overlapping set of mutants [28]. Thus, structural data derived from site-specific mutagenesis suggest that the region surrounding glutamic acid residues 41, 47, and 48 is the preferred chromatographic contact region for the anion-exchange adsorption of cytochrome b_5 .

In order to cover the surface of the protein as completely as possible, we also considered two mutations believed potentially to alter the structure of the protein. The first of these was E82Q in the carboxy end of the protein, away from any of the charge clusters mentioned above. Unlike other mutations studied, residue 82 is not completely solvent accessible, but is partially buried (14 \AA^2 solvent accessible surface area, measured with a 1.4 \AA probe radius, as compared to an average of 92 \AA^2 accessible area for the residues discussed above). Limited studies of the adsorption behavior of the E82Q protein revealed a moderate reduction in binding affinity and a large change in the apparent stoichiometry of binding ($K = 0.068$; $\Delta Z = -1.03$). The structure of cytochrome b_5 suggests that Glu82 participates in a double salt bridge with Lys32 (3.7 \AA average distance between carboxylate oxygens of Glu82 and amino nitrogens of Lys32) as well as with Arg88 (3.6 \AA). We speculate that these salt links act to stabilize this region of the protein, and their abolition may disrupt the secondary structure in the C-terminus of the protein, producing the observed changes in adsorption behavior. It is also possible that Glu82 could be involved in an alternative chromatographic contact region, but this possibility is disfavored by the absence of clustered negative charges and the proximity of the positively charged residues Lys32 and Arg88. We observed similar behavior with a mutant in which Glu96, which also lies mainly in the interior of the protein (4 \AA^2 solvent accessible surface area), is mutated to glutamine. This protein gave $K = 0.031$, $\Delta Z = -1.33$. A change in the protein's conformation as a result of this mutation is indicated by a reduced value

of R_z , the ratio of molar absorbances at 412 nm and 280 nm. This value, a commonly used index of structural integrity for cytochromes, is only 5.0 for E96Q as compared with over 5.6 for pure wild type protein.

The Van 't Hoff enthalpies of adsorption (ΔH_{ads}) of the wild type and mutant proteins are uniformly positive (Table 1). For spontaneous, high-capacity adsorption (ΔG_{ads} negative), positive enthalpies of adsorption imply an entropic driving force. This increase in entropy could arise from liberation of ions or waters of solvation, from either the ion-exchange surface or the protein. Values of $\Delta\Delta H_{\text{ads}}$ of mutation range from -0.36 to -0.55 kcal/mol ($1 \text{ cal} = 4.184 \text{ J}$) (13 – 19% of the wild type ΔH_{ads}), with no statistically significant dependence on the location of the mutation. These results show that the enthalpy of adsorption does not control either the affinity or the selectivity of adsorption in this system, under the conditions studied.

The heterogeneity index (n_{H}) calculated from Hill regression of equilibrium adsorption isotherm data was used to assess the uniformity of protein adsorption. Table 2 presents values of n_{H} calculated from 25°C adsorption isotherms measured at various ionic strengths. As noted above, the range of ionic strengths at which adsorption affinity is reliably measurable varies among the mutant proteins. Therefore, n_{H} data are available for each mutant only at a subset of the NaCl concentrations studied. The value of n_{H} is substantially below unity for all cases examined, implying that apparent adsorption affinity decreases with protein loading. A similar conclusion can be reached from a Scatchard analysis of isotherm data, and has been drawn in our previous work on the adsorption of wild type cytochrome b_5 , and by others [27,29].

The effects of mutation on adsorption heterogeneity provide insight into the sources of heterogeneity. In the interest of brevity, we discuss in detail only the data collected at 100 mM NaCl; similar conclusions follow from the results obtained under other conditions. At 100 mM NaCl, the n_{H} value for the wild type protein is 0.32 ± 0.02 . Mutations E15Q, E60Q and D64N, which affect residues outside the dominant chro-

Table 2

Hill heterogeneity indices of adsorption of cytochrome *b*₅ variants on Mono Q as a function of added NaCl concentration in 10 mM Tris buffer, pH 8.0 at 25°C

Protein	Hill heterogeneity index					
	0.05 M NaCl	0.075 M NaCl	0.1 M NaCl	0.125 M NaCl	0.15 M NaCl	0.175 M NaCl
Wild type	ND	ND	0.32 ± 0.02	0.46 ± 0.03	0.70 ± 0.03	0.82 ± 0.11
E41Q	ND	0.33 ± 0.01	0.51 ± 0.05	0.64 ± 0.05	0.84 ± 0.05	ND
E48Q	0.28 ± 0.08	0.35 ± 0.06	0.46 ± 0.09	0.79 ± 0.09	0.88 ± ND	ND
E47,48Q	0.25 ± 0.00	0.40 ± 0.00	0.59 ± 0.02	0.77 ± 0.05	ND	ND
D64N	ND	ND	0.35 ± 0.01	0.49 ± 0.03	0.71 ± 0.05	0.81 ± 0.04
E60Q	ND	ND	0.42 ± 0.01	0.60 ± 0.01	0.79 ± 0.01	0.92 ± 0.03
E15Q	ND	ND	0.36 ± 0.00	0.52 ± 0.03	0.71 ± 0.01	ND

Calculated from linear regression of adsorption isotherm data using the Hill equation (see Ref. [16]). The salt concentrations used with each variant were selected according to its adsorption behavior, as described in the text. ND = Not determined.

matographic contact region, produce relatively small changes in heterogeneity (average $n_H = 0.37$, range 0.35–0.42). The n_H values for mutants E41Q and E48Q in the primary contact region are significantly higher at 0.51 and 0.46, respectively; n_H is 0.59 ± 0.02 for the double mutant E47,48Q. In general, therefore, n_H values are most increased (heterogeneity is most reduced) for those mutants where the amino acid substitution affects *K* (and *Z*) most significantly.

Heterogeneity of protein ion-exchange adsorption can arise from heterogeneous protein orientation on uniform adsorbent sites, and/or an intrinsically heterogeneous population of adsorbent sites. We discount the possible role of lateral protein–protein interactions in the present work as all data were collected at low surface coverage. It should be noted, however, that proteins could be brought close enough to interact, even at low loadings, by heterogeneous site distribution. Heterogeneous protein adsorption on uniform adsorbent sites would involve competition among binding orientations of differing affinities. Mutations reducing charge within the preferred contact region would create a more equal competition among possible orientations. This could increase heterogeneity by allowing significant occupation of a larger set of orientations. Alternatively, in the absence of any large redistribution of protein molecules among adsorbed states, it could reduce heterogeneity by

making the populated orientations more energetically similar. Only the latter possibility is consistent with our observations, as heterogeneity is reduced (n_H increased) by all mutations tested, and most effectively reduced by mutations in the contact region.

Adsorption heterogeneity could also reflect an intrinsically heterogeneous population of sites on the adsorbent. Such heterogeneity is to be expected from the irregular topography of the hydrophilic adsorbent surface, and from the random chemical derivatization by which charges are introduced. Heterogeneity from this source would be reduced by factors which restrict the energetic diversity of sites occupied under experimental conditions, such as mutation, or changes in temperature and in ionic strength. (These factors could produce reorganization of the surface as well as reducing the overall affinity of adsorption, although the linear nature of the Van 't Hoff and stoichiometric displacement plots argues against this interpretation). The reduction in heterogeneity produced by mutations in the contact region could be ascribed to a reduction in the protein's intrinsic affinity for the surface, leading to disqualification of some sites previously acceptable by the (wild type) protein. This model is also consistent with the reduced heterogeneity observed at higher NaCl concentrations and at lower temperatures. Under each of these conditions the overall affinity is reduced,

and a smaller population of sites is expected to be energetically acceptable.

4. Conclusions

In this work we have systematically used site-directed mutant forms of cytochrome b_5 to study the structural and thermodynamic elements of protein ion-exchange adsorption. This has also allowed us to put the widely accepted stoichiometric displacement model to a rigorous test under equilibrium conditions for the first time. Our results show that the stoichiometric displacement model can effectively correlate adsorption data for this small globular protein under the low surface coverage conditions tested.

We have identified a major cluster of negative charges on the protein surface as a probable adsorbent contact region, mutations within which produce disproportionately large reductions in affinity and in the stoichiometric displacement parameter Z . Van 't Hoff analysis shows that the enthalpy of adsorption is positive (unfavorable) and is also relatively unresponsive to mutations which greatly alter adsorption affinity. For ion-exchange adsorption in this system, therefore, enthalpy does not play a dominant role in the affinity or the selectivity of adsorption. Analysis of the changes in the apparent heterogeneity of adsorption produced by mutations and by variations in ionic strength suggests the possible roles of orientation and site heterogeneity in protein adsorption. Further work, however, will be required for a complete understanding of these phenomena.

Acknowledgements

We thank Drs. Stephen Sligar and Karla Rodgers of the University of Illinois for providing us with genes for cytochrome b_5 mutants and for helpful discussions; Drs. Mario Pires and Joaquim Cabral at Instituto Superior Tecnico, Lisbon for collaboration in constructing the E96Q mutant; Dr. Tom Pochapsky of Brandeis

University for helpful information on his characterization of the cytochrome b_5 mutants by two-dimensional NMR, and Rene Ochoa, Colin Johnston and Henry Chang for skillful assistance in the experiments. This work was supported by NSF grant CTS-8910087 and by an NSF Presidential Young Investigator Award to R.C.W. We also gratefully acknowledge the support of the 3M corporation, Pharmacia, and the Waters division of Millipore Corporation.

References

- [1] J. Bonnerjea, S. Oh, M. Hoare and P. Dunnill, *Bio/Technology*, 4 (1986) 954.
- [2] R.C. Willson and M.R. Ladisch, in M.R. Ladisch, R.C. Willson, C.C. Panton and S.E. Builder (Editors), *Protein Purification: From Molecular Mechanisms to Large-Scale Processes*, American Chemical Society, Washington, DC, 1990, p. 1.
- [3] R. Scopes, *Anal. Biochem.*, 114 (1981) 8.
- [4] L.A. Haff, L.G. Fagarstam and A.E. Barry, *J. Chromatogr.*, 266 (1983) 409.
- [5] W. Kopaciewicz, M.A. Rounds, J. Fausnaugh and F.E. Regnier, *J. Chromatogr.*, 266 (1983) 3.
- [6] E. Ruckenstein and V. Lesins, *J. Colloid Interface Sci.*, 132 (1989) 566.
- [7] F.E. Regnier, *Science*, 238 (1987) 319.
- [8] N.K. Boardman and S.M. Partridge, *Biochem. J.*, 59 (1955) 543.
- [9] D.L. Brautigan, S. Ferguson-Miller and E. Margoliash, *J. Biol. Chem.*, 253 (1978) 130.
- [10] J. Fausnaugh-Pollitt, G. Thevenson, L. Janis and F.E. Regnier, *J. Chromatogr.*, 443 (1988) 221.
- [11] R.M. Chicz and F.E. Regnier, *J. Chromatogr.*, 443 (1988) 193.
- [12] R.M. Chicz and F.E. Regnier, *Anal. Chem.*, 61 (1989) 2059.
- [13] M.H. Heng and C.E. Glatz, submitted for publication.
- [14] A.N. Hodder, K.J. Machin, M.I. Aguilar and M.T.W. Hearn, *J. Chromatogr.*, 517 (1990) 317.
- [15] L. Haggerty and A.M. Lenhoff, *J. Phys. Chem.*, 95 (1991) 1472.
- [16] D.J. Roush, D.S. Gill and R.C. Willson, *Biophys. J.*, 66 (1994) 1290.
- [17] A.V. Hill, *J. Physiol. (London)*, 40 (1910) iv.
- [18] S.B. von Bodman, M.A. Schuler, D.R. Jollie and S.G. Sligar, *Proc. Natl. Acad. Sci. U.S.A.*, 83 (1986) 9443.
- [19] M.J. Pires, P.T. Martel, A. Baptista, S.B. Petersen, R.C. Willson and J.M.S. Cabral, submitted for publication.
- [20] D.S. Gill, D.J. Roush and R.C. Willson, *J. Colloid Interface Sci.*, in press.

- [21] D.J. Roush, D.S. Gill and R.C. Willson, *J. Chromatogr. A*, 653 (1993) 207.
- [22] *Ion-Exchange Chromatography: Principles and Methods*, Pharmacia LKB Biotechnology, Uppsala, 1987.
- [23] F.S. Mathews, M. Levine and P. Argos, in D. Dolphin (Editor), *The Porphyrins*, Vol. VIIB, Academic Press, New York, 1979, p. 107.
- [24] K.K. Rodgers, T.C. Pochapsky and S.G. Sligar, *Science*, 240 (1988) 1657.
- [25] F.S. Mathews and E.W. Czerwinski, in A.M. Martonosi (Editor), *The Enzymes of Biological Membranes*, Vol. 4, Plenum, New York, 1983, Ch. 52, p. 235.
- [26] D.S. Gill, D.J. Roush and R.C. Willson, *J. Biomolec. Struct. Dynam.*, 11 (1994) 1.
- [27] R.D. Whitley, R. Wachter, F. Liu and N.-H.L. Wang, *J. Chromatogr.*, 465 (1989) 137.
- [28] D.J. Roush, D.S. Gill and R.C. Willson, in preparation.
- [29] R. Janzen, K.K. Unger, W. Muller and M.T.W. Hearn, *J. Chromatogr.*, 522 (1990) 93.



ELSEVIER

Journal of Chromatography A, 684 (1994) 65-75

JOURNAL OF
CHROMATOGRAPHY A

Separation of arachidonic acid metabolites by on-line extraction and reversed-phase high-performance liquid chromatography optimized by computer simulation

H. Fritsch^a, I. Molnar^b, M. Wurl^{c,*}

^aSolvay Pharma France, Department of Pharmacology, B.P. 25, F-01400 Chatillon-sur-Chalaronne, France

^bMolnar-Institut, Blücherstrasse 22, D-10961 Berlin, Germany

^cSolvay Pharma Deutschland GmbH, Department of Cardiovascular Research, Hans-Böckler-Allee 20, D-30173 Hannover, Germany

First received 26 January 1994; revised manuscript received 9 June 1994

Abstract

A complex mixture of arachidonic acid metabolites was separated by reversed-phase HPLC using a multi-step gradient, which was modelled by computer-assisted HPLC method development. The metabolites were extracted on-line on a precolumn connected to the analytical column in the same HPLC system. The predictions of the resolution and also the retention times calculated by computer simulation were very accurate when compared with the corresponding experimental run (maximum deviation 0.86%). An appropriate HPLC method and additionally an on-line extraction procedure could be developed with just three experimental HPLC runs. This method could be useful for evaluating the concentrations of arachidonic acid metabolites involved in inflammatory diseases.

1. Introduction

Arachidonic acid (20:4) is one of the major lipid constituents of cell membranes, which can be converted into a variety of extremely potent mediators exhibiting important physiological roles [1,2]. For example, 20:4 can be metabolized to 5-hydroperoxyeicosatetraenoic acid (5-HPETE) by 5-lipoxygenase, which is primarily found in cells of the immune system. 5-HPETE is further converted either into leukotriene A₄ (LTA₄) via 5-lipoxygenase [3] or into 5-hydroxyeicosatetraenoic acid (5-HETE) by unspecific peroxidases [4]. Leukotriene A₄ is further me-

tabolized in two ways: (i) in human polymorphonuclear granulocytes (PMN) to leukotriene B₄ (LTB₄) which possesses chemotactic activity to PMN [5] and (ii) in mast cells and basophilic granulocytes to vasoconstrictive leukotrienes C₄, D₄, E₄ (LTC₄, D₄, E₄) [6,7]. In addition to these pathways, 20:4 is converted into 12-hydroperoxyeicosatetraenoic acid [12-H(P)ETE] by 12-lipoxygenase in human platelets [8,9] or porcine leukocytes [10]. Further, in PMN from various species 20:4 can be converted into 15-hydroperoxyeicosatetraenoic acid [15-H(P)ETE] [11,12], which can be further metabolized to biological active lipoxins [13].

Reversed-phase high performance liquid chromatography (RP-HPLC) has become a powerful

* Corresponding author.

tool for the separation of 20:4 metabolites from biological samples [14–17]. When investigating 20:4 metabolites it is highly desirable to examine a complex mixture of leukotrienes (LTs), hydroxyeicosatetraenoic acids (HETEs) and lipoxins. In order to resolve 20:4 metabolites from biological samples they have to be extracted prior to separation by HPLC. Various extraction techniques have been investigated such as solid-phase extraction and procedures with cartridges containing octadecylsilica (ODS) as the stationary phase [18–20] or liquid–liquid extraction with ethyl acetate [21] or diethyl ether [22]. The main disadvantage of these time-consuming techniques is the low recovery. Therefore, in recent studies on-line extraction methods have been investigated [23,24]. This approach is very effective in terms of the time reduction required for the analysis of samples. It also yields more reliable results as sample loss and deterioration could be excluded. Nevertheless, all of these procedures need additional equipment that is not available in most laboratories and additional time in HPLC method development.

For the development of a reversed-phase gradient method, technical experience with HPLC is necessary in order to establish appropriate separation conditions with a minimum of effort and time. Many experimental chromatograms have to be obtained in order to optimize the stationary phase, the mobile phase and the appropriate temperatures.

Taken together, every individual step during optimization needs a single chromatogram to be obtained without the prospect of success. To minimize the time for method development, without experimentally changing columns and mobile phases, the computer-assisted HPLC optimization program Drylab/Windows has been developed [25]. The software simulates experimental HPLC traces after entering the results of only two experimental runs. Completely new experimental conditions can be modelled. It is able to calculate the influence of gradient compositions for different column conditions with respect to column diameter, column length, particle size, temperature and flow-rate. Poor resolution of bands as a result of unsuitable

elution conditions can be monitored early without wasting time on optimization. Finally, the optimum HPLC separation conditions simulated can usually be confirmed by one final experimental run.

The aim of this work was to develop an on-line extraction HPLC method for the detection of a complex mixture of arachidonic acid metabolites, without additional equipment, using Drylab for optimization.

2. Experimental

2.1. Standards

Prostaglandin B₂, LTB₄, 20-OH-LTB₄, 20-COOH-LTB₄, 6-*trans*, 12-*epi*-LTB₄, all-*trans*-LTB₄, 12-HETE, 15-HETE, 5-HETE, and 5-HPETE were obtained from Cayman Chemicals (Ann Arbor, MI, USA). A mixture of the above 20:4 metabolites was diluted to a final concentration of 1 µg/ml in ethanol [cleaned by passing through SepPak C₁₈ solid-phase extraction columns (Waters/Millipore, Eschborn, Germany)]. The diluted mixture was thoroughly degassed with nitrogen in order to diminish the autooxidation of the 20:4 metabolites. Mobile phase components were of HPLC grade and purchased from Riedel-de Haën (Seelze, Germany). All other reagents were of analytical-reagent grade.

2.2. HPLC equipment

The mobile-phase delivery system consisted of a Sykam (Gilching, Germany) S1000 pump, an S2110 lower gradient mixer and an S4110 column oven. The S3300 UV detector was connected to an Axxiom integration system. For on-line extraction an Axxiom-controlled pneumatic switching valve (Rheodyne Model 7010) integrated into the column oven was used (Fig. 1). Sample injection was performed with an autosampler (Promis Spark-Holland, Friedrichsdorf, Germany). Drylab/Windows (LC Resources) was purchased from Molnar-Institut (Berlin, Germany).

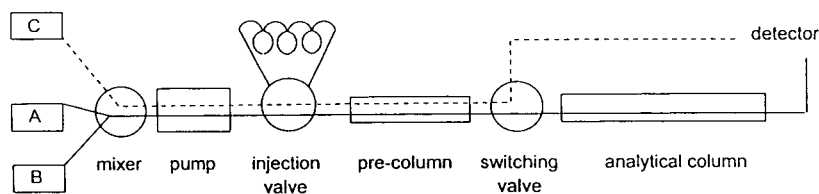


Fig. 1. Scheme of the apparatus used for on-line extraction RP-HPLC of lipxygenase products.

2.3. Procedures for on-line extraction

The precolumn of 3- μm Spherisorb ODS-2 (1×0.46 cm I.D.), (Grom, Herrenberg, Germany) was equilibrated with eluent C [acetonitrile–water–trifluoroacetic acid (TFA) (10:90:0.02 (v/v/v))] for 10 min. at a flow-rate of 1.5 ml/min at 40°C before injection. After injection of the sample (50 μl) the precolumn was eluted with eluent C at a flow-rate of 1.5 ml/min at 40°C for 10 min before the precolumn was automatically switched in front of the 3- μm Ultrasphere ODS highspeed analytical column (7.5×0.46 cm I.D.) (Beckman Instruments, Palo Alto, CA, USA). A mixture of 20:4 metabolites (30 ng each of 20-COOH-LTB₄, 20-OH-LTB₄, PGB₂, LTB₄, 15-HETE, 12-HETE, 5-HETE, 25 ng each of 6-*trans*, 12-*epi*-LTB₄ and 10 mg of all-*trans*-LTB₄ diluted in 100% ethanol) was eluted with different compositions of eluent A [acetonitrile–water–TFA (20:80:0.02 (v/v/v))] vs. eluent B [acetonitrile–methanol–water–TFA (75:22:3:0.02 (v/v/v))]. Leukotrienes were monitored at 270 nm and HETEs at 235 nm. Finally, the columns were re-equilibrated.

3. Results

3.1. Mobile phase optimization

In order to optimize the mobile phase for RP-HPLC methods using the computer, two initial experimental runs had to be performed. These two runs had to differ at least three-fold with respect to their gradient run times (t_G). Therefore, the first run was performed by injecting a mixture of 20:4 metabolites (for concen-

trations see Section 2.3) on to the precolumn, which was flushed with eluent C (on-line extraction) for 10 min prior to elution of the metabolites from the analytical column with a linear gradient from 10% to 95% eluent B in 30 min. The resulting chromatogram is shown in Fig. 2. The second experimental run was performed by eluting the same mixture with a 90-min linear gradient from 10% to 95% B after on-line extraction (Fig. 3). The operating variables of the gradient ranges, such as dwell volume, flow-rate, column width, length and number of bands, were entered into the corresponding menus of the mobile-phase optimization option (Drylab). Finally, the retention times and band areas were entered (Table 1).

3.2. Determination of system variables

For the prediction of gradient runs it was essential to determine the system dwell volume, V_D , which is the volume between the place of mixing A and B and the column inlet. The volume is responsible for the gradient delay, leading to different retentions of bands in different HPLC systems. The dwell volume was calculated by comparing an experimental run of 60 min with the prediction obtained by simulation. The dwell volume was changed manually in the Drylab options until the prediction of the retention times was close to those in the experimental run. The calculated value for the dwell volume of this HPLC system was $V_D = 3.4$ ml. Table 2 shows that following adaption of the dwell volume the maximum difference in retention time was less than 0.14 min for the bands of the 20:4 metabolite mixture.

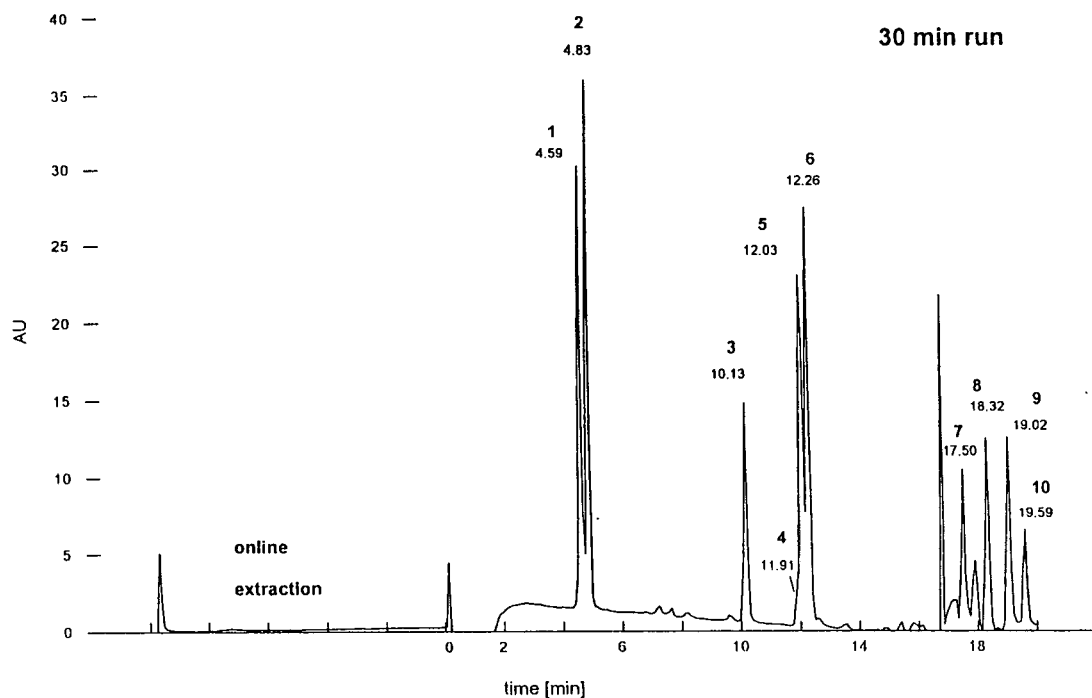


Fig. 2. Experimental chromatogram for the separation of a mixture of 20:4 metabolites (for concentrations and RP-HPLC method, see Experimental) with a linear gradient over 30 min. The gradient was excluded because the influence of the dwell volume could not be monitored by the chromatographic program.

3.3. Gradient optimization

In order to see how well the 20:4 metabolite mixture could be resolved by changing the values of %B/min during linear gradients without changing the mobile phase and the stationary phase, the k^* value calculated by Drylab had to be taken into account. The k^* value (see Eq. 1) affects the overall sample resolution and defines the retention behaviour of bands with respect to their chemical properties (S), the change in %B ($\Delta\phi$), the flow-rate (F), the column dead volume (V_m) and the gradient time (t_G). The k^* value depends on the above-mentioned parameters and therefore directly influences the resolution (R_s) of bands (Eqs. 2–4).

$$k^* = t_G F / (1.15 V_m \Delta\phi S) \quad (1)$$

$$k' = (t_R - t_0) / t_0 \quad (2)$$

$$\alpha = k' (\text{band 2}) / k' (\text{band 1}) \quad (3)$$

$$R_s = \frac{1}{4} (\alpha - 1) n^{0.5} [k^* / (k^* + 1)] \quad (4)$$

In order to obtain accurate separation of bands, k^* (Eq. 1) should be in the range of 5–20 kbar; $k^* < 5$ would lead to poor resolution as a result of the sample bands bunching together, whereas bands with $k' > 20$ are more widely separated and would lead to a decrease in sensitivity.

To monitor the quality of equal band spacing of the 30 and 90-min runs the software simulated a relative resolution map (RRM). The RRM provides information on the resolution of the poorest separated band pair vs. gradient time, based on a selected column plate number.

The resolution of bands 5 and 6 is, experimentally, $R_s = 1.1$ for a 90-min linear gradient. To obtain the same resolution in the software chro-

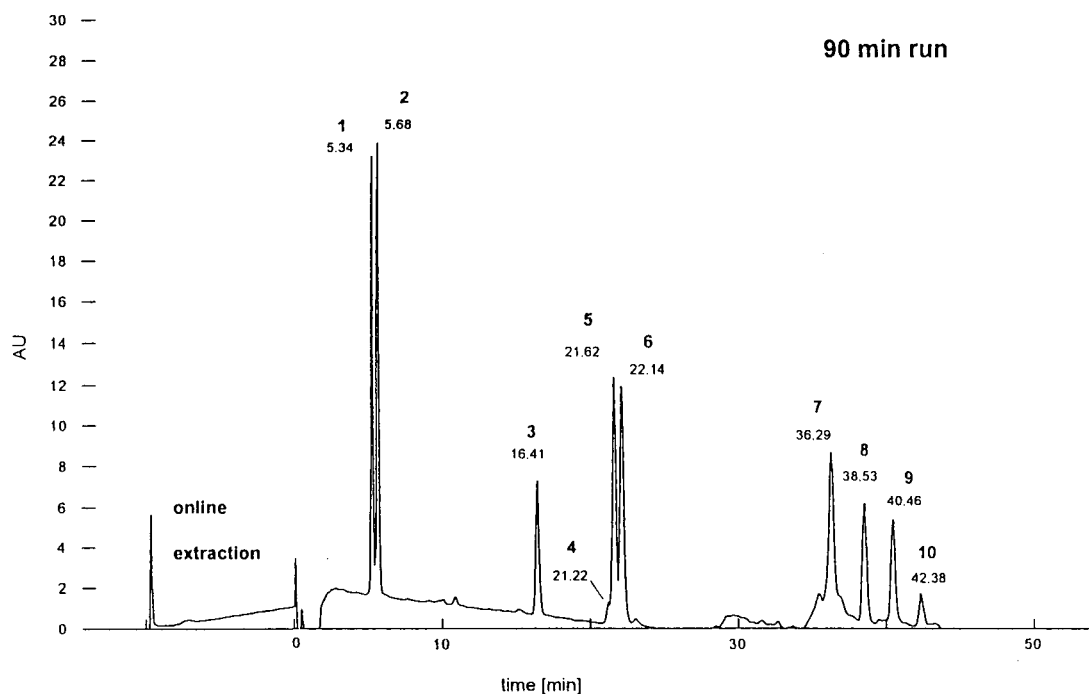


Fig. 3. Experimental chromatogram for the separation of a mixture of 20:4 metabolites (for concentrations and RP-HPLC method, see Experimental) with a linear gradient over 90 min.

matogram, a column plate number of $N = 6000$ was examined. All further calculations were based on a plate number of $N = 6000$.

The RRM provides evidence that the most critical band pair 4 and 5 (all-*trans*-LTB₄ and 6-*trans*, 12-*epi*-LTB₄) could be resolved maxi-

Table 1

Retention data for the separation of 20:4 metabolite mixture (for concentrations and HPLC method, see Experimental) using experimental linear gradients over 30 and 90 min

Peak No.	20:4 metabolite	Retention time (min)		Area (V min)
		30-min run	90-min run	
1	20-COOH-LTB ₄	4.59	5.34	1421
2	20-OH-LTB ₄	4.83	5.68	1431
3	PGB ₂	10.13	16.41	737
4	All- <i>trans</i> -LTB ₄	11.91	21.22	500
5	6- <i>trans</i> -12- <i>epi</i> -LTB ₄	12.03	21.62	1436
6	LTB ₄	12.26	22.14	1472
7	15-HETE	17.50	36.29	746
8	12-HETE	18.32	38.53	703
9	5-HETE	19.02	40.46	755
10	5-HPETE	19.59	42.38	359

Table 2

Differences in retention data based on an experimental 60-min linear gradient and Drylab-calculated retentions after adjustment of the system's dwell volume (for HPLC methods, see Experimental)

Peak No.	20:4 metabolite	Retention time (min)		
		DrylabG-predicted, 60-min run	Experimental, 60-min run	Predicted – experimental (min)
1	20-COOH-LTB4	5.12	4.98	0.14
2	20-OH-LTB4	5.41	5.32	0.09
3	PGB2	13.83	13.81	0.02
4	All-trans-LTB4	17.21	17.30	-0.09
5	6-trans-12-epi-LTB4	17.47	17.50	-0.03
6	LTB4	17.85	17.88	-0.03
7	15-HETE	27.71	27.71	0.00
8	12-HETE	29.26	29.24	0.02
9	5-HETE	30.59	30.56	0.03
10	5-HPETE	31.82	31.80	0.02

Optimum system dwell volume calculated by DrylabG = 3.4 ml.

mally by a factor of 0.83 for linear gradients (Fig. 4). Thus bands 4 and 5 could not be resolved using these separation conditions, as R_s has to exceed 1.5 for the resolution of adjacent peaks.

Changes in %B/min had only a marginal influence of the resolution of bands 5 and 6, (6-trans, 12-epi-LTB₄ and LTB₄) (Fig. 3). Hence the separation of bands 4–6 is not much affected by the gradient steepness. The remaining bands were less influenced by changes in %B/min.

3.4. Simulation of multi-segmented gradient runs

The gradient was theoretically performed in four steps starting with the isocratic elution of the metabolites after on-line extraction with 10% B for 1 min. Bands 1 and 2 were eluted shortly after the system dwell volume (dwell volume 3.425 ml = 2.28 min) and they were separated with a resolution $R_s = 1.87$ shortly after initiating the next step (see modelled chromatogram, Fig.

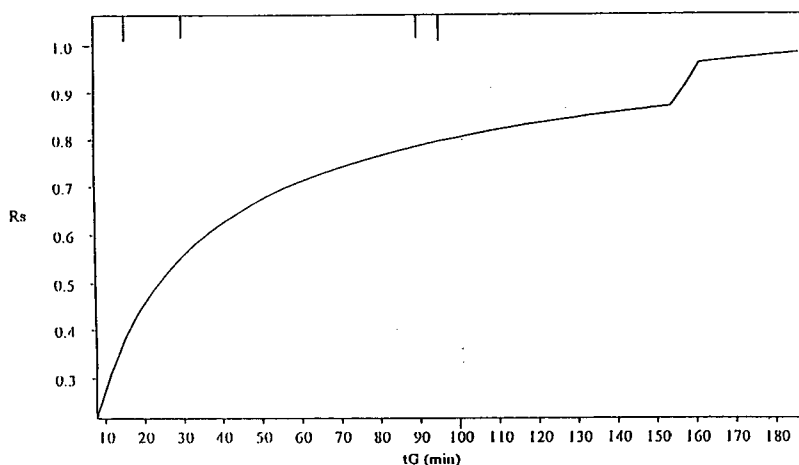


Fig. 4. Relative resolution map for bands 4 and 5 in the separation of the 20:4 metabolite mixture. The calculated resolutions (R_s) are based on the input data for 30- and 90-min linear gradients (t_G) from 10% to 90% B. For input data, see Table 1.

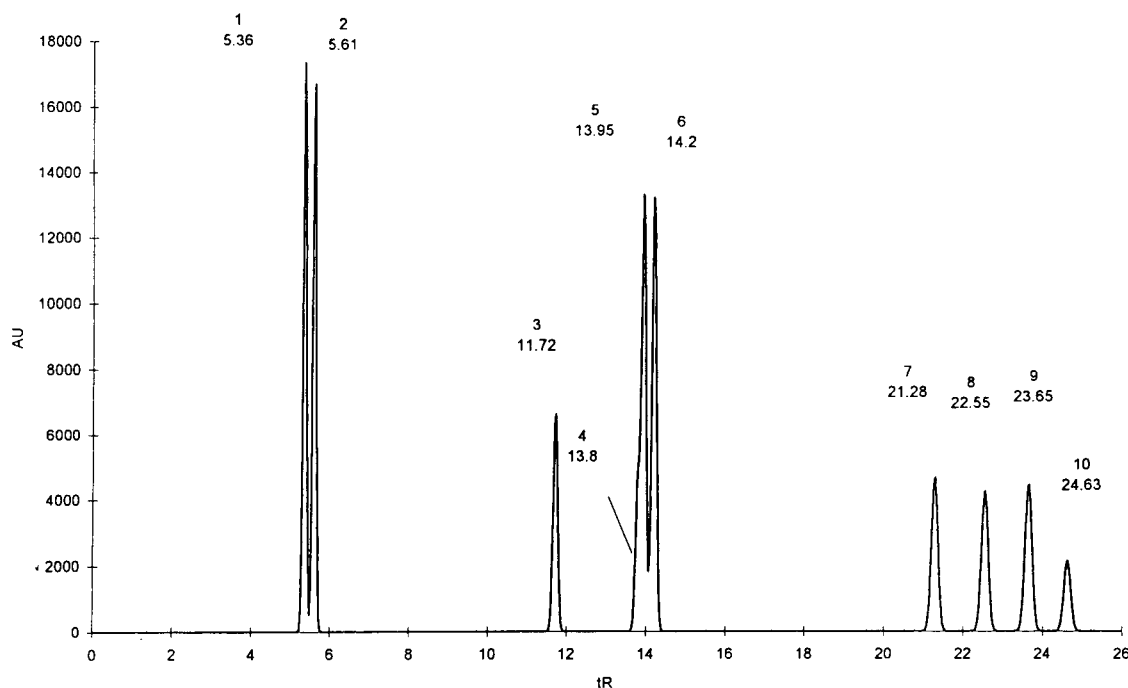


Fig. 5. Simulated chromatogram for the separation of 20:4 metabolite mixture based on a four-step gradient (for gradient, see Table 3).

5). This was achieved by changing from 10 to 37% B in 11 min. The slope of the %B/min change was flatter than for the 30-min linear gradient in order to obtain a better resolution of bands 4 and 5. During this gradient time band 3 eluted without overlapping bands (Fig. 5).

Bands 4 and 5 could only be resolved with $R_s = 0.85$. The system gave a non-baseline separation of these three peaks. However, the resolution was slightly better compared with the 30-min linear gradient run ($R_s = 0.62$). Bands 5 and 6 were only resolved with $R_s = 1.11$.

After the elution of leukotrienes and prostaglandins, the wavelength of the detector was changed to 235 nm in order to monitor eicosatetraenoic acids. This next gradient step was performed by an increase from 23% to 58% B in 13 min until all eicosatetraenoic acids were eluted. Finally, the column was cleaned with 95% B. Bands 7–10 were all eluted with a resolution of at least 2.89.

The last band was eluted with a retention time

of 24.66 min. Instead of a rapid increase of %B/min a more shallow gradient was selected for the elution of bands 7–10 in order to decrease the baseline drift after changing the detector wavelength to 235 nm. However, on comparing the resulting resolutions of bands 7–10 examined in the 90-min linear gradient with those in the four-step gradient, the conclusion was drawn that essentially the same resolution was obtained but the retention time was 20 min less. Hence about 30 ml less of mobile phase were needed to achieve the same resolution compared with the 90-min linear gradient run.

3.5. Predicted separation vs. experiment

Comparison of the chromatogram modelled by Drylab (Fig. 5) with the experimental run (Fig. 6) showed that the prediction was very close to the experimental data with a maximum deviation of 0.86% (Table 3).

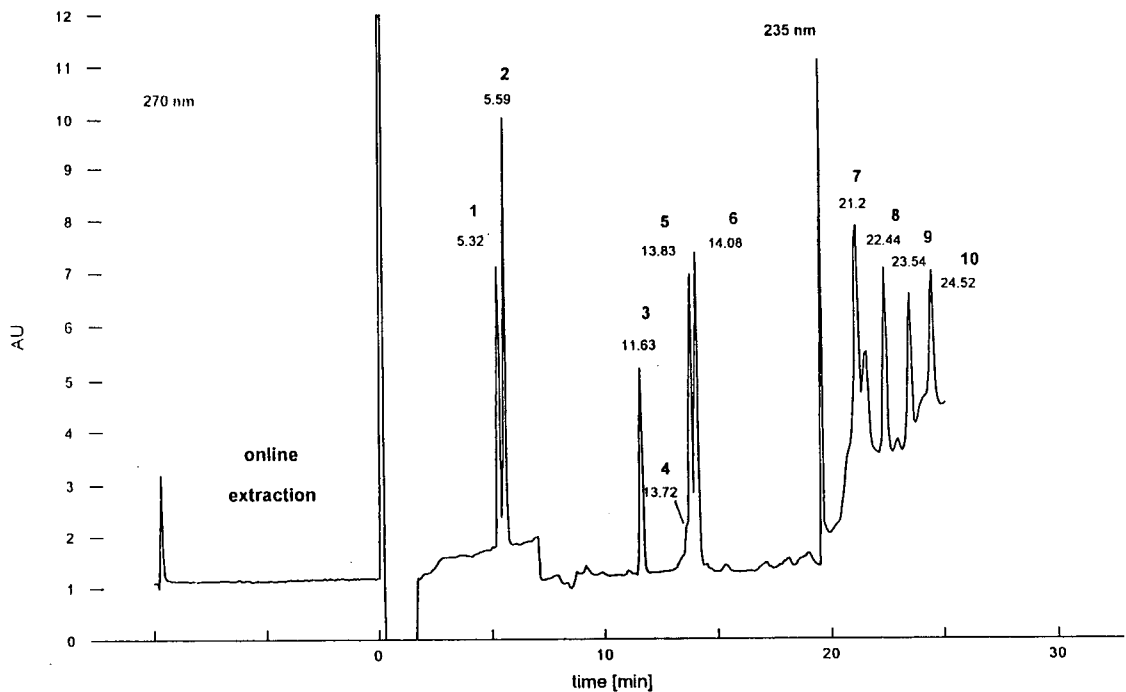


Fig. 6. Experimental chromatogram for the separation of a mixture of 20:4 metabolites (for concentrations and RP-HPLC method, see Experimental) with a four-step gradient (see Table 3).

4. Discussion

On-line extraction combined with RP-HPLC provides an efficient method for the analysis of

complex mixtures of 20:4 metabolites in a single run. This method can readily be used for automation, resulting in additional time saving. An important advantage of the on-line extraction

Table 3

Comparison and differences in retention data obtained from experimental and Drylab-calculated separation of 20:4 metabolites using a four-step gradient (0–1 min, 10% B; 1–12 min, 10–37% B; 12–25 min, 37–58% B; 25–26 min, 58–95% B)

Peak No.	20:4 metabolite	Retention time (min)		Difference, predicted – experimental (%)
		Experimental run	DrylabG-predicted	
1	20-COOH-LTB4	5.32	5.36	0.75
2	20-OH-LTB4	5.59	5.61	0.36
3	PGB2	11.63	11.72	0.77
4	All-trans-LTB4	13.72	13.80	0.58
5	6-trans-12-epi-LTB4	13.83	13.95	0.86
6	LTB4	14.08	14.20	0.85
7	15-HETE	21.20	21.28	0.38
8	12-HETE	22.44	22.55	0.49
9	5-HETE	23.54	23.65	0.47
10	5-HPETE	24.52	24.63	0.45

RP-HPLC is that the sample is transferred directly from the precolumn to the analytical column. Therefore, sample extraction procedures followed by evaporation of the eluent prior to injection are no longer necessary. This technique provides accurate method in order to save time and decrease sample losses and also to decrease sample deterioration (unpublished data). Additionally, the same precolumn could be used several times because it is always cleaned in connection with the analytical column.

The computer modelled very accurate predictions and was a rapid and reliable tool for optimizing the separation of a complex mixture of 20:4 metabolites.

Most of the 20:4 metabolites were well resolved using linear gradients. Nevertheless, the separation of three bands had to be optimized. These critical band pairs correspond to all-*trans*-LTB₄ (band 4), 6-*trans*, 12-*epi*-LTB₄ (band 5), which are non-enzymatic hydrolysis products of LTA₄, and the main LTA₄-hydrolase product LTB₄ (band 6). The structures of these LTs are closely related. All three stereoisomeric compounds are hydroxylated at positions 5 and 12 of the arachidonic acid. The conformational structures of these leukotrienes, however, differ: 5(*S*),12(*S*)-DiHETE = 6-*trans*, 12-*epi*-LTB₄, 5(*S*),12(*R*)-DiHETE with a *trans* conformation = all-*trans*-LTB₄, and 5(*S*),12(*R*)-DiHETE with a *cis* conformation = LTB₄.

The retention behaviour and band width of biological samples are influenced by the chemical properties of the sample [26,27]. All injections were performed with acidic samples in order to protonate the 20:4 metabolites and to exclude silanol interactions, which affect the separation. Parameters such as the ionic strength of the mobile phase and the ionic strength of the samples cannot be entered for column optimization by Drylab. However, the predicted resolutions, after changing the column plate number in Drylab, were close to the calculated resolutions from the experimental run. As LTB₄ (band 6), the major LTA₄-hydrolase product of human PMN, which was the metabolite of main interest, was eluted 1.2 min after the two stereo-

isomeric LTs, the reduced column plate number of the column used was of minor importance.

5. Conclusions

The prediction of the retention times of the 20:4 metabolites, using the four-step gradient, was very accurate. The maximum difference in retention time between the prediction and the corresponding experimental run was 1.21%.

The on-line extraction RP-HPLC method described here is suitable for the detection of less than 1 ng of LTs and 1 ng of HETEs in biological samples. The 5-lipoxygenase product 5-HPETE is one of the most critical metabolites in the 20:4 metabolite mixture. It is unstable and will be reduced to 5-HETE. Additionally, 5-HETE could not be resolved from 5-HPETE by RP-HPLC using gradients with only acetonitrile as the organic eluent [16]. Therefore, until now 5-HPETE has been reduced by NaBH₄ [28] in order to examine the 5-lipoxygenase activity or to separate 5-HPETE by normal-phase HPLC (NP-HPLC). The reported detection limit of 5-HPETE was above 10 ng owing to quenching effects of the organic eluents used [16]. In contrast, the on-line extraction RP-HPLC method reported here demonstrated that 5-HPETE, in addition to 5-HETE, could be resolved and determined. The detection limit (5 ng) of 5-HPETE was lower than in NP-HPLC.

In addition to the above-mentioned separation of the 20:4 metabolite mixture, this four-step gradient optimized by Drylab is also capable of separating peptido-leukotrienes (LTC₄, LTD₄, LTE₄), LTA₄ hydrolase products (5,6-DiHETEs) and the corresponding lipoxygenase products 15-HPETE and 12-HPETE together with the 20:4 metabolites in a single run. These data will be published in subsequent paper.

In summary, Drylab was useful and accurate in this application, but not much improvement in resolution was achieved by computer simulation. The use of the software avoided the need for additional experimental runs and showed that with these separation conditions no improvement in performance could be obtained.

Abbreviations and symbols

20-COOH-LTB ₄	[5(S),6Z,8E,10E,12(R),14Z]-5,12-dihydroxy-20-carboxyeicosatetraen-1-oic acid
20-OH-LTB ₄	[5(S),6Z,8E,10E,12(R),14Z]-5,12,20-trihydroxy-eicosatetraen-1-oic acid
LTB ₄	[5(S),6Z,8E,10E,12(R),14Z]-5,12-dihydroxy-eicosatetraen-1-oic acid
6-trans,12-epi-LTB ₄	[5(S),6E,8E,10E,12(S),14Z]-5,12-dihydroxy-eicosatetraen-1-oic acid
All-trans-LTB ₄	[5(S),6E,8E,10E,12(R),14Z]-5,12-dihydroxy-eicosatetraen-1-oic acid
5-HETE	[5(S),6E,8Z,11Z,14Z]-5-hydroxyeicosatetraen-1-oic acid
12-HETE	[5Z,8Z,10E,12(R),14Z]-12-hydroxyeicosatetraen-1-oic acid
15-HETE	[5Z,8Z,11Z,13E,15(S)]-15-hydroxyeicosatetraen-1-oic acid
5-HPETE	[5(S),6E,8Z,11Z,14Z]-5-hydroperoxyeicosatetraen-1-oic acid
20:4	(5Z,8Z,11Z,14Z)-eicosatetraen-1-oic acid (arachidonic acid)
k'	capacity factor
k^*	average k' value during gradient runs
N	theoretical column plate number
R_S	resolution
t_R	retention time for samples (min)
t_0	column dead time (min)
t_G	gradient time (min)
F	flow-rate (ml/min)
V_m	column dead volume (ml) = $t_0 F$
S	100S is the negative slope of log k' vs. % organic component plots

 $\Delta\phi$

change in organic volume fraction of the mobile phase (%B/100)

Acknowledgement

We are grateful to Dr. M.J. Peck for his helpful suggestions and reviewing the manuscript.

References

- [1] B. Samuelsson, *Science*, 220 (1983) 568–575.
- [2] R.A. Lewis and K.F. Austen, *J. Clin. Invest.*, 73 (1984) 889–897.
- [3] B. Samuelsson, C.A. Rouzer and T. Matsumoto, *Adv. Prostaglandin Thromboxane Leukotriene Res.*, 17 (1987) 1–11.
- [4] P. Borgeat, M. Nadeau, H. Salari, P. Poubelle and B. Fruteau de Laclous, *Adv. Lipid Res.* 21 (1985) 47.
- [5] C.W. Parker, in B. Samuelsson and R. Paoletti, *Leukotrienes and Other Lipoxygenase Products*, Raven Press, New York, 1982, pp. 115–126.
- [6] B. Samuelsson, *Leukotrienes and Other Lipoxygenase Products*, Raven Press, New York, 1982, pp. 1–17.
- [7] S.J. Feinmark and P.J. Cannon, *J. Biol. Chem.*, 261 (1986) 16466–16472.
- [8] F. Hullin, J.M.F. Ragad-Thomas, C. Sepulchre, M. Pascal, H. Chap and L. Douste-Blazy, *Biochem. Pharmacol.* 38 (1989) 2763–2772.
- [9] M. Guichardant, F. Petit and M. Lagarde, *Eicosanoids*, 2 (1989) 117–12.
- [10] S. Yamamoto, C. Yokoyama, N. Ueda, F. Shinjo and S. Kaneko, *Adv. Prostaglandin Thromboxane Leukotriene Res.*, 16 (1986) 17–26.
- [11] R.J. Soberman, *Methods Enzymol.* 163 (1988) 334–349.
- [12] S. Narumiya, J.A. Salmon, F.H. Cottee, B.C. Weatherley and R.J. Flower, *J. Biol. Chem.*, 256 (1981) 9583–9592.
- [13] S. Yamamoto, N. Ueda, C. Yokoyama, B.J. Fitzsimmons and J. Rokach, *Adv. Exp. Med. Biol.*, 229 (1988) 15–26.
- [14] M. Van Rollins, M.I. Aveladano, H.W. Sprecher and L.A. Horrocks, *Methods Enzymol.*, 86 (1982) 518–530.
- [15] W.S. Powell, *Methods Enzymol.*, 86 (1982) 530–543.
- [16] B.A. Jakschik, T. Harper and R.C. Murphy, *Methods Enzymol.*, 86 (1982) 30–37.
- [17] S.R. McColl, W.H. Betts, G.A. Murphy and L.G. Cleland, *J. Chromatogr.*, 378 (1986) 444–449.
- [18] W.S. Powell, *Methods Enzymol.*, 86 (1982) 467–477.
- [19] D.J. Osborne, B.J. Peters and C.J. Meade, *Prostaglandins*, 26 (1983) 817–832.
- [20] H. Salari and S. Steffenrud, *J. Chromatogr.*, 378 (1986) 35–44.

- [21] A. Hatzelmann and V. Ullrich, *Eur. J. Biochem.*, 169 (1987) 175–184.
- [22] D. Riendeau and Y. Leblanc, *Biochem. Biophys. Res. Commun.*, 141 (1986) 534–540.
- [23] W.S. Powell, *Anal. Biochem.*, 164 (1987) 117–131.
- [24] P. Borgeat and S. Picard, *Anal. Biochem.*, 171 (1988) 283–289.
- [25] J.W. Dolan, D.C. Lommen and L.R. Snyder, *J. Chromatogr.*, 485 (1989) 91–112.
- [26] L.R. Snyder, J.W. Dolan and D.C. Lommen, *J. Chromatogr.*, 485 (1989) 64–89.
- [27] H. Engelhardt and M. Jungheim, *Chromatographia*, 29 (1990) 59–68.
- [28] N. Ueda and S. Yamamoto, *J. Biol. Chem.*, 263 (1988) 1937–1941.

Chromatographic behaviour of phenylurea pesticides in high-performance liquid chromatography with nitrile- and amino-bonded stationary phases

Jan Fischer, Pavel Jandera*

Department of Analytical Chemistry, University of Chemical Technology, Nám. Legií 565, 532 10 Pardubice, Czech Republic

First received 10 March 1994; revised manuscript received 21 June 1994

Abstract

The retention of phenylurea pesticides on nitrile- and amino-bonded stationary phases was measured over a broad composition range of 2-propanol–*n*-hexane and 2-propanol–water mobile phases. Minima of retention were observed on the nitrile phase in mobile phases containing 80–90% 2-propanol in water. In organic mobile phases, the plots of $\log k'$ versus the concentration of 2-propanol in *n*-hexane are significantly curved. This behaviour can be attributed to combined effects of polar and hydrophobic interactions as the driving force of the retention.

Simple two-parameter equations can be used to first-approximation description of retention on the nitrile bonded phase in mobile phases containing up to 50–60% 2-propanol in water and on the two bonded phases in mobile phases containing up to 60–80% 2-propanol in *n*-hexane. Four-parameter equations taking into account mixed mechanism of retention involving polar and hydrophobic interactions can be used to describe the retention of phenylurea compounds over the whole composition range of organic and aqueous–organic mobile phases and to allow prediction of retention and optimization of separation.

The retention of phenylurea pesticides on the amino-bonded phase in mobile phase containing 2-propanol in water is too low to allow chromatographic separation of the compounds tested. The retention in aqueous–organic mobile phases is higher on the nitrile- than on the amino-bonded phase, but the selectivity of separation is unsatisfactory for most phenylurea pesticides. Most compounds tested can be separated in 2-propanol–*n*-hexane mobile phases, but significant differences in selectivities and even in the order of elution were observed between the two bonded phases.

1. Introduction

The retention in normal-phase systems is controlled primarily by polar interactions of sample solutes with the adsorbent. Amino and nitrile stationary phases bonded on a silica gel support are less polar than non-modified (“naked”) silica gel or alumina adsorbents. The functional groups

are usually bonded on to the surface of the silica gel support by means of a short hydrocarbonaceous spacer, most often comprising three carbon atoms (aminopropyl or cyanopropyl phases). The spacer is not only responsible for the mobility of the bonded groups with respect to the surface of the silica gel [1,2], but because of the non-polar character it gives rise to possible retention of the solute by a hydrophobic (lipophilic) mechanism, especially in strongly polar mobile phases. In

* Corresponding author.

addition, the bonded chains are not long enough to provide efficient shielding of the residual silanol groups, which could not be modified in the silanization procedure because of steric reasons. In addition to the aminopropyl or cyanopropyl groups, the residual silanols may participate in polar interactions with sample solutes and contribute to the retention in non-aqueous mobile phases [3,4]. Weisser et al. [5] even assume a predominant role of the residual silanol groups in the retention on cyanopropyl bonded phases in the mobile phases with low polarities.

In organic mobile phases, the energy of interaction of the solutes and of the mobile phase with the chemically bonded amino and nitrile stationary phases is weaker and the solutes are usually less strongly retained than on the "naked" silica gel or alumina. Consequently, the interactions between the solutes and the mobile phase, which are often neglected in the description of retention on the columns packed with silica gel or alumina, become more important when polar chemically bonded stationary phases are used.

Because of different acidobasic properties of the amino group and of the silanols, the selectivity of separation on the bonded amino stationary phase differs from that on the unmodified silica gel [6,7]. This holds true also for cyanopropyl bonded phases, which can demonstrate either weakly basic (e.g. in chloroform) or weakly acidic (e.g. in methyl-*tert.*-butyl ether) properties in dependence on the nature of the components of the mobile phase [8].

To describe the retention on cyanopropyl and aminopropyl bonded phases, the competitive model of adsorption can be used. This model yields, with some simplification, Eq. 1 describing the dependence of the retention (capacity factor, k') on the mole fraction of the polar solvent, N_b , in a binary mobile phase comprised of a polar solvent and a non-polar one [1,9]:

$$\log k' = \text{constant} - n \log N_b \quad (1)$$

In this equation, n is the constant giving the ratio of the molecular area on the adsorbent surface occupied by one molecule of the sample solute to that occupied by one molecule of the

polar solvent. The concentration can often be expressed as volume fraction, φ , instead of the mole fraction, for convenience sake [9]:

$$\log k' = \text{constant} - n \log \varphi \quad (2)$$

or

$$k' = k'_0 \varphi^{-n} \quad (3)$$

where $k'_0 = 10^{\text{constant}}$. Eq. 3 fails for φ equal or very close to 0.

Hennion et al. [10] suggested the retention model on amino-bonded phases, where the association of one to three molecules of a solvent on to the amino group is considered: low-polarity solvents associate one molecule and strongly polar alcohols three molecules to one polar adsorption site. Based on this model, they derived the following relationship for the retention in binary mobile phases:

$$1/k' = A' - B'\varphi + C'\varphi^2 \quad (4)$$

and in the low concentration range of strongly polar solvents [alcohols, up to 0.2% (v/v)], the quadratic term can be neglected:

$$1/k' = A' - B'\varphi \quad (5)$$

This relationship takes into account the adsorption of only one molecule of alcohol on an amino group and is formally identical with the equation proposed by Scott and Kucera [11]:

$$k' = \frac{1}{c + d\varphi} \quad (6)$$

A' , B' , C' , c and d are constants depending on the nature of the solute and of the polar solvent.

Further discussion of the retention on columns with bonded amino phases can be found in Ref. 12.

In reversed-phase systems, Eq. 7 is widely used to describe the dependence of the capacity factor on the composition of a binary aqueous-organic mobile phase [9,13]:

$$k' = a \cdot 10^{-b\varphi} \quad (7)$$

where φ is the concentration (volume fraction) of the organic solvent in the mobile phase and a and b are constants which depend on the nature of the solute and of the organic solvent.

The description of the retention as a function

of the mobile phase composition allows to predict the retention and the selectivity under changing operation conditions, which is useful for the optimization of separation.

The objective of this work was to investigate the retention behaviour of selected compounds (phenylurea herbicides) on columns packed with nitrile- and amino-bonded stationary phases in both non-aqueous and aqueous–organic two-component mobile phases.

Generally, stationary phases with polar groups bonded via a non-polar spacer onto the surface of silica gel exhibit reversed-phase behaviour in aqueous–organic mobile phases, where the retention is controlled mainly by lipophilic (hydrophobic) interactions and normal-phase behaviour in organic mobile phases, where the polar interactions between the solutes and the stationary phase are most important. However, if we gradually change the composition of the mobile phase from pure water via aqueous–organic mixtures to pure polar organic solvent and then via binary organic mixtures to the pure non-polar solvent, it would be unrealistic to expect a sharp reversal in retention mechanism exactly in the pure polar solvent—especially if we realize that different polar solvents with various polarities can be used as mobile phase components. Rather, different interactions of sample components with the stationary phase contribute simultaneously to the retention and one type of interactions is enhanced while the other is suppressed when the composition of the mobile phase is changed. Smooth transition between the predominating role of the two mechanisms results and the composition of the mobile phase where the two types of interactions are of equal magnitude is close to, but not necessarily exactly at 100% polar solvent. The retention of sample components is very low in the vicinity of this transition point and its location has practical impact on the selection of the range of mobile phase compositions for the optimization of separation.

We intended to determine the composition range where simple two-parameter equations such as Eqs. 3, 5 and 7 can be used to describe the retention and to find out whether deviations from these equations can be explained by a

mixed retention mechanism so that the curvatures of the k' versus φ plots can be characterized to allow accurate prediction of the retention data over a wide composition range of the mobile phases, which is necessary for successful optimization of separation.

2. Theoretical

Horváth and co-workers [14,15] proposed the following equation to describe the retention (k') in reversed-phase systems where the retention results from the combination of the non-polar and the polar mechanisms:

$$k' = \psi_1 K_1 + \psi_2 K_2 = k'_1 + k'_2 \quad (8)$$

where ψ_1 and ψ_2 are the phase ratios of the hydrocarbonaceous ligates and of the polar groups (silanols) in the column, respectively, K_1 is the equilibrium constant for the purely solvophobic retention and K_2 that for the polar (silanophilic) retention on the column. The capacity factor is here expressed as the sum of the solvophobic, k'_1 , and of the polar (silanophilic), k'_2 , contributions.

Using this approach to columns with polar bonded phases in aqueous–organic mobile phases and introducing Eqs. 3 and 7 for the contributions k'_1 and k'_2 , respectively, we obtain:

$$\begin{aligned} k' &= a \cdot 10^{-b\varphi_1} + k'_0 \varphi_2^{-n} \\ &= a \cdot 10^{-b\varphi_1} + k'_0 (1 - \varphi_1)^{-n} \end{aligned} \quad (9)$$

where φ_1 is the concentration of the less polar (organic) solvent and φ_2 the concentration of water in aqueous–organic mobile phases. Eq. 9 cannot be used for pure organic solvent as the mobile phase.

The first term in Eq. 9 decreases with increasing concentration of the organic solvent, φ_1 , in the mobile phase, while the second term increases. If the polar interactions contribute significantly to the retention, non-linear dependence of the logarithms of k' on φ_1 is to be expected and even minima on the $\log k'$ versus φ_1 plot may occur at higher concentrations of the organic solvent in the mobile phase [14,15].

Chemically bonded polar stationary phases are

more often used with organic than with aqueous–organic mobile phases. Mobile phases comprised of two organic solvents of different polarities are usually employed, three or more components are less frequent. In these mobile phases, polar interactions are of primary importance and the retention behaviour typical for normal-phase systems is observed, but the non-polar mechanism may contribute to the retention at higher concentrations of a more polar solvent in a less polar one. Eq. 8 can be applied to describe the combined effects of the two mechanisms on retention, like in aqueous–organic mobile phases. If φ_3 is the concentration of the more polar and φ_4 that of the less polar organic solvent in a binary mobile phase, combination of Eqs. 3, 7 and 8 results in the following retention equation, similar to Eq. 9:

$$k' = a \cdot 10^{-b\varphi_4} + k'_0 \varphi_3^{-n} \\ = a \cdot 10^{-b(1-\varphi_3)} + k'_0 \varphi_3^{-n} \quad (10)$$

Eq. 10 cannot be used for pure less polar organic solvent as the mobile phase.

The Eq. 10 is similar to Eq. 9 derived for aqueous–organic mobile phases. According to Eq. 10, the plots of the logarithms of k' versus the concentration of the polar solvent, φ_1 , are expected to deviate from straight lines at high φ_1 and possibly even retention minima may occur there.

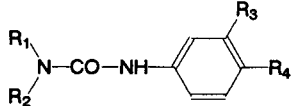
3. Experimental

The equipment used included a Model 6000A pump, a U6K injector and a Model 440 UV detector, operated at 254 nm, all from Waters-Millipore (Milford, MA, USA). The detector signal was registered using a TZ 4200 line recorder (Laboratory Instrument Works, Prague, Czech Republic). The chromatographic columns were stainless steel, 300×4.2 mm I.D., packed in the laboratory with Silasorb SPH Nitrile, $7.5 \mu\text{m}$ and Silasorb SPH Amine, $7.5 \mu\text{m}$ (both from Lachema, Brno, Czech Republic), using a high-pressure slurry-packing technique. The chromatograms were measured on a HP 1090M liquid chromatograph (Hewlett-Packard, Avondale, PA, USA).

The column dead volume, V_M , was determined as the elution volumes of the pure components of the mobile phase (water in aqueous–organic mobile phases and *n*-hexane or 2-propanol in organic mobile phases), using a Model R401 refractometric detector (Waters) and the experimental values are given in Tables 2, 5 and 8.

The sample solutes (phenylurea herbicides, see Table 1), were obtained from East-Bohemian Chemical Works (Pardubice, Czech Republic) and were dissolved in 2-propanol prior to injection. The mobile phases were prepared by mixing water (double distilled in glass with addition of potassium permanganate) with 2-pro-

Table 1
Chemical structures of phenylurea herbicides and related compounds studied

Compound					
No.	Name	R ₁	R ₂	R ₃	R ₄
1	Phenuron	–CH ₃	–CH ₃	–	–
2	Desphenuron	–CH ₃	–H	–	–
3	Hydroxymethoxuron	–CH ₃	–CH ₃	–Cl	–OH
4	Neburon	–CH ₃	–C ₄ H ₉	–Cl	–Cl
5	Deschloromethoxuron	–CH ₃	–CH ₃	–	–OCH ₃
6	Isoproturon	–CH ₃	–CH ₃	–	–CH(CH ₃) ₂
7	Bis-N,N'-(3-chloro-4-methylphenyl)urea	3-Chloro-4-methylphenyl	–H	–Cl	–CH ₃
8	N-Butyl-N'-phenylurea	–C ₄ H ₉	–H	–	–
9	N-Phenylurea	–H	–H	–	–

panol (spectroscopic grade, Lachema) or *n*-hexane (analytical-reagent grade; Loba, Fischamend, Austria) with 2-propanol. All the solvents were filtrated using a Millipore 0.45- μm filter and the premixed mobile phases were degassed by ultrasonication before use.

The capacity factors $k' = (V_R - V_M)/V_M$ were calculated from the arithmetic means of two or three experimental retention volumes V_R , in repeated experiments. From the plots of the experimental k' in dependence on the composition of the mobile phase, the parameters of the retention Eqs. 3, 7, 9 and 10 were determined by non-linear regression analysis using the Chemstat software (Trilobyte, Prague, Czech Republic). The values of the parameters are given in Tables 3, 6 and 9.

4. Results and discussion

4.1. Silasorb SPH Nitrile

The capacity factors of the phenylurea herbicides tested were calculated using the dead volume V_M determined as the elution volume of water in aqueous–propanolic mobile phases, which was almost identical to the elution volumes of *n*-hexane and 2-propanol in organic mobile phases. The values of V_M and of the experimental k' are given in Tables 2 and 5. Figs. 1–3 show the plots of k' in dependence on the concentration of 2-propanol, which is the stronger eluent in both aqueous–organic and organic mobile phases.

In 2-propanol–*n*-hexane mobile phases, the solutes containing polar functional groups such as hydroxyl (hydroxymethoxuron), primary amino (N-phenylurea) or methoxy (deschlor-methoxuron) on the benzene ring are most strongly retained. On the other hand, compounds with bulky non-polar substituents such as bis-N,N'-(3-chloro-4-methylphenyl)urea, neburon and N-butyl-N'-phenylurea are the least retained.

Fig. 1 shows a linear decrease (on a log–log scale) of the capacity factors with increasing volume fraction φ of 2-propanol in *n*-hexane in

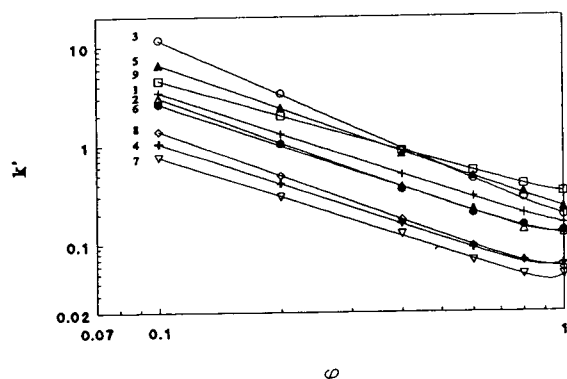


Fig. 1. Retention of phenylurea herbicides on a Silasorb SPH Nitrile column in mobile phases containing 2-propanol in *n*-hexane. Column: Silasorb SPH Nitrile, 7.5 μm , 300 \times 4.2 mm I.D. For data, see Table 2. Numbers of compounds as in Table 1. k' = capacity factor; φ = volume fraction of 2-propanol, in % (v/v) $\times 10^2$.

mobile phases containing 80% or less of 2-propanol. In mobile phases with less than 20% *n*-hexane, the plots of $\log k'$ versus $\log \varphi$ are curved. Higher values of the experimental capacity factors than those predicted from Eq. 3 were observed for all compounds tested, which suggests that the experimental behaviour in propanol-rich mobile phases is more likely to be explained by simultaneous contributions of polar and non-polar interactions to the retention than only by possible errors in measuring low ex-

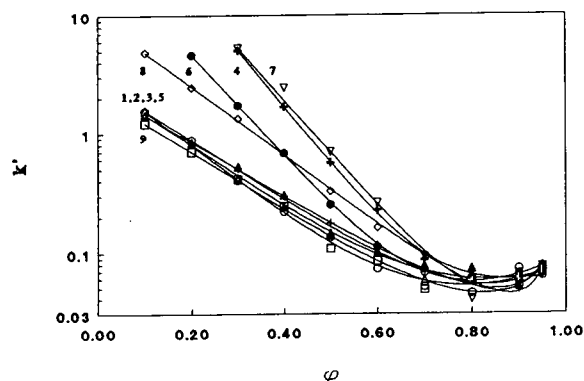


Fig. 2. Retention of phenylurea herbicides on a Silasorb SPH Nitrile column in mobile phases containing 2-propanol in water. Column: Silasorb SPH Nitrile, 7.5 μm , 300 \times 4.2 mm I.D. For data, see Table 5. Numbers of compounds as in Table 1, symbols as in Fig. 1.

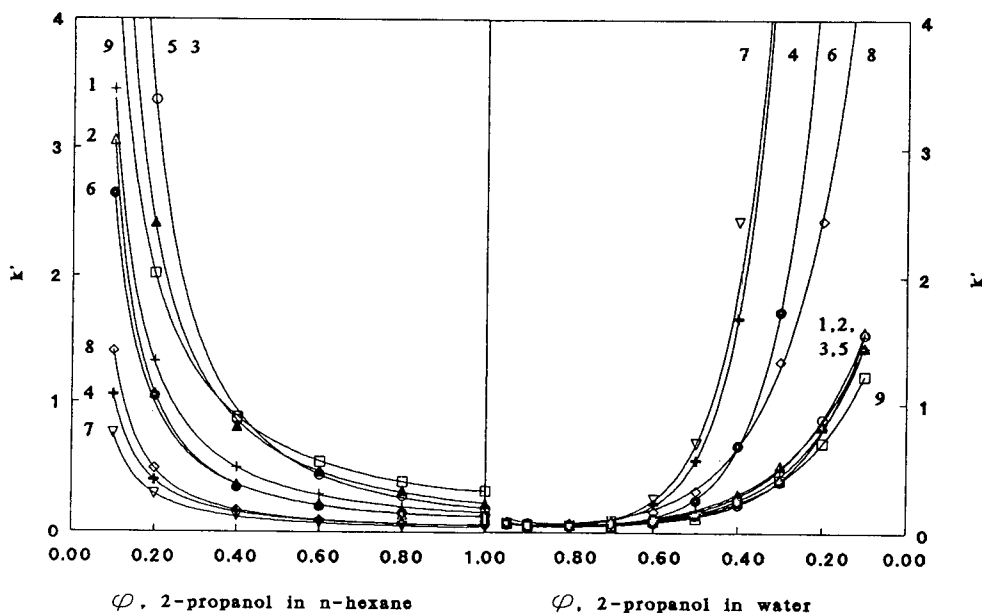


Fig. 3. Retention of phenylurea herbicides on a Silasorb SPH Nitrile column over a wide range of the mobile phase polarity from 10% 2-propanol in *n*-hexane to 10% 2-propanol in water. Column: Silasorb SPH Nitrile, 7.5 μm , 300 \times 4.2 mm I.D. For data, see Tables 2 and 5. Numbers of compounds as in Table 1, symbols as in Fig. 1.

perimental values of k' (see more detailed discussion below). This means that Eq. 3 can be used to describe the retention behaviour of phenylurea herbicides on the nitrile bonded phase only in mobile phases containing less than 80% (v/v) 2-propanol in *n*-hexane.

Fitting Eq. 3 to the experimental data in the mobile phases containing from 10 to 80% 2-propanol in *n*-hexane yielded significantly better results than fitting Eq. 6. This applied also to other chromatographic systems tested and consequently only the data calculated using Eq. 3 and Eqs. 9 and 10 are presented in this work.

Eq. 10 was fitted to the retention data in the whole composition range of mobile phases (10–100% 2-propanol in *n*-hexane) and the results in Table 2 show that this equation is well suited to describe the retention on the Silasorb SPH Nitrile column.

Table 3 lists the values of the parameters of Eqs. 3 and 10 obtained by the regression of the experimental dependencies of the capacity factors of phenylurea herbicides on the volume fraction of 2-propanol in *n*-hexane.

The parameters k'_0 and n calculated from Eq. 3 for mobile phases containing 10–80% 2-propanol agree very well with the values of the corresponding parameters of Eq. 10 measured over the whole range of mobile phase compositions.

Because the first term on the right-hand side of Eq. 10 represents the non-polar contribution to the retention whereas the second term the contribution of the polar interactions, it is possible to use the coefficients of these equations determined by regression to calculate the contributions of the two mechanisms to the retention from the ratio of the first and of the second terms to the predicted capacity factor. The values of the solvophobic contribution to retention in 2-propanol–*n*-hexane mobile phases calculated in this way from Eq. 10 indicate more significant contribution of the solvophobic mechanism to retention only in the mobile phases containing 80% or more of 2-propanol (Table 4). It is interesting to note that neburon, *N*-butyl-*N'*-phenylurea, isoproturon, phenuron and desphenuron without –OH, –OCH₃ or aromatic sub-

Table 2
Capacity factors of phenylurea herbicides on Silasorb SPH Nitrile column in mobile phases containing 2-propanol in *n*-hexane

Compound		k'					
		Concentration of 2-propanol in <i>n</i> -hexane (% v/v)					
		100	80	60	40	20	10
		V_M (ml)					
		–	3.55	3.55	–	3.56	–
1	a	0.158	0.199	0.296	0.501	1.324	3.456
	b	0.144	0.196	0.291	0.510	1.327	3.455
	c	0.158	0.200	0.291	0.507	1.322	3.456
2	a	0.126	0.139	0.221	0.374	1.064	3.057
	b	0.096	0.134	0.207	0.381	1.077	3.054
	c	0.123	0.148	0.211	0.376	1.065	3.057
3	a	0.190	0.286	0.448	0.862	3.374	11.841
	b	0.176	0.265	0.448	0.942	3.337	11.846
	c	0.193	0.270	0.448	0.931	3.334	11.846
4	a	0.062	0.067	0.091	0.161	0.408	1.055
	b	0.049	0.062	0.092	0.159	0.411	1.054
	c	0.062	0.064	0.090	0.157	0.407	1.055
5	a	0.227	0.326	0.476	0.812	2.416	6.644
	b	0.222	0.309	0.473	0.860	2.391	6.647
	c	0.231	0.312	0.473	0.859	2.389	6.649
6	a	0.132	0.152	0.201	0.311	1.046	2.643
	b	0.104	0.142	0.214	0.378	1.001	2.651
	c	0.133	0.145	0.211	0.374	0.996	2.653
7	a	0.047	0.048	0.067	0.125	0.299	0.760
	b	0.036	0.049	0.071	0.121	0.304	0.759
	c	0.047	0.048	0.069	0.119	0.302	0.760
8	a	0.055	0.066	0.094	0.174	0.494	1.402
	b	0.045	0.062	0.096	0.176	0.496	1.402
	c	0.055	0.065	0.096	0.174	0.493	1.402
9	a	0.326	0.395	0.547	0.886	2.020	4.563
	b	0.304	0.395	0.555	0.893	2.019	4.563
	c	0.326	0.394	0.551	0.889	2.014	4.564

V_M = Column dead volume; k' = capacity factor; a = experimental values; b = calculated from Eq. 3; c = calculated from Eq. 10. The parameters k'_0 , n , a and b of these equations are given in Table 3. Numbers of compounds as in Table 1.

Table 3

Experimental parameters of Eqs. 3 and 10 (10–100% 2-propanol) for phenylurea herbicides on Silasorb SPH Nitrile column in mobile phases containing 2-propanol in *n*-hexane

Compound	Parameters of equations							
	Eq. 3			Eq. 10				
	k'_0	n	R^2	k'_0	n	a	b	R^2
1	0.1438	1.381	0.9999	0.1416	1.387	0.0162	1.654	1.0000
2	0.0959	1.503	0.9998	0.0907	1.527	0.0326	0.965	0.9999
3	0.1762	1.828	0.9999	0.1756	1.829	0.0177	2.264	0.9999
4	0.0460	1.361	0.9995	0.0445	1.374	0.0178	3.616	0.9999
5	0.2225	1.475	0.9999	0.2217	1.477	0.0092	1.944	0.9999
6	0.1044	1.405	0.9983	0.1024	1.414	0.0303	4.054	0.9986
7	0.0361	1.322	0.9985	0.0353	1.333	0.0117	7.871	0.9999
8	0.0446	1.497	0.9999	0.0437	1.507	0.0152	2.353	1.0000
9	0.3041	1.176	0.9999	0.3016	1.180	0.0244	5.585	1.0000

Numbers of compounds as in Table 1.

stituents and with alkyl substituents (see Table 1) show higher non-polar contributions than the other phenylurea compounds in mobile phases containing 60–80% 2-propanol, which is in agreement with general structural effects usually observed in reversed-phase systems and supports the idea of the mixed retention mechanism.

Fig. 2 shows the dependencies of the capacity

factors of phenylurea herbicides on the volume fraction φ of 2-propanol in binary aqueous–organic mobile phases. In mobile phases containing 10–70% 2-propanol in water, bis-*N,N'*-(3-chloro-4-methylphenyl)urea, neburon, isoproturon and *N*-butyl-*N'*-phenylurea with largest alkyl or aryl substituents on the phenylurea skeleton are most strongly retained, while the compounds without (or with small) alkyl substituents (phenylurea,

Table 4

Hydrophobic (non-polar) contribution (in per cent of the first term in Eq. 10 to the capacity factor) to the retention of phenylurea herbicides on a Silasorb SPH Nitrile column in mobile phases containing 2-propanol in *n*-hexane

Compound	Relative contribution (%)				
	Concentration of 2-propanol (% v/v)				
	10	40	60	80	100
1	0.0	0.2	1.2	3.5	9.8
2	0.1	0.7	6.7	13.8	26.3
3	0.1	0.0	0.2	1.8	20.5
4	0.0	0.1	0.2	5.5	28.2
5	0.0	0.0	0.3	0.9	4.8
6	0.0	0.0	0.1	3.2	23.0
7	0.1	0.3	0.5	1.0	24.9
8	0.0	0.1	1.7	5.9	20.5
9	0.0	0.0	0.0	0.4	7.5

Numbers of compounds as in Table 1.

phenuron, desphenuron) and with a strongly polar substituent (hydroxymethoxuron) are eluted much earlier.

The dependencies of $\log k'$ on the volume fraction of 2-propanol in water in Fig. 2 show minima in 80–90% 2-propanol. This behaviour can be explained by the balance between non-polar and polar interactions in these mobile phases. Non-polar interactions control the retention in mobile phases with lower concentrations of 2-propanol, but with increasing concentration of 2-propanol the contribution of polar interactions gradually becomes more important and it predominates in mobile phases with less than 10–20% water, giving rise to the retention behaviour characteristic for a normal-phase system. As in reversed-phase systems the retention decreases with increasing concentration of the less polar solvent (2-propanol), while the opposite applies in normal-phase systems, the two opposite effects result in a minimum of retention at a certain composition of the mobile phase.

Possible experimental errors are not significant enough to explain the retention minima observed. The values of V_M in 10–100% 2-propanol in water are constant in the range 3.46–3.54 ml and an experimental error in this range may lead to deviations at the third decimal place in the values of k' . To avoid systematic errors caused by extra-column contributions, we used the shortest possible connections between the injector, the column and the detector, so that the extra-column volumes were approximately 20–30 μl , constant during the measurement of all experimental k' and V_M values, so that all the capacity factors would be affected in the same way (if this error is significant) and the absolute values of k' would be slightly modified, but the occurrence of the minima on the k' versus φ curves would not be affected at all.

The plots of $\log k'$ vs. φ are fairly linear in mobile phases containing less than 50–70% of 2-propanol, like in many reversed-phase systems with alkyl-bonded stationary phases. This is demonstrated by the agreement of the experimental capacity factors with the values calculated from the regression equation obtained by

fitting the Eq. 7 to the experimental data (Table 5).

To describe the retention in the whole composition range of the mobile phase, i.e., from 10 to 95% 2-propanol in water, the model taking into account dual mechanism of retention can be used. The values of the capacity factors calculated from the regression equations obtained by fitting Eq. 9 to the experimental data are listed in Table 5.

Table 6 lists the values of the parameters of Eqs. 7 and 9 determined by the regression of the experimental capacity factors of phenylurea herbicides in 2-propanol–water mobile phases. The correlation coefficients for Eq. 9 describing the retention in the whole range of mobile phase composition are slightly better than the correlation coefficients for Eq. 7 applied to the capacity factors in mobile phases containing 10–60% of 2-propanol in water.

The values of the contributions in this composition range of the mobile phases may be subject to some errors because of low values of the capacity factors. The values of the polar contributions to the retention of all the phenylurea herbicides tested (calculated as the per cent ratio of the second term in Eq. 9 to the value of the capacity factor) in mobile phases with different concentrations of 2-propanol in water are given in Table 7. The polar contribution to the retention can possibly be attributed mainly to the interactions of the solutes with residual silanol groups in the chemically bonded phase. For some polar compounds such as hydroxymethoxuron or chlortoluron, this contribution may be significant even in mobile phases containing 50% 2-propanol. In mobile phases with more than 70% of 2-propanol, the contribution of polar interactions to the retention increases rapidly and it amounts to 80–93% of the value of the capacity factors in 95% 2-propanol.

The data in Table 7 indicate that the equilibration of non-polar and polar contributions to the retention occurs in mobile phases with 70–90% 2-propanol in water, where the retention minima are observed (Fig. 2), supporting the idea of the reversal of the mechanism controlling the retention. Consequently, the contribution of the

Table 5
Capacity factors of phenylurea herbicides on Silasorb SPH Nitrile column in mobile phases containing 2-propanol in water

Compound		k'									
		Concentration of 2-propanol in water (% v/v)									
		95	90	80	70	60	50	40	30	20	10
		V_M (ml)									
		3.48	3.50	3.49	3.50	3.51	3.54	3.50	–	3.51	3.49
1	a	0.078	0.048	0.059	0.068	0.116	0.178	0.299	0.509	0.842	1.437
	b	0.018	0.023	0.039	0.065	0.109	0.183	0.306	0.512	0.855	1.423
	c	0.077	0.053	0.053	0.072	0.111	0.181	0.300	0.503	0.848	1.435
2	a	0.071	0.058	0.062	0.058	0.103	0.146	0.305	0.527	0.844	1.570
	b	0.014	0.018	0.031	0.055	0.096	0.167	0.291	0.509	0.889	1.552
	c	0.072	0.056	0.054	0.068	0.103	0.167	0.285	0.498	0.878	1.561
3	a	0.063	0.073	0.045	0.051	0.073	0.136	0.223	0.404	–	1.547
	b	0.007	0.009	0.018	0.034	0.063	0.120	0.227	0.430	–	1.542
	c	0.069	0.057	0.052	0.058	0.079	0.125	0.219	0.409	–	1.546
4	a	0.063	0.059	0.068	0.087	0.227	0.565	1.673	5.035	–	–
	b	0.004	0.007	0.022	0.064	0.191	0.569	1.692	5.031	–	–
	c	0.062	0.060	0.064	0.098	0.214	0.572	1.671	5.035	–	–
5	a	0.068	0.051	0.074	0.078	0.101	0.141	0.242	0.432	0.832	1.445
	b	0.014	0.015	0.027	0.047	0.084	0.148	0.261	0.462	0.817	1.443
	c	0.068	0.059	0.058	0.070	0.098	0.152	0.255	0.447	0.801	1.454
6	a	0.075	0.065	0.061	0.072	0.113	0.253	0.679	1.724	4.590	–
	b	0.003	0.005	0.014	0.037	0.097	0.253	0.665	1.747	4.584	–
	c	0.078	0.061	0.055	0.069	0.121	0.267	0.663	1.729	4.589	–
7	a	0.076	0.066	0.040	0.093	0.262	0.694	–	5.270	–	–
	b	0.008	0.012	0.034	0.094	0.257	0.703	–	5.269	–	–
	c	0.080	0.049	0.052	0.102	0.257	0.693	–	5.270	–	–
8	a	0.072	0.058	0.057	0.066	0.163	0.329	0.680	1.330	2.440	4.858
	b	0.017	0.024	0.047	0.090	0.175	0.340	0.661	1.284	2.492	4.884
	c	0.067	0.050	0.059	0.098	0.180	0.343	0.661	1.282	2.490	4.845
9	a	0.071	0.054	0.058	0.048	0.085	0.109	0.246	0.412	0.700	1.215
	b	0.012	0.016	0.028	0.048	0.082	0.140	0.241	0.412	0.706	1.211
	c	0.073	0.049	0.044	0.057	0.085	0.139	0.234	0.403	0.699	1.217

V_M = Column dead volume; k' = capacity factor; a = experimental values; b = calculated from Eq. 7; c = calculated from Eq. 9. The parameters k'_0 , n , a and b of these equations are given in Table 6. Numbers of compounds as in Table 1.

polar interactions to the retention predominates not only in the whole range of concentrations of 2-propanol in *n*-hexane, but also in mobile phases containing 90–100% 2-propanol in water.

The parameter k'_0 of Eq. 9 represents the polar contribution to the capacity factor in pure water as the mobile phase and is approximately 1–2 orders of magnitude lower than the corre-

Table 6

Experimental parameters of Eqs. 7 and 9 for phenylurea herbicides on Silasorb SPH Nitrile column in mobile phases containing 2-propanol in water

Compound	Parameters of equations							
	Eq. 7			Eq. 9				
	<i>a</i>	<i>b</i>	<i>R</i> ²	<i>a</i>	<i>b</i>	<i>k</i> ' ₀	<i>n</i>	<i>R</i> ²
1	2.387	2.230	0.9973	2.462	2.294	0.0041	0.899	0.9992
2	2.711	2.421	0.9958	2.772	2.525	0.0109	0.578	0.9992
3	2.919	2.771	0.9950	3.036	2.994	0.0223	0.357	0.9997
4	132.3	4.733	0.9993	143.0	4.854	0.0325	0.205	1.0000
5	2.551	2.473	0.9942	2.636	2.651	0.0223	0.333	0.9990
6	31.59	4.191	0.9992	32.78	4.280	0.0222	0.408	1.0000
7	108.2	4.375	0.9997	112.1	4.427	0.0042	0.965	1.0000
8	9.408	2.883	0.9989	9.427	2.893	0.0063	0.947	0.9997
9	2.075	2.340	0.9948	2.118	2.426	0.0051	0.839	0.9990

Numbers of compounds as in Table 1.

sponding parameter *k*'₀ of Eq. 10, which has the meaning of the polar contribution to *k*' in pure 2-propanol (Tables 3 and 6). The reason is increasing contribution of polar interactions to the retention when the polarity of the mobile phase is decreased.

Fig. 3 shows the dependence of the retention (capacity factors) of phenylurea herbicides on the composition of the mobile phase over a wide range of polarities, from 10% 2-propanol in *n*-

hexane to 10% 2-propanol in water. From these plots it is obvious that much better selectivities of separation can be achieved in non-aqueous mobile phases than in aqueous–propanolic media. In mobile phases containing more than 60% 2-propanol in water, all the solutes investigated are almost unretained, which contrasts to the behaviour in mobile phases with high concentrations of 2-propanol in *n*-hexane. A discontinuous change in retention of most her-

Table 7

Polar contribution (in per cent of the second term in Eq. 9 to the capacity factor) to the retention of phenylurea herbicides on a Silasorb SPH Nitrile column in mobile phases containing 2-propanol in water

Compound	Relative contribution (%)					
	Concentration of 2-propanol (% v/v)					
	10	50	70	80	90	95
1	0.4	4.4	16.7	32.7	60.4	79.2
2	0.8	9.6	30.9	50.9	73.2	85.0
3	1.5	23.0	58.6	76.9	89.5	93.9
4	–	6.1	41.6	70.3	86.7	92.4
5	1.5	18.3	47.1	65.5	81.3	89.0
6	–	10.9	52.2	77.7	87.5	93.9
7	–	1.2	12.7	38.5	76.0	91.6
8	0.0	0.5	4.3	14.8	47.8	78.2
9	0.5	6.5	25.0	45.5	71.4	85.1

Numbers of compounds as in Table 1.

bicides is apparent between 100% 2-propanol and 95% 2-propanol in water. This behaviour possibly can be explained by deactivation of the residual silanol groups as the polar adsorption centers by adsorption of water, which has leveling effect on retention and results in much lower separation selectivity for the separation of phenylurea herbicides on the bonded nitrile phases in aqueous-propanolic than in non-aqueous mobile phases.

Fig. 4 shows an example of separation of phenylurea herbicides on a Silasorb SPH Nitrile column in 2-propanol-*n*-hexane mobile phases. Strong tailing is apparent for the most strongly retained peak of unsubstituted N-phenylurea, which probably can be attributed to the hydrogen-bonding interactions with residual silanol groups in the stationary phase. This compound—the most simple in the phenylurea series—does not show herbicide properties and its peak is not of primary interest in the samples of herbicides. The peaks of herbicides of the N'-substituted N-phenylurea type in Fig. 4 are symmetrical and the efficiency of the column used (5000 theoretical plates) is sufficient for their separation. The shape of the peak of unsubstituted phenylurea can be possibly improved by the addition of small amounts of an alkylamine to the mobile phase.

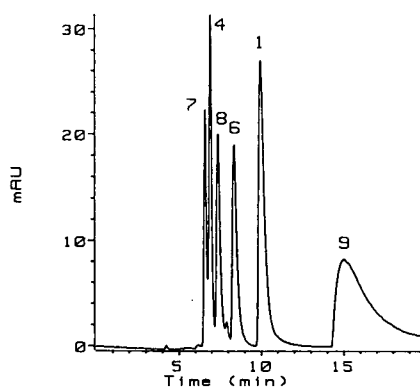


Fig. 4. Separation of phenylurea herbicides on a Silasorb SPH Nitrile column in a normal-phase system. Column: Silasorb SPH Nitrile, 7.5 μ m, 300 \times 4.2 mm I.D.; mobile phase: 10% 2-propanol in *n*-hexane, flow-rate 1.0 ml/min, UV detection at 254 nm. Numbers of compounds as in Table 1.

4.2. Silasorb SPH Amine

The capacity factors of most phenylurea herbicides on a Silasorb SPH Amine column are low and close to each other in mobile phases containing 10–90% 2-propanol in water. Some solutes show retention minima in 60% 2-propanol, but with a few exceptions, the capacity factors of sample solutes are lower than 0.5 even in mobile phases with 10% 2-propanol.

In non-aqueous mobile phases, much higher retention and selectivity of separation of substituted phenylureas are observed. The elution volume of *n*-hexane was almost independent of the composition of 2-propanol-*n*-hexane mobile phases and was used as the column dead volume for calculations of capacity factors of the analytes in mobile phases containing 5–100% 2-propanol in *n*-hexane (Table 8). Fig. 5 shows the logarithmic plots of k' in dependence on the volume fraction φ of 2-propanol in the mobile phase. The plots are approximately linear in mobile phases containing less than 60% 2-propanol and can be described by Eq. 3.

To characterize the retention over the whole range of concentrations of 2-propanol in *n*-hexane, Eq. 10 based on the model of retention taking into account simultaneous contribution of polar and non-polar interactions yields predicted capacity factors in better agreement with the experimental k' than Eq. 3.

The parameters a , b , k'_0 and n obtained by fitting the retention Eqs. 3 and 10 to the experimental data are listed in Table 9. The parameters k'_0 and n of Eq. 3 are almost identical with corresponding parameters obtained by fitting the non-linear Eq. 10 to the retention data.

Table 10 lists the values of the non-polar contributions to the retention of the individual phenylurea herbicides, calculated as the ratios of the second term in Eq. 10 to the capacity factors calculated from this equation. The non-polar contribution to the retention increases with increasing concentration of 2-propanol in the organic mobile phase. It does not exceed 10% of k' in mobile phases containing less than 60% 2-propanol and its value is higher for compounds with bulky hydrocarbon substituents such as

Table 8
Capacity factors of phenylurea herbicides on Silasorb SPH Amine column in mobile phase containing 2-propanol in *n*-hexane

Compound		k'							
		Concentration of 2-propanol in <i>n</i> -hexane (% v/v)							
		100	80	60	40	30	20	10	5
		V_M (ml)							
		2.98	2.95	2.96	–	3.01	3.01	–	3.02
1	a	0.357	0.508	0.700	1.185	1.824	3.544	10.020	–
	b	0.308	0.432	0.667	1.231	1.903	3.513	10.020	–
	c	0.376	0.469	0.681	1.227	1.888	3.849	10.028	–
2	a	0.549	0.598	0.842	1.625	2.629	5.355	17.935	–
	b	0.335	0.491	0.807	1.628	2.678	5.402	17.922	–
	c	0.502	0.594	0.844	1.619	2.646	5.346	17.936	–
3	a	0.606	0.921	1.653	3.945	7.203	–	–	–
	b	0.564	0.904	1.662	3.992	7.211	–	–	–
	c	0.606	0.916	1.617	3.929	7.207	–	–	–
4	a	0.224	0.229	0.258	0.379	0.536	0.845	2.297	5.404
	b	0.122	0.162	0.233	0.389	0.561	0.937	2.251	5.410
	c	0.231	0.209	0.249	0.387	0.551	0.919	2.223	5.418
5	a	0.515	0.629	0.970	1.741	2.733	5.569	17.921	–
	b	0.374	0.543	0.881	1.742	2.826	5.586	17.911	–
	c	0.518	0.636	0.929	1.744	2.799	5.527	17.925	–
6	a	0.357	0.393	0.534	0.871	1.372	2.222	6.174	15.244
	b	0.274	0.371	0.545	0.939	1.382	2.380	6.029	15.273
	c	0.358	0.382	0.548	0.936	1.377	2.373	6.021	15.247
7	a	0.426	0.418	0.471	0.676	1.007	1.776	5.382	13.726
	b	0.208	0.284	0.425	0.749	1.121	1.977	5.214	13.756
	c	0.441	0.365	0.469	0.745	1.107	1.952	5.181	13.767
8	a	0.301	0.308	0.371	0.591	0.895	1.682	5.303	15.005
	b	0.154	0.217	0.337	0.626	0.972	1.806	5.209	15.020
	c	0.310	0.274	0.355	0.627	0.966	1.793	5.188	15.026
9	a	0.774	0.972	1.544	2.665	4.207	7.672	–	–
	b	0.705	0.981	1.503	2.742	4.200	7.662	–	–
	c	0.769	0.998	1.493	2.718	4.179	7.675	–	–

V_M = Column dead volume; k' = capacity factor; a = experimental values; b = calculated from Eq. 3; c = calculated from Eq. 10. The parameters k'_0 , n , a and b of these equations are given in Table 9. Numbers of compounds as in Table 1.

neburon, bis-*N,N'*-(3-chloro-4-methylphenyl)-urea and *N*-butyl-*N'*-phenylurea. These compounds are the most early eluted ones in mobile

phases containing 5–40% 2-propanol, where the non-polar contribution to retention can be neglected. On the other hand, in these mobile

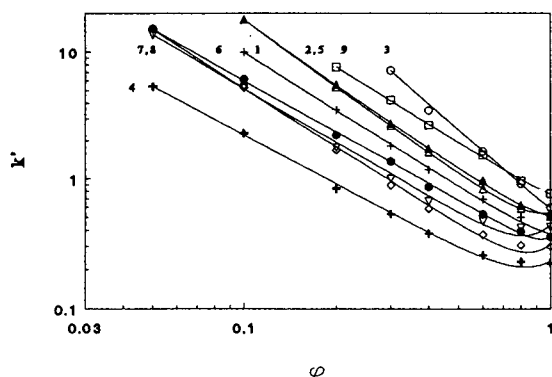


Fig. 5. Retention of phenylurea herbicides on a Silasorb SPH Amine column in mobile phases containing 2-propanol in *n*-hexane. Column: Silasorb SPH Amine, 7.5 μm , 300 \times 4.2 mm I.D. For data, see Table 8. Numbers of compounds as in Table 1, symbols as in Fig. 1.

phases hydroxymethoxuron with polar OH group is retained most strongly, but it shows the lowest non-polar contribution to retention of all the compounds tested. This behaviour suggests that the model based on Eq. 10 is suitable to describe the experimental behaviour of phenylurea herbicides on the amino-bonded phase in organic mobile phases. Changing proportions of the polar and of the non-polar contributions to the retention can probably explain the strong dependence of the selectivity of separation on the

concentration of 2-propanol in the mobile phase (Fig. 5) accompanied with changes in the order of elution of some compounds, such as hydroxymethoxuron and phenylurea, which are the most strongly retained ones.

Because the amino group is more polar than the nitrile group, the phenylurea herbicides are retained more strongly on the Silasorb SPH Amine column than on the Silasorb SPH Nitrile column. Deschlormethoxuron is eluted before *N*-phenylurea, and phenuron before desphenuron on the Silasorb SPH Amine column, while the order of elution of these pairs of compounds is reversed on the Silasorb SPH Nitrile column. Fig. 6 shows an example of the separation of phenylurea herbicides on the Silasorb SPH Amine column to illustrate this behaviour. Like on the nitrile column, unsubstituted *N*-phenylurea is most strongly retained and its peak is unsymmetrical—probably because of the hydrogen-bonding interactions with the residual silanol groups in the stationary phase. The efficiency of the column used was rather low (approximately 1500–2000 theoretical plates) and also the peaks of less retained compounds showed some tailing, caused by the previous history of the column used for several hundreds of experiments. An example of a more efficient separation of a mixture of phenylurea herbicides

Table 9

Experimental parameters of Eqs. 3 and 10 for phenylurea herbicides on Silasorb SPH Amine column in mobile phases containing 2-propanol in *n*-hexane

Compound	Parameters of equations							
	Eq. 3			Eq. 10				
	k'_0	n	R^2	k'_0	n	a	b	R^2
1	0.3063	1.515	0.9997	0.2976	1.527	0.0779	0.962	0.9998
2	0.3292	1.736	0.9997	0.3185	1.750	0.2317	1.368	1.0000
3	0.5572	2.127	0.9998	0.5689	2.109	0.0374	1.841	1.0000
4	0.1289	1.247	0.9988	0.1158	1.284	0.1157	1.610	0.9995
5	0.3703	1.685	0.9998	0.3517	1.706	0.1670	0.686	1.0000
6	0.2715	1.345	0.9996	0.2716	1.343	0.0849	3.953	0.9997
7	0.2049	1.404	0.9990	0.2012	1.411	0.2398	2.142	0.9994
8	0.1532	1.531	0.9997	0.1514	1.535	0.1596	2.098	0.9998
9	0.6957	1.491	0.9996	0.6839	1.502	0.0853	1.552	0.9998

Numbers of compounds as in Table 1.

Table 10

Solvophobic contribution (in per cent of the first term in Eq. 10 to the capacity factor) to the retention of phenylurea herbicides on a Silasorb SPH Amine column in mobile phases containing 2-propanol in *n*-hexane

Compound	Relative contribution (%)				
	Concentration of 2-propanol (% v/v)				
	10	40	60	80	100
1	0.1	1.7	4.7	10.8	20.9
2	0.1	2.2	7.7	20.8	36.6
3	—	0.0	0.0	0.6	6.1
4	0.0	3.0	10.4	26.2	49.9
5	0.2	3.7	9.5	19.1	32.1
6	0.6	0.7	1.6	4.1	24.1
7	0.1	1.7	11.8	24.5	54.4
8	0.0	1.5	6.6	22.2	51.2
9	—	0.4	1.3	4.2	11.1

Numbers of compounds as in Table 1.

(most of which have not been studied in detail in all the mobile phases reported in this work) on a more fresh and efficient column is shown in Fig. 7.

5. Conclusions

(1) For the polar bonded stationary phases Silasorb SPH Nitrile and Silasorb SPH Amine,

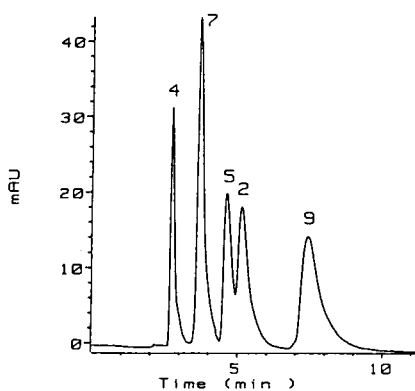


Fig. 6. Separation of phenylurea herbicides on a Silasorb SPH Amine column in a normal-phase system. Column: Silasorb SPH Amine, 7.5 μ m, 300 \times 4.2 mm I.D.; mobile phase: 40% 2-propanol in *n*-hexane, flow-rate 1.0 ml/min, UV detection at 254 nm. Numbers of compounds as in Table 1.

the dependence of the retention of phenylurea herbicides on the concentration of a polar organic solvent in a non-polar one or in water can be adequately described by two-parameter equations only over a limited composition range of the mobile phases. In aqueous-organic and in non-aqueous binary mixtures with concentrations of 2-propanol higher than 60–70%, significant curvature of the plots of $\log k'$ versus the volume fraction of propanol, or its logarithm, respectively, is observed. If the composition of the mobile phase is changed gradually from 0 to 100% 2-

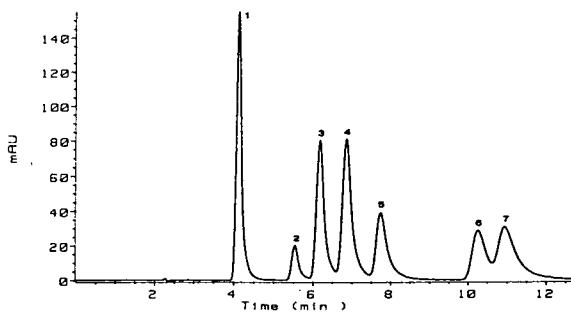


Fig. 7. Separation of phenylurea herbicides on a Silasorb SPH Amine column in a normal-phase system. Column: Silasorb SPH Amine, 7 μ m, 250 \times 4 mm I.D.; mobile phase: 20% 2-propanol in *n*-hexane, flow-rate 1.0 ml/min, UV detection at 254 nm, column temperature 40°C. Peaks: 1 = neburon; 2 = fluormethuron; 3 = diuron; 4 = monuron; 5 = phenuron; 6 = methoxuron; 7 = deschlormethoxuron.

propanol in *n*-hexane and then to 0% 2-propanol in water, minima of retention are observed in mobile phases containing 80–90% 2-propanol in water. The retention behaviour can be described over the whole range of compositions of binary mobile phases using a four-parameter equation derived on the basis of the mechanism of retention taking into account simultaneous effects of non-polar and polar interactions in the chromatographic systems studied.

(2) For the two stationary phases, the separation selectivity of phenylurea herbicides is higher in non-aqueous than in aqueous–organic mobile phases, so that binary organic solvents are to be preferred for practical separations of these compounds on chemically bonded nitrile and amino stationary phases. Because of a higher polarity of the amino group with respect to the nitrile substituent, the retention is higher on Silasorb SPH Amine than on Silasorb SPH Nitrile stationary phases and the separation selectivity differs significantly for the two stationary phases, which makes separations of phenylurea herbicides on the two columns complementary each to the other.

Acknowledgement

This research was supported by the Grant Agency of the Czech Republic, Project No. 203/94/1397.

References

- [1] L.R. Snyder, *Anal. Chem.*, 46 (1981) 1384.
- [2] L.R. Snyder and T.C. Schunk, *Anal. Chem.*, 54 (1982) 1764.
- [3] R.J. Hurtubise, A. Hussain and H.F. Silver, *Anal. Chem.*, 53 (1981) 1993.
- [4] C.A. Chang and C.-S. Chuang, *Anal. Chem.*, 57 (1985) 997.
- [5] E.L. Weisser, A.W. Salotto, S.M. Flach and L.R. Snyder, *J. Chromatogr.*, 303 (1984) 1.
- [6] J. Chmielovec and A.E. George, *Anal. Chem.*, 52 (1980) 1154.
- [7] K.-G. Liphard, *Chromatographia*, 13 (1980) 603.
- [8] W.T. Cooper and P.L. Smith, *J. Chromatogr.*, 335 (1986) 57.
- [9] P. Jandera and J. Churáček, *J. Chromatogr.*, 91 (1974) 207.
- [10] C.M. Hennion, C. Picard, C. Combellas, M. Caude and R. Rosset, *J. Chromatogr.*, 210 (1981) 211.
- [11] R.P.W. Scott and P. Kucera, *Anal. Chem.*, 45 (1973) 749.
- [12] L.R. Snyder, in Cs. Horváth (Editor), *High-Performance Liquid Chromatography — Advances and Perspectives*, Vol. 3, Academic Press, Orlando, FL, 1983, p. 186.
- [13] L.R. Snyder, J.W. Dolan and J.R. Gant, *J. Chromatogr.*, 165 (1979) 3.
- [14] A. Nahum and Cs. Horváth, *J. Chromatogr.*, 203 (1981) 53.
- [15] K.E. Bij, Cs. Horváth, W.R. Melander and A. Nahum, *J. Chromatogr.*, 203 (1981) 65.



ELSEVIER

Journal of Chromatography A, 684 (1994) 93–101

JOURNAL OF
CHROMATOGRAPHY A

Evaluation of liquid chromatography–ion spray mass spectrometry for the determination of substituted benzoic acids and their glycine conjugates[☆]

F. Kasuya*, K. Igarashi, M. Fukui

Faculty of Pharmaceutical Sciences, Kobe-gakuin University, 518, Arise, Ikawadani, Nishiku, Kobe 651-21, Japan

First received 4 March 1994; revised manuscript received 31 May 1994

Abstract

Liquid chromatography combined with pneumatically assisted electrospray (ion spray) mass spectrometry was evaluated for the characterization of low-molecular-mass compounds such as a variety of substituted benzoic acids and their glycine conjugates. Each substituted benzoic acid and its glycine conjugate formed with rat liver mitochondria were separated with a conventional C₈ packed column or a semimicro C₈ column using three mobile phases. The positive- and negative-ion mass spectra of the glycine conjugates gave abundant [M + H]⁺ and [M – H][–] ions, respectively. However, the positive-ion mass spectra of the acids were dominated by [M + H – H₂O]⁺ ions, with the exception of [M + H]⁺ ions for acids having an amino, an acetylamino or a dimethylamino group. All of the negative-ion mass spectra of acids gave dominant [M – H][–] ions. The negative-ion mass spectra of acids with halogen, nitro and cyano groups showed the ions equivalent to the mass of each functional group. Further, the alkoxy group gave a characteristic fragmentation representing loss of the alkyl moiety. The abundances of the fragment ions due to the functional groups gave information on the position of the ring substituents in the negative-ion mass spectra. The positive- and negative-ion mass spectra of the glycine conjugates revealed the presence of glycine.

1. Introduction

Compounds containing the carboxylic acid group are of great significance as drugs, herbicides and insecticides owing to a variety of interesting biological activities. In addition, xenobiotics are readily converted into carboxylic acids by metabolism. A wide range of carboxylic acids can undergo amino acids conjugations,

which vary with the animal species and the structure of the acids. Glycine conjugation has been observed to be a feature of a diversity of carboxylic acids in a wide range of species. Correlations between the chemical structure of acids and glycine conjugation are also important in order to understand detoxification mechanisms and have been discussed [1–4]. We have also elucidated the influence of chemical structure on the extent of glycine conjugation [5–7], which required methods for the determination of these compounds. Conventional gas chromatography–mass spectrometry (GC–MS) has been

* Corresponding author.

[☆] This paper is dedicated to Professor Yasumitsu Tamura on the occasion of his 70th birthday.

widely applied to the determination of the glycine conjugates. However, no information is available about pneumatically assisted liquid chromatography–electrospray mass spectrometry (LC–ion spray MS), which has been used to detect and identify a series of organic acids and their glycine conjugates. In addition, there is no report about their spectral features. It is useful for metabolism studies to elucidate the spectral characteristics of a series of acids and their glycine conjugates using different analytical techniques.

Liquid chromatography–mass spectrometry (LC–MS), which permits the separation and ionization of polar, non-volatile or thermally labile compounds without derivatization, has been widely applied in various analytical biomedical and environmental fields. Recent advances in electrospray ionization (ESI) have expanded the capabilities of LC–MS. Using this ionization technique, high-molecular-mass compounds such as proteins and peptides have been ionized and measured [8,9]. ESI has shown superior performance to other ionization methods in biomolecular analysis. In addition, the technique has allowed detection of very polar and ionic compounds. Another advantage of ESI is the low chemical background. We have previously characterized various substituted benzoic acids and their glycine conjugates by liquid chromatography–atmospheric pressure chemical ionization mass spectrometry (LC–APCI–MS) [10]. However, the acids and their glycine conjugates have very low molecular masses. Therefore, it was difficult to measure and identify lower concentrations of acids and their glycine conjugates by LC–APCI–MS owing to the higher chemical background. ESI has an excellent capability for application to very low-molecular-mass compounds because of its intrinsically low background.

Ionization based on the ion evaporation mechanism is known to be very soft and thus minimizes the fragmentation. Therefore, molecular mass information is readily accessible from an ion evaporation mass spectrum [11]. However, the mass spectra reveal no structural information. If extra internal energy is added to the ions, fragmentation can be promoted. Tandem mass

spectrometry (MS–MS) is well known for the structural information that it can provide in conjunction with soft ionization techniques [12,13]. On the other hand, it is necessary for structural identification to evaluate the use of collision-induced dissociation (CID) in combination with a single MS technique.

This paper reports the evaluation of LC–ion spray MS for the determination of a series of acids and their glycine conjugates. The extent to which degree structural information is gained by CID is also discussed. In addition, the mass spectrometric fragmentation properties of acids and their glycine conjugates are described.

2. Experimental

2.1. Chemicals

Benzoic acid and 2-methoxy-, 2-nitro-, 3-amino-, 3-chloro-, 3-methoxy-, 3-methyl-, 3-nitro-, 4-amino-, 4-acetylamino-, 4-bromo-, 4-chloro-, 4-cyano-, 4-ethoxy-, 4-methoxy-, 4-methyl-, 4-nitro-, 4-dimethylamino-, 2-chloro-4-nitrobenzoic acid were purchased from Nacalai Tesque (Kyoto, Japan). Hippuric acid and 4-aminohippuric acid were purchased from Wako (Osaka, Japan). All other chemicals were of analytical-reagent grade. N-(4-Acetylamino-benzoyl)glycine was synthesized by the method described previously [5].

2.2. Preparation of mitochondria

The animals used were Wistar-strain male rats weighing about 200–250 g. Mitochondria were prepared by the method described previously [6].

2.3. Formation of glycine conjugates of a series of substituted benzoic acids

The formation of glycine conjugates was carried out by using the technique described previously [6,7].

2.4. Instrumentation

HPLC separation was performed with a Hitachi (Tokyo, Japan) L-6200 instrument having a 5- μ m Cosmosil C₈ reversed-phase column

(150 mm × 4.6 mm I.D.) (Nacalai Tesque) or a 5- μ m Develosil C₈ reversed-phase semimicro column (150 mm × 1.5 mm I.D.) (Nomura Chemical, Aichi, Japan). The mobile phases consisted of water–methanol–acetic acid systems as follows: (a) 49.8:50:0.2, (b) 61.3:38.5:0.2 and (c) 77.8:22:0.2 (v/v/v). The flow-rate was 1 ml/min or 50 μ l/min. Each substituted benzoic acid and its glycine conjugate were separated using the same mobile phases as described previously [10]. A Hitachi M-2000 double-focusing mass spectrometer equipped with an atmospheric pressure chemical ionization (APCI) source was used. The interface for introducing the HPLC effluent to the APCI-MS system was pneumatically assisted electrospray. Analyte ions formed from the LC–ion spray MS interface were sampled into the mass spectrometer through 0.2- and 0.4-mm orifices. All positive- and negative-ion mass spectral data were obtained by scanning the mass range from m/z 1 to 500 in 4 s, with a dwell time of 0.5 s. The drift voltage varied in the range 30–75 V.

3. Results and discussion

In previous work we studied the mass spectral characterization of substituted benzoic acids and their glycine conjugates by LC–APCI-MS [10]. LC–APCI-MS provided some structural and molecular mass information. LC–ion spray MS–MS has recently been applied as an extremely attractive method for the characterization of proteins and peptides. On the other hand, the advantage of LC–ion spray MS is the low chemical background. Therefore, we used LC–ion spray MS for the determination of low-molecular-mass compounds such as substituted benzoic acids and their glycine conjugates. The ion formation process for ion spray is different from that for APCI. The ionization mechanism in APCI is known to be very similar to that of CI, whereas that of ESI is ion evaporation. As ion evaporation is a very soft ionization process, the molecular mass can be easily determined. However, the molecular mass information alone is not sufficient for structural identification of analytes. It is important for the identification of the

metabolites to gain some structural information. We investigated the use of CID for LC–ion spray MS analysis and the extent to which structural information was provided from CID mass spectra in a single MS mode.

The positive- and negative-ion mass spectra of benzoic acid derivatives were measured using water–methanol (50:50, v/v) as the eluent at a flow-rate of 50 μ l/min in the flow-injection mode (no column).

Table 1 shows the effect of drift voltage on the characteristic ions in the negative-ion mass spectra of 2-chloro-4-nitrobenzoic acid. The drift voltage is necessary in order to dissociate cluster ions into a high-abundance deprotonated molecular ion. When extra energy is added to the deprotonated molecular ion, fragmentation can be promoted. At a drift voltage of 30 V, the negative-ion mass spectrum of 2-chloro-4-nitrobenzoic acid gave a dominant $[M - H]^-$ ion at m/z 200 with little fragmentation. However, at a drift voltage of 40 V, increases in the signals at m/z 156 ($[M - COOH]^-$) and 35 (Cl^-) occurred owing to CID of the deprotonated molecular ion. At drift voltages more than 45 V, the characteristic ion at m/z 46 (NO_2^-) was also observed. The ease of elimination of the substituents depends on the position of the ring substituent. Even if the substituent is present in the same *para* position on the benzene ring, the degree of elimination differs in the type of the substituent. The ions equivalent to the mass of the iodo and bromo groups in the *para* position were easily observed at a lower drift voltage. At a slightly higher drift voltage, the fragment ion

Table 1
Effect of drift voltage on characteristic ions in the negative-ion mass spectra of 2-chloro-4-nitrobenzoic acid

Drift voltage (V)	Relative ion abundance (%)			
	m/z 200	m/z 156	m/z 46	m/z 35
30	100	8	0	0
40	38	100	0	80
45	30	100	22	100

Mobile phase, water–methanol (50:50, v/v); flow-rate, 50 μ l/min; amount injected, 300 ng; injection, flow-injection mode.

due to elimination of the cyano group in the *para* position appeared. The order of elimination of the functional group in the *para* position was Br^- , I^- , $\text{NO}_2^- > \text{Cl}^- > \text{CN}^-$. The drift voltage was kept at 50 V to obtain some structural information.

Table 2 shows characteristic ions of the negative-ion mass spectra of the *para*-substituted benzoic acids. The negative-ion mass spectra were relatively simple. $[\text{M} - \text{COOH}]^-$ ions were generated by the same fragmentations as observed for all benzoic acid derivatives. The same observations on the fragmentation of 2-chloro-4-nitrobenzoic acid were made for the mass spectra of the acids having a cyano or a halo group. The characteristic ions at m/z 26, 79 and 127 indicated the possible presence of cyano, bromo and iodo moieties, respectively. In the mass spectra of 4-methoxy- and 4-ethoxybenzoic acid, important diagnostic ions at m/z 92 were observed, which correspond to $[\text{M} - \text{COOH} - \text{CH}_3]^-$ and $[\text{M} - \text{COOH} - \text{C}_2\text{H}_5]^-$ ions, respectively. The alkoxy group gave a characteristic fragmentation representing loss of the alkyl moiety. An alkyl ion in the low-mass range did not appear. In contrast, the mass spectra of 4-methyl-, 4-amino- and 4-dimethylaminobenzoic acid were very simple, consisting primarily of $[\text{M} - \text{H}]^-$ and $[\text{M} -$

Table 3

Characteristic ions of the positive-ion mass spectra of 4-methyl- and 4-aminobenzoic acid

Substituent	Molecular mass	Characteristic ions ^a	
		$[\text{M} + \text{H}]^+$	$[\text{M} + \text{H} - \text{H}_2\text{O}]^+$
4-CH ₃	136	—	119 (100)
4-NH ₂	137	138 (100)	120 (76)

Mobile phase, water-methanol (50:50, v/v); flow-rate, 50 $\mu\text{l}/\text{min}$; amount injected, 500 ng; injection, flow-injection mode.

^a Values are m/z with relative intensities (%) in parentheses.

$\text{COOH}]^-$ ions. At a high drift voltage of 75 V, the ion due to the cleavage of the substituent was not observed. In addition, the negative-ion detection for acids having an amino, an acetyl-amino or a dimethylamino group decreased compared with that for other acids.

Table 3 shows characteristic ions of the positive-ion mass spectra of 4-methyl- and 4-aminobenzoic acid. The positive-ion mass spectra of the substituted benzoic acids were different from the negative-ion mass spectra. The positive-ion mass spectra of benzoic acid derivatives with an amino, an acetyl-amino or a dimethylamino group gave dominant $[\text{M} + \text{H}]^+$

Table 2

Characteristic ions of the negative-ion mass spectra of the substituted benzoic acids

Substituent	Molecular mass	Characteristic ions ^a			
		$[\text{M} - \text{H}]^-$	$[\text{M} - \text{COOH}]^-$	$[\text{M} - \text{COOH} - \text{R}^b]^-$	$[\text{X}^c]^-$
4-CN	147	146 (40)	102 (100)		26 (9)
4-Cl	156	155 (71)	111 (100)		35 (16)
4-Br	200	199 (63)	155 (100)		79 (38)
4-I	248	247 (100)	203 (89)		127 (72)
4-OCH ₃	152	151 (51)	107 (100)	92 (12)	
4-OC ₂ H ₅	166	165 (80)	121 (100)	92 (24)	
4-CH ₃	136	135 (79)	91 (100)		
4-NH ₂	137	136 (83)	92 (100)		
4-N(CH ₃) ₂	165	164 (51)	120 (100)		

Mobile phase, water-methanol (50:50, v/v); flow-rate, 50 $\mu\text{l}/\text{min}$; amount injected, 300 ng; injection, flow-injection mode. The drift voltage was kept at 65 V for 4-cyano-, 4-methoxy and 4-ethoxybenzoic acid.

^a Values are m/z with relative intensities (%) in parentheses.

^b R = CH₃ and C₂H₅.

^c X = CN, Cl, Br and I.

ions and $[M + H - H_2O]^+$ ions, whereas the positive-ion mass spectra of all the series except for these acids were dominated by $[M + H - H_2O]^+$ ions.

The influence of the position of the ring substituent on the mass spectrum was also investigated. Table 4 shows the influence of the position of the nitro group on the nitro anion abundance in the negative-ion mass spectra of nitrobenzoic acid. At a drift voltage of 50 V, no significant differences in the ion abundances at m/z 46 were observed. However, at a drift voltage of 45 V, the ion abundances at m/z 46 increased in the order 4-position < 3-position < 2-position (on the benzene ring). On the other hand, the mass spectra of the acids having a methoxy group offered different fragment ions in correlation with the position of the substituent (Table 4). In the mass spectrum of 4-methoxybenzoic acid taken at a drift voltage of 65 V, a signal at m/z 92 corresponding to $[M - COOH - CH_3]^-$ was observed. With the methoxy group in the 2-position, the signal at m/z 92 disappeared, whereas that at m/z 77 corresponding to $[M - COOH - OCH_3 + H]^-$ increased compared with the 3- and 4-positions. The fragment ions due to elimination of the substituent gave information on the position of the substituent.

Glycine conjugation was dependent not only on the lipophilicity of the chemicals but also on the size of both the *para* and *meta* substituents

on the benzene ring. The acids having chlorine, methyl, methoxy and ethoxy groups in either the *para* or *meta* position on the benzene ring showed high glycine conjugate formation. The acids bearing cyano, nitro, amino, acetyl amino and dimethylamino groups in the *para* or *meta* position resulted in decreases in glycine conjugation. On the other hand, the acids having a substituent in the *ortho* position were conjugated with glycine to only a small extent or did not undergo glycine conjugation.

Three synthetic glycine conjugates available were determined in both the positive- and negative-ion modes. When no synthetic glycine conjugates were available, the glycine conjugates were formed with rat liver mitochondria. For the HPLC separation of each acid and its glycine conjugate, the acetic acid concentration required for the mobile phase was more than 0.2% in water–methanol. Both a conventional packed column (150 mm \times 4.6 mm I.D.) and a semimicro packed column (150 mm \times 1.5 mm I.D.) were used. On-line LC with pneumatically assisted electrospray was best accomplished with low mobile phase flow-rates. Flow-rates of up to 200 μ l/min could be used. However, the optimum flow-rate was ca. 50 μ l/min. Therefore, splitting of the LC eluent with the use of the 4.6 mm I.D. column is necessary in order to increase the ionization efficiency and ensure stable liquid drop formation. When HPLC separation was performed with the use of the 4.6 mm I.D.

Table 4

Influence of the position of the functional groups on characteristic ions in the negative-ion mass spectra of methoxy- and nitrobenzoic acid

Substituent	Relative ion abundance (%)						
	m/z 166	m/z 122	m/z 46	m/z 151	m/z 107	m/z 92	m/z 77
2-NO ₂	57	100	82				
3-NO ₂	65	100	33				
4-NO ₂	56	100	12				
2-OCH ₃				62	95	0	100
3-OCH ₃				45	100	31	3
4-OCH ₃				51	100	12	0

Mobile phase, water–methanol (50:50, v/v); flow-rate, 50 μ l/min; amount injected, 300 ng; injection, flow-injection mode; drift voltage, 45 V for nitrobenzoic acid and 65 V for methoxybenzoic acid.

column at a flow-rate of 1.0 ml/min, the splitting ratio was 1:20. Most of the samples injected were split to waste. On the other hand, the major advantage of the use of the semimicro column is that it does not require a postcolumn split. The losses of samples by splitting of the LC eluent could be circumvented by the use of the semimicro column. An increase in sensitivity could be achieved by using the semimicro column when the sample amounts injected were limited. However, larger volumes (20 μ l) of samples injected into the semimicro packed column resulted in broader peaks. Separation with the use of the semimicro column was performed using the same mobile phases as with the 4.6 mm I.D. column.

Fig. 1 shows full-scan total ion and extracted ion profiles of the supernatant obtained after incubation with (A) 3-methylbenzoic and (B) 3-chlorobenzoic acid in the rat liver mitochondria. The mass spectra were measured using water-methanol-acetic acid (49.8:50:0.2, v/v/v) as the eluent for both (A) and (B) at a flow-rate of 50 μ l/min through a semimicro column. A typical mass chromatogram measured in the positive-ion mode is shown in (A) and that in the negative-ion mode in (B). Inspection of the total ion current (TIC) profile for the positive-ion mode revealed a few chromatographic peaks. The extracted ion profiles for the ions at m/z 119 and 194, corresponding to $[M + H - H_2O]^+$ and $[M + H]^+$, respectively, showed 3-methylbenzoic acid and its glycine conjugate, respectively. The

TIC profile for the negative-ion mode was noisy. One reason is that stable liquid drop formation in the negative-ion mode is more difficult than that in the positive-ion mode. The negative-ion mode of operation was less sensitive than the positive-ion detection mode. The presence of 3-chlorobenzoic acid and its glycine conjugate in the rat liver mitochondria could be detected via the extracted ion profiles at m/z 155 and 212, respectively. Characteristic ions of the mass spectra of the glycine conjugates of 3-chlorobenzoic and 3-methylbenzoic acid are shown in Tables 5 and 6. In the negative-ion mode, 100-pmol levels of the acids yielded sufficient $[M - H]^-$ and $[M - COOH]^-$ ion intensities to allow interpretation. Low-molecular-mass compounds such as acids and their glycine conjugates were detected less sensitively by using LC-ion spray MS than in the LC-ion spray MS-MS analysis of proteins reported previously [14]. One reason is that scattering losses in the interface are most likely for ions of relatively low mass. Scattering losses are expected to be less important as the ions become heavier [14]. However, LC-ion spray MS was sufficiently sensitive to be applicable to the detection and identification of acids and their glycine conjugates in rat liver mitochondria.

To obtain structural characteristic information on glycine conjugates, the negative-ion mass spectra of hippuric acid were measured at different drift voltages. The negative-ion mass spectrum of hippuric acid taken at a drift voltage of

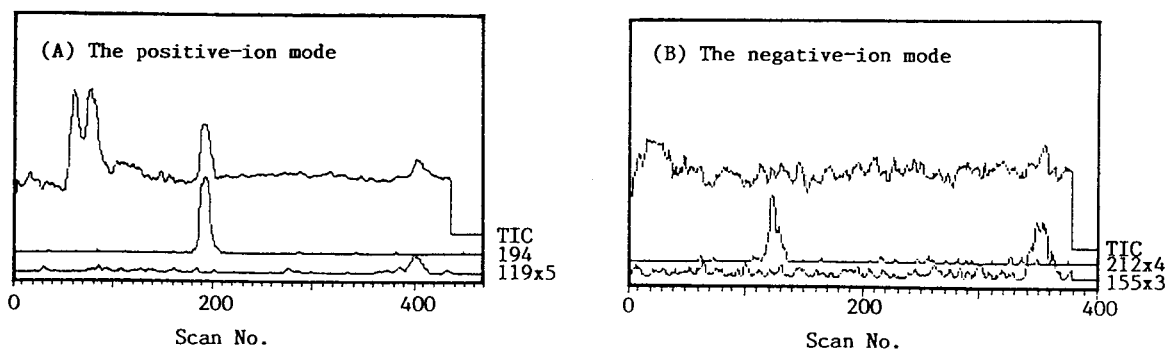


Fig. 1. Typical full-scan total ion and extracted ion profiles of the supernatant obtained after incubation with (A) 3-methylbenzoic acid and (B) 3-chlorobenzoic acid in rat liver mitochondria. Mobile phase, water-methanol-acetic acid (49.8:50:0.2, v/v/v); flow-rate, 50 μ l/min.

Table 5
Characteristic ions of the negative-ion mass spectra of glycine conjugates

Substituent	Molecular mass	Characteristic ions ^a			
		[M - H] ⁻	[M - COOH] ⁻	[M - CONHCH ₂ COOH] ⁻	Others
H	179	178 (100)	134 (46)	77 (66)	
3-Cl	213	212 (80)	168 (55)	111 (60)	35 (100)
4-Cl	213	212 (100)	168 (51)	111 (61)	35 (88)
3-CH ₃	193	192 (100)	148 (29)	91 (82)	
4-CH ₃	193	192 (100)	148 (41)	91 (53)	
4-CH ₃ O	209	208 (100)	164 (39)	107 (71)	
4-NH ₂	194	193 (100)	149 (43)	92 (71)	
4-CH ₃ CONH	236	235 (100)	191 (41)	134 (80)	92 (18)

Column, Develosil 5C₈; drift voltage, 65 V; flow-rate, 50 μl/min; mobile phase, water-methanol-acetic acid (49.8:50:0.2, v/v/v) for the glycine conjugates of 3-chloro-, 4-chloro-, 3-methyl- and 4-methylbenzoic acid, (61.3:38.5:0.2, v/v/v) for the glycine conjugates of benzoic acid and 4-methoxybenzoic acid and (77.8:22:0.2, v/v/v) for the glycine conjugates of 4-amino- and 4-acetylamino benzoic acid.

^a Values are *m/z* with relative intensities (%) in parentheses.

30 V showed a dominant [M - H]⁻ ion at *m/z* 178 with very low-abundant fragment ions. The mass spectrum at a drift voltage of 50 V gave only abundant [M - H]⁻ and [M - COOH]⁻ ions, which were observed in the negative-ion mass spectra of the acids. At a drift voltage of 75 V, an additional signal at *m/z* 77 ([M - CONHCH₂COOH]⁻) increased (Table 5). The drift voltage was set to 65 V in order to promote specific fragmentations of glycine conjugate.

Table 5 shows characteristic ions in the negative-ion mass spectra obtained from tracing the deprotonated molecular ions of glycine conjugates. The mass spectra were measured using three mobile phases at a flow-rate of 50 μl/min through a reversed-phase semimicro column. All negative-ion mass spectra gave characteristic ions of the glycine conjugates, consisting of [M - H]⁻, [M - COOH]⁻ and [M - CONHCH₂COOH]⁻ ions. The mass spectrum of

Table 6
Characteristic ions of the positive-ion mass spectra of glycine conjugates

Substituent	Molecular mass	Characteristic ions ^a			
		[M + H] ⁺	[M - NHCH ₂ COOH] ⁺	[M - CONHCH ₂ COOH] ⁺	Others ([M + Na] ⁺ etc.)
H	179	180 (48)	105 (100)	77 (16)	202 (10)
3-Cl	213	214 (62)	139 (100)	111 (14)	236 (8)
4-Cl	213	214 (55)	139 (100)	111 (10)	236 (12)
3-CH ₃	193	194 (21)	119 (100)	91 (17)	216 (13)
4-CH ₃	193	194 (18)	119 (100)	91 (11)	216 (18)
4-CH ₃ O	209	210 (20)	135 (100)		232 (9), 121 (10)
4-NH ₂	194	195 (26)	120 (100)	92 (26)	217 (10)
4-CH ₃ CONH	236	237 (35)	162 (100)		259 (16), 120 (63)

Column, Develosil 5C₈; drift voltage, 65 V; flow-rate, 50 μl/min; mobile phase, water-methanol-acetic acid (49.5:50:0.2, v/v/v) for the glycine conjugates of 3-chloro-, 4-chloro-, 3-methyl- and 4-methylbenzoic acid, (61.3:38.5:0.2, v/v/v) for the glycine conjugates of benzoic acid and 4-methoxybenzoic acid and (77.8:22:0.2, v/v/v) for the glycine conjugates of 4-amino- and 4-acetylamino benzoic acid.

^a Values are *m/z* with relative intensities (%) in parentheses.

4-acetylaminohippuric acids showed an additional signal at m/z 92, corresponding to a characteristic loss of CH_2CO from the $[\text{M} - \text{CONHCH}_2\text{COOH}]^-$ ion. In the presence of a chloro group, the chloride anion was observed in the low-mass region. The ions due to the cleavage of the substituent were also observed in the same fragmentation as with the acids.

The positive-ion mass spectra were determined by the same method as for the negative-ion mode. In the mass spectrum of the glycine conjugate of 4-aminobenzoic acid, a drift voltage of 30 V led to a dominant $[\text{M} + \text{H}]^+$ ion, but a change from 40 to 75 V led to higher fragmentation levels, resulting in increases in signals at m/z 120 ($[\text{M} - \text{NHCH}_2\text{COOH}]^+$) and 92 ($[\text{M} - \text{CONHCH}_2\text{COOH}]^+$). These fragmentations in the positive-ion mass spectra were characteristic for all glycine conjugates. However, a signal corresponding to loss of CH_2COOH from the protonated molecular ion, which is one of characteristic ions for the glycine conjugates obtained by LC-APCI-MS, could not be observed in the ion spray mass spectrum. The positive-ion mass spectra of glycine conjugates provided more useful structural information for the presence of glycine than the negative-ion mass spectra. Apart from these fragment ions, the mass spectrum of 4-acetylaminohippuric acid taken at a drift voltage of 75 V showed $[\text{M} - \text{NHCH}_2\text{COOH} - \text{CH}_3\text{CO} + \text{H}]^+$ ion at m/z 120. In the presence of an alkyl or an amino group, no information on the substituents was obtained in either the positive- or the negative-ion mode. The chloride anion also was not observed in the low-mass region.

4. Conclusions

LC-ion spray MS was applied to the determination of low-molecular-mass compounds such as benzoic acid derivatives and their glycine conjugates. LC-ion spray MS could make interpretation of the spectrum obtained from low levels of the analyte easier than with LC-APCI-MS. LC-ion spray MS did not always provide molecular

information. All of the negative-ion mass spectra of the substituted benzoic acids and their glycine conjugates gave dominant $[\text{M} - \text{H}]^-$ ions with little fragmentation. However, all of the positive-ion mass spectra of glycine conjugates were dominated by $[\text{M} + \text{H}]^+$ ions, whereas those of acids gave dominant $[\text{M} + \text{H} - \text{H}_2\text{O}]^+$ ions, except for the $[\text{M} + \text{H}]^+$ ions for the acids having an amino, an acetyl amino or a dimethylamino group. LC-ion spray MS provided less structural information than LC-APCI-MS. However, the CID technique was beneficial for obtaining some structural information on the substituted benzoic acids and their glycine conjugates even using the single MS mode. The negative-ion mass spectra of the substituted benzoic acids permitted identification of the position and kind of substituent. The negative- and positive-ion mass spectra of glycine conjugates revealed the presence of glycine and the kind of substituent from the characteristic fragmentation patterns. The mass spectrometric fragmentation properties obtained from LC-ion spray MS allow the detection and identification of metabolites in biological samples.

References

- [1] J. Caldwell, in A. Aitio (Editor), *Conjugation Reactions in Drug Biotransformation*, North-Holland, Amsterdam, 1978, p. 111.
- [2] J. Caldwell, J.R. Idle and R.L. Smith, in T.E. Gram (Editor), *Extrahepatic Metabolism of Drug and Other Foreign Compounds*, SP Medical and Scientific Books, New York, 1980, p. 453.
- [3] J. Caldwell, in W.B. Jakoby (Editor), *Metabolic Basis of Detoxification*, Academic Press, New York, 1982, p. 271.
- [4] H.V. de Waterbeemd, B. Testa and J. Caldwell, *J. Pharm. Pharmacol.*, 38 (1986) 14.
- [5] F. Kasuya, K. Igarashi and M. Fukui, *J. Pharm. Sci.*, 76 (1987) 303.
- [6] F. Kasuya, K. Igarashi and M. Fukui, *J. Pharmacobiodyn.*, 13 (1990) 432.
- [7] F. Kasuya, K. Igarashi and M. Fukui, *J. Pharmacobiodyn.*, 14 (1991) 671.
- [8] J.A. Loo, H.R. Udseth and R.D. Smith, *Anal. Biochem.*, 179 (1989) 404.
- [9] J.A. Loo, C.G. Edmons, H.R. Udseth and R.D. Smith, *Anal. Chem.*, 62 (1990) 693.

- [10] F. Kasuya, K. Igarashi and M. Fukui, *J. Chromatogr.*, 654 (1993) 221.
- [11] A.P. Bruins, T.R. Covey and J.D. Henion, *Anal. Chem.*, 59 (1987) 2642.
- [12] K. Biemann, *Anal. Chem.*, 58 (1986) 1228A.
- [13] D.F. Hunt, J.R. Yates, J. Shabanowitz, S. Winston and C.R. Hauer, *Proc. Natl. Acad. Sci. U.S.A.*, 83 (1986) 6233.
- [14] S.A. McLuckey, G.J. Van Berkel, G.L. Glish, E.C. Huang and J.D. Henion, *Anal. Chem.*, 63 (1991) 375.



ELSEVIER

Journal of Chromatography A, 684 (1994) 103–111

JOURNAL OF
CHROMATOGRAPHY A

Analysis of neutral nitrogen compounds in diesel oil by direct injection high-performance liquid chromatography–mass spectrometry–ultraviolet spectrometry methods

John Mao^{a,b,*}, Carlos R. Pacheco^{a,c}, Daniel D. Traficante^{a,d}, William Rosen^a

^aDepartment of Chemistry, University of Rhode Island, Kingston, RI 02881, USA

^bSpringborn Laboratories, Inc., 790 Main Street, Wareham, MA 02571, USA

^cChemistry Division of Petrobras/Cenpes, Rio de Janeiro, Brazil

^dNMR Concepts, University of Rhode Island, Kingston, RI 02881, USA

First received 29 March 1994; revised manuscript received 21 June 1994

Abstract

An analytical methodology has been developed for the direct analysis of neutral nitrogen compounds in diesel oil by HPLC with subsequent detection using MS and/or photodiode-array UV spectrometry. By diluting diesel oils with one volume of hexane, diesel samples could be injected directly onto an alumina analytical column and then eluted with a gradient mobile phase consisting of hexane and dioxane. Nitrogen compounds were selectively retained on the alumina column, eluted using LC, and then detected by particle beam LC-MS or UV at 254, 270 and 290 nm. Two Brazilian and one Arabian diesel distillates were investigated. Alkylcarbazoles and alkylindoles were identified as the major neutral nitrogen components. Structural identification was accomplished by combination of electron impact MS and UV analyses. The concentration of carbazoles and indoles was estimated using calibration standards of carbazole and indole, respectively.

1. Introduction

It has been known for sometime that nitrogen compounds in petroleum adversely affect many of the important petroleum refining processes that are important in industry [1]. Many different nitrogen compounds, even at very low concentration levels (ppm), may poison the catalysts used in cracking and hydrocracking reforming

processes presumably through interactions with the acid sites of these catalysts [2]. Because of the deleterious effects that nitrogen-containing compounds exhibit numerous studies have been conducted leading to the isolation, characterization and identification of the nitrogen compounds extant in petroleum [3–8]. Generally, both basic and neutral (non-basic) nitrogen compound types are found in petroleum distillates, with the neutral nitrogen compounds usually being the predominant entity types. The basic nitrogen compounds can be obtained by acid (HCl or H₂SO₄) extraction of the oil [8], while the neutral nitrogen compounds can be isolated

* Corresponding author. Address for correspondence: Springborn Laboratories, Inc., 790 Main Street, Wareham, MA 02571, USA.

through adsorption to an active adsorbent [8] like activated aluminum oxide. Although many of the established methods for the analysis of nitrogen-containing compounds in petroleum are effective, they often are time consuming and labor intensive. This is partially attributable to the lack of selectivity and sensitivity with respect to both separation and detection. As a result, extensive sample clean-up is usually necessary prior to analytical measurements. For instance, gas chromatography coupled to mass spectrometry (GC–MS) is widely used in the petroleum industry to monitor nitrogen compounds [9–11]. The high separation power of GC when coupled with MS detection has made this methodology particularly successful for analyzing samples of a complex nature, such as diesel oils. Nevertheless, certain non-volatile and polar compounds are not suitable for GC and further, to eliminate matrix interference, sample clean-up is essential. Because of the extreme complexity of petroleum products, very little attention has been given to the direct analysis of diesel oils by either gas or liquid chromatography. Our work explored the possibility of direct analysis of diesel oils by selective normal-phase liquid chromatography (LC) so that oil samples can be quickly screened for nitrogen compounds without labor-intensive sample preparation. Our results are therefore reported below.

Three samples were investigated: a Brazilian diesel oil (laboratory distilled), a Brazilian light cycle oil, and a commercial Arabian straight run diesel. In a previous study [12], we reported the isolation and identification of major nitrogen compounds in the three diesel samples by particle beam LC–MS and UV spectrometry. Alkyl carbazoles were identified as the major neutral nitrogen compounds in the Brazilian and Arabian straight run diesel samples [12], while alkyl indoles were the major neutral nitrogen compounds in the light cycle oil sample [13]. Alkyl benzoquinolines were identified as the major basic nitrogen compounds in the Brazilian diesel sample [12,13]. The results obtained in the present work are comparable to those obtained previously [12,13] and demonstrate the potential

application of this direct analysis methodology to these very complex mixtures.

2. Experimental

2.1. Materials

The Brazilian diesel and light cycle oil were provided by Petrobras, Brazil. The Brazilian diesel sample was laboratory distilled at Petrobras with a boiling range of 200–400°C. The total nitrogen content of this sample was approximately 700 ppm. The Brazilian light cycle oil (boiling range: 206–314°C) contained approximately 2000 ppm of total nitrogen. The Arabian straight run diesel was also provided by Petrobras, Brazil. This sample had a boiling range of 171–377°C and contained approximately 102 ppm of total nitrogen, while reference standards of carbazole, indole, acridine and benzo[*h*]quinoline were purchased from Aldrich and were analytical grade. Chemical structures of these compounds are shown in Fig. 1. All other chemicals were obtained from commercial sources and were at a minimum reagent grade. All solvents were HPLC grade.

2.2. Sample preparation

Prior to high-performance liquid chromatography (HPLC), all samples were diluted with one volume of hexane and solutions were ana-

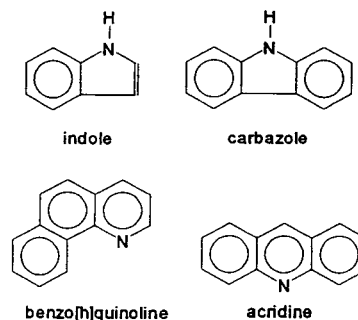


Fig. 1. Chemical structures of the nitrogen compounds investigated.

lyzed directly by HPLC–UV or particle beam LC–MS.

2.3. HPLC

HPLC–UV analyses were conducted using a Hewlett-Packard Model 1090 liquid chromatograph equipped with a gradient solvent pump, an autosampler and a photodiode-array detector. Samples were monitored at 254, 270 and 290 nm and UV spectra were collected at a scan range of 220–400 nm. LC–MS analyses were conducted using a Hewlett-Packard Model 1050 gradient solvent pump, a Hewlett-Packard Model 1050 autosampler and a Hewlett-Packard Model 5989A MS Engine (mass spectrometer) equipped with a particle beam interface. Full-scan electron impact (EI) mass spectra were obtained using 70

eV electron energy. The ion source temperature was 250°C and the analyzer temperature was 120°C. The interface was maintained at 50°C at a carrier gas (helium) flow of 50 p.s.i. (1 p.s.i. = 6894.76 Pa). The instrument was optimized by adjusting nebulizer and helium flow using flow injection analysis of a carbazole standard. Under the normal-phase HPLC conditions, the ion source pressure was approximately $1 \cdot 10^{-4}$ – $2 \cdot 10^{-4}$ Torr (1 Torr = 133.322 Pa).

Normal-phase HPLC separations of oil samples were achieved on a Spherisorb alumina (5 μ m, 250 \times 4.6 mm) column using gradient elution at 0.7 ml/min. Elution solvent A was hexane and solvent B was hexane–dioxane (50:50). The linear gradient program was: 0 min, 100% A; 20 min, 100% A; 120 min, A–B (90:10).

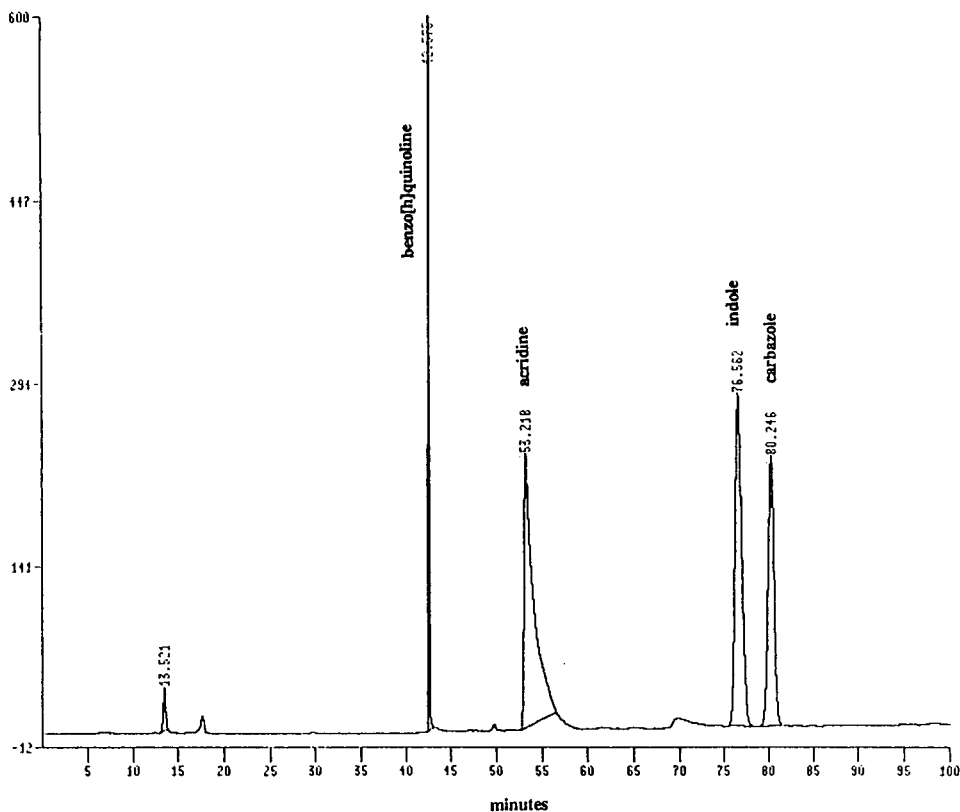


Fig. 2. HPLC–UV chromatogram (254 nm) of a standard mixture. Injection volume: 5 μ l.

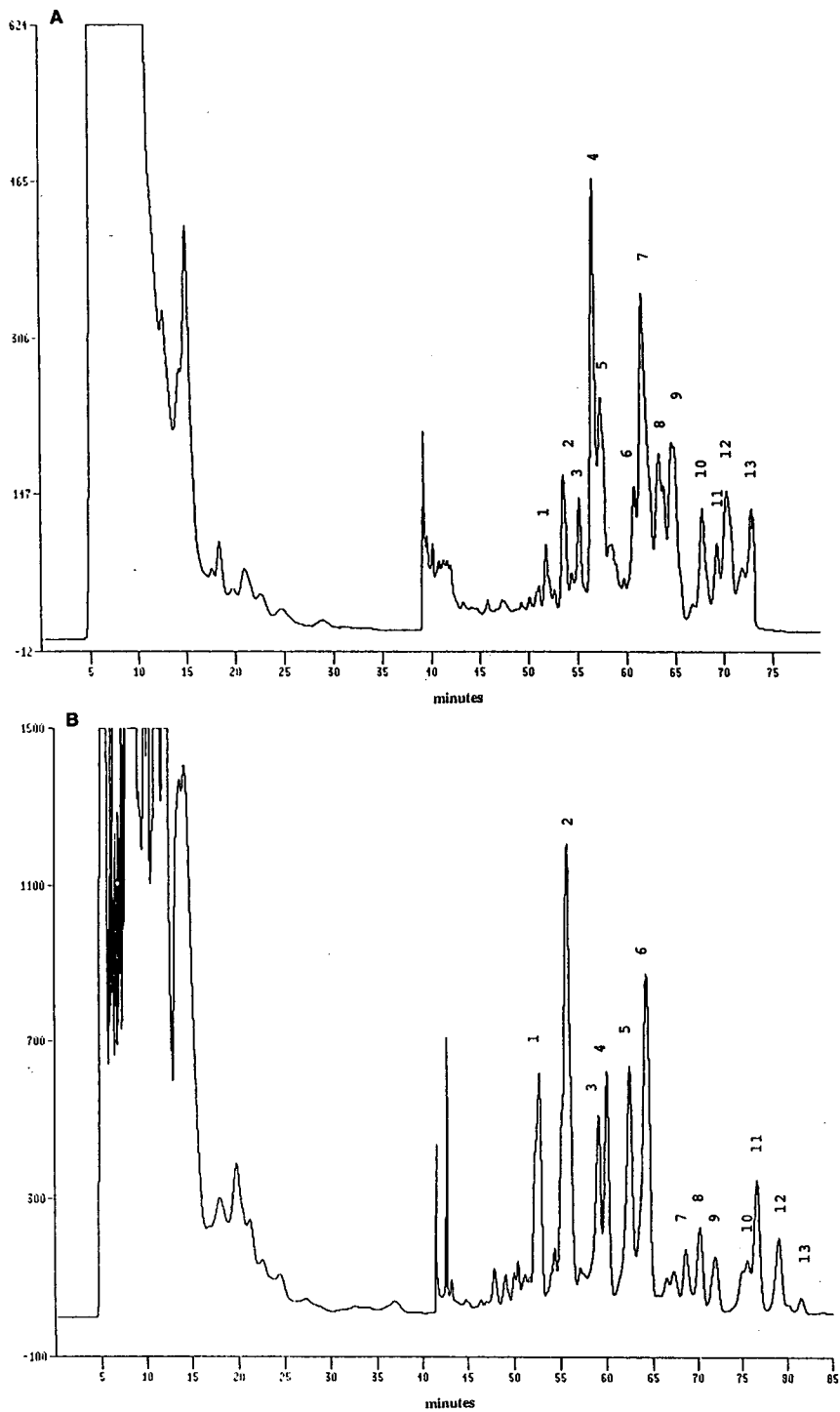


Fig. 3. (A) HPLC-UV chromatogram (290 nm) of the Brazilian diesel sample. Injection volume: 25 μ l. Major alkylcarbazole peaks are numbered (1–13). (B) HPLC-UV chromatogram (270 nm) of the Brazilian light cycle oil sample. Injection volume: 25 μ l. Major alkylindole and alkylcarbazole peaks are numbered (1–13).

2.4. Estimation of the concentrations of carbazoles and indoles

The concentrations of carbazoles and indoles in oil samples were estimated by HPLC–UV at 290 and 270 nm, respectively, using external calibration. External calibration standards of carbazole and indole were prepared in hexane at 500 ppm and analyzed with the samples. Because of the long HPLC runtime, the quantitation was based on a single-point calibration using peak area. The detector linearity was demonstrated over a range of 10–500 mg/l for both carbazole and indole using isocratic elution (to shorten the analysis time). Based on the detector response for the lowest calibration standard (10 mg/l), a ppm method detection limit was a reasonable estimation for both carbazoles and indoles in diesel samples.

3. Results and discussion

Neutral nitrogen compounds in petroleum products are frequently isolated by normal-phase column chromatography using activated

aluminum oxide [8]. While hydrocarbons and other interfering components have very little or no retention on the column, the nitrogen compounds are selectively retained and can be eluted with stronger normal-phase solvents (e.g. chloroform, methylene chloride). This principle can certainly be extrapolated onto the analytical scale where nitrogen compounds can be analyzed directly using an HPLC analytical column without precolumn concentration enrichment.

In this work, we investigated four classes of compounds: carbazoles, indoles, benzoquinolines and acridines. The separation of a standard mixture containing these four reference standards is shown in Fig. 2. Neutral nitrogen compounds (carbazole and indole) retained significantly longer on the alumina column than the basic nitrogen compounds (benzo[*h*]quinoline and acridine). This separation was used successfully to monitor carbazoles and indoles in oil samples. On the other hand, because of the relatively short retention times, benzoquinolines and acridines were not adequately separated from the matrix polyaromatic hydrocarbons and the interference from the matrix militated against using direct injection methods for these basic nitrogen compounds. Thus the method

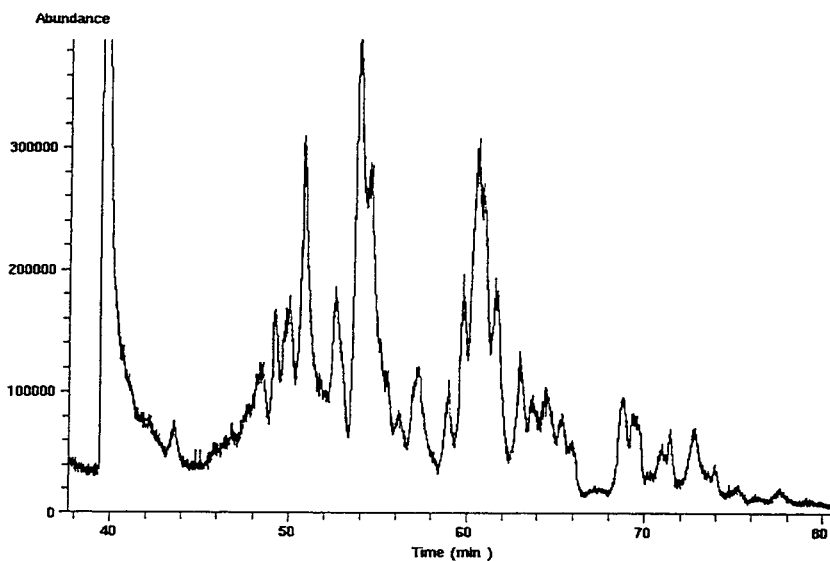


Fig. 4. Total ion chromatogram of the Brazilian diesel sample. Ion source temperature: 250°C; scan range: 110–250 u; injection volume: 50 μ l.

developed in this work is more useful for the neutral nitrogen compounds than for the basic nitrogen compounds. (Because of the polar nature of the basic nitrogen compounds, reversed-phase HPLC is the preferred separation technique.) HPLC–UV analyses of the Brazilian diesel and light cycle oil are presented in Fig. 3. As shown, hydrocarbons were eluted with hexane during the first 30–35 min, while the neutral nitrogen compounds were retained and eluted with a gradual increase of the mobile phase strength (through gradient elution). Although the runtime was relatively long (100 min), peak broadening was not severe and adequate quantitation was achieved.

Approximately 13 major peaks were observed at 290 nm in the Brazilian diesel sample (Fig. 3A). They were identified as the C₁–C₅-carbazoles (mostly methyl and multiple methyl substitutions). The identification was based on EI-MS and UV spectrometry of each peak. The *m/z* values of molecular ions were used to differentiate carbazole homologues. The LC–MS total ion chromatogram of this sample is presented in Fig. 4. Extracted ion chromatograms of *m/z* 181, 195, 209, 223 and 237 are presented in Fig. 5, showing the distribution of C₁–C₅-carbazoles. Full-scan EI mass spectra of selected peaks are shown in Fig. 6. Although there were ion contributions resulting from fragmentation of

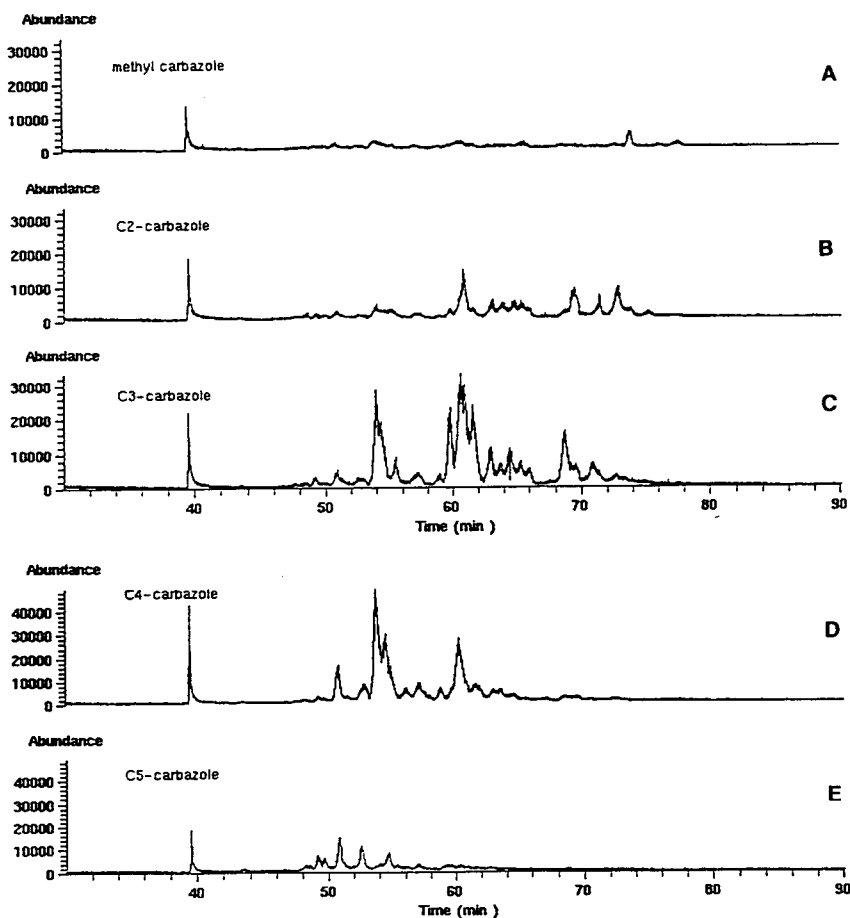


Fig. 5. Extracted ion chromatograms [*m/z* 181 (A), 195 (B), 209 (C), 223 (D) and 237 (E)] of the Brazilian diesel sample.

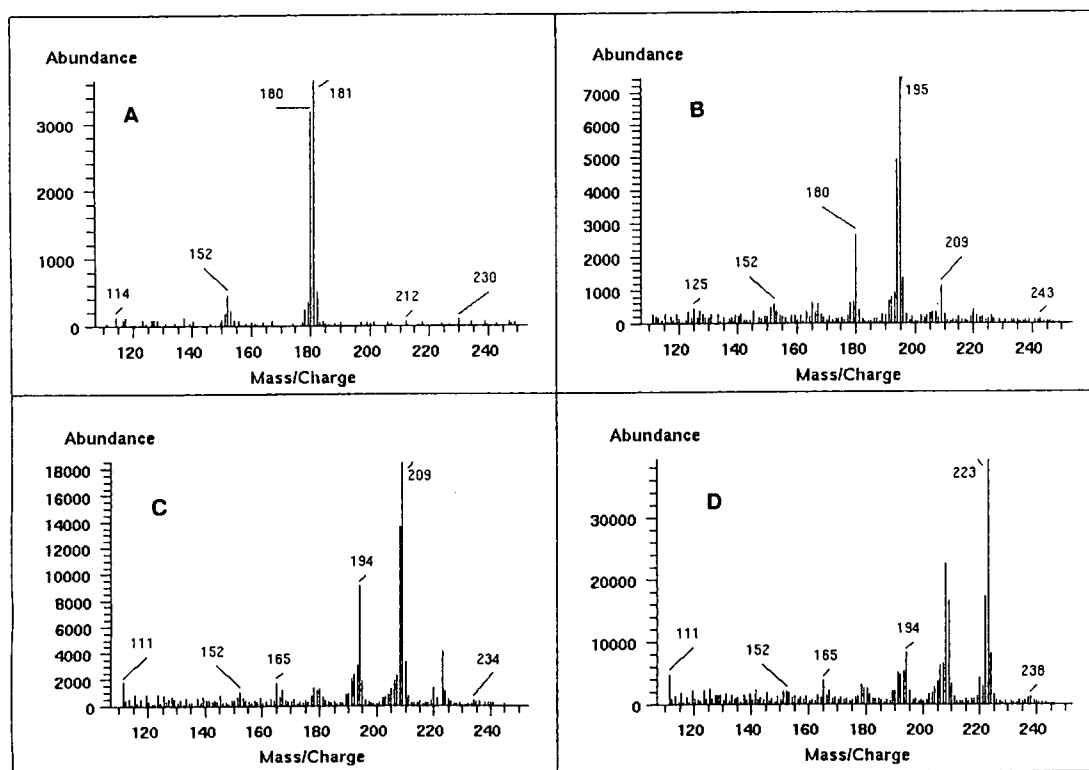


Fig. 6. Full-scan LC-EI-MS mass spectra of (A) methyl carbazole, (B) C₂-carbazole, (C) C₃-carbazole and (D) C₄-carbazole identified in the Brazilian diesel sample.

higher carbazole homologues (for example, C₄-carbazole, molecular ion 223, also produces m/z 209), it was apparent that the C₃- and C₄-carbazoles were the major carbazole homologues and represented the majority of the neutral nitrogen compounds in this sample. Carbazole itself was not detected in this sample. The elution order generally was C₅- < C₄- < C₃- < C₂- < methyl carbazole < carbazole although some overlapping does occur. To confirm peak assignments, the UV spectrum (220–400 nm) of each peak was collected online using a photodiode-array detector. Two representative UV spectra (peak 4 and 7) are presented in Fig. 7A. (UV spectra for the authentic standards of carbazole and indole exhibited characteristic λ_{\max} at 270 and 290 nm with little overlap.) Peak 4 was identified by LC-MS to be C₄-carbazole and peak 7 to be C₃-carbazole. The two UV spectra

were very similar, indicating that alkyl groups had little effect on the UV absorption of carbazoles [12].

The analysis of the Brazilian light cycle oil revealed that the major neutral nitrogen compounds were indoles (indole, methyl indoles, and dimethyl indoles [13]) (Fig. 3B). Approximately 13 major peaks representing indoles and carbazoles were observed. Representative UV spectra of different alkyl indoles (peaks 2 and 6) are shown in Fig. 7B. Although indoles and carbazoles eluted at approximately the same retention time region (Fig. 3A and B), they can be distinguished by signal ratios at 290 and 270 nm. The signal ratio (290 nm/270 nm) is greater than 2 for carbazoles and less than 0.6 for indoles. LC-MS analysis of this sample, however, showed only carbazoles because of the low mass sensitivity of LC-MS for indoles. The LC-MS

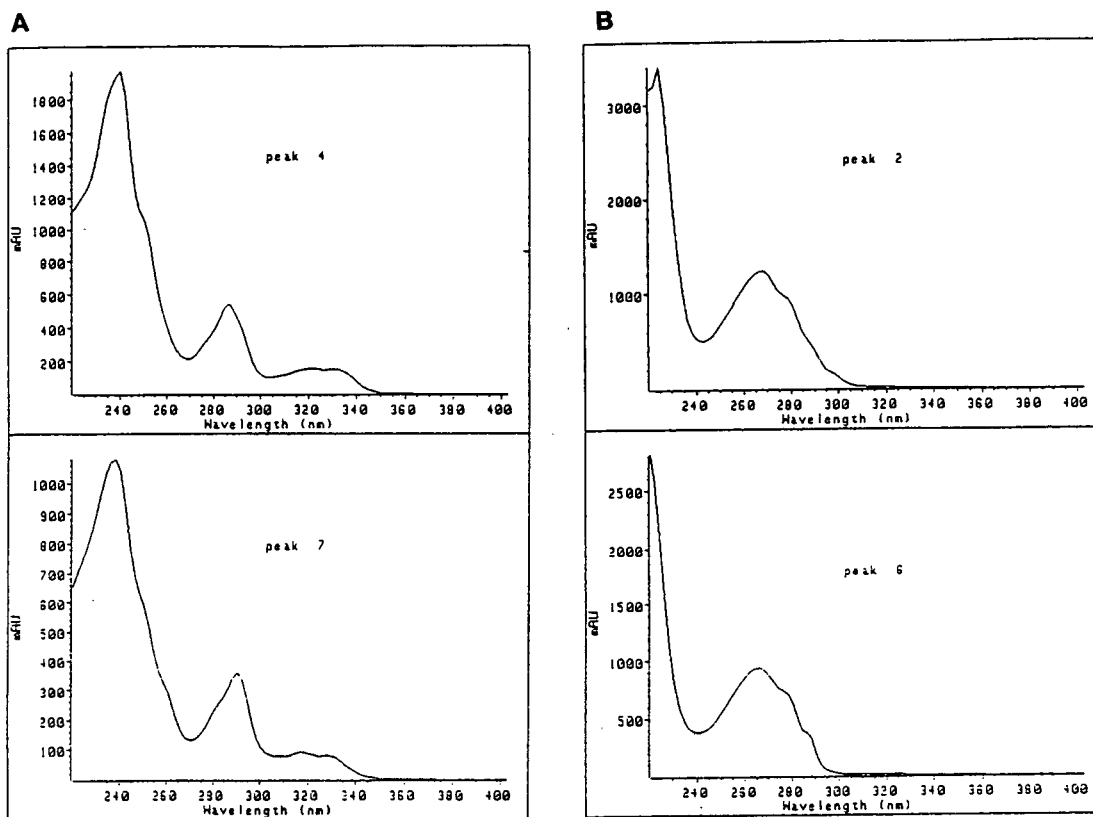


Fig. 7. UV spectra of (A) carbazoles in the Brazilian diesel sample and (B) indoles in the Brazilian light cycle oil.

sensitivity for indole was approximately three orders of magnitude less than for carbazole, presumably due to the relatively high volatility of indole. As a result, direct analysis of indoles by particle beam LC-MS was not possible. (Enrichment of indoles by extraction or column chromatography is needed for analysis by particle beam LC-MS.) Among the carbazoles detected in this light cycle oil sample (by LC-MS), carbazole (peak 13) and methyl carbazoles were the major homologues. The HPLC profile of the Arabian straight run diesel sample was very similar to that of the Brazilian diesel. As with the Brazilian diesel, carbazoles were determined to be the major neutral nitrogen compounds in the Arabian straight run diesel sample, but in much lower quantities.

The concentrations of total carbazoles and

indoles in the three samples were estimated by HPLC-UV. The total carbazole concentrations were approximately 2440, 435 and 514 mg/l in the Brazilian diesel, the Brazilian light cycle oil and the Arabian straight run diesel, respectively. The total indole concentration was measured to be approximately 21 770 mg/l in the Brazilian light cycle oil. Indoles were not found in the other two oil samples. Due to the lack of reference standards, carbazole and indole were used to quantify their alkyl homologues at 290 and 270 nm, respectively. Thus, the concentrations reported can only serve as an estimation. Based on the UV detector sensitivity for standards of carbazole and indole, a method detection limit of ppm level can be readily achieved for analysis of both classes of compounds in diesel oils by normal-phase HPLC.

4. Conclusions

By using alumina normal-phase liquid chromatography, we have demonstrated the usefulness of a direct analysis method for determination of neutral nitrogen compounds in diesel oils. Combining MS and photodiode-array detection, we analyzed three diesel samples of different origins and illustrated the potential application of such a direct analysis method for petroleum products. Although particle beam LC-MS showed poor sensitivity for indoles, it displayed exceptionally good sensitivity and selectivity for carbazoles and therefore can be used to screen for carbazoles in petroleum products without labor-intensive sample preparations. This method, however, is not applicable to basic nitrogen compounds because of their high polarities.

Acknowledgement

The authors would like to thank Petrobras for providing the oil samples. This project was funded by Petrobras, Springborn Laboratories, Inc. and NMR Concepts.

References

- [1] L. Chan, J. Ellis and P.T. Crisp, *J. Chromatogr.*, 292 (1984) 355.
- [2] H.V. Drushel and A.L. Sommers, *Anal. Chem.*, 38 (1966) 19.
- [3] M. Dorbon and C. Bernasconi, *Fuel*, 68 (1989) 1067.
- [4] J.F. McKay, J.H. Weber and D.R. Latham, *Anal. Chem.*, 48 (1976) 891.
- [5] B.A. Tomkins and C.-H. Ho, *Anal. Chem.*, 54 (1982) 91.
- [6] S.J. Marshman, *Fuel*, 70 (1991) 967.
- [7] J.-M. Schmitter, H. Colin, J.L. Excoffier, P. Arpino and G. Guiochon, *Anal. Chem.*, 54 (1982) 769.
- [8] G.K. Hartung and D.M. Jewell, *Anal. Chim. Acta*, 26 (1962) 514.
- [9] G. Grimmer, J. Jacob and K.-W. Naujack, *Anal. Chem.*, 55 (1983) 2398.
- [10] M. Dorbon, I. Ignatiadis, J.-M. Schmitter, P. Arpino, G. Guiochon, H. Toulhoat and A. Huc, *Fuel*, 63 (1983) 565.
- [11] D.W. Later, T.G. Andros and M.L. Lee, *Anal. Chem.*, 55 (1983) 2126.
- [12] J. Mao, C.R. Pacheco, D.D. Traficante and W. Rosen, *Fuel*, (1994) in press.
- [13] J. Mao, C.R. Pacheco, D.D. Traficante and W. Rosen, *Anal. Chem.*, (1994) submitted for publication.



ELSEVIER

Journal of Chromatography A, 684 (1994) 113–119

JOURNAL OF
CHROMATOGRAPHY A

Identification of potentially mutagenic contaminants in the aquatic environment by liquid chromatographic–thermospray mass spectrometric characterization of *in vitro* DNA adducts

Douglas W. Kuehl^{a,*}, Jose Serrano^a, Sandra Naumann^{b,1}

^a*Environmental Research Laboratory–Duluth, US Environmental Protection Agency, Duluth, MN 55804, USA*

^b*ASCI Corporation, Duluth, MN 55804, USA*

First received 10 May 1994; revised manuscript received 20 June 1994

Abstract

Liquid chromatographic–thermospray mass spectrometric (LC–TSP–MS) characterization of chemical adducts of DNA formed during *in vitro* reactions is proposed as an analytical technique to detect and identify those contaminants in aqueous environmental samples which have the propensity to be genotoxic, i.e. to covalently bond to DNA. The approach for direct-acting chemicals includes the *in vitro* incubation of DNA with contaminated aqueous samples at 37°C, pH 7.0 for 0.5 to 6 h, followed by enzymatic hydrolysis of the DNA to deoxynucleosides and LC–TSP–MS analysis of the resultant solution. A series of allylic reagents was used as model reactive electrophiles in synthetic aqueous samples to demonstrate that adduct formation was linear with both contaminant concentration and electrophilic reactivity potential. The characterizations can also estimate the proportion of bonding to different sites on a base, for instance, the ratio of O⁶- to 7-alkylguanine (oxygen vs. nitrogen bonding) products, which is an important parameter in assessing the genotoxicology of chemicals.

1. Introduction

Potentially mutagenic chemical agents are recognized as being contaminants in the aquatic environment, including municipal and industrial discharges, hazardous waste leachates and contaminated sediments. The development of protocols for the regulation of discharges and the remediation of contaminated areas is dependent upon the careful detection and identification of potential mutagens. Those identifications, how-

ever, can be very difficult because the potentially mutagenic chemicals are often (1) at very low concentrations, (2) in the presence of much higher concentrations of non-mutagenic contaminants and (3) poorly recovered during sample processing. Their identification has been based primarily upon extensive gas chromatographic–mass spectrometric (GC–MS) characterizations of all (or as many as possible) chemicals in an extract, followed by an assessment of the structures to determine which might possibly be mutagenic [1]. The use of MS–MS spectra [2] and the integration of GC–MS with mutagenic response bioassays [3] have been added to improve the chances of mutagen detection. An

* Corresponding author.

¹ Present address: PACE Laboratories, Charlotte, NC 27808, USA.

alternative approach for the selective detection and identification of mutagens was proposed by Cheh and Carlson [4]. They assessed the ability of low-molecular-mass nucleophilic reagents to selectively label electrophilic (mutagenic) contaminants in complex solutions after sample enrichment. The label provided an easily identifiable moiety with which to detect potential mutagens.

The use of selective labeling to identify potentially mutagenic contaminants in complex environmental samples is also being investigated in these laboratories. First, using a gas chromatograph interfaced to the collision cell of a tandem quadrupole mass spectrometer, it was demonstrated that potentially mutagenic environmental contaminants could be selectively detected after reaction with gas phase nucleophilic labeling reagents in the collision cell of the mass spectrometer [5–7], and second, we have been assessing aqueous *in vitro* reactions of electrophiles with their ultimate *in vivo* target, DNA, as the labeling reagent. In contrast to reactions with low-molecular-mass nucleophilic reagents, reactions with DNA are important because many environmental contaminants which are metabolically activated to reactive electrophiles, such as polynuclear aromatic hydrocarbons, require the DNA double helix structure for adduct formation to occur [8]. Further, DNA adducts formed *in vitro* have the analytical advantage over adducts formed *in vivo* of not being destroyed by cellular DNA repair mechanisms before they can be identified.

The second technique, using DNA as a labeling reagent, is the subject of this report. Our objective was to conduct a feasibility study to determine if liquid chromatography–thermospray mass spectrometry (LC–TSP–MS) can be used to identify potentially mutagenic chemicals isolated from aqueous environmental samples (effluents, leachates, etc.) by selectively bonding to DNA during *in vitro* reactions. Although the non-chemospecific measurement of DNA adducts by ^{32}P -postlabelling has previously been proposed as a technique to assess the presence of mutagenic contaminants in environmental samples [9], to the best of our knowledge, LC–TSP–

MS has not been applied to the characterization of potentially mutagenic chemical contaminants isolated in such a manner.

A series of allylic reagents has been selected to test the proposed protocol. The potential of these reagents to alkylate nucleophiles has previously been correlated to their mutagenic potential [10,11]. Some of the compounds selected, because of their highly reactive nature, may not necessarily be identified as an environmental contaminant. However, they can serve as a good set of demonstration chemicals because of their previous extensive characterization.

2. Experimental

2.1. Chemical reagents

Acetonitrile (spectrograde) was obtained from EM Scientific (Gibbstown, NJ, USA). Ammonium acetate (ACS reagent grade), allylchloride, allylbromide, allyliodide and allylisothiocyanate were obtained from Aldrich (Milwaukee, WI, USA) and used without further purification. Nucleosides, enzymes and calf thymus DNA were obtained from Sigma (St. Louis, MO, USA).

Caution: Allyl reagents should be used with care in a well ventilated area or chemical fume hood.

2.2. Instrumentation

A Finnigan-MAT (San Jose, CA, USA) Model TSQ-70 triple quadrupole mass spectrometer coupled through a Finnigan-MAT Model TSP-2 thermospray interface to a Beckman Model 340 liquid chromatograph was used to characterize DNA hydrolysates. The HPLC system was equipped with a Supelcosil LC-18s reversed-phase column (Supelco, Bellefonte, PA, USA). The mobile phases were programmed after 3 min from 3% to 15% B in 6 min and to 85% B in an additional 6 min. The system was then maintained at 85% B for an additional 10 min. Simultaneously, the flow-rate was increased after 3 min from 1.2 to 1.4 ml/min in 12 min,

and similarly maintained at that value for an additional 10 min. Mobile phases A and B were 1.5% and 30% acetonitrile in water, respectively. Both mobile phases were 0.05 M ammonium acetate, pH 6.5. The mass spectrometer was operated in both the positive ion and pulsed positive/negative ion scan modes. The positive ion scan was 105–405 u/s. The pulsed scan was 105–405 u/0.5 s for positive ions and 120–405 u/0.5 s for negative ions. Argon at approximately 1 Torr (1 Torr = 133.322 Pa) was used as the collision gas for MS–MS experiments. Collision energies varied from –0.5 to –20.0 V, and mass spectrometer–mass spectrometer voltage correction (MSMSC) was 50 V.

2.3. Alkylation of deoxyguanosine

To 100 μ mol of deoxyguanosine in 500 μ l 50 mM Tris–HCl (pH 7.0) were added 100 μ mol allylbromide in 100 μ l dimethyl sulfoxide (DMSO). The reaction mixture was stirred at 37°C for 2 h. The reaction was stopped by placing it on ice, and analyzed directly by LC–TSP-MS.

2.4. *In vitro* DNA alkylation reactions

Calf thymus DNA (200 μ g) was dissolved in 100 mM Tris–HCl pH 7.0 (500 μ l). To this was added from 0.5 to 25 μ mol allyl reagent in 10 to 100 μ l DMSO. The reaction was maintained at 37°C for 0.5 to 6 h. The reactions were stopped by placing the reaction on ice for 10 min. The DNA was then precipitated from the reaction mixture by the addition of 50 μ l of 3 M LiCl followed by the slow addition of 450 μ l isopropanol, chilling the mixture to –20°C, and centrifuging for 30 min at 10 000 g. The solvent and excess reagent were removed by drying the DNA in a rotary vacuum evaporator.

2.5. DNA hydrolysis

Hydrolysis of DNA to deoxynucleosides was achieved by the consecutive application of nuclease P₁, phosphodiesterase I and alkaline phosphatase as previously described [12].

2.6. Quality assurance/quality control

Performance of the LC–TSP-MS for analyte elution, signal response and mass calibration was evaluated using calibration standards of deoxynucleosides [12]. Alkylation reactions were conducted and analyzed in replicate.

3. Results and discussion

Products formed during the *in vitro* reaction of unsubstituted allylic compounds with DNA have previously been identified by Eder et al. [13]. Product distribution was dominated by reactions with the purine bases, guanine and adenine. They observed that 7-allylguanine (7-A-Gua) and 3-allyladenine were released spontaneously during alkylation while N⁶-allyladenine and O⁶-allylguanosine (O⁶-A-Dguo) were released only during enzymatic hydrolysis of DNA to free deoxynucleosides. Alkylation of guanine at the 7 position (nitrogen) is expected to be the predominant product formed during reactions of double-stranded DNA with low-molecular-mass direct-acting electrophiles [14]. The proportion of bonding at O⁶ relative to N-7, however, is an important parameter in the evaluation of genotoxic risk [15].

The experiments performed here were based upon the results of Eder et al. [13] and were designed to assess several factors necessary to determine if the proposed protocol was a feasible approach to developing a method for the chemospecific identification of environmental mutagens. It was necessary to demonstrate whether (1) alkylation product formation was linear with the concentration of a mutagenic contaminant in an aqueous sample, (2) alkylation product formation was proportional to the relative reactivity of various mutagenic contaminants in an aqueous sample and (3) it was possible to determine the relative proportion of guanine alkylation products which had been formed, i.e. N-7 vs O⁶ allylguanine.

Identification of the products of alkylation of deoxyguanosine (dGuo) and DNA by allylbromide using LC–TSP-MS are presented in

Table 1

Identification of three alkylated guanines produced during in vitro reactions of allylbromide with deoxyguanosine and calf thymus DNA

Analyte	M + H	RRT (dCyd = 0) ^a	Nucleophile	
			dGuo (%) ^b	DNA (%) ^b
dGuo	268	1.00	–	–
N ² -A-dGuo	308	2.61	53	0.4
7-A-Gua	192	2.89	35	99
O ⁶ -A-dGuo	308	3.90	12	0.6

The table provides *m/z* values of M + H ions and relative LC retention time of products. Data also show the difference in product distribution of modified dGuo relative to the total amount of modified dGuo obtained when dGuo is free in solution vs. held in the DNA double helix during the reaction. (Product distributions from the two reactions are estimated by calculating [M + H]⁺ TSP peak area ratios, and are not quantitative.) Reaction conditions: 37°C, pH 7.0, 2 h, 5 μmol allylbromide, 100 μg DNA or 5 μmol dGuo.

^a RRT = Relative retention time.

^b Modification/total modification × 100.

Table 1. Identification of modified products was based upon increasing reversed-phase liquid chromatography elution order presented by Eder et al. [13] (N²-allylguanosine before 7-A-Gua followed by O⁶-A-dGuo), upon appropriate mass spectral *m/z* values (*m/z* 192, B + 2H allylguanosine and M + H allylguanine; and *m/z* 308, M + H allylguanosine), and upon the detection of a predominant product resulting from N-7 alkylation of guanine in the DNA structure compared to dGuo free in solution. Further, the N-7 reaction product was confirmed to be a modified base by the inability to detect an ion at *m/z* 308 during a MS–MS product ion experiment. The reaction product determined to be O⁶-A-dGuo was further characterized by determining that the ion at *m/z* 308 produced an ion at *m/z* 192 during a MS–MS precursor-ion experiment.

DNA alkylation product formation, as a function of the concentration of the mutagenic contaminant in the sample, was assessed by determining the amount of 7-A-Gua and O⁶-A-dGuo formed relative to the amount of dGuo present in the final reaction product hydrolysate. The results are presented in Table 2. The production of 7-A-Gua increased rapidly with the dose of allylbromide, exceeding the amount (peak area ratio, *m/z* 192 M + H 7-A-Gua:*m/z* 152 B + 2H dGuo) of dGuo at a dose of just over

5.0 μmole allylbromide. In spite of the large loss of dGuo, the formation of O⁶-A-dGuo increased linearly from 0.5 to 25 μmol allylbromide ($r^2 = 0.995$).

DNA alkylation product formation, as a function of the reactivity of individual mutagenic components in an aqueous sample, was assessed by determining the relative amount of 7-A-Gua formed during the reaction of 5 μmol of each of four allylic reagents, allylisothiocyanate, allylchloride, allylbromide and allyliodide, with DNA. The amount of product formed relative to

Table 2

Product formation during in vitro reactions of allylbromide with DNA

Dose (μmol) allylbromide	Modification/dGuo	
	7-A-Gua	O ⁶ -A-dGuo
0.5	0.12	<0.0001
5.0	0.93	0.015
7.5	2.11	0.025
12.5	–	0.05
25.0	–	0.11

Data show an increase in product formation relative to dGuo as the amount of allylbromide added to the reaction increases. Product formation calculated from [M + H]⁺ TSP peak areas; not quantitative. Reaction conditions: 37°C, pH 7.0, 6 h, 100 μg DNA.

dGuo (peak area measured as before) was compared to alkylating activity [4-nitrobenzylpyridine (NBP)] and mutagenic activity (*Salmonella typhimurium* TA 100) previously presented by Eder et al. [11] (Table 3). NBP activity was found to correlate with mutagenic activity at $r^2 = 0.999$. The correlation between DNA alkylation product formation determined by LC-TSP-MS with NBP reactivity was $r^2 = 0.891$. Allyliodide was not found to be as reactive in the DNA alkylation experiment as was expected from the mutagenicity results. The reason for this is not known; however, it is possible that because of the high reactivity of this compound, some of it had hydrolyzed to the less reactive allyl alcohol.

The propensity of an environmental contaminant to be more or less carcinogenic relative to other contaminants can potentially be estimated by evaluating its initial N-7:O⁶ alkylation ratio [15]. The data presented in Table 1 indicate that it was possible to estimate this ratio using LC-TSP-MS characterizations of in vitro DNA alkylation reactions. For instance, for the reaction conditions of 5 μmol allylbromide, 37°C and 6 h and 100 μg DNA, the estimated ratio of N-7:O⁶ calculated using peak areas of M+H ions was found to be 62:1. Accurate ratio determinations, of course, would require analytical quantification standards.

These studies indicate that the proposed protocol for the chemospecific detection of po-

tentially mutagenic environmental contaminants is feasible, and therefore further experiments should be conducted to extend the technique. Additional studies will include sample-enrichment procedures [4,16], integration of the protocol into toxicity identification evaluation (TIE) procedures [17] and complex mixture analysis. Our preliminary investigations into LC-TSP-MS characterization of contaminants metabolized by liver microsomal preparations to reactive species indicate that the protocol can be readily extended to contaminants such as polynuclear aromatic hydrocarbons (PAHs) [18], where the reactive form of the molecule, the diol epoxide metabolite, covalently bonds with N² of dGuo.

It must be remembered that the modifying moiety which has covalently bonded to DNA is not the intact environmental contaminant which one wishes to identify, but a only portion of the original molecule which remains after it has been modified to become the reactive species. Although systematic studies to optimize TSP analyses have shown that TSP can be reproducible and highly sensitive [19], TSP spectra of deoxynucleosides are generally quite simple and usually do not contain sufficient information for a complete characterization of the modifying moiety. However, numerous instrumental techniques are available to enhance fragmentation and thus provide more structural information. These techniques include variation of vaporizer and/or source temperature, selection of filament and/or

Table 3

Comparison of the formation of 7-A-Gua ($[M+H]^+$ TSP peak area ratio) produced during the in vitro alkylation of DNA by four different allyl reagents to the alkylating (NBP) and mutagenic activity obtained by Eder et al. (11)

Allyl reagent	LC-TSP-MS, 7-A-Gua/dGuo	Alkylating activity, NBP (ΔE_{560}) ^a	Mutagenic activity (revertants/ μmol)
Thiocyanate	<0.0001	0.03	1
Chloride	0.002	0.3	9
Bromide	0.012	54	700
Iodide	0.018	164	2000

Formation of 7-A-Gua relative to dGuo was estimated from $[M+H]^+$ TSP peak area; not quantitative. Reaction conditions: 37°C, pH 7.0, 2 h, 5 μmol allylbromide, 100 μg DNA.

^a Data from Ref. 11. ΔE_{560} = Molar extinction coefficient measured at 560 nm.

discharge ionization and collision-induced dissociation with the TSP repeller [20] and by MS–MS. A review of MS techniques for the characterization of the modifying moiety in DNA alkylations has been presented by McCloskey and Crain [21].

Sensitivity (full mass range scanning, positive ion) for the characterization of a modifying moiety using the protocol proposed here was assessed by analyzing a series of standards each containing Guo (500 pg/ μ l) and decreasing amounts of 7-methylGuo (to 1 pg/ μ l). It was found that at the greatest concentration ratio for Guo to 7-methylGuo (500:1), the ratio of the TSP peak area of M + H for each analyte was 228:1, and that 1 pg/ μ l (100 μ l injected) of 7-methylGuo produced a signal-to-noise ratio (*S/N*) of 7:1. For an injection volume of 100 μ l taken from 500 μ l of solution produced by the hydrolysis of 100 μ g DNA, this sensitivity represents the detection of approximately 1 modified guanine per 10 000 guanine residues.

Alternative analytical techniques to LC–TSP–MS, such as LC–continuous-flow fast atom bombardment MS (LC–FAB–MS) may also be feasible for these types of analyses. For instance, Kostianen et al. [22] have recently used LC–FAB–MS to successfully characterize butadienemoxide/deoxyadenosine reaction products, and Wolf and Vouros [23] have used it to characterize N-acetoxy-N-acetyl-2-aminofluorene/dGuo adducts with a sensitivity of one adduct per 10^6 normal bases. Finally, we believe that low-molecular-mass nucleophilic reagents, such as 4-nitrothiophenol [4] and NBP [11], which have been used to assess the reactivity of electrophilic chemicals can be used to conduct a preliminary assessment of environmental samples for reactive contaminants. We have therefore also been pursuing the development of alternative nucleophilic reagents suitable for high-sensitivity characterization by GC–MS, using highly selective precursor and product ion scans in both positive and negative ionization modes [24]. No single analytical technique or biological assay can be expected to completely characterize all potentially mutagenic contaminants in an environmental sample, but the proto-

col described in this paper can serve as a complementary technique to other existing techniques.

Acknowledgements

The authors are grateful for the assistance of University of Minnesota–Duluth, Department of Chemistry students Monica Bostrom, Mya-Lisa Crotty, Sandra Fisketjon and Jon Engstrom. We are also grateful to Drs. James McCloskey and Pamela Crain, University of Utah, for their advice. Mention of trade names or commercial products does not constitute endorsement or recommendation by the US Environmental Protection Agency.

References

- [1] S. Lesage, *J. Chromatogr.*, 642 (1993) 65–74.
- [2] W.J. Dunn III and D. Swain, *Chemometrics Intelligent Lab. Syst.*, 19 (1993) 175–179.
- [3] K.C. Donnelly, P. Davol, K.W. Brown, M. Estiri and J.C. Thomas, *Environ. Sci. Technol.*, 21 (1987) 57–64.
- [4] A.M. Cheh and R.E. Carlson, *Anal. Chem.*, 53 (1981) 1001–1006.
- [5] J.A. Freeman, J.V. Johnson, M.E. Hail, R.A. Yost and D.W. Kuehl, *J. Am. Soc. Mass Spectrom.*, 1 (1990) 110–115.
- [6] J.A. Freeman, J.V. Johnson, R.A. Yost and D.K. Kuehl, *Anal. Chem.*, 66 (1994) 1902–1910.
- [7] B.V. Rozynov, D.W. Kuehl and R.M. Carlson, in preparation.
- [8] R.G. Harvey and N.E. Geacintov, *Acc. Chem. Res.*, 21 (1988) 66–72.
- [9] N.J. Jones and J.M. Parry, *Aq. Toxicol.*, 22 (1992) 323–344.
- [10] E. Eder, T. Neudecker, D. Lutz and D. Henschler, *Chem.-Biol. Interactions*, 38 (1982) 303–315.
- [11] E. Eder, D. Henschler and T. Neudecker, *Xenobiotica*, 12 (1982) 831–848.
- [12] J. Serrano, D.W. Kuehl and S. Naumann, *J. Chromatogr.*, 615 (1993) 203–213.
- [13] E. Eder, D. Lutz and M. Jörns, *Chem.-Biol. Interactions*, 61 (1987) 97–108.
- [14] B. Singer, in J.F. Lemontt and W.M. Generoso (Editors), *Molecular and Cellular Mechanisms of Mutagenesis*, Plenum, New York, 1982, pp. 1–42.
- [15] H. Bartsch, B. Terracini, C. Malaveille, L. Tomatis, J. Wahrendorf, G. Brun and B. Dodet, *Mutation Res.*, 110 (1983) 181–219.

- [16] D.W. Kuehl and R.C. Dougherty, *Environ. Sci. Technol.*, 14 (1980) 447–449.
- [17] D.W. Kuehl, G.T. Ankley, L.P. Burkhard and D. Jensen, *Hazard. Waste Hazard. Materials*, 7 (1990) 283–291.
- [18] J. Serrano, D.W. Kuehl and M.L. Crotty, *J. Chromatogr. A*, (1994) in preparation.
- [19] C.E.M. Heeremans, R.A.M. van der Hoven, W.M.A. Niessen, U.R. Tjaden and J. van der Greef, *J. Chromatogr.*, 474 (1989) 149–162.
- [20] W.H. McFadden and S.A. Lammert, *J. Chromatogr.*, 385 (1987) 201–211.
- [21] J.A. McCloskey and P.F. Crain, *Int. J. Mass Spectrom. Ion Processes*, 118/119 (1992) 593–616.
- [22] R. Kostianen, P. Koivisto and K. Peltonen, *J. Chromatogr.*, 647 (1993) 91–94.
- [23] S.M. Wolf and P. Vouros, *Chem. Res. Toxicol.*, 7 (1994) 82–88.
- [24] R.M. Carlson, *Cooperative Research Project CR816783*, Department of Chemistry, University of Minnesota–Duluth, Duluth, MN/ERL-Duluth, US Environmental Protection Agency, Duluth, MN, 1993.



ELSEVIER

Journal of Chromatography A, 684 (1994) 121–131

JOURNAL OF
CHROMATOGRAPHY A

Automated headspace analysis of fumigants 1,3-dichloropropene and methyl isothiocyanate on charcoal sampling tubes

Jianying Gan* Scott R. Yates, William F. Spencer, Marylynn V. Yates

*US Department of Agriculture–Agricultural Research Service Pesticide and Water Quality Research Unit,
Department of Soil and Environmental Sciences, University of California, Riverside, CA 92521, USA*

First received 6 April 1994; revised manuscript received 17 June 1994

Abstract

Charcoal tubes are widely used for collecting organic vapor in the atmosphere, and the measurement is usually completed by analyzing an aliquot of the solvent phase following solvent extraction, typically with carbon disulfide. However, the sensitivity of this method is limited and sometimes too low for monitoring contaminants at trace levels in the environmental atmosphere. In this study, the potential of static headspace analysis techniques was explored on two common fumigants, 1,3-dichloropropene (1,3-DCP) and methyl isothiocyanate (MITC), on both coconut- and petroleum-based charcoal sampling tubes, using an automated and programmable headspace sampler. Three important parameters in the headspace analysis, equilibrating temperature and time, and amount of extracting solvent, were optimized individually for each compound–charcoal tube combination to achieve maximum sensitivity of GC analysis. Higher stability was observed for both isomers of 1,3-DCP and MITC on petroleum-based charcoal, and 180 and 190°C, and 5 min were selected as the equilibrating temperatures and time, respectively. On coconut-based charcoal tubes, however, all the compounds were more sensitive to the temperature, and 160 and 140°C, and 5.0 and 3.0 min were therefore determined as the equilibrating temperatures and times for the 1,3-DCP isomers and MITC, respectively. Reducing solvent volume from 3 to 1 ml in 9-ml headspace vials improved the sensitivity and 1.0 ml benzyl alcohol was therefore selected for all the compound–charcoal tube combinations. Compared to the conventional extraction method with CS₂, the optimized headspace methods were 10–35 times more sensitive, and equivalently reproducible except for MITC on coconut-based ORBO-32 tubes. Better sensitivity and precision of measurements were consistently obtained on petroleum-based charcoal tubes, and the minimum detection limits were estimated as 0.2 and 0.5 ng per tube for the (*Z*)- and (*E*)-isomers of 1,3-DCP, respectively, and 2.0 ng per tube for MITC. With the automated headspace method, sample preparation was simplified and sample throughput was greatly enhanced, and up to 200 samples could be analyzed on a 24-h basis under the optimum conditions.

1. Introduction

The (*Z*)- and (*E*)-isomers of 1,3-dichloro-

propene (1,3-DCP) and metham-sodium (sodium N-methyldithiocarbamate) are widely used as soil fumigants for parasitic plant nematodes [1,2].

In soil, metham-sodium decomposes quickly to produce methyl isothiocyanate (MITC) [3]. A

* Corresponding author.

significant fraction of the applied fumigants may diffuse up to the soil surface and escape into the atmosphere as organic vapor due to their extremely high vapor pressures [4]. As found with chlorofluorocarbons, methyl chloroform, halons and methyl bromide, many chlorine and bromine-containing compounds may possess the power of ozone destruction. The continuation of the soil-disinfection practice using these fumigants may largely rely on the extent of their emission into the atmosphere and the possible adverse impact on the environment. To monitor the behavior of 1,3-DCP and MITC after application, methods of sampling and analysis with high sensitivity and sample throughput need to be developed.

Though many sampling methods such as solvent scrubbing and cryogenic concentration exist, solid adsorption is the most effective and widely used method for collecting organic contaminants in the atmosphere [5]. Two basic types of solid adsorbent are commonly used. The more traditional method, used in many procedures recommended by the National Institute for Occupational Safety and Health (NIOSH), utilizes charcoal as the adsorbent, followed by solvent desorption and GC analysis of an aliquot of the solvent extract [5,6]. The other method uses porous polymer adsorbents, such as Tenax and polyurethane foams. Direct thermal desorption into the GC system is commonly used for Tenax, while exhaustive solvent extraction, usually Soxhlet extraction, is used for polyurethane foams [5,7,8]. Both methods have advantages and disadvantages. Collection using charcoal tubes usually allows high flow-rates and large sampling volumes, and charcoal sampling tubes are inexpensive and easy to handle both in the field and in the laboratory [9]. However, since only a few μl of the entire solvent extract (a few ml) are injected into the GC system, two to three orders of magnitude dilution is often involved, which results in relatively low sensitivity of detection for this method. Besides, the interferences from solvent and the dissolved impurities are sometimes also disadvantages. With Tenax and thermal desorption, since the entire or main portion of the sample is introduced into

the GC system, the sensitivity of analysis is usually high. However, sampling tubes packed with Tenax-GC (or other types of Tenax) only allows small safe sampling volumes and low flow-rates, especially for compounds with low boiling points, for which the sampling volumes are often limited to $< 1\text{ l}$ and flow-rates to $< 50\text{ ml min}^{-1}$ [7]. Tenax is expensive and conditioning prior to installation is usually required. Sample stability on Tenax is sometimes also poor, and each analysis is destructive and usually takes long time which results in low sample throughput [10]. Soxhlet extraction of samples on polyurethane foams is time and solvent consuming, and the impurities are extracted together with the interested compounds. Therefore, improvements leading to better analytical sensitivity for air samples on charcoal tubes are highly desirable and of great practical importance.

Measurement of interested analytes from the vapor phase in the headspace in a closed system instead of directly from the sample matrix, i.e., headspace analysis, has been extensively used in the qualitative and quantitative determination of chemical residues and flavors in food products [11,12], and pollutants in water and other aqueous solutions [13,14] and soil and other solids [15,16]. Headspace analysis eliminates the entry of sample solution or solvent and the interfering non- or semi-volatile impurities into the GC column, simplifies the sample preparation process, and often offers better sensitivity for the analysis of volatile compounds. Jentzsch et al. [17] and Kolb [18] first reported the use of an electropneumatic dosing device in the place of a manual gas-tight syringe to automate some of the steps in their headspace-GC applications. Automated dynamic headspace samplers, or purge-and-trap systems, and static headspace samplers, have become commercially available, which provide enhanced precision and sample throughput through the automation. However, so far very little effort has been made to investigate the applicability of headspace analysis techniques in analyzing air samples on charcoal adsorbents [19,20].

Charcoals of two different origins, coconut-based and petroleum-based, are currently used

in packing charcoal sampling tubes. Charcoal in a glass tubing is divided into a larger front adsorption bed (A) and a smaller backup adsorption bed (B) with glass wool plugs and glass wool or polyurethane spacers. Charcoal tubes with this type of configuration are generally classified as ORBO tubes [5]. Different types of ORBO tubes are recommended for different compounds by NIOSH [5]. Use of charcoal tubes for the sampling of fumigants in air has been reported for 1,3-DCP and MITC, and the safe flow-rates and sampling volumes which did not cause any significant breakthrough have been well defined [21,22]. However, in those studies, solvent desorption with CS₂ or other solvents (such as acetone and benzene) was used, and the sensitivity of analysis and sample throughput were relatively low. The reported best minimum detection limits (MDLs) were 0.2 µg m⁻³ for 1,3-DCP and 1.0 µg m⁻³ for MITC when 40 l of air were sampled [21]. These limits may be sufficient for monitoring the atmosphere at workplaces, but not high enough for environmental monitoring in the field.

In this paper, headspace analysis methods for the (*Z*)- and (*E*)-isomers of 1,3-DCP and MITC using a static headspace autosampler are reported. Conditions including the equilibrating temperature and time, and solvent volume, were optimized to generate maximum sensitivity and precision of measurement. The sensitivity and precision of measurements using the optimized headspace methods were compared to the conventional solvent extraction method using CS₂ as the solvent.

2. Experimental¹

2.1. Chemicals and ORBO tubes

Standard of 1,3-DCP in a mixture of the (*Z*)- (71%) and (*E*)- (27%) isomers was purchased

from Chem Service (West Chester, PA, USA). MITC standard was purchased from Sigma (St. Louis, MO, USA) with a purity of >99.0%. Benzyl alcohol and carbon disulfide were all from Fisher Scientific (Fair Lawn, NJ, USA) and used without further purification.

Two types of charcoal sampling tubes, coconut-based ORBO-32 and petroleum-based ORBO-306, were purchased from Supelco (Bellefonte, PA, USA). Both tubes had the same configuration, and 600 mg charcoal (20–40 mesh, 0.08–0.16 mm) in a 100 × 8 mm O.D. tubing was divided into bed A (400 mg) and bed B (200 mg) by using glass wool plugs and polyurethane spacers. The unused ORBO tubes were flame-sealed at both ends. Before use, the tubes were prepared by cutting both ends off using a tube-cutter (Supelco) and smoothed with a file.

2.2. Headspace autosampler and gas chromatograph

A Tekmar (Cincinnati, OH, USA) 7000 static headspace autosampler connected in tandem with a HP 5890 GC (Hewlett-Packard, Fresno, CA, USA) was used for the sample introduction in all the headspace analyses. Manual injection on the GC system was performed when an aliquot of the CS₂ extract was analyzed.

The GC carrier gas (helium for both electron-capture and nitrogen–phosphorus detectors) was split into two flows before entering the headspace autosampler: a carrier flow through a 6-port valve, the heated oven section in the headspace autosampler, the transfer line between headspace autosampler and GC system, and then into the GC column; and a pressurization flow through the lines, sample loop and stationary needle. While in operation, headspace vials containing samples were heated, mixed and equilibrated at a preset temperature for a programmed period of time, and then raised onto the stationary needle, puncturing the septum. Pressurization gas filled the vial via the side pore on the needle, and the original static pressure and the added pressure together drove a fraction of the headspace atmosphere in the vial through the needle and the line into the sample loop. The

¹ Names of products are included for the benefit of the reader and do not imply endorsement or preferential treatment by the US Department of Agriculture.

6-port valve was then switched and the sample in the sample loop was swept into the GC column by the carrier gas. The concentration of the analyte in the headspace determines the amount of analyte to be delivered to the GC system and therefore the signal output from each injection, and the equilibration of the analyte among the three phases, i.e., headspace, solvent and solid phases, determines the precision of the measurement.

A capillary column (RTX 624, 25 m × 0.25 mm, 1.4 μm; Restek, Bellefonte, PA, USA) was used for the analysis of both 1,3-DCP isomers and MITC. GC conditions used for 1,3-DCP isomers were: electron-capture detector; 1.7 ml min⁻¹ column flow-rate; 130°C isothermal oven temperature; 230°C injection port temperature; and 270°C detector temperature. GC conditions used for MITC were: nitrogen-phosphorus detector; 1.7 ml min⁻¹ column flow-rate; 170°C isothermal oven temperature; 230°C injection port temperature; and 270°C detector temperature. (*Z*)-1,3-DCP, (*E*)-1,3-DCP and MITC were eluted approximately at 3.6, 3.8 and 3.1 min when manual injections were used. A 0.15-min delay was observed for all the retention times when the injections were made from the headspace autosampler.

2.3. Optimization of parameters on headspace autosampler

Many factors contribute to the partition and equilibration of an analyte in a closed headspace vial, among which sample vial equilibrating temperature and time, and the amount of solvent present in the vial, are the most important. Optimization of these three parameters were made by changing one parameter step-wise while maintaining the other two parameters unchanged. All the other parameters other than these three were kept consistent as below in all the optimization processes: 9-ml headspace vial (Tekmar); benzyl alcohol as the solvent; PTFE-faced silicone septa and aluminum seals (Tekmar); 2.0-ml sample loop; 0.5-min mixing time at power level 2; 0.1-min mixing equilibrating time;

12 p.s.i. (1 p.s.i. = 6894.76 Pa) pressurization pressure; 0.25-min pressurization time and 0.1-min stabilizing time; 0.25-min sample loop fill time; 0.1-min sample loop equilibrating time; and 0.5-min sample injecting time. Benzyl alcohol was chosen as the solvent primarily due to its very high boiling point (205.3°C). Canela and Muehleisen [23] used benzyl alcohol and water as extracting solvents in analyzing organic volatiles adsorbed on charcoal by a manual headspace-GC method.

A 20-μg amount of 1,3-DCP (*Z*)- or (*E*)-isomer, or MITC in 2 μl methanol was added into the A bed of prepared ORBO-32 or ORBO-306 tubes using a gas-tight syringe, and air was drawn through the tubes at 100 ml min⁻¹ for 1 h to simulate samples taken off from an active air sampling device. The charcoal in the spiked ORBO tubes was then emptied into the headspace vials, and glass wool and polyurethane foams were carefully removed.

For the optimization of equilibrating temperature, 1.0 ml benzyl alcohol was added and the sample vials were sealed immediately with septalined aluminum caps using a hand crimper. The vials were equilibrated in the headspace autosampler for 5 min at 100, 110, 120, 130, 140, 150, 160, 180 or 200°C. Higher temperatures were not tested since the maximum temperature allowed in the headspace autosampler was 200°C. The optimal temperature was selected based on the GC signal output (in peak area) from each measurement. Two duplicates were used for each temperature level.

Using the optimal equilibrating temperature and 1.0 ml benzyl alcohol, the spiked standards were heated for 1, 2, 3, 4, 5, 6, 8, 10 or 20 min in the headspace autosampler, and the optimal equilibrating time was then selected based on the produced GC signal output from each injection. Two duplicates were included for each time step.

For the optimization of the solvent volume, 0.5, 1.0, 2.0 and 3.0 ml benzyl alcohol were added into the vials containing the spiked standards, and analysis was then completed using the optimal equilibrating temperature and time. The optimal solvent volume was then decided based on the produced signal output of each GC

analysis. Two duplicates were used for each different solvent volume.

2.4. Sensitivity and precision of analysis

The sensitivity and precision of analysis were measured for each compound–ORBO tube combination using the respective optimized headspace methods, and comparisons were made to the analysis using the conventional CS₂ extraction method. Various known amounts (0.1 to 100 μg) of 1,3-DCP (*Z*)- or (*E*)-isomer or MITC in methanol were spiked on ORBO-32 or ORBO-306 tubes. The spiked ORBO tubes were exposed to air flux and the charcoal content was transferred into headspace vials as described above. The optimized headspace methods or the CS₂ extraction method were then used to analyze the spiked samples. When the CS₂ method was used, the charcoal was extracted with 4.0 ml CS₂ in sealed headspace vials for 60 min with periodical shaking, and 5 μl of the extract were injected manually into the GC system using a gas-tight syringe (Hamilton, Reno, NV, USA). Two duplicates were used for each concentration level, and the averaged response in peak area from each concentration was plotted against the amount of chemical spiked to generate the calibration curves. The MDL was estimated from the lower end of the calibration curves by assuming the detectable peak area to be three times the background noise. Sensitivity of analysis for each method was also evaluated by comparing the slopes of the linearized calibration curves.

The precision of each method was measured as the standard deviation of multiple analyses using the same method. The mixture of the (*Z*)- and (*E*)-isomers of 1,3-DCP, or MITC, was spiked onto ORBO-32 or ORBO-306 tubes at rates equivalent to 4 and 20 μg per tube for (*Z*)-1,3-DCP and MITC, or 1.52 and 7.61 μg per tube for (*E*)-1,3-DCP, and the spiked tubes were then analyzed using the respective optimized headspace methods or the CS₂ method. Four replicates were used for each method and concentration level. The calibration curves generated above were used for the quantitation of each measurement.

3. Results and discussion

3.1. Optimization of headspace analysis conditions

When a sealed vial containing charcoal sample is heated in one of the platens in the headspace autosampler, some of the analyte adsorbed on the surfaces of charcoal particles was desorbed by the solvent and redistributed among the vapor, solvent and solid phases. The relationships among the concentrations and these three phases can be described as in Eqs. 1–3, assuming the total distribution of the analyte among the three phases equals P :

$$C_1/C_a = K_H \quad (1)$$

$$C_s/C_1 = K_d \quad (2)$$

$$C_a V_a + C_1 V_1 + C_s M_s = P \quad (3)$$

where C_a , C_1 and C_s are the concentrations of analyte in the headspace, solvent and solid phase, respectively; V_a , V_1 and M_s are the volumes of headspace and solvent, and the mass of charcoal, respectively; K_H is the partition coefficient between the headspace and solvent phases, or the Henry's constant; and K_d is the partition coefficient between the solvent and solid phases, or the adsorption coefficient. Rearranging the equations will result in the expression for the concentration of analyte in the headspace phase:

$$C_a = \frac{P}{V_a + K_H V_1 + K_H K_d M_s} \quad (4)$$

Obviously, reducing the headspace volume V_a , volume of solvent V_1 or mass of charcoal M_s , or decreasing K_H or K_d will all lead to the increase of C_a and therefore maximize the amount of analyte entering the GC system.

Two sizes of headspace vials, 21 and 9 ml, were available for the Tekmar 7000 headspace autosampler. To reduce the headspace volume, the smaller version of the headspace vials (9 ml) was chosen in this study. Mass of charcoal is usually decided based on the trapping efficiency

and the initial concentration in the air. Large ORBO tubes are necessary when large sampling volume and high flow-rate are required. Solvent volume cannot be indefinitely small since the amount of solvent should be sufficient to bring all the charcoal particles into contact with the solvent to obtain maximum desorption.

K_H and K_d are functions of the analyte as well as the chosen solvent and charcoal types. Once the types of solvent and charcoal are chosen, K_H and K_d can be influenced by the equilibrating temperature in the closed vial as well as the equilibrating time of the vial. Increases of temperature drive the analyte from solvent phase into the vapor phase, and accelerate the desorption of the analyte from the solid surface into the solvent phase. However, a high temperature may cause the decomposition of the analyte in the presence of solvent and charcoal adsorbent and therefore, as a net result, C_a may decrease. Using a longer equilibrating time may also lead to increased decomposition and a smaller C_a . However, if the equilibrating time is too short, equilibrium of the analyte among the three phases is not achieved, which may affect the reproducibility of the analysis.

Signal output generated from the analysis of ORBO tubes spiked with 20 μg 1,3-DCP (*Z*)- or (*E*)-isomer or MITC revealed a close dependence of response on the equilibrating temperature (Fig. 1). Equilibrating temperature had different effects on the detection response for different ORBO tubes. On petroleum-based ORBO-306 charcoal tubes, using the same equilibrating time, the produced response increased steadily with increases of equilibrating temperature from 100 to 200°C for both 1,3-DCP isomers and MITC (Fig. 1). The increases were almost linear over the range of 100 to 200°C for all the three compounds, and at 200°C, the signal output was enhanced 5.3, 6.0 and 12.5 times compared to that at 110°C for (*Z*)-1,3-DCP, (*E*)-1,3-DCP and MITC, respectively. The selected optimum equilibrating temperature for 1,3-DCP isomers and MITC on ORBO-306 were 190 and 180°C, which were slightly below the maximum temperature allowed on the instrument and the boiling point of benzyl alcohol. On coconut-

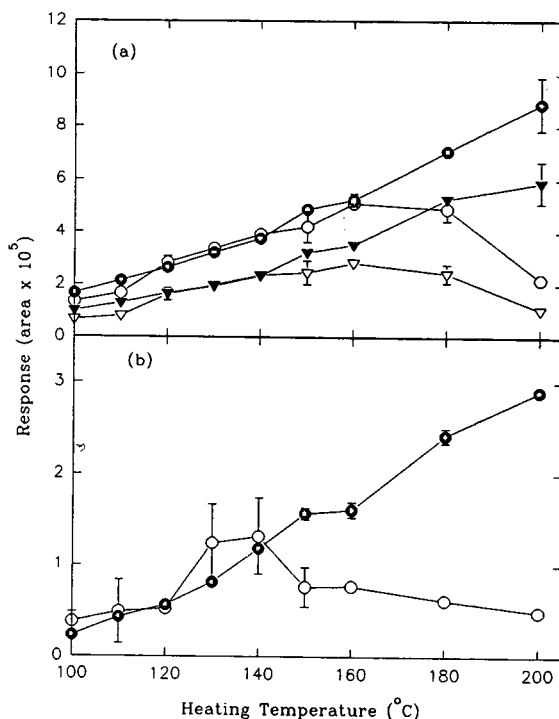


Fig. 1. Effect of equilibrating temperature in the headspace autosampler on response of analysis. (a) 1,3-DCP: equilibrating time 5.0 min and solvent volume 1.0 ml; ○, ● = (*Z*)-isomer; ▽, ▼ = (*E*)-isomer; ○, ▽ = ORBO-32; ●, ▼ = ORBO-306. (b) MITC: equilibrating time 5.0 min and solvent volume 1.0 ml; ○ = ORBO-32; ● = ORBO-306.

based ORBO-32 charcoal tubes, however, the produced response first increased and then decreased rapidly with the increase of equilibrating temperature, and therefore an optimal temperature point existed for all the three compounds. When a 5-min equilibrating time was used, the determined optimal equilibrating temperature on ORBO-32 tubes was approximately 160°C for both (*Z*)- and (*E*)-isomers of 1,3-DCP, and 140°C for MITC. More variation was consistently observed on ORBO-32 tubes, particularly for MITC (Fig. 1b). It could be concluded that coconut charcoal had higher reactivity towards these compounds at high temperature, which might be attributed to the catalytic contents such as bases in the plant-based charcoal. Poor storage stability was reported for 1,2-dichloropropane and 1,2-dibromo-3-chloropropane on

coconut-based charcoal at room temperature [21,24]. A daily loss of 7% for a 10- μg spike of 1,2-dibromo-3-chloropropane on coconut-based charcoal at 24°C was observed [24]. Alkyl isocyanates are known for their additive reactions with aliphatic alcohols to form thiocarbamates, and the reaction is catalyzed in the presence of alkoxide anions [25]. The catalytic ability of coconut-based charcoal at elevated temperatures and the potential reaction of MITC with benzyl alcohol may be combined to explain the observed enhanced decomposition of MITC on ORBO-32 charcoal at high temperatures. When coconut-based charcoal tubes have to be used, alternative high-boiling solvents, such as tetrahydronaphthalene, benzyl esters, or polyethers, should be tried to substitute benzyl alcohol for the extracting agent. The effect of benzyl alcohol–MITC reaction on petroleum-based charcoal was not significant, since good reproducibility and linear increase of sensitivity with increasing equilibrating temperature were clearly observed (Fig. 1b). Petroleum-based charcoal tubes are therefore recommended over coconut-based tubes for MITC sampling if headspace analysis is to be performed.

At the same equilibrating temperature, the signal output produced from the same amount of the (*E*)-isomer of 1,3-DCP was consistently lower than that from the (*Z*)-isomer (Fig. 1a). This difference could be explained by the higher boiling point (112°C) and smaller vapor pressure (34 mmHg at 25°C; 1 mmHg = 133.322 Pa) of the (*E*)-isomer than the (*Z*)-isomer, which had a boiling point of 104.3°C and a vapor pressure of 43 mmHg at 25°C.

The equilibrating time at the selected optimal temperatures was varied from 1 to 20 min, and the signal output of each analysis was correlated to the equilibrating time (Fig. 2). When the ORBO-32 and -306 tubes spiked with 1,3-DCP isomers were heated at 160 and 190°C, respectively, the response increased within the first 4–5 min, and then gradually decreased with the increase of equilibrating time (Fig. 2a). Similar dependence of the detection response on the equilibrating time was observed for both the (*Z*)- and (*E*)-isomers of 1,3-DCP on both ORBO

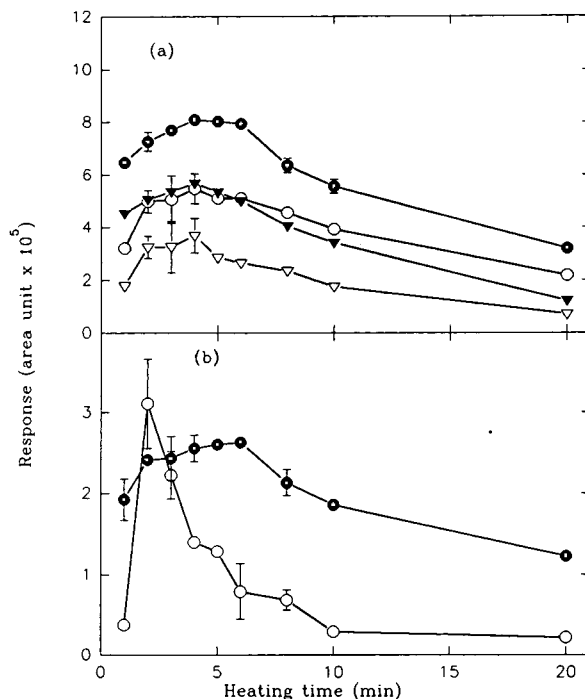


Fig. 2. Effect of equilibrating time in the headspace auto-sampler on response of analysis. (a) 1,3-DCP: equilibrating temperature 160°C for ORBO-32 (○, ∇) and 190°C for ORBO-306 (●, ▼) tubes, and solvent volume 1.0 ml; ○, ● = (*Z*)-isomer; ∇, ▼ = (*E*)-isomer. (b) MITC: equilibrating temperature 140°C for ORBO-32 (○) and 180°C for ORBO-306 (●) tubes, and solvent volume 1.0 ml.

tubes. However, more significant variations were observed on ORBO-32 tubes when the equilibrating time was less than 5 min, indicating equilibrium of the distribution of 1,3-DCP among the phases was not well achieved within such a short period of time. A 5-min period was therefore selected as the optimal time for the equilibrating temperatures used for both isomers of 1,3-DCP on both ORBO tubes. The signal output reached the maximum at 2 min for MITC on ORBO-32 tubes when 140°C was used as the equilibrating temperature, but decreased rapidly with further increases of time (Fig. 2b). A 3-min period was therefore determined as the optimal equilibrating time for MITC on ORBO-32 tubes. On petroleum-based ORBO-306 tubes, the response almost remained constant from 2–6 min

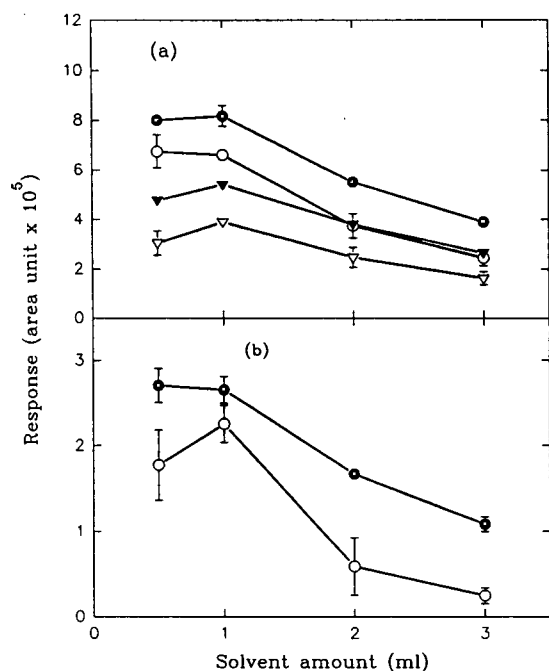


Fig. 3. Effect of solvent volume in the headspace vials on response of analysis under the optimum equilibrating temperature and time. (a) 1,3-DCP; ○, ● = (Z)-isomer; ▼, ▼ = (E)-isomer; ○, ▼ = ORBO-32; ●, ▼ = ORBO-306. (b) MITC; ○ = ORBO-32; ● = ORBO-306.

and then decreased gradually with further increases of the equilibrating time, and 5 min was decided as the optimal time. MITC was apparently more resistant to longer equilibrating time on ORBO-306 tubes than on ORBO-32 tubes. Longer equilibrating time may affect the response of analysis by increasing the decomposition of the analyte in the heated headspace vials.

Using the optimal equilibrating temperatures

and times, the effect of solvent volume on the production of response from each analysis was determined (Fig. 3). The signal output was approximately the same when 0.5 or 1.0 ml benzyl alcohol was added into the headspace vials, but decreased proportionally when the solvent volume further increased to 2.0 and 3.0 ml. However, more variations were noticed for most of the compound–charcoal tube combinations when 0.5 ml solvent volume was used, which may be attributed to the possibility that not all of the charcoal particles were in contact with the solvent when the amount of solvent was so small. A 1-ml volume was therefore determined as the optimal amount of solvent for all the headspace methods. Effect of the amount of solvent on the detection sensitivity was obviously due to that more solvent increased the partition of the analyte into the solvent phase and concurrently decreased its concentration in the vapor phase.

The parameters of the optimized headspace methods for 1,3-DCP isomers and MITC on ORBO-32 and -306 tubes were summarized in Table 1. It is obvious that different optimal parameters exist for different compound–charcoal tube combination, and therefore different conditions should be used to achieve the maximum sensitivity of analysis.

3.2. Sensitivity and precision of measurements

Calibration curves between peak area and amount of compound spiked on ORBO tubes were constructed for each optimized headspace method as well as for the CS₂ method on

Table 1
Optimized parameters for headspace analysis of 1,3-DCP and MITC on ORBO-32 and -306 charcoal tubes

Parameter	1,3-DCP		MITC	
	ORBO-32	ORBO-306	ORBO-32	ORBO-306
Equilibrating temperature(°C)	160	190	140	180
Equilibrating time (min)	5	5	3	5
Solvent volume (ml) (benzyl alcohol)	1.0	1.0	1.0	1.0

different ORBO tubes (Fig. 4). Good linearity was noticed over the concentration range of 0.1–100.0 μg per tube for all the methods ($r^2 > 0.99$ in all situations). All the optimized headspace methods were significantly superior to the solvent-phase analysis method on the sensitivity of measurement. The calculated slopes of the linearized calibration curves on ORBO-32 and -306 tubes obtained with the optimized headspace methods were 12 and 32 times of those obtained with the CS_2 method for (*Z*)-1,3-DCP, 8 and 21 times for (*E*)-1,3-DCP, and 12 and 14 times for MITC, respectively. Petroleum-based

ORBO-306 tubes constantly gave better sensitivity than coconut-based ORBO-32 tubes for all the three compounds (Fig. 4). A large dilution factor may be used to explain the relatively low sensitivity for the CS_2 method. With the CS_2 method, since only 5 μl of the 4 ml extract were eventually injected into the GC system, the dilution was 800 times even when a complete desorption was assumed.

The estimated MDL was at least one order of magnitude smaller for the optimized headspace methods than the CS_2 method for all the compound–charcoal tube combinations (Table 2). Assuming 40 l of air are collected using the ORBO-32 or -306 tubes, the estimated minimum detectable concentrations of the analyte in air would be 0.01 and 0.005 $\mu\text{g m}^{-3}$ for (*Z*)-1,3-DCP, 0.03 and 0.01 $\mu\text{g m}^{-3}$ for (*E*)-1,3-DCP, and 0.05 and 0.08 $\mu\text{g m}^{-3}$ for MITC, respectively, which were significantly improved from the MDL of 0.2 and 1.0 $\mu\text{g m}^{-3}$ reported for 1,3-DCP and MITC on petroleum-based charcoal tubes [21].

Measurements of replicated spiked samples using the above calibration curves showed that except for MITC on ORBO-32 tubes, analysis with the optimized headspace methods was highly reproducible and the precision was approximately the same as using the CS_2 method (Table 2). The standard deviation calculated from four replicate analyses was less than 10% for all the measurements made by using the headspace methods except for the MITC–ORBO-32 combination. Analysis of ORBO-32 tubes spiked with MITC was low in reproducibility, which may be attributed to the poor stability of this compound on the coconut-based charcoal at the selected equilibrating temperature. It is important to point out that the optimized headspace methods, due to the complete automation, are less labor-intensive and high in sample throughput. For the GC conditions used in this study, one analysis was completed within 6 min, and up to 200 charcoal samples may be analyzed on a 24-h basis. The consumption of solvent is significantly reduced. Since CS_2 is highly flammable and toxic, the safety of operation is also improved when the headspace methods are used.

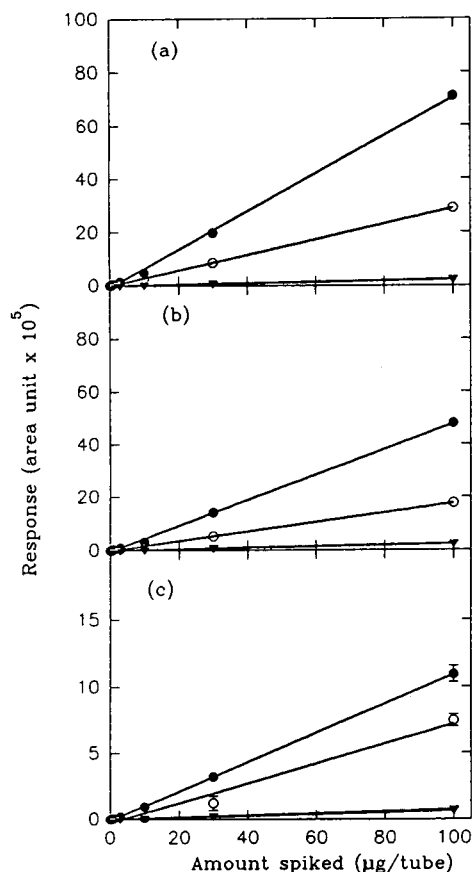


Fig. 4. Calibration curves of the optimized headspace methods (HS) and the solvent extraction method with CS_2 (CS_2). (a) (*Z*)-1,3-DCP; (b) (*E*)-1,3-DCP; (c) MITC. \circ = ORBO-32, HS; ∇ = ORBO-32, CS_2 ; \bullet = ORBO-306, HS; \blacktriangledown = ORBO-306, CS_2 .

Table 2
MDL \pm S.D. of analysis by different methods

	Amount spiked (μg per tube)	ORBO-32		ORBO-306	
		HS method ^a	CS ₂ method ^b	HS method	CS ₂ method
<i>MDL (ng per tube)</i>					
MITC		3.0	30	2.0	20
(Z)-Isomer		0.5	7.7	0.2	10.8
(E)-Isomer		1.1	7.3	0.5	10.6
<i>Recovery (μg per tube; n = 4)</i>					
MITC	4.0	3.16 \pm 1.29	2.89 \pm 0.26	4.20 \pm 0.44	3.92 \pm 0.17
	20.0	16.20 \pm 7.68	18.43 \pm 2.04	20.48 \pm 1.58	19.28 \pm 0.40
(Z)-1,3-DCP	4.0	4.07 \pm 0.07	3.71 \pm 0.33	3.78 \pm 0.22	4.20 \pm 0.32
	20.0	19.01 \pm 0.22	19.77 \pm 0.55	20.15 \pm 0.54	21.09 \pm 0.60
(E)-1,3-DCP	1.52	1.49 \pm 0.07	1.45 \pm 0.14	1.48 \pm 0.08	1.61 \pm 0.12
	7.61	7.14 \pm 0.19	7.61 \pm 0.22	7.79 \pm 0.25	8.04 \pm 0.25

^aHS method: the optimized headspace methods.

^bCS₂ method: analysis of solvent extract after extraction with CS₂.

4. Conclusions

Headspace techniques are applicable for the analysis of 1,3-DCP isomers and MITC on charcoal sampling tubes, and more than one order of magnitude higher sensitivity than the standard solvent-phase analysis approach was achieved under optimum conditions. Equilibrating temperature and time, and the amount of extracting solvent, could all be adjusted to maximize the signal output of each GC analysis. All the three compounds were less stable on coconut-based charcoal at high temperature, and a lower equilibrating temperature and a short equilibrating time therefore had to be used. However, better sensitivity and reproducibility were observed for all the three compounds on petroleum-based charcoal tubes. The estimated minimum detection limits for the (Z)- and (E)-isomer of 1,3-DCP and MITC were 0.2, 0.5 and 2.0 ng per tube on the petroleum-based ORBO-306 tubes, and 0.5, 1.1 and 3.0 ng per tube on coconut-based ORBO-32 tubes, respectively. Assuming 40 l of air are sampled, the corresponding MDLs in concentration were 0.005, 0.01 and 0.05 $\mu\text{g m}^{-3}$ on ORBO-306 tubes, and 0.01, 0.03 and 0.08 $\mu\text{g m}^{-3}$ on ORBO-32 tubes, respectively.

Precision of measurement was comparable to the CS₂ method except for MITC on ORBO-32 tubes. Sample output and safety of operation were also significantly improved compared to the conventional solvent-phase analysis using CS₂. Applications of the headspace method to other volatile compounds, including some common pollutants of industrial origin, are worth further exploration.

References

- [1] R.S.H. Yang, *Residue Rev.*, 97 (1986) 19.
- [2] M. Ottnad, N.A. Jenny and C.H. Röder, in G. Zweig and J. Sherma (Editors), *Analytical Methods for Pesticides and Plant Regulators*, Vol. 10, Academic Press, New York, 1978, pp. 563–573.
- [3] J.H. Smelt and M. Leistra, *Pestic. Sci.*, 5 (1974) 401.
- [4] M. Basile, N. Senesi and F. Lamberti, *Agric., Ecosyst. Environ.*, 17 (1986) 269.
- [5] S.A. Ness, in S.A. Ness (Editor), *Air Monitoring for Toxic Substances: an Integrated Approach*, Van Nostrand Reinhold, New York, 1991, pp. 51–92.
- [6] E.V. Kring, G.R. Ansul, T.J. Henry, J.A. Morello, S.W. Dixon, J.F. Vasta and R.E. Hemingway, *Am. Ind. Hyg. Assoc. J.*, 45 (1984) 250.
- [7] R.H. Brown and C.J. Purnell, *J. Chromatogr.*, 178 (1979) 79.

- [8] W.T. Jr. Winberry, N.Y. Murphy and R.M. Riggan, in W.T. Winberry, Jr., N.Y. Murphy and R.M. Riggan, (Editors), *Methods for Determination of Toxic Organic Compounds in Air; EPA Methods, Method T010*, Noyes Data Corp., Park Ridge, NJ, 1990, pp. 257–293.
- [9] J.B. Mann, J.J. Freal, H.F. Enos and J.X. Danauskas, *J. Environ. Sci. Health*, B15 (1980) 507.
- [10] L.G.M. Th. Tuinstra, W.A. Traag and A.H. Roos, *J. High Resolut. Chromatogr. Chromatgr. Commun.*, 11 (1988) 106.
- [11] B.D. Page and R.J. Avon, *J. Assoc. Off. Anal. Chem.*, 72 (1989) 815.
- [12] K.N.T. Norman, *Pestic. Sci.*, 33 (1991) 23.
- [13] R. Otson and D.T. Williams, *Anal. Chem.*, 54 (1982) 942.
- [14] Z. Penton, *J. High Resolut. Chromatogr.*, 15 (1992) 834.
- [15] P.H. Kiang and R.L. Grob, *J. Environ. Sci. Health*, A21 (1986) 71.
- [16] T.C. Voice and B. Kolb, *Environ. Sci. Technol.*, 27 (1993) 709.
- [17] D. Jentzsch, J. Krüger, H.G. Lebrecht, G. Dencks and J. Gut, *Z. Anal. Chem.*, 236 (1968) 96.
- [18] B. Kolb, *J. Chromatogr.*, 122 (1976) 553.
- [19] J.E. Woodrow, M.M. McChesney and J.N. Seiber, *Anal. Chem.*, 60 (1988) 509.
- [20] J. Gan; S.R. Yates and W.F. Spencer, *J. Agric. Food Chem.*, submitted for publication.
- [21] F. van den Berg, M. Leistra, A.H. Roos and L.G.M. Th. Tuinstra, *Water, Air, Soil Pollut.*, 61 (1992) 385.
- [22] A. Collina and P. Maini, *Bull. Environ. Contam. Toxicol.*, 22 (1979) 400.
- [23] A.M. Canela and H. Muehleisen, *J. Chromatogr.*, 456 (1988) 241.
- [24] W.N. Albrecht, M.R. Hagadone and K. Chenchin, *Bull. Environ. Contam. Toxicol.*, 36 (1986) 629.
- [25] W. Walter and K.-D. Bode, *Angew. Chem., Int. Ed. Engl.*, 6 (1967) 281.



ELSEVIER

Journal of Chromatography A, 684 (1994) 133–142

JOURNAL OF
CHROMATOGRAPHY A

Evaluation of Tenax TA for the determination of chlorobenzene and chloronitrobenzenes in air using capillary gas chromatography and thermal desorption

S.F. Patil^{a,*}, S.T. Lonkar^b^aDepartment of Chemistry and School of Environmental Sciences, University of Poona, Poona 411007, India^bIndustrial Hygiene Laboratory, Hindustan Organic Chemicals Ltd., Rasayani 410207, India

First received 25 January 1994; revised manuscript received 9 June 1994

Abstract

A method for the determination of chloronitrobenzenes (CNBs) and chlorobenzene (CB) in air was developed. CNBs and CB were sampled on Tenax TA sampling tubes, thermally desorbed and analysed by capillary gas chromatography (cGC) with flame ionization detection. The sampling efficiency was found to be independent of flow-rate (25 and 50 ml/min) and relative humidity (30–90%) generated in the laboratory. Recovery studies on Tenax TA (20–35, 35–60 and 60–80 mesh) in the concentration range 0.041–8.212 mg/ml were conducted using cGC coupled with an automatic thermal desorption system (ATD-50). Nearly quantitative recoveries were obtained at all levels of concentrations. Further, it was observed that flow-rates and relative humidity had no effect on the adsorption and thermal desorption efficiency of CNBs and CB when present as a mixture in workplace air. No loss of sample was observed up to 30 days of storage at room temperature. With this method, a time-weighted average concentration of less than 0.04 mg/m³ could be determined in an 8-h sampling period with a precision of 1.4–12% for the whole method.

1. Introduction

Chloronitrobenzenes (CNBs, *o*-, *m*- and *p*-) and chlorobenzene (CB) are used extensively for manufacturing dyes, pesticides, agrochemicals, pharmaceuticals and rubber chemicals. It has been known for a long time that CNBs and CB are irritants to the eyes and mucous membranes in the respiratory tract and have acute and chronic effects. The threshold limit values (TLVs) for *o*-, *m*- and *p*-CNB and CB are 1, 1, 3

and 350 mg/m³, respectively, for an 8-h exposure [1].

For the last two decades, preconcentration of toxic organic vapours used in most NIOSH procedures [2] utilizes charcoal or silica gel as the adsorbent followed by solvent desorption [3] and gas chromatographic (GC) analysis [4–6]. However, charcoal and silica gel have certain disadvantages. Air humidity may reduce their sorption efficiency and the attendant contaminants may displace the target substances on the sorbent.

Another approach uses a porous polymer for

* Corresponding author.

contaminant adsorption and thermal desorption into a gas chromatograph [7], which offers better sensitivity with respect to solvent extraction as the whole sample is injected [8]. Porous polymer sorbents (e.g., Tenax, Chromosorbs, Polysorbs, Porapak and Amberlite XAD series) are relatively inert and hydrophobic and normally have large surface areas. Porous polymers are most successfully used to trap toxic agents of high molecular mass and low- or non-volatile substances [8–11]. Among different sorbents, Tenax GC/TA, a polymer of 2,6-diphenyl-*p*-phenylene oxide, has been used extensively in air pollution monitoring applications because of its excellent properties of trapping the pollutants and high thermal (350–400°C) stability, which in turn facilitates thermal desorption [12,13]. The suitability of Tenax and its ability to concentrate diverse organic compounds with a wide range of boiling temperatures have made it indispensable in the analysis of the complex composition of toxic agents in GC and thermal desorption techniques [8,14].

The determination of chlorobenzene in air using a solid sorption technique and subsequent gas chromatographic analysis has been described [8,15,16]. However, to our knowledge, no method for monitoring chloronitrobenzenes in the presence of chlorobenzene has been described. The serious effects of CNBs and CB on human health necessitate the development of a reliable method of monitoring the workplace environment. This study was aimed at determining traces of these pollutants in humid workplace air where the temperature varied from 20 to 40°C, in a chemical plant involving the process of nitration of CB to CNB. The process chemicals were adsorbed on Tenax TA solid sorbent and analysed using GC coupled with an automatic thermal desorption system.

Experimental

2.1. Chemicals

Chlorobenzene and *o*-, *m*- and *p*-chloronitrobenzenes were of analytical-reagent grade

from Fluka (Buchs, Switzerland). Methanol used as a solvent was of analytical-reagent grade from S.D. Fine Chemicals (Bombay, India).

2.2. Apparatus

For the analysis of standard test atmosphere samples, spiked samples and samples of workplace air, a Perkin-Elmer (Beaconsfield, UK) Model 8500 gas chromatograph with a flame ionization detector and coupled with an ATD-50 automatic thermal desorption system was used. The chromatograms obtained were recorded on a Perkin-Elmer GP 100 printer-plotter and the areas under the curve were evaluated with the help of a built-in data processor.

Sampling rates were maintained by a water-siphoning system for field samples, the details of which were described in a previous paper [8]. Portable sampling pumps (SKC, USA) supplied by Spantech Products (UK) were used during the sampling from standard test atmospheres with different relative humidities.

2.3. Sample tubes

For sampling in the solid sorbent method, stainless-steel sampling tubes (Perkin-Elmer) of 89 mm × 5 mm I.D. with stainless-steel wire gauges on both ends to hold the adsorbent were used. Metal sealing caps were used during the storage of samples. Outer and inner analytical end-caps were used during the thermal desorption and the analysis of samples.

2.4. Columns

A DB 225 fused-silica wide-bore capillary column of 15 m × 0.53 mm I.D. (J and W Scientific, Folsom, CA, USA) with a film thickness of 1 μm was used for the analysis of samples obtained under various experimental conditions.

Retention volumes and safe sampling volumes were determined on laboratory-packed glass columns (1 m × 2 mm I.D.) of Tenax TA of 60–80, 35–60 and 20–35 mesh (180–250, 250–500 and 500–850 μm).

2.5. Solid adsorbents

Tenax TA of three different mesh sizes was obtained from Ohio Valley Speciality Chemicals (Marietta, OH, USA) and was used throughout the experiments.

2.6. Retention volume

The retention volumes and safe sampling volumes of CNBs and CB on Tenax TA porous polymer of three different mesh sizes were evaluated for concentrating all the compounds in the course of sampling without breakthrough.

Three glass chromatographic columns (1 m × 2 mm I.D.) were filled with a known mass of Tenax TA of 20–35, 35–60 and 60–80 mesh. Each column was conditioned at 25°C for 45 min. Thereafter, the temperature was increased by 2°C/min to the final temperature of 300°C, which was maintained for 24 h with a nitrogen flow-rate of 20 ml/min. After conditioning of the columns, standard solutions of *o*-, *m*- and *p*-CNB and CB were injected separately at different column temperatures with a nitrogen flow-rate of 20 ml/min. The retention volumes were recorded along with the absolute column temperatures.

2.7. Preparations of standard solutions

Stock standard solutions were prepared by

dissolving 1.030, 1.024, 1.027 and 1.026 g of *o*-, *m*- and *p*-CNB and CB, respectively, in 100 ml of methanol. Working standard solutions in the concentration range of interest (0.041–8.212 mg/ml) were prepared by serial dilution of the stock standard solutions with methanol in a 25-ml volumetric flask. To these working standard solutions, 2 ml of a standard solution of aniline (20.37 mg/ml) was added as an internal standard.

2.8. Calibration of method by GC

A 0.2- μ l volume of each standard solution was injected into the GC column (DB 225). The initial temperature of the column was 40°C, held for 3 min, then the temperature was increased at 30°C/min to 115°C, which was maintained for 8 min. The temperatures of the injector and the detector were maintained at 280 and 300°C, respectively. The flow-rate of nitrogen through the column was 11 ml/min.

2.9. Generation of test atmosphere

Chloronitrobenzenes and chlorobenzene in air were generated by the dynamic generation equipment shown in Fig. 1. A tube containing each analyte was inserted into a 200-ml glass vessel, placed in a water-bath. A stream of the analyte of interest was generated by blowing dried air into the vessel. The outlet was con-

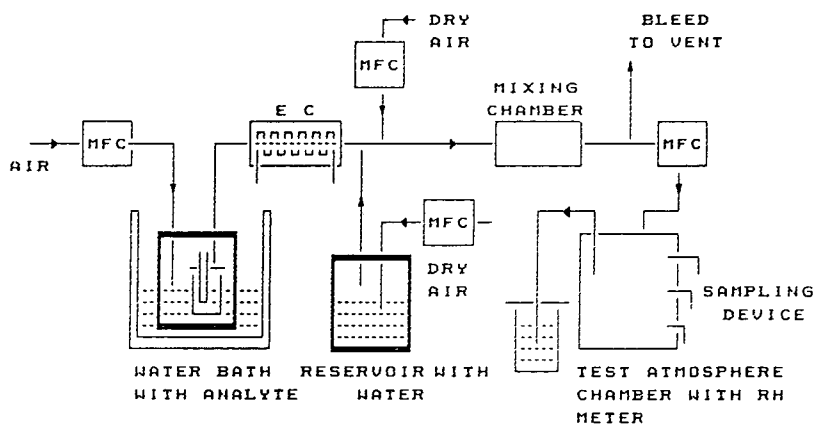


Fig. 1. Scheme of the dynamic dilution system. MFC = Electronic mass flow controller; EC = evaporation chamber.

nected to a mixing chamber where the analyte atmosphere was further diluted with air using a mass flow controller (Porter Instrument Co., USA). Further dilution with a controlled relative humidity (RH) were made by using another mass flow controller in the system. The air stream, after appropriate dilution and thorough mixing, was fed into a glass exposure chamber of 5 l capacity with an air-tight removable lid with the help of the mass flow controller. The flow-rate was kept at 40–60 ml/min.

Samples were drawn at each concentration of CNBs and CB through the two sampling tubes of Tenax TA. The sampling flow-rates were maintained at 25 and 50 ml/min with the help of portable sampling pumps for different periods of time. During the sampling the RH was maintained at 30, 60 and 90%, which were achieved by mixing dry air with air bubbled through deionized water. The exposure chamber was provided with two outlets for sampling and a third outlet was left in water to maintain atmospheric pressure in the exposure chamber during sampling.

The concentration in the exposure chamber was monitored at 30-min intervals using the Tenax sampling tubes with GC determination for control purpose. Different concentrations were obtained by varying the temperature in the water-bath between 50 and 100°C and by changing the flow-rate of the air blowing over the vessel and in the mixing chamber. Relative humidities between 30 and 90% could be generated.

2.10. Thermal desorption recovery

To determine the thermal desorption recovery of Tenax TA of three different mesh sizes in the concentration range of interest, a set of 35 sampling tubes were filled with 200 mg of Tenax TA of a chosen particle size. All the tubes were conditioned in a specially made tube conditioner (SkyLab, India) at 300°C for 24 h with a nitrogen flow-rate of 20 ml/min and were sealed before use with storage caps supplied by Perkin-Elmer. Each conditioned sample tube was fitted into the GC injection port maintained at 280°C with a nitrogen flow-rate of 15 ml/min and a set of five

tubes were spiked with 0.2 μ l of each standard solution at room temperature. The spiked tube was disconnected after 2 min and exposed to different RH for 4–8 h in order to check the potential losses during field sampling.

These tubes were then immediately desorbed under the following optimum desorption conditions: desorption temperature, 250°C; desorption time, 10 min; transfer line temperature, 110°C; cold trap low temperature, –30°C; cold trap high temperature, 300°C; cold trap adsorbent, Tenax TA (60–80 mesh). After desorption, the cold trap was heated spontaneously and desorbed material was fed to the GC capillary column for analysis. The analysis were performed using the optimized GC conditions used for the calibration of the method.

2.11. Storage of samples

Storage tests were performed by loading a set of five tubes with standard solutions as mentioned above. The tubes were sealed with storage caps and stored at room temperature (25–27°C) for 5, 15 and 30 days. Each set of tubes was analysed after a specified time using the optimized conditions of thermal desorption and GC.

2.12. Workplace environment atmosphere

Air samples were collected in a chemical plant manufacturing CNBs using CB as raw material. To achieve more or less the same pressure drop and constant flow-rates during sampling, each tube was filled with an equal amount (200 mg) of Tenax TA of 20–35, 35–60 and 60–80 mesh. Before starting the field sampling, all sampling tubes were preconditioned for 12 h at 300°C with a nitrogen flow-rate of 20 ml/min. After conditioning, the tubes were sealed immediately with storage caps to avoid cross-contamination due to the diffusion process. The RH and temperature of the workplace during the period of investigation were found to vary in the ranges 50–90% and 20–40°C, respectively.

Sample volumes in the range 4–20 l with flow-rates of 25 and 50 ml/min were collected. Samples were also collected for short periods with

higher flow-rates using portable pumps, to establish the suitability of Tenax TA for short-term monitoring, often required prior to shut-down jobs in a plant.

The tubes were fitted with analytical end-caps and placed on the turntable of thermal desorption system for analysis. The tubes were thermally desorbed and analysed using the optimized conditions of thermal desorption and GC.

3. Results and discussion

3.1. Standards

The identities of the CNBs and CB were confirmed by GC–MS. The purity was also checked using GC with flame ionization detection and found to be more than 99%.

3.2. Retention volumes

The retention volumes of each analyte at different temperatures were recorded. The logarithm of the specific retention volume was plotted against the reciprocal of the absolute column temperature, which gave a linear relationship. The retention volumes at 25 and 30°C were obtained by extrapolation (Table 1). Half of the retention volume was considered as a safe sampling volume for sampling purposes in the field. It was observed that with this retention volume, the determination of CNBs and CB is feasible without any breakthrough in 10–20-l air samples.

Table 1
Adsorptive properties of Tenax TA of different mesh sizes

Compound	Retention volume (l/g) ^a		
	60–80 mesh	35–60 mesh	20–35 mesh
CB	281 (184)	280 (181)	232 (153)
<i>m</i> -CNB	18 836 (11 290)	16 463 (9767)	6994 (4363)
<i>p</i> -CNB	25 119 (14 944)	24 126 (14 150)	10 455 (6445)
<i>o</i> -CNB	25 699 (15 313)	21 739 (12 841)	8142 (5083)

^a Values at 25°C; values in parentheses are retention volumes at 30°C.

2.3. Gas chromatography and quantitative analysis

The calibration graph for each analyte was obtained by plotting the average peak area ratio against the amount injected. A typical chromatogram of a mixture is shown in Fig. 2. A linear graph passing through the origin was obtained in the investigated concentration range of 0.04–8.212 mg/ml for each analyte. The pooled ac-

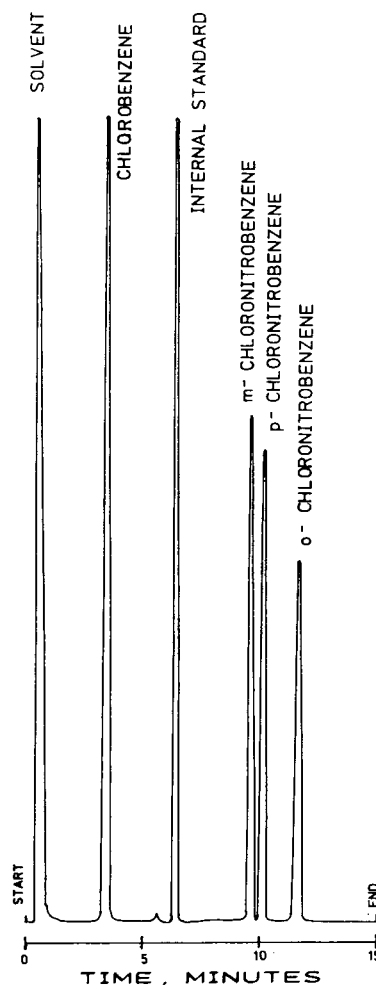


Fig. 2. Chromatogram of calibration mixture containing 4.1 mg/ml of CB and *m*-, *p*- and *o*-CNB. Injection volume, 0.2 μ l; column (polar), DB 225 (15 M \times 0.53 mm I.D.) with film thickness 1 μ m; oven programme, 45°C for 5 min, increased at 30°C/min to 115°C, held for 8 min. Aniline was added as an internal standard.

curacy of the method is better than 99.95%. The regression coefficients for CB and *o*-, *m*- and *p*-CNB are 0.9999, 0.9305, 0.9999 and 0.9999 respectively.

For establishing the suitability of the column with respect to the identification and determination of analytes, a comparison between the results obtained using non-polar (DB 1701 and DB 210) and polar (DB 225) columns was made. It was found that a fused-silica capillary column (DB 225) gave a better performance than the others under identical conditions of length, internal diameter and film thickness. When the DB 225 column was used, no signs of adsorption or decomposition were observed. The overall analytical precision of the method was found to be in the range 0.30–7%.

3.4. Sampling efficiency

The sampling efficiency for different concentrations of *o*-, *m*- and *p*-CNB and CB was determined by analysing sampling tubes exposed to known concentrations of test atmosphere. The results are summarized in Table 2. Neither the concentration nor the RH seems to affect the sampling efficiency seriously for sampling rates

of 25 and 50 ml/min. Three parallel samplings with flow-rates of 25 and 50 ml/min were performed at 30, 60 and 90% RH. The overall sampling efficiency at different flow-rates and RH was found to be more than 99%, showing complete adsorption and thermal desorption of CNBs and CB from Tenax TA.

3.5. Thermal desorption recovery

The recovery of *o*-, *m*- and *p*-CNB and CB on solid sorbent tubes packed with Tenax TA of different mesh sizes was investigated at various concentrations. The tubes were spiked with different concentrations of standard solutions. After the spiking, each tube was connected to the pump and exposed to different RH for 4–8 h in order to check for potential losses during the field sampling. As the recoveries of the analytes were found to be independent of the mesh size of Tenax TA, only the data for 35–60-mesh Tenax TA are presented in Table 3.

The results in Table 3 indicate nearly quantitative recoveries (>95%) of all the analytes at all levels of spiking within relative standard deviations of 1–10% for the whole method for a sampling volume of 10 l. A typical chromato-

Table 2
Sampling efficiency of Tenax TA sorbent for CNBs and CB at different concentrations and relative humidity in air

Compound	Concentration in air (mg/m ³)	Relative humidity (%)	Sampling volume (l)	Sampling efficiency (%)	No. of determinations	Precision (R.S.D., %)
CB	4.75	30	8	105	5	2.80
	9.35	90	7.5	103	5	2.69
	13.50	60	8	108	6	2.64
<i>m</i> -CNB	0.56	30	10	105	5	7.15
	2.15	90	9	103	5	6.05
	3.24	60	8	99	4	5.51
<i>p</i> -CNB	1.0	30	8	103	5	6.87
	2.15	90	9	99	5	3.10
	6.73	60	12	102	4	2.50
<i>o</i> -CNB	0.45	30	8	102	5	7.38
	1.85	90	10	103	5	5.78
	3.57	60	8	101	5	4.67

The sampling rate was 25 and 50 ml/min.

Table 3
Thermal desorption recovery on Tenax TA (35–60 mesh) at 250°C

Standard No.	Recovery (μg) ^a			
	CB	<i>m</i> -CNB	<i>p</i> -CNB	<i>o</i> -CNB
1	0.049 (121) [6.03]	0.045 (110) [7.53]	0.042 (102) [10.28]	0.046 (111) [7.03]
2	0.088 (108) [7.27]	0.085 (104) [11.8]	0.076 (94) [12.17]	0.093 (114) [10.97]
3	0.174 (106) [2.78]	0.166 (101) [6.105]	0.162 (99) [5.378]	0.173 (105) [5.80]
4	0.428 (104) [2.47]	0.428 (104) [5.466]	0.415 (101) [3.501]	0.431 (105) [4.587]
5	0.852 (104) [2.388]	0.795 (97) [3.566]	0.786 (96) [3.459]	0.820 (99) [2.438]
6	1.322 (107) [2.44]	1.265 (103) [1.196]	1.256 (102) [1.824]	1.268 (102) [1.445]
7	1.720 (105) [1.695]	1.674 (102) [1.638]	1.647 (100) [1.322]	1.669 (101) [1.479]

^a Each value is the average of five independent measurements with the percentage recoveries in parentheses and the R.S.D. (%) in square brackets.

gram of thermal desorption is shown in Fig. 3. It was observed that the adsorption of substances from the calibration mixtures and subsequent thermal desorption were complete under the conditions specified. Further, it was also found that RH and flow-rate had no effect on the adsorption and thermal desorption using Tenax TA.

3.6. Storage

The stability of *o*-, *m*- and *p*-CNB and CB on Tenax TA was studied. A set of five tubes at three concentrations were immediately analysed while another set of tubes were kept at room temperature (25–27°C) for 5, 15 and 30 days until analysis. The recoveries during storage were not influenced by the RH in the sampled air. At lower concentration, the recovery of CB was found to be 141%, which is relatively high compared with the results obtained at higher concentrations. This is attributed to the blank values contributed by Tenax TA arising from

storage. A typical chromatogram depicting the higher background levels is shown in Fig. 4. The results presented in Table 4 indicate nearly quantitative recoveries of 96–115, 97–117 and 100–119% for 5, 15 and 30 days, respectively. Almost no change in recovery was observed for samples stored in a refrigerator (5°C) for 8 weeks.

3.7. Workplace air sample analyses

Air samples taken by Tenax TA adsorption tubes were analysed using the standard conditions for GC and thermal desorption mentioned previously. The results obtained at each location for three individual samples are in good agreement with each other. A typical representative example of air sample analyses obtained by using 35–60-mesh Tenax TA is presented in Table 5. The concentrations of CNBs and CB were found to be well within the threshold limit values prescribed for the individual compounds. It should also be noted that no breakthrough was

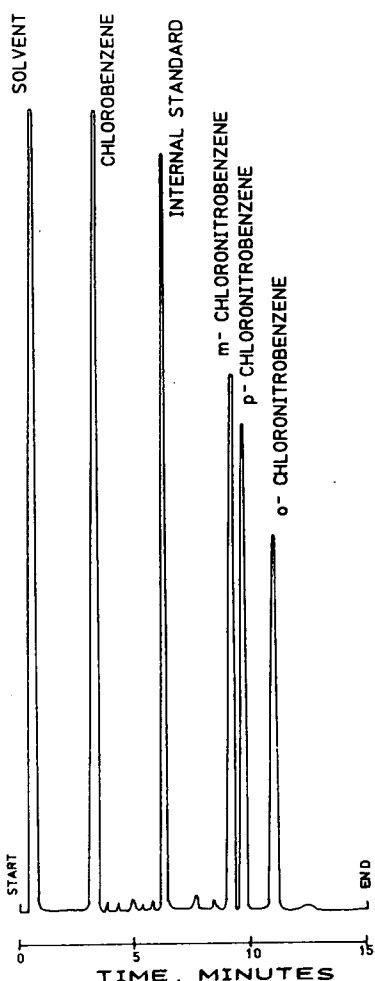


Fig. 3. Chromatogram of thermal desorption recovery of CB and *m*-, *p*- and *o*-CNB on 35–60-mesh size Tenax TA. Thermal desorption conditions: desorption temperature, 250°C; desorption time, 10 min; transfer line temperature, 110°C; cold trap low temperature, -30°C; cold trap high temperature, 300°C; cold trap adsorbent, Tenax TA (60–80 mesh); injection volume, 0.2 μ l.

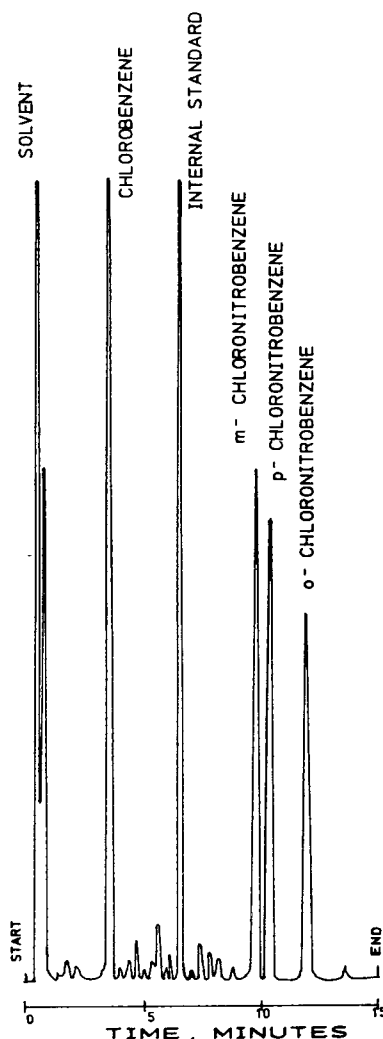


Fig. 4. Chromatogram of thermal desorption recovery after storage for 30 days. Thermal desorption conditions as in Fig. 3.

observed under the different prevailing conditions existing in the workplace air during sampling.

3.8. Hygienic effect

The hygienic effect [5] of the contaminants in an air sample is defined as the sum of the ratios

between the concentrations and threshold limit values (TLV) of each component. This is valid assuming that each component has a similar effect on man. When the sum of the ratios exceeds unity, the TLV of the mixture is exceeded. The hygienic effect (Table 5) was found to be less than unity for the compounds studied in the workplace air, confirming that the analyte concentrations are well below the prescribed limits.

Table 4
Recovery and precision for sample storage for 5, 15 and 30 days at room temperature (25–27°C)

Compound	Amount added (μg)	5 days		15 days		30 days	
		Found (μg) ^a	R.S.D. (%)	Found (μg) ^a	R.S.D. (%)	Found (μg) ^a	R.S.D. (%)
CB	0.082	0.098 (120)	11.7	0.099 (121)	4.46	0.116 (141)	4.1
	0.410	0.440 (107)	2.7	0.480 (117)	5.61	0.489 (119)	8.46
	1.231	1.332 (108)	0.7	1.383 (112)	0.41	1.382 (112)	1.11
<i>m</i> -CNB	0.082	0.080 (98)	4.1	0.090 (110)	8.24	0.093 (113)	1.33
	0.409	0.406 (99)	5.3	0.410 (100)	2.31	0.427 (104)	1.99
	1.228	1.210 (99)	1.7	1.315 (107)	1.11	1.270 (103)	0.23
<i>p</i> -CNB	0.082	0.079 (96)	6.2	0.082 (100)	7.65	0.085 (104)	0.2
	0.411	0.400 (97)	6.9	0.397 (97)	3.22	0.411 (100)	1.46
	1.233	1.199 (97)	2.4	1.300 (105)	1.18	1.247 (101)	0.57
<i>o</i> -CNB	0.082	0.094 (115)	26.4	0.081 (106)	5.26	0.095 (116)	4.27
	0.412	0.434 (105)	7.5	0.407 (99)	3.05	0.435 (106)	0.74
	1.236	1.215 (98)	1.9	1.324 (107)	1.73	1.266 (102)	0.49

^a Each value is the average of five independent measurements with percentage recoveries in parentheses.

4. Conclusions

The proposed method for monitoring CNBs and CB in air was found to be reliable with a detection limit much below the expected average

Table 5
Results of workplace air sample analysis on Tenax TA (35–60 mesh)

Sample No.	Concentration (mg/m^3) ^a				Hygienic effect ^b
	CB	<i>m</i> -CNB	<i>p</i> -CNB	<i>o</i> -CNB	
1	0.070	0.165	0.178	0.242	0.47
2	0.128	–	0.156	0.265	0.32
3	0.030	0.033	0.564	0.030	0.25
4	0.115	0.062	0.364	0.222	0.40
5	0.264	–	0.958	0.044	0.36
6	0.069	0.028	0.223	0.147	0.25
7	0.174	0.037	0.427	0.269	0.45
8	0.864	0.027	0.562	0.524	0.74
9	0.112	–	0.242	0.424	0.50
10	0.056	0.027	0.348	0.276	0.42

^a Average of three independent measurements at the same location.

^b See text for definition.

concentration found in the workplace environment. The sampling efficiency of Tenax TA is not affected by the RH and temperature prevailing in the air. Further, this method can also be used for monitoring the analytes using high flow-rates as the adsorption and thermal desorption processes were found to be independent of flow-rate. No significant loss of CNBs and CB was observed during storage for up to 1 month on Tenax TA.

For long-term monitoring sampling rates of 25 and 50 ml/min are preferable. This method gave the same results (within experimental errors) for monitoring CNBs and CB in both a standard test atmosphere and a workplace environment. This method could be used routinely for monitoring CNBs and CB in the workplace environment.

Acknowledgements

The authors thank Mr. V.K. Aundhe, Chairman and Managing Director, Hindustan Organic Chemicals Ltd., for permitting them to publish these results and Dr. P.D. Joshi (Chief Industrial Health Physician) for useful suggestions.

References

- [1] *Threshold Limit Values and Biological Exposure Indices for 1988–1989*, American Conference of Governmental Industrial Hygienists, Cincinnati, 1988.
- [2] National Institute of Occupational Safety and Health (NIOSH), *Manual of Sampling Data Sheets*, Publ. 77-159, Department of Health, Education and Welfare (NIOSH), Cincinnati, 1977.
- [3] L. Weber and U. Knecht, *Fresenius' Z. Anal. Chem.*, 321 (1985) 544.
- [4] R.A. Lunsford, Y.T. Gagnon, J. Palassic, J.M. Fajen, D.R. Roberts and P.M. Eller, *Appl. Occup. Environ. Hyg.*, 5 (1990) 310.
- [5] O. Einarsson, J. Gorczak, B.O. Lundmark and U. Palmqvist, *J. Chromatogr.*, 498 (1990) 381.
- [6] E. Searle, *Analyst*, 114 (1989) 113.
- [7] E.D. Pellizzari, J.E. Bunch, B.H. Carpenter and E. Sawiki, *Environ. Sci. Technol.*, 9 (1975) 552.
- [8] S.F. Patil and S.T. Lonkar, *J. Chromatogr.*, 600 (1992) 344.
- [9] B. Jonsson, H. Welinder and G. Skarping, *J. Chromatogr.*, 558 (1991) 247.
- [10] K.E. Noll and J.N. Sarlis, *JAPCA*, 38 (1988) 1512.
- [11] J.C. Chuang and M.R. Kuhlman, *Environ. Sci. Technol.*, 24 (1990) 661.
- [12] R.H. Brown and C.J. Purnell, *J. Chromatogr.*, 178 (1979) 79.
- [13] K. Schoene, *Anal. Chem.*, 336 (1990) 114.
- [14] J.H. Raymer and E.D. Pellizzari, *Anal. Chem.*, 59 (1987) 1043.
- [15] M.T. Zaranski, G.W. Patton, L.L. McConnel, T.F. Bidleman and J.D. Mulik, *Anal. Chem.*, 63 (1991) 1228.
- [16] R.F. Mouradian, S.P. Levine, K.H. Qiong and H.H. Alvord, *J. Air Waste Manage. Assoc.*, 41 (1991) 1067.

Simple approach to eliminating disturbances in isoelectric focusing caused by the presence of salts

Jia-Li Liao*, Rong Zhang

Department of Biochemistry, University of Uppsala, Biomedical Centre, P.O. Box 576, S-751 23 Uppsala, Sweden

First received 5 April 1994; revised manuscript received 22 June 1994

Abstract

It is well known that the resolution in isoelectric focusing (IEF) is impaired by the presence of salts, partly due to a decrease in the width of the pH gradient. In addition, the risk of precipitation increases and the mobilization time for focused protein zones, an important step in IEF in capillary electrophoresis, is prolonged. To eliminate these drawbacks, an on-tube desalting technique for IEF was developed, based on an automatic substitution of the salts with an ampholyte solution in a short focusing step prior to the final analytical isoelectric focusing procedure.

1. Introduction

Capillary electrophoresis (CE) allows rapid separations with high efficiency and resolution. One of the greatest advantages of CE is the use of minute sample amounts, which range from a few nanolitres of sample to the cytosolic fluid of a single cell [1]. Capillary isoelectric focusing (cIEF) has been applied to the separation of haemoglobins [2], transferrins [3] and immunoglobulins [4]. It is known that the presence of salt in a sample changes the pH gradient and confines the protein zone to a small segment of the capillary. This narrow gradient will result in high protein concentrations and consequently an increased risk of precipitation, loss of resolution and long mobilization times [5]. For these reasons, desalting of biological samples prior to IEF is recommended, which usually entails large sample losses when the volume is below 5 μ l. So

far, no desalting methods are available for sample volumes in the nanolitre range. Therefore, there is a need for a microscale desalting technique. In this paper, we described an on-tube desalting method specific for IEF and its theoretical basis.

2. Experimental and results

2.1. Materials and equipment

An IEF protein standard mixture and Bio-Lyte (pH 3–10) ampholytes were obtained from Bio-Rad Labs. (Richmond, CA, USA). The separations capillary, made from fused silica and obtained from Polymicro Technologies (Phoenix, AZ, USA), was 150 mm \times 0.1 mm I.D. with a wall thickness of 0.1 mm. The on-tube detector was a modified Spectroflow 783 from ABI Analytical Kratos Division (Ramsey, NJ, USA) [6].

* Corresponding author.

The detection point was 15 mm from the cathodic end of the capillary.

2.2. Replacement of salt with ampholytes

The capillary was coated internally with linear polyacrylamide covalently attached to the wall using the method of Hjertén [7]. The IEF protein standard mixture was diluted 1:20 in 1.5% Bio-Lyte (pH 3–10) and to this solution various amounts of solid sodium chloride were added. The coated capillary was filled with this solution. A 3% Bio-Lyte (pH 3–10) solution was titrated to pH 4.0 with 2.0 M hydrochloric acid and served as the anolyte. The Bio-Lyte was titrated to pH 11.0 with 2.0 M sodium hydroxide and used as the catholyte. Electrophoretic replacement of salt with ampholytes was performed at a 30- μ A constant current, and completed when the voltage reached 3000 V. The time for replacement of salt was dependent on the salt concentration (Table 1).

2.3. Focusing and mobilization of proteins

Focusing was performed at a 3000-V constant voltage for 8 min (the time was determined by the use of coloured proteins). Phosphoric acid (0.02 M) served as the anolyte and 0.02 M sodium hydroxide as the catholyte. The width of the pH gradient was determined by measuring the distance with the aid of a ruler between the two coloured focused protein zones, phycocyanin

($pI = 4.65$) and cytochrome *c* ($pI = 9.6$) (Table 1). Cathodic mobilization was initiated by replacing the 0.02 M sodium hydroxide catholyte with 0.02 M phosphoric acid. Mobilization was performed at a constant voltage of 3000 V. The migrating zones were monitored at 280 nm as they passed a stationary UV detector. Mobilization occurs in one direction only. Therefore, proteins which focus at a pH around 10 may not be detected by the UV monitor on cathodic mobilization (e.g., cytochrome *c* in Fig. 1A,B), as their steady-state positions may be between the detector window and the cathode. However, on desalting cytochrome *c* can easily be detected (Fig. 1F–H).

For the study of IEF without replacement of salt we were able to avoid the risk of overheating during focusing by using a constant current of 30 μ A until the voltage reached 3000 V, and then keeping the voltage constant for 8 min (Fig. 1A–E).

3. Theoretical

Ampholytes are small molecules with different pI values. In cIEF, the whole capillary is filled with diluted ampholytes to a concentration of about 1.5%. When a voltage is applied the negatively charged acidic ampholytes migrate towards the anode and decrease the pH at the anodic section, while the positively charged basic ampholytes migrate towards the cathode and increase the pH at the cathodic section. These pH changes will continue until each ampholyte species has come to its isoelectric point, where it will then concentrate. Because each ampholyte has its own buffering capacity, a virtually continuous pH gradient will be formed. To prevent the ampholytes from migrating into the electrode vessels by either diffusion or gradient drift [8], 0.02 M phosphoric acid and 0.02 M sodium hydroxide were used as anolyte and catholyte, respectively.

Consider the boundary between the anolyte and the medium in the separation tube during the focusing step. The number of protons, N_{H^+} ,

Table 1
Influence of desalting on the width of the pH gradient

Conditions	NaCl concentration in sample (mol/l)	Desalting time (min)	Width of pH gradient (cm)
A	0	0	9.0
B	0.010	0	8.0
C	0.025	0	6.0
D	0.050	0	4.7
E	0.100	0	3.2
F	0.100	5	9.3
G	0.300	15	9.0
H	0.500	30	8.8

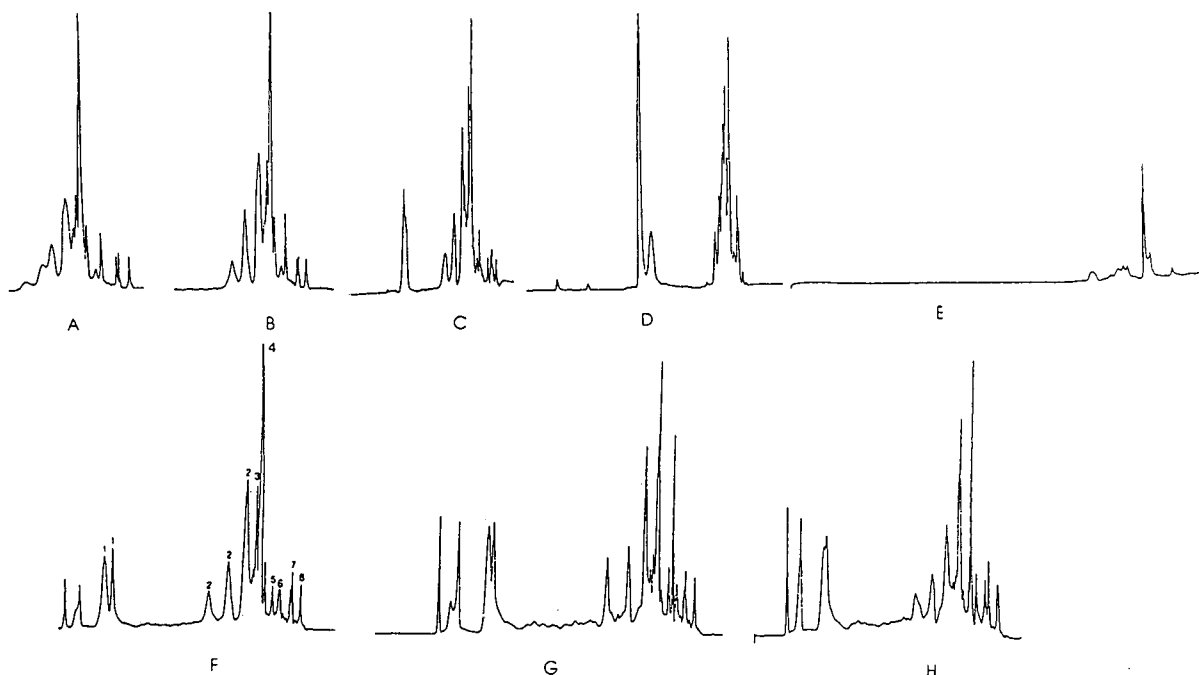


Fig. 1. Isoelectric focusing of IEF protein standard mixture with and without desalting. The protein mixture consisted of cytochrome *c* (peak 1), lentil lectin (2), human haemoglobin A (3), equine myoglobin A (4), human carbonic anhydrase (5), bovine carbonic anhydrase (6), β -lactoglobulin B (7) and phycocyanin (8). Replacement of salt with ampholytes was performed at a 30- μ A constant current and completed when the voltage reached 3000 V. A 3% Bio-Lyte (pH 3–10) solution titrated to pH 4.0 and 11.0 served as the anolyte and catholyte, respectively. The letters A–H refer to the experimental conditions listed in Table 1.

passing electrophoretically from the anolyte to the boundary per time unit can be expressed by

$$N_{H^+} = Iu_{H^+}n_{H^+}/\kappa \quad (1)$$

where I = current, u_{H^+} = mobility of the protons in the anolyte, n_{H^+} = number of protons per unit volume and κ = conductivity in the anolyte [8]. Ampholytes that are diluted in water have a high ohmic resistance, which increases further during focusing when a voltage is applied. Owing to the low current, the number of protons entering the capillary is limited according to Eq. 1, so the buffering ampholyte pH gradient is not affected.

In the presence of a sample containing salt (e.g. 0.1 M NaCl), we obtain a similar expression:

$$N'_{H^+} = I'u'_{H^+}n'_{H^+}/\kappa' \quad (2)$$

where I' = current in the tube in the presence of salt, $u'_{H^+} = u_{H^+}$, $n'_{H^+} = n_{H^+}$ and $\kappa' = \kappa$. In a 0.1 M NaCl sample solution the current, I' , is about twenty times greater than the current with NaCl is absent.

Combination of Eqs. 1 and 2 gives

$$N_{H^+}/N'_{H^+} = I/I' \quad (3)$$

i.e., $N'_{H^+} = 20 N_{H^+}$.

The number of protons entering the tube from the anolyte increases about twentyfold, then gradually decreases until most of the Na^+ ions have moved out electrophoretically. This decrease in pH at the anodic section causes the ampholytes to become positively charged and migrate towards the cathode. A similar situation occurs at the cathode, where a large number of OH^- ions enter the tube, giving rise to a pH

increase that forces the ampholytes to migrate towards the anode. As a result, the focused zones will be confined to a distance of 3–4 cm in the central part of the capillary, where a large degree of heat is generated, increasing the risk of protein precipitation [5]. As expected, the length of the pH gradient decreased with increasing amount of salt in the sample (Table 1).

To replace the salts in the capillary with ampholytes and to avoid proteins from either moving out of the capillary or being confined to the centre, 3% Bio-Lyte (pH 3–10) is titrated to pH 4.0 and 10.0 with 2.0 M HCl and 2.0 M NaOH and employed as anolyte and catholyte, respectively. Eq. 1 now takes the form

$$N''_{H^+} = I''u''_{H^+}n''_{H^+}/\kappa'' \quad (4)$$

where $\kappa'' = 2\kappa'$ (found experimentally) and $n''_{H^+} = (1/200)n'_{H^+}$ (0.0001/0.02) and $I'' = I'$. Accordingly, $N''_{H^+} = (1/400)N'_{H^+}$. Similarly, at the cathodic end $N''_{OH^-} = (1/400)N'_{OH^-}$. Therefore, the amount of H^+ at the anodic end and OH^- at the cathodic end during the removal of salt decreases about 400-fold when the sample contains 0.1 M NaCl. The concentrations of H^+ and OH^- decrease further along the capillary as they meet and react with the buffering ampholytes from the electrode vessels. The mobility of the ampholytes is much lower than that of Na^+ , so the current will decrease as the Na^+ ions are replaced by ampholytes moving into the capillary tube. The salt replacement is complete when the conductivity in the capillary tubing becomes close to that of a 1.5% ampholyte solution in the absence of salt, e.g., in our experiments when the voltage has increased to 3000 V at a constant current of 30 μA .

4. Discussion

IEF is a rapid and high-resolution separation technique that can resolve proteins based on small differences in isoelectric points. An obvious disadvantage with all methods based on IEF is that many proteins precipitate at their isoelectric points, particularly at high protein and salt

concentrations, and at elevated temperature. The presence of salt in a sample solution will shorten the ampholyte gradient (see Theoretical) and decrease the resolution (see Fig. 1B–D). When the concentration of salt increases above 0.05 M the proteins will focus into a very narrow pH gradient (see Table 1) where they tend to precipitate (see Fig. 1E). The mobilization towards the cathode was achieved by replacing the sodium hydroxide with phosphoric acid, which will decrease the pH in the capillary in accordance with the electroneutrality condition [8]. As the proteins and ampholytes become confined towards the centre of the capillary, H^+ and OH^- will accumulate at the margins. The field strength ($\propto 1/\kappa$) at the end of the capillary where phosphate ion enters is much smaller than that in the centre region owing to the higher conductivity at the ends of the capillary. Therefore, the velocity of phosphate ions is lower at the start of the mobilization when the sample contains salt according to the equation

$$v = Eu \quad (5)$$

where v = velocity of the phosphate ions, E = field strength and u = their mobility. Accordingly, the mobilization time is longer. The high pH in the basic region of the capillary hydrolyses the Si–O–Si–C bonds of the inner wall, causing electroendosmosis, which will distort any further IEF experiments.

We shall now show that desalting can be accomplished not only by ampholytes but also by ions of low mobility. From Eq. 1, one recognizes that a decrease in N can be achieved by a decrease in current (I), which is governed by the expression

$$I = V/R \quad (6)$$

and

$$R = l/q\kappa \quad (7)$$

where l = length of capillary and q = its cross-sectional area. Combining Eqs. 6 and 7 gives

$$I = Vq\kappa/l \quad (8)$$

The conductivity, κ , is determined by the expres-

$$\kappa = \frac{F}{1000} \cdot \sum C_i u_i \quad (9)$$

where F = the Faraday constant and C = concentration in gram equivalents per litre of solution.

Inexpensive cations and anions (with $pK \geq 11$ and ≤ 3 , respectively), that have high molecular masses and low mobilities, may be used for desalting instead of expensive ampholytes in the electrode vessel. Owing to the low ampholyte concentration in the sample solution (below 0.01 M) and neglecting the influence from H^+ and OH^- , the Kohlrausch regulating function, ω , [9] for the phases separated by the moving boundary between Na^+ in the α phase and the displacing ion X^+ in the β phase (migrating into the capillary from the anode) can be written as

$$\omega^\alpha = \frac{C_{Na^+}^\alpha}{U_{Na^+}^\alpha} + \frac{C_{Cl^-}^\alpha}{U_{Cl^-}^\alpha} \quad (10)$$

and

$$\omega^\beta = \frac{C_{X^+}^\beta}{U_{X^+}^\beta} + \frac{C_{Cl^-}^\beta}{U_{Cl^-}^\beta} \quad (11)$$

respectively. As $\omega^\alpha = \omega^\beta$,

$$\frac{C_{Na^+}^\alpha}{U_{Na^+}^\alpha} + \frac{C_{Cl^-}^\alpha}{U_{Cl^-}^\alpha} = \frac{C_{X^+}^\beta}{U_{X^+}^\beta} + \frac{C_{Cl^-}^\beta}{U_{Cl^-}^\beta} \quad (12)$$

Utilizing the conditions for electroneutrality and putting $C_{Na^+}^\alpha \approx C_{Cl^-}^\alpha$, $C_{X^+}^\beta = C_{Cl^-}^\beta$, $U_{Cl^-}^\alpha = U_{Cl^-}^\beta \approx U_{Na^+}^\alpha$ (the mobility of Cl^- is about 50% higher than that of Na^+), one obtains the following equation:

$$C_{X^+}^\beta = \frac{2C_{Na^+}^\alpha + U_{X^+}^\beta}{U_{Na^+}^\alpha + U_{X^+}^\beta} \quad (13)$$

Therefore, if the displacing ion has one tenth of the mobility of Na^+ , the concentration of this ion will be 2/11 of the Na^+ concentration [$U_{X^+}^\beta = (1/10)U_{Na^+}^\alpha$, $C_{X^+}^\beta = (2/11)C_{Na^+}^\alpha$]. Eq. 9 gives the following approximate value of the conductivity (κ_2) in the capillary following removal of the salt in the sample:

$$\kappa_2 = \frac{F}{1000} \left(\frac{2}{11} \cdot C_{Na^+} \cdot \frac{1}{10} \cdot U_{Na^+} + \frac{2}{11} \cdot C_{Cl^-} \cdot \frac{1}{10} \cdot U_{Cl^-} \right) \quad (14)$$

Similarly, the conductivity (κ_1) prior to removal of salt is

$$\kappa_1 = \frac{F}{1000} (C_{Na^+} U_{Na^+} + C_{Cl^-} U_{Cl^-}) \quad (15)$$

Consequently, $\kappa_2/\kappa_1 = 2/110$. Therefore, the contribution from the displacing ion to the current will also be reduced, as can be seen from Eq. 8. Owing to this lower current there will be a decrease in the number of H^+ and OH^- ions to the extent that the pH gradient will remain unaffected. The advantage of using the displacing ion instead of the ampholyte solution is that the pI of the displacing ion is outside the pH range of the ampholyte gradient. Therefore, this ion will be removed during IEF.

The on-tube desalting technique described here is rapid, highly reproducible and gives a high recovery compared with dialysis.

Acknowledgements

The authors thank Professor Stellan Hjertén for stimulating discussions and criticism of the manuscript. This work was supported by the Swedish National Science Research Council and the Knut and Alice Wallenberg and Carl Trygger Foundations.

References

- [1] T.M. Olefirowicz and A.G. Ewing, *Anal. Chem.*, 62 (1990) 1872–1876.
- [2] S. Hjertén and M. Zhu, *J. Chromatogr.*, 346 (1985) 265–270.
- [3] F. Kilár and S. Hjertén, *Electrophoresis*, 10 (1989) 23–29.
- [4] T. Wehr, M. Zhu, R. Rodriguez, D. Burke and K. Duncan, *Am. Biotechnol. Lab.*, 8 (1990) 22–29.

- [5] M. Zhu, R. Rodriguez and T. Wehr, *J. Chromatogr.*, 559 (1991) 479–488.
- [6] S. Hjertén, in H. Hirai (Editor), *Electrophoresis '83*, Walter de Gruyter, Berlin, 1984, pp. 71–79.
- [7] S. Hjertén, *J. Chromatogr.*, 347 (1985) 191–198.
- [8] S. Hjertén, J.-L. Liao and K. Yao, *J. Chromatogr.*, 387 (1987) 127–138.
- [9] S. Hjertén, in G. Milazzo (Editor), *Topics in Bioelectrochemistry and Bioenergetics*, Vol. 2, Wiley, Chichester, 1978, pp. 103–106.



ELSEVIER

Journal of Chromatography A, 684 (1994) 149–161

JOURNAL OF
CHROMATOGRAPHY A

Model of electrophoretic focusing in a natural pH gradient moving in a tapered capillary

Karel Šlais

Institute of Analytical Chemistry, Academy of Sciences of the Czech Republic, 611 42 Brno, Czech Republic

First received 17 May 1994; revised manuscript received 14 June 1994

Abstract

The principle and theoretical description of zone focusing in electrophoretic migration in a tapered capillary are presented. The model involves moving zones which gradually reduce their volume. The variance of a single Gaussian zone is discussed to illustrate the dynamics of this process. In order to derive the solution of the continuity equation, previous models of idealized focusing of ampholytes were modified to represent zone electrophoretic focusing in migration in a capillary with a shallow taper. The relations between the departure from the local steady state, the ratio of the inlet to outlet capillary cross-section, the ampholyte effective mobility and the pH gradient were established. They allow a comparison of described process with conventional isoelectric focusing and also the selection of the operating conditions such that the departure from the local steady state can be decreased to an acceptable extent. The relations predict that focusing in the capillary with a shallow taper should maintain constant the ratio of the actual zone width to the local steady state width, provided that the local capillary cross-section is indirectly proportional to the migration length coordinate. The significance of some assumptions needed for the model formulation is analysed. Numerical examples demonstrate the feasibility of the method.

1. Introduction

The trace determination of ionizable compounds often needs some means of sample concentration. Focusing electrophoretic methods as isotachopheresis (ITP) and isoelectric focusing (IEF) advantageously combine the powerful focusing and separation features. ITP also permits the transfer of analytes from a large capillary cross-section to a smaller one [1–3] which is used also in the combination of ITP with capillary zone electrophoresis (CZE) [4–7]. It has been shown [8] that some modes of IEF, including IEF with electrophoretic mobilization [9–11], have certain features similar to ITP. Therefore, it

seems reasonable to examine the possibilities of focusing ampholytes in a capillary with a non-constant cross-section. However, it is known from ITP that migration through a tapered channel brings about deterioration of the boundaries and zone broadening, which needs to be improved by using a coupled capillary with a constant cross-section [3]. Svensson [12] mentioned the idea of the numerical solution of focusing in a channel with a non-constant cross-section.

This contribution presents a simplified theoretical model that allows the shape and the degree of the continuous capillary taper to be related to other operational parameters of the focusing

process. The model used is consistent with the simplified approaches used previously to develop the theory of IEF in a channel with a constant cross-section [8,12–16].

2. Description of model

Let us examine focusing with net electrophoretic transport in a capillary with a non-constant cross-section A (see Fig. 1). The initial configuration consists of the near steady-state zone surrounded by the background of volume V_g , which spans the pH gradient with a total pH difference $\delta(\text{pH})$. The background together with the ampholytic analyte is positioned between the leading and terminating electrolytes, which adjust the mean gradient effective mobility, $\bar{\mu}$, and, together with the amount of the background components, the pH gradient volume. At time $t = t_0$, the zone position is $y = y_0$, where the capillary cross-section is A_0 . Owing to the constant electric current, I , the whole gradient including the analyte zone moves toward the detection point with coordinate y_d and cross-section $A_d < A_0$. Together with the movement to positions with a smaller cross-section, the length of the pH gradient gradually increases. In

this way, the local steepness of the pH gradient, $d(\text{pH})/dy$, decreases and the field strength, E , around the zone increases with decrease in A . The changes in the concentration profile due to the migration into the narrower cross-section unbalance the establishment of the steady state. The ampholyte tends to respond by re-establishing a new steady state but even as this proceeds, the unbalancing effect of the taper continues. With ongoing transport into locations with a smaller cross-section, the steady state remains just out of reach.

To allow the approximate solution of the process described above, the previous simple models of IEF [8,12–16] were used here for the initial considerations. They include the displacement of the gradient components due only to the electrophoretic transport so that the local velocity can be regarded as uniform over the capillary cross-section. Thus, the radial components of the transport can be neglected in comparison with the transport of the zone along the axis of the capillary. The current models of the background in idealized IEF consist of the system of ampholytes with equal diffusion coefficients, D , equal mass of the components and similar derivative of the pH dependence of their effective mobility, $d\mu/d(\text{pH})$ around their iso-

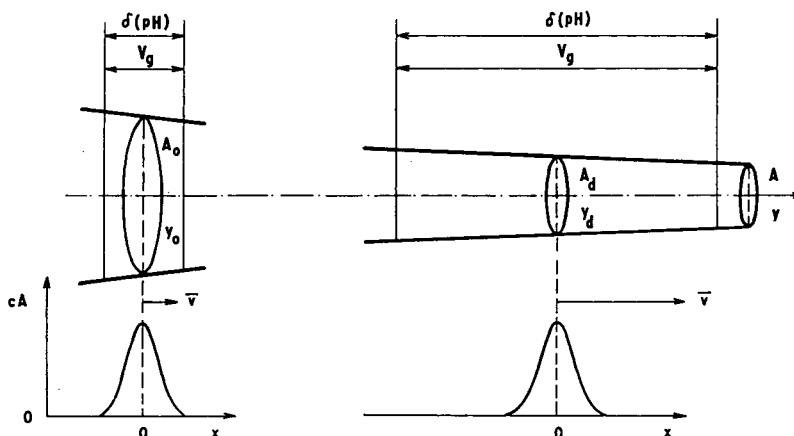


Fig. 1. Model of electrophoretic focusing of ampholytes in a natural pH gradient moving in a tapered capillary. A = Variable capillary cross-section; A_0 , A_d = cross-sections at the inlet and at the detection point, respectively; y = separation coordinate, zone position along the capillary axis; y_0 , y_d = zone positions at the inlet and at the detection point, respectively; x = distance from the zone centre in the direction of zone migration; c = ampholyte analytical concentration; $\delta(\text{pH})$ = pH difference across the volume of the separation medium, V_g ; \bar{v} = zone mean velocity along the separation coordinate. For further explanation, see text.

electric point, pI . The analyte amount is assumed to be small enough to make no essential contribution to the properties of the background. Because of the large number (up to thousands) of background components with approximately equally spaced isoelectric points, an essentially linear gradient is formed in the capillary of constant cross-section. The large number of components and a sufficiently large field strength imply that the zone width is small in comparison with the length of the capillary. Further, the contribution of solvent ions to the background conductivity is neglected. Assumptions of constant steepness of the pH gradient and constant field strength around the zone in a capillary with constant cross-section used previously in order to develop a theory simple enough for practical use do not, in fact, imply any serious oversimplification [14].

The above models are modified here in such a way that the pH gradient and the peak of the ampholytic analyte are allowed to move electrophoretically in the capillary with a shallow taper. The electric current, I , is constant, which implies a constant volume displacement of the considered zone. The pH difference, $\delta(\text{pH})$, over the volume of the focusing medium, V_g , and its conductivity are regarded as independent of the field intensity. Further, the ampholyte net dissociation is allowed to be small so that the local pH is not very different from the component isoelectric point, pI , which enables the derivative of the component mobility vs. pH dependence, $d\mu/d(\text{pH})$, to be regarded as equal to that at its pI . The mean effective mobilities of the components of the background and also that of the analyte are determined by the $d\mu/d(\text{pH})$ parameter and the composition of the leading electrolyte. As the diffusivities of both the background components and analyte are here considered to be the same, their mean effective mobilities can still be regarded as mutually equal. Hence it is accepted that the field intensity varies along the capillary due only to the current density. As the above conditions are not very different from the steady state in IEF, it is reasonable to regard the concentration profile of the zone as a Gaussian curve [8,12–18].

3. Theory

3.1. Relation of zone variance to the gradient of migration velocity

In the initial part of the theory, let us describe the influence of the local migration velocity, v , on the zone width as outlined in the model description and Fig. 1. The zone is regarded as that of the analyte or that of the background component. As the local velocity can be regarded as uniform over the capillary cross-section and the zone is close to the steady state, the radial concentration gradients can be neglected in comparison with the axial ones. When we accept the above assumptions, the continuity equation for the considered ampholyte can be written in a one-dimensional form:

$$\frac{dc}{dt} = D \cdot \frac{d^2c}{dy^2} - \frac{d(v c)}{dy} \quad (1)$$

where c is the local concentration of the ampholyte. The transformation to the system in which the coordinate origin moves with the zone centre enables the concentration changes to be related to the position of the concentration maximum. In the new system, x is the distance from the zone centre, expressed as

$$x = y - \int_0^t \bar{v} dt \quad (2)$$

where \bar{v} is the mean zone velocity along the separation coordinate, $\bar{v} = dy/dt$. Actually, it is the local velocity of the zone concentration maximum. With the use of Eq. 2, Eq. 1 transforms to

$$\frac{dc}{dt} = D \cdot \frac{d^2c}{dx^2} - c \cdot \frac{dv}{dx} - (v - \bar{v}) \cdot \frac{dc}{dx} \quad (3)$$

As stated above, electrophoretic focusing with transport in the tapered capillary leads to non-steady-state zones. This means that the term dc/dt in Eq. 3 is different from zero. Whereas in a capillary with constant cross-section the local steady-state concentration profile remains constant along the capillary axis [8], the local steady-state concentration profile in a tapered capillary

changes owing to the variations in the field strength and pH gradient. If the actual profile approaches the local steady-state profile very rapidly, it could be described by the relationships used in the description of the simple model of IEF. As the flux that equilibrates the difference between the actual profile and local steady state is only finite, the actual profile only tends to reach the local steady-state profile. Hence, the zone dispersion varies both by changes in the local steady-state profile and by the departure of the actual profile from the steady-state profile. As the concentration profile is regarded as Gaussian, the temporal changes in the local concentration originated by both effects can be expressed with help of the apparent dispersion coefficient, D^* , by the relation

$$\frac{dc}{dt} = \frac{d}{dx} \cdot \left(D^* \cdot \frac{dc}{dx} \right) \quad (4)$$

The insertion of Eq. 4 into Eq. 3 yields

$$\frac{d}{dx} \left[(D - D^*) \cdot \frac{dc}{dx} \right] = c \cdot \frac{dv}{dx} + (v - \bar{v}) \cdot \frac{dc}{dx} \quad (5)$$

In a tapered capillary, the local actual velocity, v , varies with the local cross-section, A , and thus with the x coordinate. As a shallow taper is considered, this variation can be described by a Taylor expansion. However, the shape of the capillary taper may be generally very different. In order to permit a simplified analytical solution of Eq. 5, we shall examine only a single kind of taper which generates a velocity variation described by only the first two terms in the expansion

$$v = \bar{v} + x \cdot \frac{dv}{dx} \quad (6)$$

By insertion of Eq. 6 into Eq. 5 and coupling the exact differential, we obtain

$$\frac{d}{dx} \left[(D - D^*) \cdot \frac{dc}{dx} \right] = \frac{dv}{dx} \cdot \frac{d(cx)}{dx} \quad (7)$$

As long as the dv/dx term is treated as a constant in the entire capillary, Eq. 7 can be directly integrated. The assumption of a long capillary in comparison with the zone width means that the boundary conditions imply van-

ishing of the concentration and the appropriate derivations towards both capillary ends. We obtain after integration, the use of the relation $dc/(c dx) = d(\ln c)/dx$ and rearrangement,

$$(D - D^*) \cdot \frac{d(\ln c)}{dx} = x \cdot \frac{dv}{dx} \quad (8)$$

The Gaussian concentration profile can be described by the relation

$$c = c_{\max} \exp\left(\frac{-x^2}{2\sigma^2}\right) \quad (9)$$

where σ is the standard deviation of the curve in length units and c_{\max} is the concentration in the zone concentration maximum, where $x = 0$. Since, as will be verified further, σ can be regarded as a constant along the whole capillary, from Eq. 9 it is for the particular zone

$$\frac{d(\ln c)}{dx} = \frac{-x}{\sigma^2} \quad (10)$$

By insertion of Eq. 10 into Eq. 8, we obtain the sought relation between the length-based zone variance and the constant velocity gradient. For further treatment, it is convenient to write this relation in the form

$$\frac{D^* - D}{\sigma^2} = \frac{dv}{dx} \quad (11)$$

Below, dv/dx and D^* will be expressed in terms of mobility, field strength and capillary taper.

3.2. Gradient of migration velocity in a tapered capillary

As the zone is transported only by the electromigration, the component velocity is the product of the component effective mobility, μ , and the local field strength, E :

$$v = \mu E \quad (12)$$

The focusing occurs by means of two gradients in the direction of the transport, the mobility gradient and field strength [12,15,18]. As the curvature of the velocity gradient is shallow, the same is expected for the both of the above. Further, the zone width is regarded as small in comparison with the capillary length. These gradients

can then be approximated as linear within the zone. The actual effective mobility can then be related to the mobility gradient, $d\mu/dx$, within the zone by the relation

$$\mu = \bar{\mu} + x \cdot \frac{d\mu}{dx} \quad (13)$$

Let us remember again that $\bar{\mu}$ is the component effective mobility at the zone maximum (see also Fig. 2). The mobility gradient of the ampholyte, $d\mu/dx$, can be related to the background pH gradient, $d(\text{pH})/dx$, by the equation

$$\frac{d\mu}{dx} = \frac{d\mu}{d(\text{pH})} \cdot \frac{d(\text{pH})}{dx} \quad (14)$$

where $d\mu/d(\text{pH})$ is the gradient of the pH dependence of the component effective mobility. It is generally function of μ but, as the ampholyte $\bar{\mu}$ is here constant and the zones are narrow, the $d\mu/d(\text{pH})$ term can be regarded as constant within the zone. This approximation is similar to that made in the simple IEF models with the only difference that the mean effective mobility of the zone centre is different from

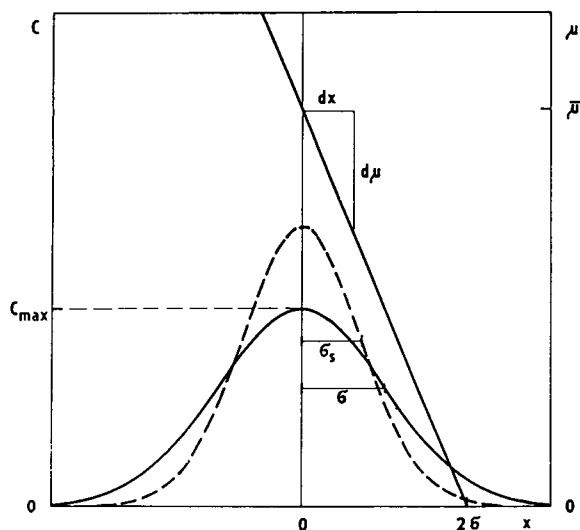


Fig. 2. Illustration of the zone mobility and the zone width. σ , σ_s = Actual and local steady-state standard deviation of the zone concentration profile, respectively; c_{max} = maximum ampholyte concentration in the zone; $d\mu/dx$ = derivative of the dependence of the ampholyte effective mobility on the distance along the separation coordinate; $\bar{\mu}$ = the zone mean effective mobility. For further explanation, see text.

zero. As stated in the model description, the background pH gradient can be treated as the pH continuum. In the steady state, it generates a linear pH gradient in a capillary of constant cross-section. The influence of variable capillary cross-section on the local steepness of the pH gradient can be expressed as

$$\frac{d(\text{pH})}{dx} = A \cdot \frac{\delta(\text{pH})}{V_g} \quad (15)$$

where $\delta(\text{pH})$ is the pH difference over the gradient volume, V_g . As the ratio $\delta(\text{pH})/V_g$ is constant, it allows us to assume that the local pH gradient can be expressed by Eq. 15 also when the background composed of a series of zones of ampholytes moves in the capillary with a non-constant cross-section under conditions that are close to the steady state. It should be noted that V_g can be only a fraction of the capillary volume and only a small part of that volume which surrounds the particular zone can be taken into the consideration for the estimation of the local steepness of the pH gradient. Therefore, the volume-based steepness of the pH gradient need not be constant over the whole V_g . When this is the case, then, instead of $\delta(\text{pH})/V_g$, the volume steepness of the pH gradient can be written in terms of the small finite differences, $\Delta(\text{pH})/\Delta V_g$.

The local field strength is related to A by the equation

$$E = \frac{I}{\kappa A} \quad (16)$$

where I is the total electric current over the capillary cross-section and κ is the background electrolyte conductivity. In conventional IEF, the background conductivity is inversely proportional to the degree of separation of the background component or, in other words, to the field intensity. However, in IEF with electrophoretic mobilization, this influence is reduced owing to the presence of a common counter ion which adjusts the non-zero mean effective mobility of both the background and the analytes. In Section 4, the conditions will be specified under which the background conductivity can be regarded as constant. Similarly to

the description of the local pH gradient, the conductivity need not be constant over the entire V_g . It is sufficient when the κ of the background surrounding the considered zone is constant. Therefore, in subsequent considerations, a constant conductivity environment of the particular zone during its transport through the tapered capillary is taken as a first approximation. When the constant current is applied to a tapered capillary filled with a medium of the constant conductivity, we obtain for the derivative of the dependence of the field strength on x with use of Eq. 16

$$\frac{dE}{dx} = -E \cdot \frac{d \ln A}{dx} \quad (17)$$

For evaluation of the dv/dx term in Eq. 11, the product $E d\mu/dx$ has an important role. The combination of Eqs. 14, 15 and 16 gives

$$E \cdot \frac{d\mu}{dx} = \frac{d\mu}{d(\text{pH})} \cdot \frac{\delta(\text{pH})}{V_g} \cdot \frac{I}{\kappa} \quad (18)$$

It appears that, for the first approximation, the $E d\mu/dx$ term can be regarded as independent of the capillary cross-section; the increase in E by the capillary taper is just counterbalanced by the same decrease in the $d\mu/dx$ term. It further yields the invariability of the $E d\mu/dx$ term with respect to the position relative to the zone centre not only in a capillary with a constant cross-section but also in a tapered capillary. This conclusion has key importance in the treatment of zone variance in the next section. Further, when we take the $E d\mu/dx$ term as constant, it can be verified with the use of Eqs. 12, 13 and 17 that the sought relation for the velocity gradient, dv/dx , is

$$\frac{dv}{dx} = E \cdot \frac{d\mu}{dx} - E \bar{\mu} \cdot \frac{d(\ln A)}{dx} \quad (19)$$

Insertion of Eq. 19 in Eq. 11 yields the relation

$$\frac{D^* - D}{\sigma^2} = E \cdot \frac{d\mu}{dx} - E \bar{\mu} \cdot \frac{d(\ln A)}{dx} \quad (20)$$

which brings us closer to the final solution.

3.3. Departure from the local steady state

Now, let us consider the system with no mean electrophoretic transport of the zone, i.e., $\bar{\mu} = 0$. It corresponds to the simple model of IEF, which means $dc/dt = 0$ and $D^* = 0$ in the steady state. Applying this condition to Eq. 20 yields the known relation for the length-based variance of the focused Gaussian zone in the steady state, σ_s^2 [8,12–16]:

$$\sigma_s^2 = \frac{-D}{E \cdot \frac{d\mu}{dx}} \quad (21)$$

Together with conclusion following from Eq. 18, the last relation indicates that, under the approximations made, the length-based width of the steady-state focused zone is independent on the capillary cross-section. Further, as $dx = dy$ for the steady state (see Eq. 2), σ_s is constant along the entire capillary. This conclusion also supports the assumptions used for the derivation of Eqs. 10 and 11. However, the steady-state volume-based standard deviation expressed as $A\sigma_s$ decreases proportionally to the decrease in A . As the model adopted involves the background composed from the series of ampholyte zones with the same amounts of respective components, c_{\max} is proportionally higher for the zones positioned at the smaller cross-section relative to the zones focused at larger A .

Now, let the series of the zones move from the broader end of the capillary towards the narrower end. When this movement is very slow, the zones can almost adjust their concentration profiles to the local steady-state ones. The result of such a process would be a continuous increase in c_{\max} of every particular zone. According to the model adopted, the position with certain A is bound to the corresponding c_{\max} for every zone passed. However, when we are treating a particular moving zone, the assumption of equal amounts of the gradient components is not necessary. Therefore, we can follow a single moving zone of an analyte in the same way as the zone of the background.

As discussed in Section 3.1, the zones moving

in a tapered capillary do not reach the local steady-state profile. When comparing Eq. 21 with Eq. 20, we can see that there are two terms more in the relation for the focusing with the finite mean zone velocity, i.e., D^*/σ^2 and $\bar{\mu}E d(\ln A)/dx$, which make the difference from the description of the local steady state. The departure from the equation for the steady-state focusing arises from the fact that the transport of the zone through a tapered capillary prevents a steady state from occurring.

First, the higher field strength in front of the zone continuously speeds up this part of the zone relative to the centre. Similarly, the zone rear, where the field strength is smaller relative to the centre, is slowed. This source of departure relative to the steady state is described by the second term on the right-hand side (RHS) of Eq. 20.

Second, as σ_s is constant and we examine a system with a small departure of the actual σ from σ_s , the ever decreasing capillary cross-section sweeps the concentration in the zone maximum to an increase relative to the actual value. As the zone concentration profile remains Gaussian, this process seems like negative diffusion towards the zone centre. This contribution to the departure of the actual state from the steady state reflects the term D^*/σ^2 in Eq. 20.

Owing to this effect, the steady state remains just out of reach, with the actual zone width lagging slightly behind the local steady-state zone width. The diagram of concentration profiles in Fig. 2 illustrates the above description; the standard deviation of the actual concentration profile exceeds the local steady state one.

Further, we shall discuss here the case when the actual zone width can be expressed as a multiple of the local steady state width with a proportionality coefficient not very different from unity. This is advantageous when the departure from the steady state is small and finite over the entire capillary. Then the proportionality coefficient should also be constant. To conclude, we shall seek a shape of the capillary taper that should maintain the ratio of the actual to the local steady-state zone width constant and not very different from unity.

It is conventional to express the changes in zone dispersion in terms of plate height, H . Then, we may relate D^* to H and the zone mean velocity explicitly as

$$D^* = \frac{\bar{v}H}{2} \quad (22)$$

Although the use of the theoretical plate concepts is particularly inappropriate for continuous processes, the rate of variance generation, $H = d\sigma^2/dy$, is still of utmost significance. It applies also for techniques operating in a non-uniform, gradient mode [17–19]. Thus, more universally, H may be regarded as a local increment of the zone variance. For a capillary with a non-constant cross-section, the volume-based changes in zone variance, σ_v^2 , should apply. As a shallow taper is under consideration, the theoretical plate volume can be expressed as the product of H and A . Then, we can write for H

$$H = \frac{1}{A} \cdot \frac{d\sigma_v^2}{dV} \quad (23)$$

and for σ_v , $\sigma_v = \sigma A$. The length-based zone variance may be regarded here as constant, to a first approximation (see also Eqs. 18 and 21). Then, the volume-based changes of the zone variance are originated from the variation of the cross-section along the separation coordinate. As $dV = A dy = A dx$, we obtain from Eq. 23

$$H = 2\sigma^2 \cdot \frac{d(\ln A)}{dx} \quad (24)$$

It should be noted that, contrary to the common understanding, there is some difference in the meaning of H . In conventional kinetic processes, e.g., in chromatography, the local departure from equilibrium leads to an increase in the zone variance. Here, the causality is changed, i.e., the continuously forced change in the volume-based variance leads to the departure from its local steady-state value.

Further, following Eq. 12, the local mean zone velocity is

$$\bar{v} = \bar{\mu}E_0 \quad (25)$$

where E_0 is the field intensity at the zone centre.

For a narrow zone in a capillary with a shallow taper, E and E_0 can be related by

$$E = E_0 + x \cdot \frac{dE}{dx} \quad (26)$$

E_0 in Eq. 25 may be approximated by E when the second term on the RHS of Eq. 26 is much smaller than the first, $|x dE/dx| \ll |E_0|$. When applied to a zone with width 4σ , this condition can be written with help of Eq. 17 as

$$2\sigma \ll \frac{-1}{d(\ln A)/dx} \quad (27)$$

In Section 4, the conditions for the use of E instead of E_0 will be further specified. With the last approximation, the insertion of Eqs. 24 and 25 in Eq. 22 yields the sought relation for D^* :

$$D^* = \bar{\mu} E \sigma^2 \cdot \frac{d(\ln A)}{dx} \quad (28)$$

Finally, insertion of Eq. 28 into Eq. 20 yields the expression for the actual zone variance:

$$\sigma^2 = \frac{D}{E \left[2\bar{\mu} \cdot \frac{d(\ln A)}{dx} - \frac{d\mu}{dx} \right]} \quad (29)$$

The last equation is more general than Eq. 21 because both for the zero net mobility and/or for no taper, it converts to the equation for σ_s . However, it should be kept in mind that Eq. 29 is derived for conditions where the denominator of the RHS is treated as constant or, in other words, for a special kind of capillary taper. Nevertheless, the last equation shows that the focused zone can be obtained, provided that the first term in the brackets is smaller than the second and, for a small departure of the actual zone width from the local steady-state one, it should be even much smaller. For a more explicit formulation of this relation, let us introduce the departure from the local steady state, ϵ , by the equation

$$\epsilon = 1 - \frac{\sigma_s^2}{\sigma^2} \quad (30)$$

This term not only simplifies the subsequent equations, but also explicitly relates the actual

zone variance to the local steady-state one. Apparently, the smaller ϵ is, the closer is the zone to the local steady state; zero ϵ means achieving the local steady state. The magnitude of ϵ can be obtained by the treatment of the equations for σ^2 and σ_s^2 . From combination of Eqs. 21, 29 and 30, we arrive at the relation between the capillary taper, the effective mobility gradient and ϵ as a simple expression achieving the desired purpose:

$$\frac{d(\ln A)}{dx} = \frac{\epsilon}{2} \cdot \frac{d\mu/dx}{\bar{\mu}} \quad (31)$$

By insertion of Eqs. 14 and 15 into Eq. 31, we obtain for the steepness of the capillary taper explicitly

$$\frac{d(1/A)}{dx} = \frac{\epsilon}{2} \cdot \frac{-d\mu/d(\text{pH})}{\bar{\mu}} \cdot \frac{\delta(\text{pH})}{V_g} \quad (32)$$

A relation similar to Eq. 32 can be obtained by evaluation of the changes in the resolution of the zones focused with migration in a tapered capillary [20]. The last equation can be used to calculate the relation of the capillary geometry to the acceptable departure from the steady state as a function of other experimental parameters.

3.4. Relation between the capillary geometry and the departure from the local steady state

Eq. 32 relates the local capillary taper to ϵ and important parameters of focusing such as the gradient volume and pH difference, the analyte mobility and the mobility vs. pH dependence. For the evaluation of the feasibility of the method, the dependence of the departure from the steady state on the entire capillary geometry is necessary. The following calculations are formulated so that the geometrical parameters are expressed as explicit functions of other experimental parameters including ϵ , which is regarded as a constant determined by the acceptable departure of the actual zone profile from the local steady-state one (see Eq. 30).

Because, for the sought geometry, the whole RHS of Eq. 32 and the zone volume displacement are regarded as positive constants along the

entire length of the capillary, the x variable can be substituted back to the y coordinate. After integration, we have for the dependence of the local cross-section on the y coordinate

$$A = \frac{1}{y} \cdot \frac{2}{\epsilon} \cdot \frac{\bar{\mu}}{-d\mu/d(\text{pH})} \cdot \frac{V_g}{\delta(\text{pH})} \quad (33)$$

When we solve the equation obtained for the particular capillary dimensions, let us recall that the cross-section A_0 is at the beginning of the capillary, $y = y_0$, and the cross-section A_d is at the detection point, $y = y_d$ (see Fig. 1). Then, the capillary length is $L = y_d - y_0$. Further, it is convenient to relate the changes in the capillary cross-section to its narrowest value, A_d . Therefore, we introduce the ratio of the inlet cross-section to the detection cross-section as a ratio, q :

$$q = A_0/A_d \quad (34)$$

Then, the particular solution of Eq. 32 has the form

$$1 - \frac{1}{q} = \frac{\epsilon}{2} \cdot \frac{-d\mu/d(\text{pH})}{\bar{\mu}} \cdot \frac{\delta(\text{pH})}{V_g} \cdot A_d L \quad (35)$$

The parameter q is also related to the capillary volume, V_L , which can be obtained by integration:

$$V_L = \int_{y_0}^{y_d} A \, dy \quad (36)$$

By insertion of Eqs. 33 and 34 into Eq. 36, we obtain after integration

$$\ln q = \frac{\epsilon}{2} \cdot \frac{-d\mu/d(\text{pH})}{\bar{\mu}} \cdot \frac{V_L}{V_g} \cdot \delta(\text{pH}) \quad (37)$$

Usually, capillaries of circular cross-section are used with $A = \pi r^2$, where r is the local capillary radius. With help of Eqs. 33 and 37, the sought dependence of r on y can be formulated as a relation involving only the geometrical parameters:

$$r = \left(\frac{1}{y} \cdot \frac{V_L}{\pi \ln q} \right)^{1/2} \quad (38)$$

which indicates the decrease in the capillary radius with the square root of the y coordinate.

The needed V_L and q variables should be optimized with the help of the previous equations.

4. Discussion

For the discussion of the calculation procedure, Eq. 32 has a key position. It relates the capillary taper to the departure from the steady state, ϵ , steepness of the pH gradient, $\delta(\text{pH})/V_g$, and the relative change in compound mobility vs. pH. Note that no electrical variables enter this equation except for their influence on the assumption of a narrow zone. As postulated in course of the calculation, the departure from the steady state which can be expressed in terms of ϵ is set constant along the whole capillary. The second term in Eq. 32 is the property of the focused substance and the magnitude of its effective mobility adjusted by the leading electrolyte. Therefore, it is independent of the capillary shape. The volume-based steepness of the pH gradient can be considered as constant for small departures from the steady state. Hence the left-hand side (LHS) of Eq. 32 can be regarded as a constant which determines the capillary geometry described by Eqs. 33–38. On the other hand, the invariability of the LHS of Eq. 32 justifies some approximations made through the calculations. Namely, together with Eq. 16, it leads to invariability of the dE/dx term in Eq. 17, which further justifies Eq. 26 and leads to invariability of the dv/dx term expressed by Eq. 19. Finally, for the found capillary shape, it also means that no higher terms need be neglected when writing the relation for the actual v (Eq. 6).

The assumption of constant conductivity has been used throughout this theory to facilitate and simplify the calculations. Now, the significance of this assumption will be discussed in a semi-quantitative manner. In the model adopted, the changes in average effective mobility of the ampholyte within the zone have contributions from changes in the ratios of uncharged and positively and negatively charged forms of the particular ampholyte with mutual overlap of the neighbouring zones. According to the model

adopted, the separation of the zone maxima in volume units is regarded as independent of field strength and capillary cross-section. Hence the mutual overlap is determined by the zone width in volume units. When there is no counter ion, the relative content of both ionized forms of the ampholyte decreases in the same way as the zone volume becomes smaller. When some strong common counter ion (e.g., positive) is used, the state can be achieved when the fraction of one of the charged forms of the ampholyte (i.e., positive) decreases faster than the other and finely becomes negligibly small. With further zone sharpening, the fraction of the other dissociated form (i.e., negative) remains constant in order to maintain the finite mean mobility that is necessary for transport of the whole gradient. To conclude, the relative invariability of the conductivity of the zone environment with the field intensity can be achieved when most of the respective ampholyte of the background is ionized with charge of only one sign. Then, its effective charge cannot vary with the zone width and then it also cannot be function of field, and, under a constant total current, a function of cross-section and position along the capillary length. As most of the component is accumulated within the zone width expressed as 4σ (see Fig. 2), such a condition can be described by the relation

$$2\sigma < \frac{-\bar{\mu}}{d\mu/dx} \quad (39)$$

This relation shows that under the conditions prescribed, a change in the sign of the ampholyte effective charge occurs at a point that is more than 2σ distant from the zone centre and hence only a negligible fraction of the total ampholyte mass has a charge sign opposite to that of most of the component. It is apparent that in IEF where zero net mobility is adjusted, the background conductivity is always dependent on the zone shape. On the other hand, in focusing with electrophoretic mobilization where the common counter ion adjusts the finite net effective mobility, it is possible to achieve a certain σ where the conductivity remains constant with further decrease in σ . Now, as the zones are close to the

steady state, let us estimate the desired conditions from the combination of Eqs. 14, 21 and 39. In the case of migration of the gradient towards the cathode, we obtain for E

$$E > \frac{4D}{\bar{\mu}} \cdot \frac{-d\mu/d(\text{pH})}{\bar{\mu}} \cdot \frac{d(\text{pH})}{dx} \quad (40)$$

Let us examine the real conditions close to the detection point as the reference and the narrowest, most critical place. We take typical values for focusing of ampholytes with electrophoretic mobilization towards the cathode as the ampholyte mean effective charge $z = 0.1$ and $E = 50 \text{ V mm}^{-1}$ [8]. With the use of the Nernst equation, we can estimate the first term on the RHS of Eq. 40 as $4 RT/zF \approx 1 \text{ V}$. The second term does not exceed 10 pH^{-1} for biprotic ampholytes and $z \approx 0.1$. As the gradient volume is usually only a fraction of the capillary volume in methods with gradient mobilization, let us take $V_g = V_L/5$. Further, we take $V_L/A_d = 200 \text{ mm}$, which relates the discussed tapered capillary to the typical length of a capillary with constant cross-section. The typical pH difference across the pH gradient is taken as $\delta(\text{pH}) = 5 \text{ pH}$. Then, Eq. 15 gives 0.125 pH mm^{-1} for the third term of the RHS of Eq. 40. Together, this means that E should be $>1.25 \text{ V mm}^{-1}$ at $y = y_d$. Actually, E can be expected to be up to 50 V mm^{-1} at the detection point [8], which is nearly two orders of magnitude higher than Eq. 40 needs. Consequently, with the help of Eqs. 33 and 34, the conductivity should not vary considerably with changes in A even at q up to about 50 in the discussed case. It can be noted that when the background components can be treated as weak electrolytes with similar D and equally spaced $\text{p}K_a$ values [8], the conductivity of the background should not vary with the shape of the zone of its components.

The zone profile at the focusing in a pH gradient in a background with a linear conductivity gradient was calculated by Svensson [12] for $\bar{\mu} = 0$ and $dE/dx = 0$. Under these conditions, he found the equation for the skew concentration distribution. When, for a shallow conductivity gradient, his result (Eq. 34 in Ref.

[12]) is taken and the logarithm is expanded as $\ln(1+a) = a + a^2/2 - a^3/3$ with neglect of higher terms, we obtain in the present notation

$$\ln\left(\frac{c}{c_{\max}}\right) = \frac{-x^2}{2\sigma_s^2} \left[1 + \frac{2}{3} \left(1 - \frac{\kappa}{\kappa_0} \right) \right] \quad (41)$$

where κ_0 is the conductivity at the zone centre. As the change in conductivity within a narrow zone can be expected to be only a few per cent, the actual concentration profile can be still approximated by a Gaussian curve.

Further, with decrease in A , the field strength increases and the conductivity can be constant or can decrease when the zone approaches the narrow parts of the capillary. At constant I , a field strength increase higher than corresponds to the decrease in A can be expected when the assumption of constant conductivity is not appropriate. Hence, although the calculations may become complicated with variation of the conductivity, narrower zones than those predicted by Eqs. 21 and 29 can be expected.

From Eqs. 27 and 31, the condition for approximating E_0 by E is

$$\frac{1}{\sigma} \gg \epsilon \cdot \frac{-d\mu/dx}{\bar{\mu}} \quad (42)$$

which is surely met when the system obeys Eqs. 39 and 40 as ϵ is expected to be much smaller than unity.

As the amount of the ampholyte in the zone and the length-based zone width remain constant during migration in a tapered capillary, the product of the local concentration and the local cross-section should have the same profile independent of the zone position in the capillary (see Fig. 1, bottom). Hence, as the zone passes through the tapered capillary, the concentration in the zone maximum increases proportionally to the decrease in cross-section (see also discussion following Eq. 21). Explicitly, the ratio of the inlet to the outlet concentration in the zone maximum is expected to be equal to q .

The acceptable numerical value of q may be estimated from the semi-quantitative evaluation of Eq. 37. For ampholytic analytes such as proteins, the absolute value of the second term

on the RHS is 10 pH^{-1} or higher for $z = 0.1$. When we take values of V_g and $\delta(\text{pH})$ the same as those for the evaluation of E at the detection point, it appears that the ratio q may be up to hundreds even for accepted ϵ as small as $0.01 < \epsilon < 0.1$.

The example of capillary dimensions with $V_L/A_d = 200 \text{ mm}$ and $q = 10$ can be calculated as follows. The combination of Eqs. 35 and 37 yields the length of the tapered capillary, $L = V_L(1 - 1/q)(A_d \ln q) = 78 \text{ mm}$, which is a factor of 0.39 smaller than the length of a cylindrical capillary of the same V_L and A_d . When we take the values above, we obtain $\epsilon = 0.0184$ from Eq. 37. With help of Eq. 30, this leads to the conclusion that the actual σ can be expected to be only 1% higher than the local steady state σ_s in the discussed case. It is apparent that a higher acceptable ϵ permits a higher q (see Eq. 37). For example, departure from the steady state due to the capillary taper expressed as $\epsilon = 0.5$ may be practically acceptable because, according to Eq. 30, it represents a σ/σ_s ratio of 1.4 (see Fig. 2). It can be concluded that there need not be a substantial decrease in the separation efficiency in comparison with other possible sources of the departure of the actual zone width from the theoretical local steady state value expressed by Eq. 21.

The course of the ratio of the local capillary radius to the radius at the detection point, r_d , with the position along the capillary is shown for q values of 5, 10 and 20 in Fig. 3. For the calculation of the curves, Eq. 38 is modified to

$$\frac{r}{r_d} = \left[\frac{1}{\frac{(y - y_0)A_d \ln q}{V_L} + \frac{1}{q}} \right]^{1/2} \quad (43)$$

where the V_L/A_d ratio is taken as constant and equal to 200 mm . In viewing Fig. 3, it should be kept in mind that the curves are drawn with $L/r_d \approx 5$, whereas in reality the values of this ratio can be expected to be up to two orders of magnitude higher. For example with $q = 20$ and typical $r_d = 40 \text{ }\mu\text{m}$, $L/r_d \approx 1600$. Thus, even the shape with $q = 20$ can still be regarded as a shallow taper along the entire capillary.

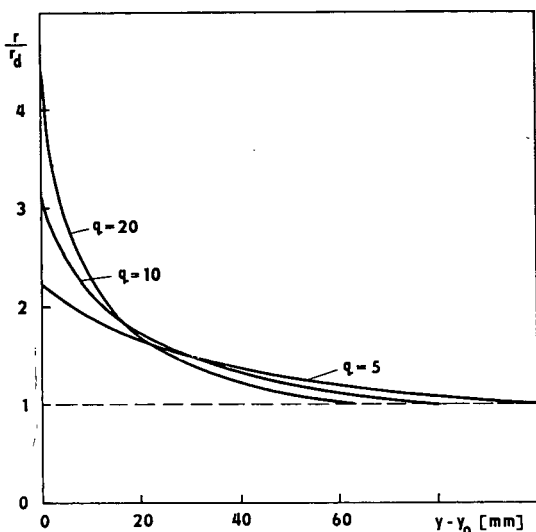


Fig. 3. Examples of calculated capillary geometry for $V_L/A_d = 200$ mm. r/r_d = Ratio of local capillary radius to the radius at the detection point; $y - y_0$ = distance from the capillary inlet; q = ratio of inlet capillary cross-section to the cross-section at the detection point.

Eqs. 32, 33 and 37 clearly show that the increase in the allowable taper steepness and/or the decrease in ϵ can be achieved by a decrease in the zone mean effective mobility. Thus, the smaller $\bar{\mu}$ is, the steeper the decrease in the capillary cross-section (or the higher q) can be with the same other parameters including ϵ . As follows from the model description, the mean effective mobility of an ampholytic analyte and that of the background components can be conveniently controlled by the leading electrolyte composition.

5. Conclusions

A simplified model of the focusing of an ampholyte zone that migrates electrophoretically in a tapered capillary has been suggested. An approximate solution of the continuity equation is possible by assuming a constant conductivity environment of the zone during its electrophoretic transport within a capillary with a shallow taper. It was found that focusing in the tapered capillary should maintain constant the departure

of the actual zone width from the local steady-state zone width and acceptably small even for a considerable ratio of the inlet to outlet capillary cross-section, provided that the local capillary cross-section is indirectly proportional to the migration length coordinate. The equations derived enable one to show the magnitude of the possible gain in operational parameters such as the decrease in the voltage and pressure drop needed, which will be discussed elsewhere together with changes in the zone resolution [20].

The method described opens up the way to increase the number of separable compounds without limitation from the excessive high voltage needed. The intended use of a constant current may obviate the problems of record interpretation associated with operation under a constant potential drop.

The discussed non-steady-state process continuously transports, separates and focuses the Gaussian zones of the ampholytes or of weak electrolytes, so it can be seen as intermediate between typical electrophoretic techniques including CZE, ITP and IEF.

6. References

- [1] F.M. Everaerts, T.P.E.M. Verheggen and F.E.P. Mikers, *J. Chromatogr.*, 169 (1979) 21.
- [2] T.P.E.M. Verheggen and F.M. Everaerts, *J. Chromatogr.*, 249 (1982) 221.
- [3] V. Dolník, M. Deml and P. Boček, *J. Chromatogr.*, 320 (1985) 89.
- [4] F. Foret, V. Šustáček and P. Boček, *J. Microcol. Sep.*, 2 (1990) 229.
- [5] F. Foret, E. Szökő and B. Karger, *J. Chromatogr.*, 608 (1992) 3.
- [6] D.S. Stegehuis, H. Irth, U.R. Tjaden and J. van der Greef, *J. Chromatogr.*, 538 (1991) 393.
- [7] D.S. Stegehuis, U.R. Tjaden and J. van der Greef, *J. Chromatogr.*, 591 (1992) 341.
- [8] K. Šlais, *J. Microcol. Sep.*, 5 (1993) 469.
- [9] S. Hjertén and M. Zhu, *J. Chromatogr.*, 346 (1985) 265.
- [10] S. Hjertén, J. Liao and K. Yao, *J. Chromatogr.*, 387 (1987) 127.
- [11] S. Hjertén, K. Elenbring, F. Kilár, J.L. Liao, A.J.C. Chen, C.J. Siebert and M.D. Zhu, *J. Chromatogr.*, 403 (1987) 47.
- [12] H. Svensson, *Acta Chem. Scand.*, 15 (1961) 325.

- [13] M. Almgren, *Chem. Scr.*, 1 (1971) 69.
- [14] H. Rilbe, *Ann. New York Acad. Sci.*, 209 (1973) 11.
- [15] J.C. Giddings and H. Dahlgren, *Sep. Sci. Technol.*, 6 (1971) 345.
- [16] J.C. Giddings, *Sep. Sci. Technol.*, 14 (1979) 871.
- [17] J.C. Giddings, *Dynamics of Chromatography, Part I*, Marcel Dekker, New York, 1963.
- [18] J.C. Giddings, *Unified Separation Science*, Wiley, New York, 1991.
- [19] J.C. Giddings, *Anal. Chem.*, 35 (1963) 353.
- [20] K. Šlais, *J. Microcol. Sep.*, submitted for publication.



ELSEVIER

Journal of Chromatography A, 684 (1994) 162-167

JOURNAL OF
CHROMATOGRAPHY A

Short communication

Diastereomeric and enantiomeric separation of monoesters prepared from *meso*-cyclopentanediols and racemic carboxylic acids on a silica phase and on amylose and cellulose chiral stationary phases

Annamarie Kunath^{a,*}, Fritz Theil^a, Jürgen Wagner^b

^aInstitute of Applied Chemistry, Rudower Chaussee 5, D-12484 Berlin-Adlershof, Germany

^bHumboldt University, Institute of Organic and Bioorganic Chemistry, Invalidenstrasse 42, D-10115 Berlin, Germany

First received 26 May 1994; revised manuscript received 15 July 1994

Abstract

The diastereomeric and enantiomeric separation of cyclopent-2-ene-1,4-diol and bicyclo[3.1.0]hexane-1,4-diol derivatives was carried out by HPLC on chiral stationary phases consisting of 3,5-dimethylphenylcarbamates of cellulose (Chiracel OD) and amylose (Chiralpak AD) coated on macroporous silica. The separation on the AD column is dramatically influenced by the kind of alcohol in the mobile phase. The retention times and separation factors increase on changing the mobile phase modifier from 2-propanol to ethanol and to a mixture of methanol and ethanol. On the OD column solutes elute faster with ethanol than with 2-propanol modifier, as expected from the higher polarity of ethanol.

1. Introduction

The lipase-catalysed transesterification of *meso*-diols with racemic carboxylic esters [1,2] leads to four stereoisomers with at least three asymmetric centers (Fig. 1). The isomers 1/1 and 1/2 and also 2/1 and 2/2 are enantiomeric. The pairs 1/1 + 1/2 and 2/1 + 2/2 are diastereomeric. Therefore, a complete analytical treatment includes first the separation of the diastereomeric pairs, which are subjected to chiral chromatography in a second step.

2. Experimental

2.1. Chemicals and materials

The synthesis of the racemic monoesters was described previously [2]. Chiracel OD and Chiralpak AD analytical columns (250 × 4.6 mm I.D.) were purchased from J.T. Baker (Gross-Gerau, Germany). Silica gel Si 60 (7 μm) (Merck, Darmstadt, Germany) was slurry packed in a stainless-steel column (150 × 4 mm I.D.) and used for diastereomeric separation. Mobile phase components were carefully dried analytical-reagent grade 2-propanol, ethanol, methanol, diethyl ether and *n*-hexane (Merck).

* Corresponding author.

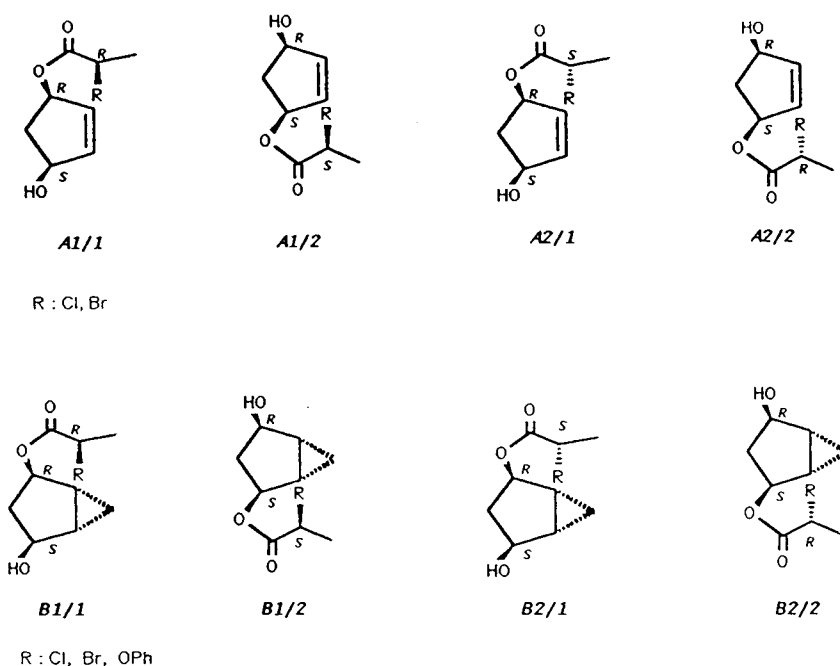


Fig. 1. Structures of compounds. A = cyclopent-2-ene-1,4-diol derivatives; B = bicyclo[3.1.0]hexane-1,4-diol derivatives.

2.2. Apparatus and chromatographic conditions

The liquid chromatographic systems consisted of a Merck–Hitachi L 6200 pump, a Rheodyne RH 7125 injection valve (20- μ l loop) a variable-wavelength spectrophotometer (Knauer, Berlin, Germany) and an Auswert 2 data system (ZIOC, Berlin, Germany). Optical rotation was followed with a Chiralyser (IBZ Messtechnik, Hannover, Germany) in series with the UV detector. The detection wavelength of the spectrophotometer and the flow-rate were set at 215 nm (except for the OPh compounds, 254 nm) and 1 ml/min, respectively. The column temperature was maintained at 23°C. The eluents used for the chiral separation were hexane–2-propanol (80:20, v/v), hexane–ethanol (80:20, v/v) and hexane–ethanol–methanol (80:10:10, v/v/v). Diastereomeric separations were carried out using hexane–2-propanol (97:3, v/v) or hexane–diethyl ether (1:1, v/v) as mobile phases. The sample concentration was about 10 mg/ml for the preparative mode and about 1 mg/ml for the analytical mode. Preparative separation of the diastereomers was achieved on

a silica gel column. Compounds with index 1 elute first (fraction F_1); index 2 represents the corresponding diastereomers with longer retention (fraction F_2) (see Fig. 2). After the evaporation of the mobile phase using a stream of nitrogen, the separated diastereomers were dissolved in 100 μ l of the mobile phase and subjected to chiral separation.

Circular dichroism (CD) spectra were recorded at room temperature on a JASCO J-710 spectropolarimeter.

3. Results and discussion

3.1. Diastereomeric separation

The capacity factors and the α -values of the diastereomeric separation are given in Table 1. Fig. 2 shows as an example the chromatogram of the preparative separation of compound B (R = OPh). The results clearly indicate that the bulkier the substituent R, the better is the separation factor and the shorter the retention time. In all

Table 1
Separation of the diastereomers on a silica gel column

Solute	Substituent	Eluent ^a	k'_1	k'_2	α
A	Cl	1	5.85	6.48	1.11
A	Br	1	5.40	6.24	1.16
B	Cl	2	5.03	5.56	1.10
B	Br	2	4.61	5.53	1.20
B	OPh	2	3.95	5.08	1.29

^a Eluent 1 = hexane–diethyl-ether (1:1, v/v); 2 = hexane–2-propanol (97:3, v/v).

instances the resolutions was sufficient enough for the preparative separation.

3.2. Enantiomeric separation

Enantiomeric separation of the solutes A1, A2, B1 and B2 was achieved on chiral stationary phases (CSP) consisting of 3,5-dimethylphenyl-carbamates of cellulose (Chiracel OD) and amylose (Chiralpak AD) coated on silica. The AD

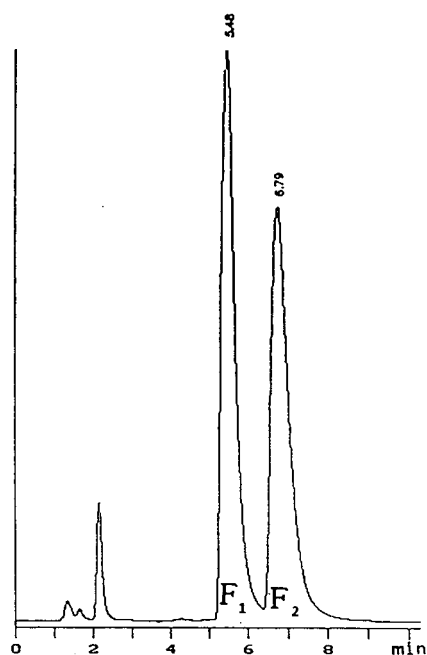


Fig. 2. Separation of the diastereomers of bicyclo[3.1.0]-hexane-1,4-diol derivatives ($R_1 = OPh$) on a silica gel column. Eluent: hexane–2-propanol (97:3, v/v). $F_1 = B1/1$ and $B1/2$; $F_2 = B2/1$ and $B2/2$.

column gave better results in all instances. The chromatographic parameters obtained are summarized in Tables 2 and 3. Examples of chromatograms are shown in Figs. 3 and 4.

Most striking is the influence of the kind of polar modifier in the mobile phase on the capacity factors k' and also the chiral recognition. With the CSP OD, as expected, the solutes elute faster with ethanol than with 2-propanol as polar modifier [3] (Table 3).

The chromatographic parameters obtained on CSP AD showed an unexpected behaviour. Both the capacity factors and the separation factors increase on changing from 2-propanol to ethanol and to ethanol–methanol (see Table 2 and Fig. 3). It is seen that with respect to retention, the second-eluting enantiomers (ester group in an *S*-configuration) are much more retained than the corresponding first-eluting *R*-enantiomers. Type B solutes are especially influenced. The retention also depends on the substituent R of the ester group. The strongest retention is obtained for solute B with the chloropropionate residue in an *S*-configuration and hexane–ethanol–methanol as eluent. The weakest retention is shown by solute A with the chloropropionate residue in an *R*-configuration and hexane–2-propanol as eluent. There seems to be no simple relationship between the type of substituent in the propionate side-chain and retention. In all instances the hexane–ethanol–methanol mobile phase system leads to an increase in optical resolution. For example, the α -value of B1 solute ($R = OPh$) increases by a factor of nine.

The chiral recognition process reflects the sum of all stereospecific interactions between the solute and the CSP [4,5]. Possible modes of the interaction arise between the free OH group and the ester carbonyl of the solutes and the CO group and the NH group of the polysaccharide carbamate as dipole–dipole interactions and/or hydrogen bonding. In addition, the chiral cavity of the CSP plays an important role. As the chemical derivatization of both cellulose and amylose is the same, the difference in chiral recognition of cellulose and amylose derivatives must be due to the different configuration of the glucose residue and higher order structure [5–7].

Table 2
Enantiomeric separation of the cyclopent-2-ene-1,4-diol and bicyclo[3.1.0]hexane-1,4-diol derivatives on a Chiralpak (AD) column

Substituent	Solute	Eluent ^a	$k'_{1/1}$	$k'_{1/2}$	α	$k'_{2/1}$	$k'_{2/2}$	α
Cl	A	1	0.65	0.78	1.20	0.67	0.77	1.14
Cl	A	2	0.95	2.10	2.21	1.01	1.66	1.64
Cl	A	3	0.94	2.30	2.45	1.05	1.78	1.69
Br	A	1	0.75	0.76	1.02	0.73	0.84	1.15
Br	A	2	1.18	1.63	1.38	0.94	2.03	2.16
Br	A	3	1.15	1.80	1.56	0.96	2.12	2.20
Cl	B	1	0.97	2.15	2.22	0.93	2.03	2.18
Cl	B	2	1.90	13.29	6.99	2.01	10.82	5.38
Cl	B	3	1.98	22.34	11.28	3.01	16.23	5.39
Br	B	1	1.17	1.81	1.55	1.02	1.67	1.64
Br	B	2	3.00	13.42	4.47	2.94	12.59	4.28
Br	B	3	3.11	18.22	5.86	3.11	18.00	5.79
OPh	B	1	0.79	1.22	1.54	0.80	1.26	1.57
OPh	B	2	0.97	9.71	10.01	2.38	11.09	4.66
OPh	B	3	0.85	12.09	14.22	2.43	16.60	6.83

^a Eluent 1 = hexane–2-propanol (80:20, v/v); 2 = hexane–ethanol (80:20, v/v); 3 = hexane–ethanol–methanol (80:10:10, v/v/v).

In order to explain the observed effect of polar organic modifiers on optical resolution, two possibilities must be taken into account: (i) the solvation or the conformation of either the solute or the CSP is affected by changes in the nature of the modifier; (ii) an alternation in the steric environment of the chiral cavity on the stationary phase is induced by changing the modifier. For example, CD experiments for solutes B1/2 (R = Cl) and B2/2 (R = Cl, Br) were performed

to confirm whether a conformational change of the solute occurred depending on the alcohol used. In each instance identical CD spectra were obtained in 2-propanol and methanol (Cotton effect $\lambda_{\max}/\text{sign}$: B1/2 233.5 nm/+; B2/2 (R = Cl) 233/5 nm/–; B2/2 (R = Br) 239.0 nm/–). These results show that the conformation of the solutes should not alter and therefore the modifier effect is probably related to changes in the CSP. To the best of our knowledge, there is no

Table 3
Enantiomeric separation of the cyclopent-2-ene-1,4-diol and bicyclo[3.1.0]hexane-1,4-diol derivatives on a Chiralcel (OD) column

Substituent	Solute	Eluent ^a	$k'_{1/1}$	$k'_{1/2}$	α	$k'_{2/1}$	$k'_{2/2}$	α
Cl	A	1	0.52	0.66	1.27	0.54	0.61	1.12
Cl	A	2	0.42	0.48	1.14	0.45	0.45	ca.1
Br	A	1	0.56	0.71	1.27	0.56	0.68	1.21
Br	A	2	0.45	0.49	1.09	0.45	0.49	1.09
Cl	B	1	0.47	0.48	1.02	0.46	0.50	1.09
Cl	B	2	0.37 ^b	0.34	1.09	0.33	0.38	1.15
Br	B	1	0.53	0.53	ca.1	0.52	0.51	ca.1
Br	B	2	0.45	0.49	1.13	0.45	0.49	1.21
OPh	B	1	0.89 ^b	0.65	1.37	0.67	1.19	1.78
OPh	B	2	0.50	0.50	ca.1	0.46	0.68	1.48

^a See Table 2.

^b Elution order has changed.

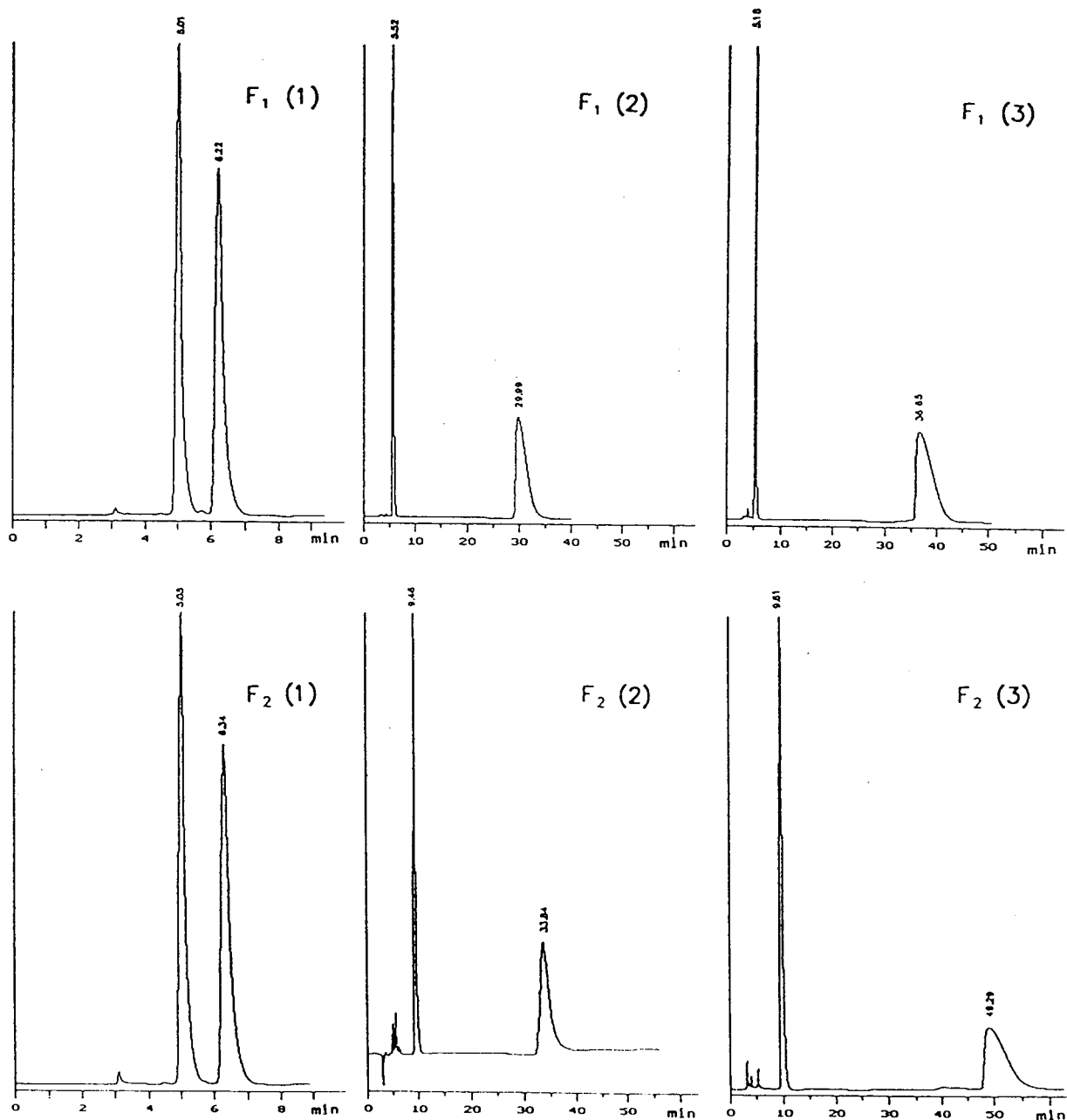


Fig. 3. Optical resolution of the silica gel fractions F₁ and F₂ on a Chiralpak AD column. The first-eluting compounds are B1/1 (F₁) and B2/1 (F₂) and the second B1/2 (F₁) and B2/2 (F₂). For eluents (1), (2) and (3), see Table 2.

information about the influence of solvents on the helix and chiral cavity of amylose carbamate derivatives. Solvents may affect the groove of the helix and the steric fit of a solute can become

better or worse during the interaction with carbamate groups of two or more glucose units.

A similar solvent effect was found by Balmer et al. [8] in the optical resolution of timoproxole

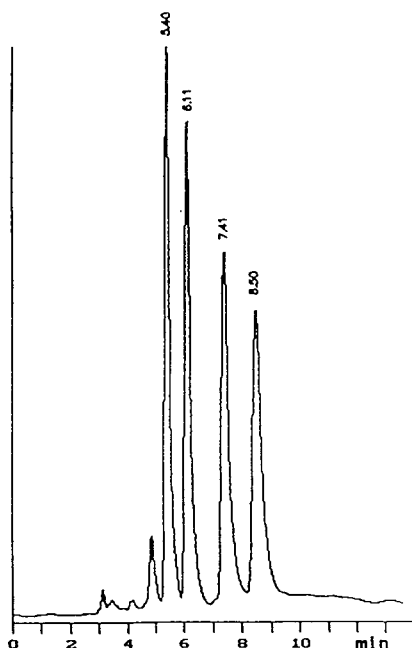


Fig. 4. Optical resolution of cyclopent-2-ene-1,4-diol derivatives ($R=Br$) on a Chiralpak AD column. Eluent: hexane-ethanol (80:20, v/v). Retention times: 540 min = A2/1, 611 min = A1/1; 7.41 min = A1/2; 8.50 min = A2/2.

on an AD column. They used hexane-2-propanol (80/20, v/v) as eluent and to this were added 1–20% of methanol. From 1% to about 6% of methanol the capacity factors decreased, as expected from the higher polarity of the eluent. On increasing the methanol content from 6 to 8%, the capacity factor of the second-eluting (+)-enantiomer increased by a factor of 2 where-

as the retention of the (–)-enantiomer was only slightly influenced. This means that an alteration of the chiral forces of the AD CSP probably occurs when the concentration of methanol in the eluent is about 5–10%.

4. Conclusion

OD and AD CSPs are suitable for the optical resolution of cyclopent-2-ene-1,4-diol and bicyclo[3.1.0]hexane-1,4-diol derivatives. Using the AD column an inverse polarity effect of the eluent is observed. Both retention and separation factor increase on changing the polar organic modifier from 2-propanol to ethanol and to a mixture of ethanol and methanol.

References

- [1] F. Theil, A. Kunath and H. Schick, *Tetrahedron Lett.*, 33 (1992) 3457–3460.
- [2] F. Theil, A. Kunath, M. Ramm, T. Reiher and H. Schick, *J. Chem. Soc., Perkin Trans. 1*, (1994) 1509.
- [3] *Instruction Manual for Chiracel OD*, Daicel Chemical Industries, Tokyo.
- [4] Y. Okamoto, M. Kawashima and K. Hatada, *J. Chromatogr.*, 363 (1986) 173.
- [5] Y. Okamoto and Y. Kaida, *J. Chromatogr. A*, 666 (1994) 403.
- [6] U. Vogt and P. Zugenmaier, *Ber. Bunsenges. Phys. Chem.*, 89 (1986) 983.
- [7] R. Aburatani, Y. Okamoto and K. Hatada, *Bull. Chem. Soc. Jpn.*, 63 (1990) 3606.
- [8] K. Balmer, B.-A. Persson and P.-O. Lagerström, *J. Chromatogr. A*, 660 (1994) 269.



ELSEVIER

Journal of Chromatography A, 684 (1994) 168–173

JOURNAL OF
CHROMATOGRAPHY A

Short communication

In vivo O-dealkylation of resorufin and coumarin ethers by the green alga *Chlorella fusca* analysed by a rapid and sensitive high-performance liquid chromatographic assay

Frank Thies, L. Horst Grimme*

Institute of Cell Biology, Biochemistry and Biotechnology, Department of Biology/Chemistry, University of Bremen, 28334 Bremen, Germany

Received 27 May 1994

Abstract

The O-dealkylation of resorufin or coumarin ethers is known to be a cytochrome P450-mediated reaction. It is used as a reference to characterize the corresponding enzyme activity and its state of induceability. In adopting this approach, an in vivo O-dealkylase assay was developed (a) using the unicellular green alga *Chlorella* as the biotransforming system and (b) applying a rapid and sensitive high-performance liquid chromatography (HPLC) assay which makes use of the wide pH stability of modified aluminium oxide packings. Separation was achieved isocratically at pH 9.8 using an Aluspher RP select B analytical column. The eluate was monitored by fluorescence detection with a detection limit of ≤ 3.5 pg for both resorufin and umbelliferone. The time needed for HPLC analysis is about 2 min, indicating that the method is suitable for automation.

1. Introduction

Cytochrome (Cyt) P450, the terminal oxygenase of the mixed function oxygenase system (mfo), is documented to be widely distributed among mammals, avians, fishes, insects, plants and unicellular organisms [1]. Although there are other oxygenase systems such as the flavin containing monooxygenase, Cyt P450 plays a major role in the metabolism of a broad range of xenobiotics. The first step (phase 1) in the biotransformation of drugs or xenobiotics is usually a Cyt P450-mediated reaction [2]. In plants, the involvement of Cyt P450 isoenzymes in the biotransformation of xenobiotics is de-

scribed particularly for herbicides [3,4]. In the case of green algae, representing the main part of primary producers in aquatic systems, references to Cyt P450 implications are rare [5] and systematic research is lacking. A common method for determining Cyt P450 activities or state of induction is to measure the O-dealkylation of alkoxy coumarins or alkoxyresorufins (ACOD, AROD) by a direct fluorimetric assay [6,7]. This approach allows one to distinguish different P450 isoforms [8,9]. In pharmacology and ecotoxicology it is used, e.g., for pharmacokinetic studies [10,11] and effect monitoring [12,13]. In contrast to a direct fluorimetric assay, HPLC analysis prevents interferences and allows the determination of both the substrate and metabolite. However, HPLC assays already described

* Corresponding author.

[14,15] showed limitations due to insensitivity or a long duration of analysis. This paper presents a simple, very sensitive and rapid HPLC method that was used to determine the O-dealkylase activities of the green alga *Chlorella fusca*.

2. Experimental

2.1. Chemicals

Methoxy-, ethoxy- and pentoxyresorufin (7-MR, 7-ER, 7-PR) were synthesized from resorufin (Res) by the method of Prough et al. [16], including the modifications of Klotz et al. [17]. The sodium salt of resorufin was purchased from Sigma (Deisenhofen, Germany) and iodoethane, 1-iodoethane and 1-iodopentane from Merck (Darmstadt, Germany). All preparative separations were performed on a 310-25 Li-Chroprep Si 60 column (Merck). The resorufin ethers were judged greater than 98% pure by HPLC with a combination of diode-array and fluorescence detection. Analytical standards were obtained from Boehringer (Mannheim, Germany) and Lambda (Graz, Austria). Acetone stock solutions were stored at -30°C . 7-Ethoxycoumarin (7-EC) and umbelliferone (7-HC) were obtained from Sigma, 7-methoxycoumarin (7-MC) from Lambda and glycine and organic solvents (analytical-reagent or HPLC grade) from Riedel-de Haën (Seelze/Hannover, Germany). Ingredients required for alga nutrient media were purchased from Merck.

2.2. Equipment

The HPLC equipment consisted of an L-6200A HPLC pump, an AS-4000 autosampler including a cooling sample rack, an F-1000 fluorescence detector, an L-4500 diode-array detector (not necessary for O-dealkylase assay) and D-6000 HPLC software (Merck). Quantification was effected by the external standard method.

Compounds were separated on an Aluspher 100 RP select B column (125 mm \times 4 mm I.D.)

with an appropriate guard column (4 mm \times 4 mm I.D.) (Merck).

2.3. Mobile phase

Separations of resorufin and alkoxyresorufin and of umbelliferone and alkoxy coumarin were performed isocratically with acetonitrile (solvent A) and 10 mM glycine in water adjusted to pH 9.8 with NaOH (solvent B). Solvent A to B ratios were as follows: MROD assay, 40:60; EROD assay, 50:50; PROD assay, 55:45; MROD assay 35:65; and ECOD assay, 42:58. Total flow-rate was 1.5 ml/min in all instances. The excitation and emission wavelengths were tuned to 370 and 455 nm respectively, for umbelliferone-alkoxy coumarin analysis and to 540 and 600 nm, respectively, for resorufin-alkoxyresorufin analysis.

2.4. In vivo O-dealkylase assay

Organism and culture conditions

The unicellular green alga *Chlorella fusca* var. *vacuolata* Shihira et Krauss, strain 211-15, culture collection Pringsheim (Göttingen, Germany), was grown photoautotrophically at $28 \pm 0.5^{\circ}\text{C}$ in an appropriate sterilized medium [18] adjusted to pH 7.6. Cultures were aerated with sterilized, water-saturated air, enriched with CO_2 (1.5–2.0%, v/v) and illuminated by a combination of two types of fluorescent tubes (L36W/41 Interna, L36W/11 daylight; Osram, Berlin, Germany) with an intensity of 13–18 W/m^2 (22–33 klux). Cells were synchronized by light-dark changes of 14–10 h and a periodic dilution to a standard cell density of $1 \times 10^6/\text{ml}$. The cell number and cell volume distribution were analysed using a Coulter Counter Model ZB Industrial and a Coulter Channelizer C-256 (Coulter Electronic, Luton, UK). For statistical treatment (mean cell volume of population, calculated as median or average of cell volume distribution), data were transferred directly to a microcomputer (Victor VPC; Victor Technologies, Scotts Valley, CA, USA) [19,20].

Assay procedure

An adequate volume of a stock solution of alkoxyresorufin/-coumarin was transferred into an erlenmeyer flask, acetone was evaporated and the flasks were filled completely with the nutrient medium, closed and incubated for about 1–2 h at 48°C in the dark with continuous stirring until dissolution was complete. The high hydrophobicity of 7-pentoxoresorufin requires acetone as a mediator. Therefore, 7-PR stock solution was applied directly to nutrient media, resulting in a final acetone concentration of 0.25%. At t_2 – t_3 of the cell cycle, algae were harvested (3250 g 5 min), washed twice, resuspended and adjusted to a biovolume of $0.8 \pm 0.02 \mu\text{l/ml}$ (average cell volume \times cell number). Aliquots of 2.5 ml of algae suspension were filled in 10-ml centrifuge tubes, each equipped with a 15-mm stirrer bar. Test-tubes were placed in a water-bath at 28°C with a multi-point magnetic stirrer (Variomag; H+P, Munich, Germany) adjusted to the maximum rpm and illuminated as described above. The layout made it possible to test up to 48 samples simultaneously. The assay was started by adding 2.5 ml of alkoxyresorufin/-coumarin solution to each test-tube, resulting in a final biovolume of $0.4 \pm 0.01 \mu\text{l/ml}$. After an adequate time of incubation the tubes were immediately put in a precooled (0°C) centrifuge and algae were separated at 3250 g for 5 min. Supernatants were analysed by HPLC as outlined above. The injection volume was 20 μl .

3. Results

Fig. 1 shows typical chromatograms for ECOD and EROD assays. The retention times for resorufin and umbelliferone are 0.65 and 0.71 min, respectively. The corresponding k' values (the hold-up time was 0.56 min determined with acetone and diode-array detection) are 0.15 and 0.27, which indicates only weak retention. For all other assays they were the same; the k' values for resorufin and coumarin ethers are 0.98 (7-MR), 0.84 (7-ER), 1.86 (7-PR), 1.07 (7-MC) and 1.02 (7-EC). Therefore, the analysis takes no longer than 1.5–2.0 min. There was no or

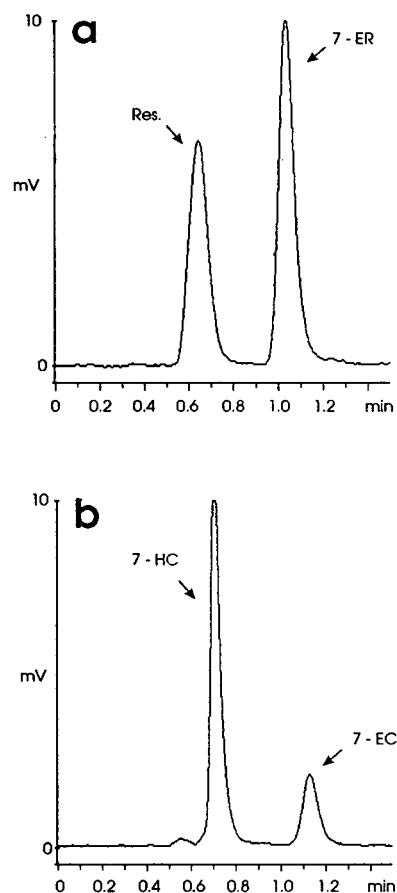


Fig. 1. Standard chromatograms of (a) resorufin–7-ethoxyresorufin and (b) 7-hydroxycoumarin–7-ethoxycoumarin (7-HC, Res $1.0 \times 10^{-8} M$; 7-EC, $2.0 \times 10^{-5} M$; 7-ER, $5.0 \times 10^{-6} M$). Substances were dissolved in alga nutrient media. Injection volume, 20 μl . Conditions as stated in the text.

only minor interference from ingredients of the medium which eluted together with resorufin or umbelliferone. The detection limits, defined by a signal-to-noise ratio of 3:1, were 2.6 pg for umbelliferone and 3.4 pg for resorufin, equivalent to a molarity of the medium supernatants of 0.8 nmol/l. The column packing was stable for over 300 days at pH 9.8.

Fig. 2 depicts the rate of umbelliferone/resorufin production versus substrate concentration. Because this curve resulted from an *in vivo* assay, it is the summation of all kinetic processes

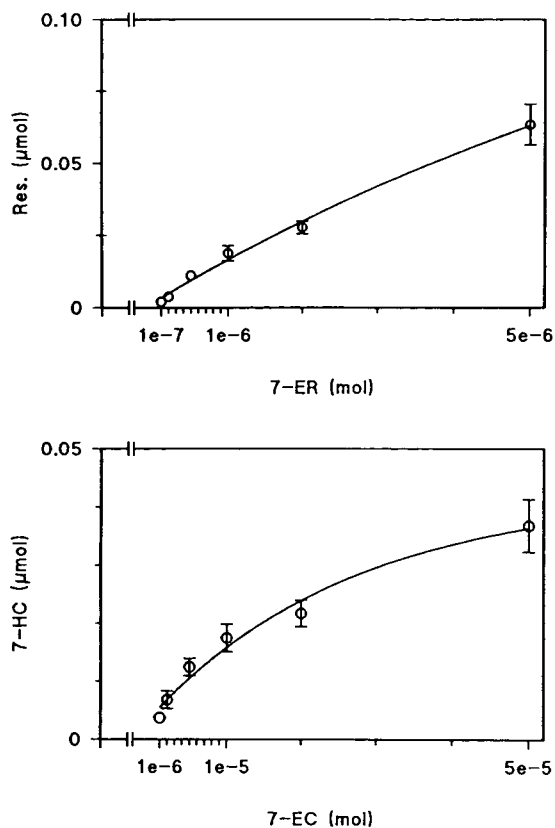


Fig. 2. Kinetic plots of umbelliferone (7-HC)/resorufin (Res) formation by *Chlorella fusca* ($0.4 \mu\text{l/ml}$) at $t_{60 \text{ min}}$ versus 7-EC/7-ER concentration. Values are means \pm S.D.

involved, including substrate absorption, enzymatic transformations and release of products. Higher substrate concentrations are not soluble without adding organic solvents (see below). Therefore, V_{max} could not be achieved. However, it is clear that alkoxyresorufin is a more suitable substrate. This becomes clearer by comparing the metabolite formation versus the time of incubation, which is shown in Fig. 3.

In addition to the methyl and ethyl ethers, the pentyl ether of resorufin was tested. In the first 120 min there is a linear increase in umbelliferone/resorufin formation accompanied by a decrease of substrate in the medium. Only with 7-MR as O-dealkylase substrate after 90 min did the resorufin formation begin to stagnate, followed by a decrease in resorufin in the medium.

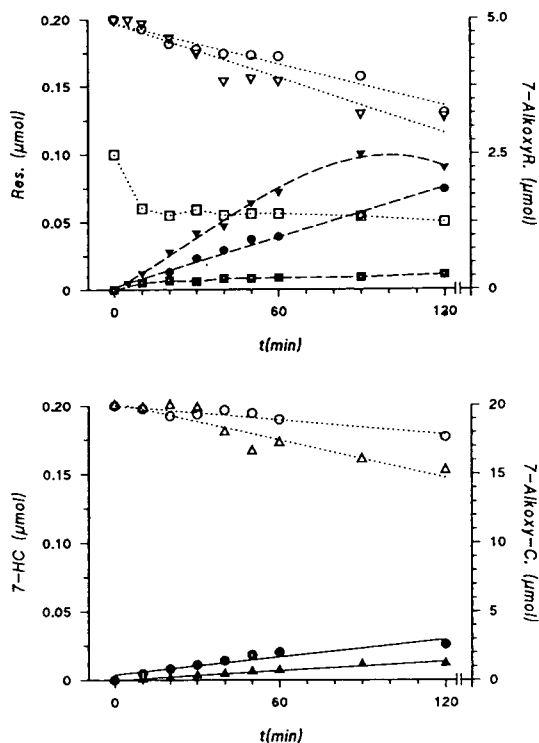


Fig. 3. Kinetic plots of umbelliferone (7-HC)/resorufin (Res) formation (solid symbols) and decrease of O-dealkylase substrates (open symbols) by *Chlorella fusca* ($0.4 \mu\text{l/ml}$) versus time. Substrate concentrations at t_0 : 7-MC, 7-EC, $2.0 \times 10^{-5} \text{ M}$; 7-MR, 7-ER, $5.0 \times 10^{-6} \text{ M}$; 7-PR, $2.5 \times 10^{-6} \text{ M}$. Δ , \blacktriangle = MCOD; \circ , \bullet = ECOD; ∇ , \blacktriangledown = MROD; \circ , \bullet = EROD; \square , \blacksquare = PROD.

For the alkoxyresorufins the order of turnover is 7-MR > 7-ER > 7-PR, indicating that the preference for one or another substrate is not only a function of its chain length. For the alkoxy-coumarins it is 7-EC > 7-MC. In the dark, the dealkylase activities decreased immediately (EROD –88%, ECOD –92%), which can be correlated with the much lower reduction power available.

As shown in Table 1, the inter-assay variances of the different O-dealkylases determined over 3 months are ca. 20%. This relatively high variance seems to depend on differences in the degree of dissolution of the substrates. The intra-assay variances are typically $\leq 10\%$. Therefore, to make use of the O-dealkylase activities of *Chlorella fusca* for the purposes of determining

Table 1
Resorufin and umbelliferone formation by *Chlorella fusca*

Substrate	$\mu\text{mol resorufin}$ (umbelliferone) $\times \text{h}^{-1}$	<i>n</i>
7-Methoxyresorufin	0.0843 ± 0.0175	10
7-Ethoxyresorufin	0.0579 ± 0.0128	14
7-Pentoxyresorufin	0.0083 ± 0.0024	8
7-Methoxycoumarin	0.0108 ± 0.0059	9
7-Ethoxycoumarin	0.0200 ± 0.0051	16

O-Dealkylase inter-assay variation over a period of 3 months. Biovolume of *Chlorella fusca* was adjusted to $0.4 \pm 0.01 \mu\text{l/ml}$. Values are means \pm S.D., *n* = number of assays. 7-MC, 7-EC, $2.0 \times 10^{-5} \text{ M}$; 7-MR, 7-ER, $5.0 \times 10^{-6} \text{ M}$; 7-PR, $2.5 \times 10^{-6} \text{ M}$. Conditions are described in the text.

potential inducers and inhibitors, great efforts have to be made to dissolve the coumarin and resorufin ethers.

Whereas it is common to use organic solvents as mediators for better dissolution, in this instance 0.1% acetone led to more than a 60% decrease in umbelliferone formation and 20% less EROD activity. MROD was inhibited significantly by acetone concentrations $\geq 0.2\%$. On the other hand, resorufin formation from 7-PR increased slightly with a higher concentration (0.25–3.0%) of acetone.

4. Discussion

The excitation and emission spectra and fluorescence intensity of umbelliferone and resorufin are affected by the degree of dissociation of the acid hydroxy group; the pK_a values are 7.75 and 6.1, respectively [21,22]. Therefore, full dissociation and maximum fluorescence occur at pH 9.8. In contrast to common RP-modified silica-based column packings, which hydrolyse under alkaline conditions, aluminium oxide-based packings are stable over a wide range of pH (2–12) [23]. This makes the appropriate "RP" phases (Aluspher RP select B is a polybutadiene-coated aluminium oxide [24]) suitable especially for separations of basic compounds, because protonation is suppressed and the chromatographic conditions are well defined. In the application presented this approach is inverted and ionization of the metab-

olites resorufin and umbelliferone is induced, leading to an improved sensitivity and minimum retention, whereas the retention of the hydrophobic alkoxyresorufins and -coumarins depends only on the concentration of acetonitrile. The detection limit of the applied HPLC method allows the supernatant to be analysed without further substance enrichment. Unlike other O-dealkylase assay procedures, using microsomes as the biotransforming system, it has been shown that it is possible to determine O-dealkylase activities of a unicellular green alga in vivo. Further investigations will demonstrate the usability of such a biotransforming system of Cyt P450, e.g., to establish the ecotoxicological relevance of environmental pollutants.

Acknowledgements

This work was supported by grants from the Senator für Bildung, Wissenschaft und Kunst der Freien Hansestadt Bremen. Thanks are due to Martin Bartsch for excellent technical assistance.

References

- [1] Y. Funae and S. Imaoka, in J.B. Schenkman and H. Greim (Editors), *Cytochrome P450, Handbook of Experimental Pharmacology*, Springer, Berlin, 1993, p. 221.
- [2] V. Ullrich, in J.W. Gorrod, H. Oelschlaeger and J. Caldwell (Editors), *Metabolism of Xenobiotics*, Taylor and Francis, London, 1988, p. 39.
- [3] C. Mougou, N. Polge, R. Scalla and F. Cabanne, *Pestic. Biochem. Physiol.*, 40 (1991) 1.
- [4] F. Durst and I. Benveniste, in J.B. Schenkman and H. Greim (Editors), *Cytochrome P450, Handbook of Experimental Pharmacology*, Springer, Berlin, 1993, p. 303.
- [5] M.F. Ladouceur, P. Weinberger, R. Greenhalgh and B. Hollebone, in H. Frehse, E. Kesseler-Schmitz and S. Conway (Editors), *Seventh International Congress of Pesticide Chemistry, Book of Abstracts*, Vol. II, GDCH, Hamburg, 1990, p. 169.
- [6] V. Ullrich and P. Weber, *Hoppe-Seyler's Z. Physiol. Chem.*, 353 (1972) 1171.
- [7] M.D. Burke and R.T. Mayer, *Drug Metab. Dispos.*, 2 (1974) 583.
- [8] M.D. Burke and R.T. Mayer, *Chem.-Biol. Interact.*, 45 (1983) 243.

- [9] M.D. Burke, S. Thompson, C.R. Elcombe, J. Halpert, T. Haaparanta and R.T. Mayer, *Biochem. Pharmacol.*, 34 (1985) 3337.
- [10] A.A.J.J.L. Rutten, H.E. Falke, J.F. Catsburk, H.M. Wortelboer, B.J. Blaauboer, L. Doorn, F.X.R. van Leeuwen, R. Theelen and I.M.C.M. Rietjens, *Arch. Toxicol.*, 66 (1992) 237.
- [11] J. Fry, M.J. Garle and K. Lal, *Xenobiotica*, 22 (1992) 211.
- [12] C.S. Elangbam, C.W. Qualls and R.L. Lochmiller, *Bull. Environ. Contam. Toxicol.*, 47 (1991) 23.
- [13] J. Snegarow, *Bull. Environ. Contam. Toxicol.*, 29 (1982) 492.
- [14] L. Esclade, D. Guillochon and D. Thomas, *J. Chromatogr.*, 341 (1985) 373.
- [15] R.R. Evans and M.V. Relling, *J. Chromatogr.*, 578 (1992) 141.
- [16] R.A. Prough, M.D. Burke and R.T. Mayer, *Methods Enzymol.*, 52C (1978) 372.
- [17] A.V. Klotz, J.J. Stegeman and C. Walsh, *Anal. Biochem.*, 140 (1984) 138.
- [18] L.H. Grimme and N.K. Boardman, *Biochem. Biophys. Res. Commun.*, 49 (1972) 1617.
- [19] R. Altenburger, W. Boedeker, M. Faust and L.H. Grimme, *Ecotoxicol. Environ. Saf.*, 20 (1990) 98.
- [20] M. Faust, R. Altenburger, W. Boedeker and L.H. Grimme, in K.G. Steinhäuser and P.-D. Hansen (Editors), *Biologische Testverfahren*, Schriftenreihe WaBoLu, Vol. 89, Fischer, Stuttgart, 1992, p. 311.
- [21] D.W. Fink and W.R. Koehler, *Anal. Chem.*, 42 (1970) 990.
- [22] H. Musso and C. Rathjen, *Chem. Ber.*, 92 (1959) 751.
- [23] K. Cabrera, G. Jung, K. Czerny and D. Lubda, *GIT Fachz. Lab.*, Chrom II (1991) 61.
- [24] G. Schomburg, J. Koehler, H. Figge, A. Deege and U. Bien-Vogelsang, *Chromatographia*, 18 (1984) 265.

CALL FOR PAPERS

1995 International Symposium & Exhibit on **PREPARATIVE CHROMATOGRAPHY**

June 11-14, 1995
Washington, DC, USA

Abstract Deadline -- NOVEMBER 8, 1994

*Organized by Professor Georges Guiochon
University of Tennessee and Oak Ridge National Laboratory*

**LECTURE & POSTER PRESENTATIONS
WORKSHOPS
SEMINARS
ROUNDTABLE DISCUSSIONS
CASE STUDIES
INSTRUMENTATION EXHIBIT**

Sponsored by the Washington Chromatography Discussion Group

For more information contact:

Janet Cunningham, c/o Barr Enterprises
P.O. Box 279, Walkersville, Maryland 21793 USA
(tele. 301-898-3772, fax 301-898-5596)

PUBLICATION SCHEDULE FOR THE 1995 SUBSCRIPTION

Journal of Chromatography A and Journal of Chromatography B: Biomedical Applications

MONTH	O 1994	N 1994	D 1994	
Journal of Chromatography A	683/1 683/2 684/1	684/2 685/1 685/2 686/1	686/2 687/1 687/2 688/1 + 2	The publication schedule for further issues will be published later.
Bibliography Section				
Journal of Chromatography B: Biomedical Applications				

INFORMATION FOR AUTHORS

(Detailed *Instructions to Authors* were published in *J. Chromatogr. A*, Vol. 657, pp. 463–469. A free reprint can be obtained by application to the publisher, Elsevier Science B.V., P.O. Box 330, 1000 AH Amsterdam, Netherlands.)

Types of Contributions. The following types of papers are published: Regular research papers (full-length papers), Review articles, Short Communications and Discussions. Short Communications are usually descriptions of short investigations, or they can report minor technical improvements of previously published procedures; they reflect the same quality of research as full-length papers, but should preferably not exceed five printed pages. Discussions (one or two pages) should explain, amplify, correct or otherwise comment substantively upon an article recently published in the journal. For Review articles, see inside front cover under Submission of Papers.

Submission. Every paper must be accompanied by a letter from the senior author, stating that he/she is submitting the paper for publication in the *Journal of Chromatography A* or *B*.

Manuscripts. Manuscripts should be typed in **double spacing** on consecutively numbered pages of uniform size. The manuscript should be preceded by a sheet of manuscript paper carrying the title of the paper and the name and full postal address of the person to whom the proofs are to be sent. As a rule, papers should be divided into sections, headed by a caption (e.g., Abstract, Introduction, Experimental, Results, Discussion, etc.). All illustrations, photographs, tables, etc., should be on separate sheets.

Abstract. All articles should have an abstract of 50–100 words which clearly and briefly indicates what is new, different and significant. No references should be given.

Introduction. Every paper must have a concise introduction mentioning what has been done before on the topic described, and stating clearly what is new in the paper now submitted.

Experimental conditions should preferably be given on a *separate* sheet, headed "Conditions". These conditions will, if appropriate, be printed in a block, directly following the heading "Experimental".

Illustrations. The figures should be submitted in a form suitable for reproduction, drawn in Indian ink on drawing or tracing paper. Each illustration should have a caption, all the *captions* being typed (with double spacing) together on a *separate sheet*. If structures are given in the text, the original drawings should be provided. Coloured illustrations are reproduced at the author's expense, the cost being determined by the number of pages and by the number of colours needed. The written permission of the author and publisher must be obtained for the use of any figure already published. Its source must be indicated in the legend.

References. References should be numbered in the order in which they are cited in the text, and listed in numerical sequence on a separate sheet at the end of the article. Please check a recent issue for the layout of the reference list. Abbreviations for the titles of journals should follow the system used by *Chemical Abstracts*. Articles not yet published should be given as "in press" (journal should be specified), "submitted for publication" (journal should be specified), "in preparation" or "personal communication".

Vols. 1–651 of the *Journal of Chromatography*; *Journal of Chromatography, Biomedical Applications* and *Journal of Chromatography, Symposium Volumes* should be cited as *J. Chromatogr.* From Vol. 652 on, *Journal of Chromatography A* (incl. Symposium Volumes) should be cited as *J. Chromatogr. A* and *Journal of Chromatography B: Biomedical Applications* as *J. Chromatogr. B*.

Dispatch. Before sending the manuscript to the Editor please check that the envelope contains four copies of the paper complete with references, captions and figures. One of the sets of figures must be the originals suitable for direct reproduction. Please also ensure that permission to publish has been obtained from your institute.

Proofs. One set of proofs will be sent to the author to be carefully checked for printer's errors. Corrections must be restricted to instances in which the proof is at variance with the manuscript.

Reprints. Fifty reprints will be supplied free of charge. Additional reprints can be ordered by the authors. An order form containing price quotations will be sent to the authors together with the proofs of their article.

Advertisements. The Editors of the journal accept no responsibility for the contents of the advertisements. Advertisement rates are available on request. Advertising orders and enquiries can be sent to the Advertising Manager, Elsevier Science B.V., Advertising Department, P.O. Box 211, 1000 AE Amsterdam, Netherlands; courier shipments to: Van de Sande Bakhuyzenstraat 4, 1061 AG Amsterdam, Netherlands; Tel. (+31-20) 515 3220/515 3222, Telefax (+31-20) 6833 041, Telex 16479 els vi nl. UK: T.G. Scott & Son Ltd., Tim Blake, Portland House, 21 Narborough Road, Cosby, Leics. LE9 5TA, UK; Tel. (+44-533) 753 333, Telefax (+44-533) 750 522. USA and Canada: Weston Media Associates, Daniel S. Lipner, P.O. Box 1110, Greens Farms, CT 06436-1110, USA; Tel. (+1-203) 261 2500, Telefax (+1-203) 261 0101.

ANALYTICAL BIOTECHNOLOGY

Proceedings of the 4th International Symposium on Analytical Methods, Systems and Strategies in Biotechnology (ANABIOTEC '92), Noordwijkerhout, The Netherlands. 21-23 September 1992

Edited by **C. van Dijk**

Previously published as part of the 1993 subscription to the journals
Analytica Chimica Acta and *Journal of Biotechnology*

ANABIOTEC '92 focused on the further integration of biotechnology and analytical chemistry. The results of this symposium clearly demonstrated that a substantial progress could be reported in the application of both conventional and new analytical techniques, the latter essentially based on natural analytical tools such as biomolecules. The main themes covered during this meeting are fermentation monitoring, chromatography, instrumental analysis, biosensors and bioanalysis.

A selection of the contents.

Preface.

Process Control. Monitoring and control of recombinant protein production (K. Schügerl *et al.*). Rapid and quantitative analysis of bioprocesses using pyrolysis mass spectrometry and neural networks: application to indole production (R. Goodacre, D.B. Kell). Characterization of a sampling unit based on tangential flow filtration for on-line bioprocess monitoring (T. Buttler, L. Gorton, G. Marko-Varga). Automated monitoring of biotechnological processes using on-line ultrafiltration and column liquid chromatography (N.C. Van de Merbel *et al.*). On-line monitoring of penicillin V during penicillin fermentations: a comparison of two different methods based on flow-injection analysis (M. Carlsen *et al.*). Development of an on-line method for the monitoring of vicinal diketones and their precursors in beer fermentation (C. Mathis *et al.*). Monitoring of fermentation by

infrared spectrometry. Alcoholic and lactic fermentations.

(D. Picque *et al.*).

Chromatography and other Separation Techniques.

Chromatographic analysis of biopolymers distribution in "poly-hemoglobin"; an intermolecularly crosslinked hemoglobin solution (J. Simoni, G. Simoni, M. Feola). Application of multivariate mathematical-statistical methods for the comparison of the retention behaviour of porous graphitized carbon and octadecylsilica columns (E. Forgács, T. Cserhádi, B. Bordás).

Antibodies. Catalytic antibodies: new developments (R. Hiltorst).

Biosensors. Measurements of nitric oxide in biological materials using a porphyrinic microsensor (T. Malinski *et al.*). Reusable fiber-optic-based immunosensor for rapid detection of imazethapyr herbicide (R.B. Wong, N. Anis, M.E. Eldefrawi). Biosensor monitoring of blood lactate during open-heart surgery (M. Kyröläinen *et al.*).

Instrumental Techniques.

Introduction to the dielectric

estimation of cellular biomass in real time, with special emphasis on measurements at high volume fractions (C.L. Davey *et al.*).

Spectral analysis of interactions between proteins and dye ligands (J. Hubble, A.G. Mayes, R. Eisenthal).

Enzymatic Analysis. Preservation of shelf life of enzyme based analytical systems using a combination of sugars, sugar alcohols and cationic polymers or zinc ions (T.D. Gibson, J.N. Hulbert, J.R. Woodward).

Colloidal Carbon Particles.

Colloidal carbon particles as a new label for rapid immunochemical test methods: Quantitative computer image analysis of results (A. van Amerongen *et al.*). Author Index.

© 1993 208 pages Hardbound
Price: Dfl. 265.00 (US \$ 151.50)
ISBN 0-444-81640-2

ORDER INFORMATION

For USA and Canada
ELSEVIER SCIENCE INC.

P.O. Box 945
Madison Square Station
New York, NY 10160-0757
Fax: (212) 633 3880

In all other countries
ELSEVIER SCIENCE B.V.

P.O. Box 330
1000 AH Amsterdam
The Netherlands

Fax: (+31-20) 5862 845
US\$ prices are valid only for the USA & Canada and are subject to exchange rate fluctuations; in all other countries the Dutch guilder price (Dfl.) is definitive. Customers in the European Union should add the appropriate VAT rate applicable in their country to the price(s). Books are sent postfree if prepaid.



**ELSEVIER
SCIENCE**
B.V.



0021-9673(19941028)684:1;1-I

13 S.F. 2537

zone